

Fundamentals and Multi-Objective Design of Inductive Power Transfer Systems

Roman Bosshard & Johann W. Kolar

Power Electronic Systems Laboratory
ETH Zurich, Switzerland



ICPE 2015
ECCE Asia



ACKNOWLEDGEMENT

The authors would like to express their sincere appreciation to ABB Switzerland Ltd. for the support of research on IPT that lead to the results presented in this Tutorial



The authors also acknowledge the support of CADFEM (Suisse) AG concerning the ANSYS software

Agenda



Slide Download:
www.pes.ee.ethz.ch
Publications → Tutorials

Introduction		System Components & Design Considerations		Power Electronics Concept for 50 kW	
14 slides	45 slides	68 slides	23 slides	24 slides	12 slides
	Fundamentals: Isolated DC/DC → IPT		Multi-Objective Optimization		Summary & Conclusions

Introduction

Features & Limitations
Potential Applications
Existing Industry Solutions



► Future Electric Vehicle Charging

■ Electric Vehicles – Key Limitations

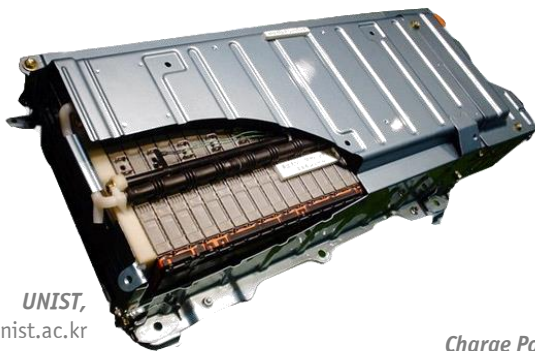
- Driving Range / Battery Capacity
- Availability of Charging Stations
- Time for Battery Re-Charging

■ Drivers for Future Development

- Battery Technology
- Infrastructure Development
- Charging Technology



Nissan Leaf,
www.nissan.com



UNIST,
www.unist.ac.kr



Charge Point,
www.chargepoint.com



Network World, www.networkworld.com

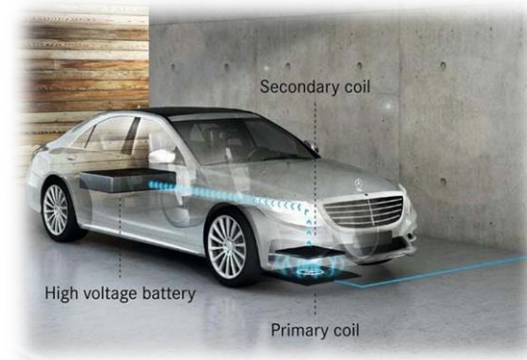
► Wireless Electric Vehicle Battery Charging



Charge Point,
www.chargepoint.com



Delphi, www.delphi.com



Daimler & BMW,
www.daimler.com, www.bmw.de

■ Higher Convenience & Usability

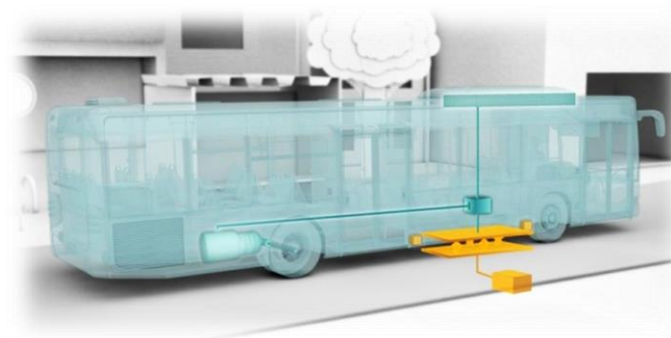
- No Plug Required: Quick Charging at Traffic Lights, Bus Stops, ...

■ More Frequent Recharging

- Longer Battery Lifetime
- Smaller Battery Volume & Weight

■ Reduced Fleet in Public Transportation

- Shorter Time for Depot Re-Charging



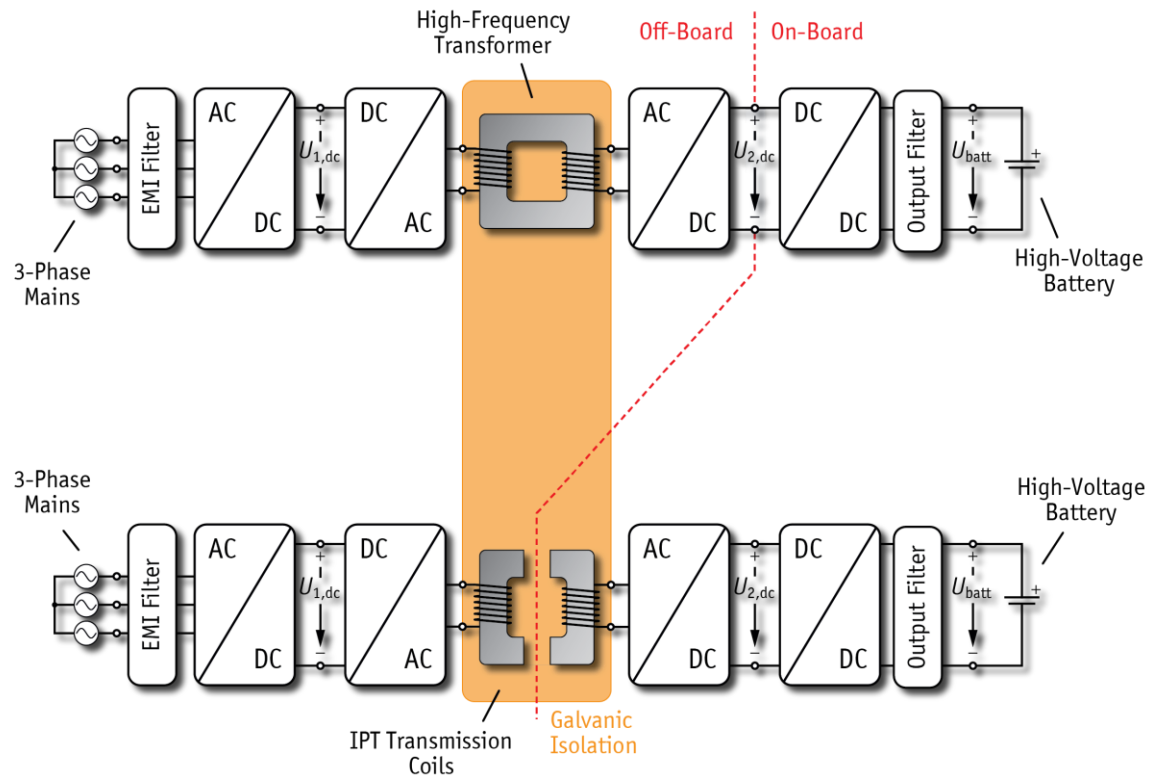
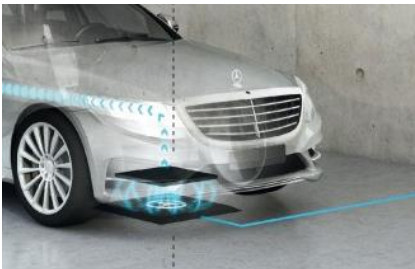
Bombardier PRIMOVE,
<http://primove.bombardier.com>.

► EV Charging – Typical AC/DC Power Conversion Chain

■ Conductive EV Charging



■ Wireless EV Charging



▲ Structure of a 3-Φ Isolated 2-Stage High-Power Battery Charging System with High-Frequency Transformer or IPT Transmission Coils

► Electrical Ratings of Conductive EV Chargers

■ SAE J1772 Definition (USA)

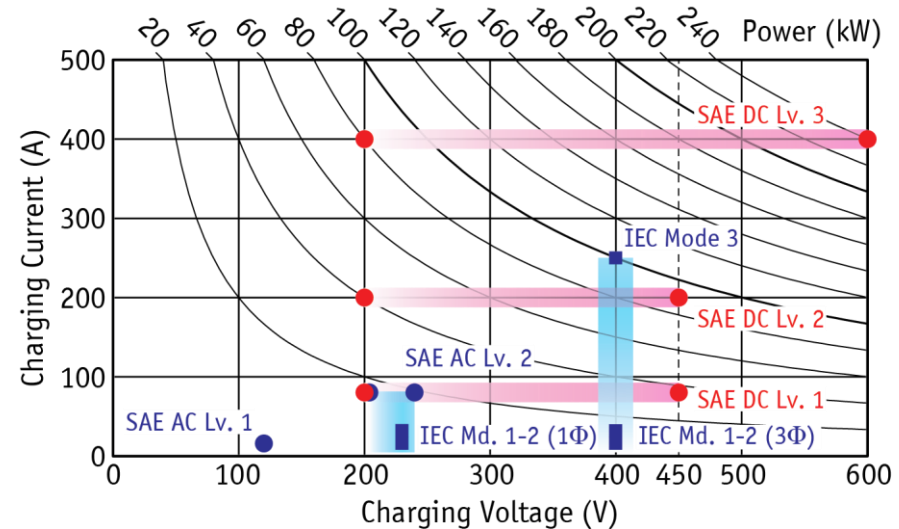
- AC Level 1: 120 V, 16 A → 1.92 kW
- AC Level 2: 204-240 V, 80 A → 19.2 kW
- AC Level 3: n/a → ≥ 20 kW
- DC Level 1: 200-450 V, 80 A → 36 kW
- DC Level 2: 200-450 V, 200 A → 90 kW
- DC Level 3: 200-600 V, 400 A → 240 kW

■ IEC 62196 Definition (Europe, Int.)

- Mode 1: 1x230 V / 3x400 V, 16 A → 7.7 kW
- Mode 2: 1x230 V / 3x400 V, 32 A → 15.4 kW
- Mode 3: 3x400 V, 32-250 A → ≥ 20 kW
- Mode 4: ≤ 1000 V, 400 A (DC) → 240 kW



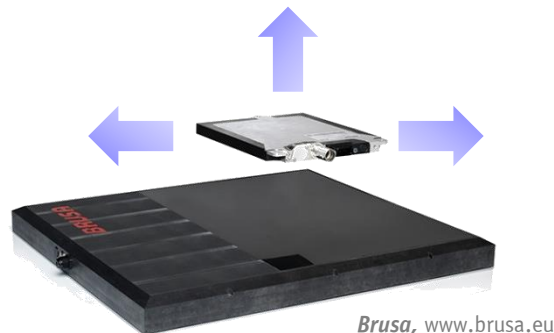
▲
SAE J1772 Combo Connector
for AC or DC (Level 1-2)



► Regulations & Standards for Inductive EV Charging (1)

■ SAE J2954 Wireless Charging Standard (under Development, Nov. 2013)

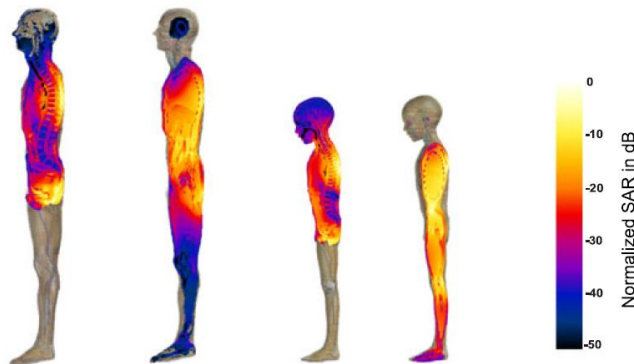
- Common Operating Frequency 85 kHz
- Minimum Charging Efficiency > 90%
- Charging Levels:
 - 3.7 kW (WPT1: Private Low Power)
 - 7.7 kW (WPT2: Private/Publ. Parking)
 - 22 kW (WPT3: Fast Charging)
- Interoperability: Air Gap, Coil Dimensions, Tolerance, Communication, Receiver-Side Interface
- Safety Features: Foreign Object Detection, Electromagnetic Stray Field
- Validation Methods: Performance, Safety



► Regulations & Standards for Inductive EV Charging (2)

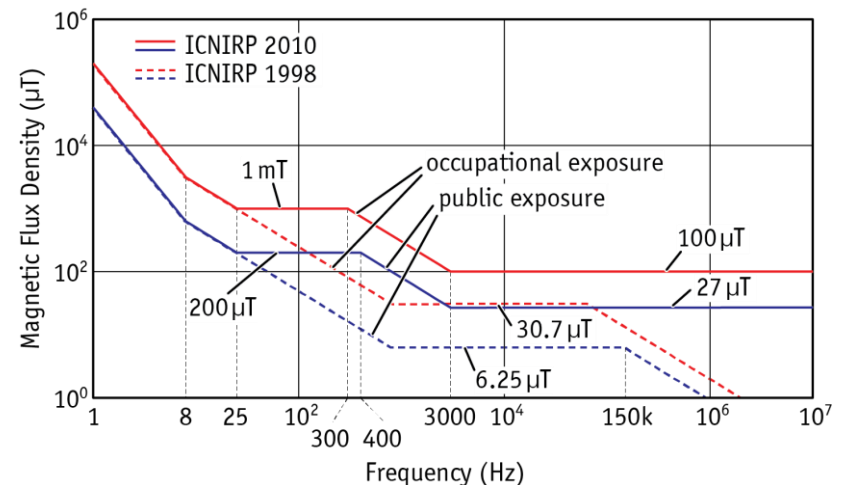
■ ICNIRP 1998/2010: Guidelines for Limiting Exposure to Time-Varying EM Fields

- Living Tissue affected by Power Dissipation caused by Electromagnetic Fields
- Limitation of Human Body SAR (=Specific Absorption Rate, [W/kg]) by Limiting Electric and Magnetic Fields
- Distinction between “General Public” and “Occupational Exposure”



Christ et al., «Evaluation of Wireless Resonant Power Transfer Systems With Human Electromagnetic Exposure Limits,” IEEE Trans. Power Electron., vol. 55, no. 2, 2013.

▲ SAR caused by 8 MHz 4-Coil IPT System



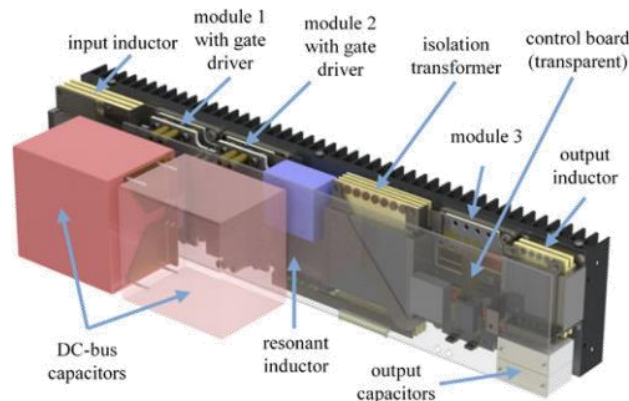
▲ ICNIRP 1998/2010 Reference Values for B-Field

► EV Battery Charging: Key Design Challenges

■ Conductive Isolated On-Board EV Battery Charger:

- Charging Power 6.1 kW
- Efficiency > 95%
- Power Density 5 kW/dm³
- Spec. Weight 3.8 kW/kg

→ Engineering Goal:
Design Competitive IPT System



*B. Whitaker et al. (APEI),
«High-Density, High-Efficiency,
Isolated On-Board Vehicle Battery
Charger Utilizing SiC Devices,”
IEEE Trans. Power Electron.,
vol. 29, no. 5, 2014.*



■ High Power Density (kW/dm², kW/kg)

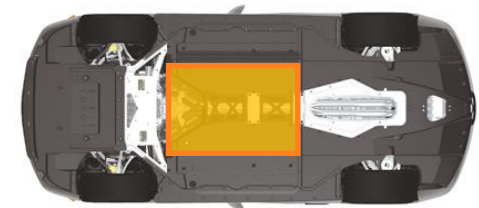
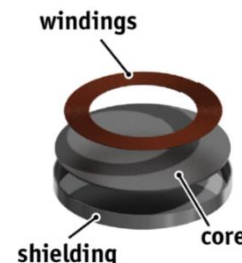
- High Ratio of Coil Diameter / Air Gap
- Heavy Shielding & Core Materials

■ Low Magnetic Stray Field $B_s < B_{lim}$

- Limited by Standards (e.g. ICNIRP)
- Eddy Current Loss in Surrounding Metals

■ High Magnetic Coupling

- Physical Efficiency Limit def. by k
- Sensitivity to Coil Misalignment



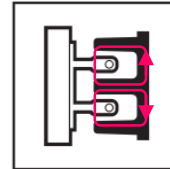
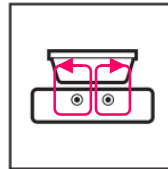
Lexus, www.lexus.com, 2014

Realization Examples

► IPT for Industry Automation Applications

■ Industry Automation & Clean-Room Technology

- Automatic Guided & Monorail Transportation Vehicles
- Stationary/Dynamic Charging in Closed Environment
- Key Features: Wireless, Maintenance-Free, Clean & Safe



▲ Wireless Powered Floor Surface Conveyors





▲ Ceiling-Mounted Monorail Transportation System

Conductix-Wampfler, www.conductix.ch (1.11.2014),
«Product Overview: Inductive Power Transfer»

► IPT for EV: Selected Demonstration/Research Activities



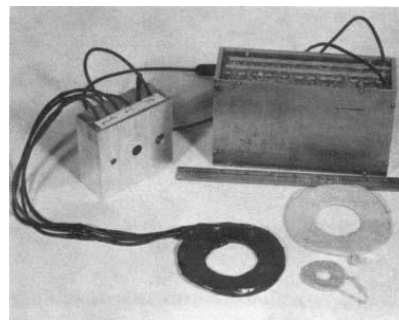
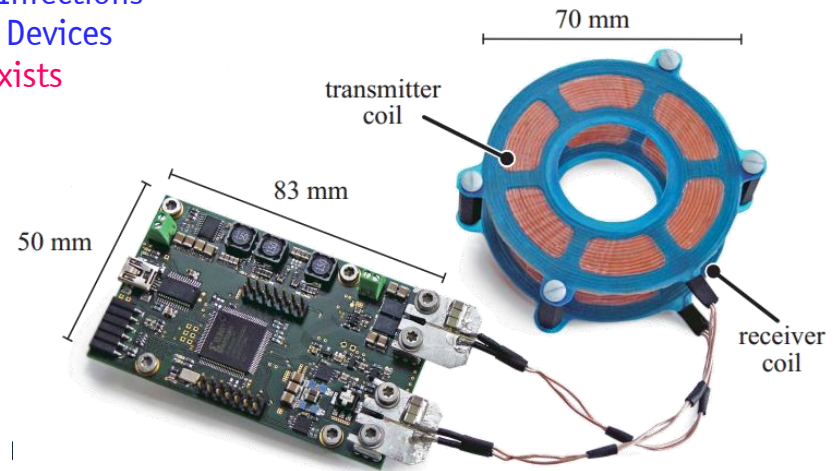
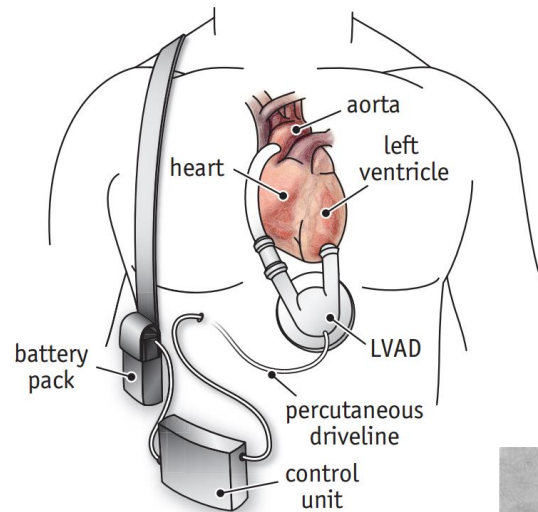
► IPT Public Transportation Systems

	Conductix-Wampfler IPT Charge	Bombardier PRIMOVE	KAIST On-Line EV	Wave IPT
				
Location	Genoa (IT) Hertogenbosch (NL)	Augsburg, Braunschweig, Mannheim (DE) Lommel (BE)	Seoul, Daejeon, Yeosu, Gumi (KR)	Salt Lake City, McAllen Monterey-Salinas, Lancaster (USA)
Year	2002 - 2012	2010 - 2015	2010 - 2015	2014 - 2015
Air Gap	Approx. 4 cm	Approx. 4 cm	Up to 20 cm	Up to 20 cm
Power	Up to 60 kW	150-200 kW	3-100 kW	50 kW
Details	<ul style="list-style-type: none"> • Coil Lowered to Ground at Bus Stations • Charging Efficiency > 90% • ICNIRP 1998 Compliant • 50% Red. Battery Capacity (240→120 kWh) 	<ul style="list-style-type: none"> • Coil Lowered to Ground at Bus-Stations • Reduced Number of Fleet Vehicles • Extended Battery Life • Lower Total Cost 	<ul style="list-style-type: none"> • Electrified Track for In-Motion Charging • ICNIRP 1998 Compl. • 30% Reduced Battery Weight • Reduced Number of Fleet Vehicles 	<ul style="list-style-type: none"> • Wireless Charging at Bus-Stations without Lowering the Coil • Charging Efficiency > 90% • ICNIRP Compliant

► Historic Background: Medical Applications

■ Electro-Mechanical Heart Assist Devices

- Percutaneous Driveline Major Cause of Lethal Infections
- Transcutaneous Power Supply for Heart Assist Devices
- No Reliable and Medically Certified Solution Exists



J. C. Schuder, "Powering an artificial heart: birth of the inductively coupled-radio frequency system in **1960**," *Artificial Organs*, vol. 26, no. 11, pp. 909–915, 2002.

O. Knecht, R. Bosshard, and J. W. Kolar, "Optimization of Transcutaneous Energy Transfer Coils for High Power Medical Applications," in *Proc. Workshop on Control and Modeling for Power Electron. (COMPEL)*, **2014**.

► Inductive Power Transfer: Summary of Key Features

- Easy-to-Use and Fast EV Charging: **Increased Convenience** for Users
- **Reduced Number of Fleet Vehicles** for Public Transportation
- **Galvanic Isolation** - No Additional Transformer Required

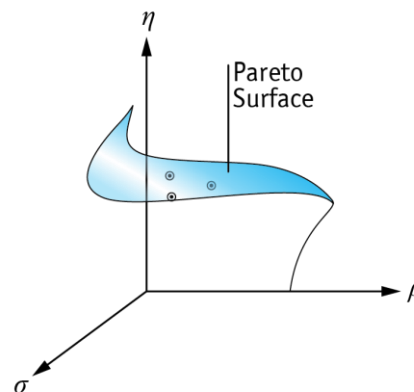
► Remaining Challenges for Further Industry Adaptation

- Transmission of **High Power @ Highest Possible Efficiency Despite Low Coupling**
- Compliance with Standards Regulating Magnetic Stray Fields
- Clarification of Technical Feasibility and **Physical Limitations**

■ Easy-to-Follow Optimization Methods for the Practicing Engineer

- Coil Size
- Efficiency
- Stray Field
- Thermal Limit

**Multi-Objective
Design Problem** ! ●



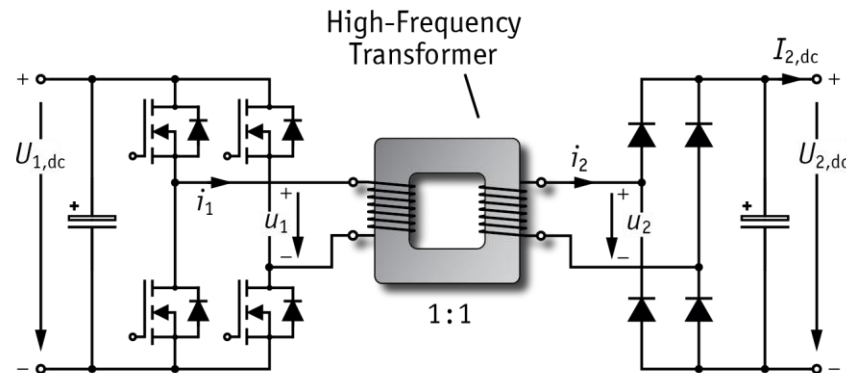
Fundamentals: Isolated DC/DC → IPT



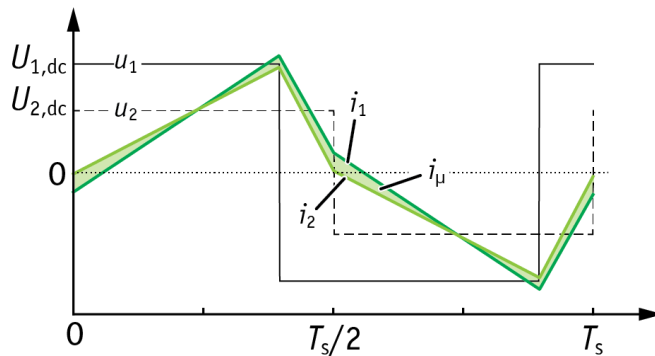
*Transformer Equivalent
Series Resonant Topologies
Zero-Voltage Switching
Inductive Power Transfer*

► Isolated DC/DC-Converter for Conductive EV Charging

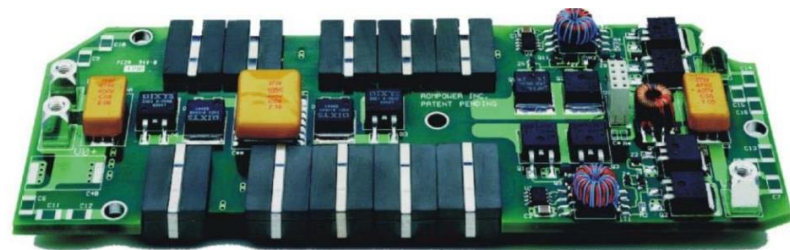
- **Soft-Switching DC/DC-Converter without Output Inductor**
 - Galvanic Isolation
 - Minimum Number of Components
 - Clamped Voltage across Rectifier
- **Constant Switching Frequency of Full-Bridge Inverter on Primary**
 - di/dt given by Voltage Levels & Transformer Stray & Magn. Induct.



▲ Isolated DC/DC Converter Topology with MF Transformer



▲ Schematic Converter Waveforms
(i_1 - i_2 not to Scale)



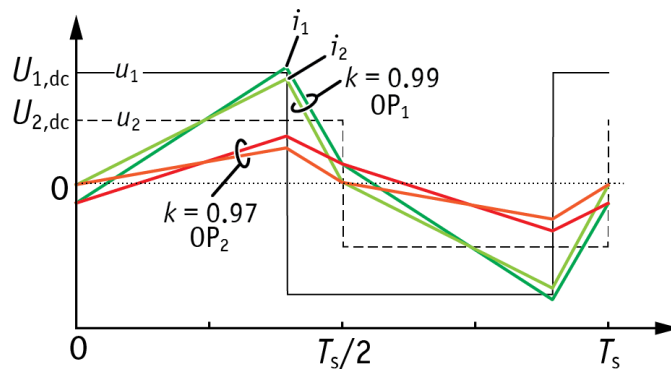
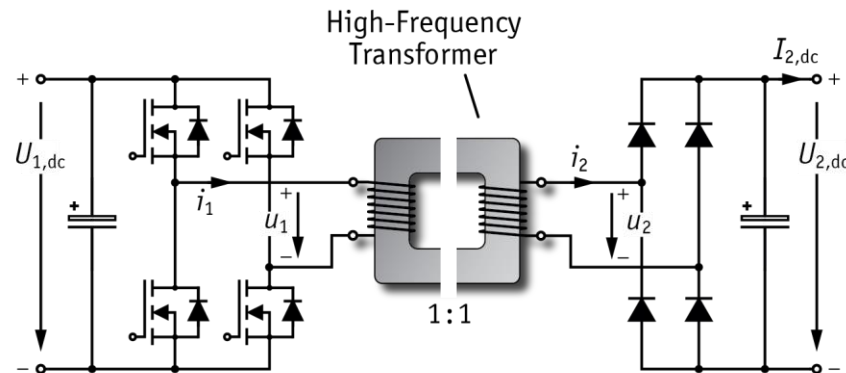
I. D. Jitaru, «A 3 kW Soft-Switching DC-DC Converter," Proc. IEEE APEC, pp. 86-92, 2000.

▲ Realization Example (1 kW Module, Rompower)

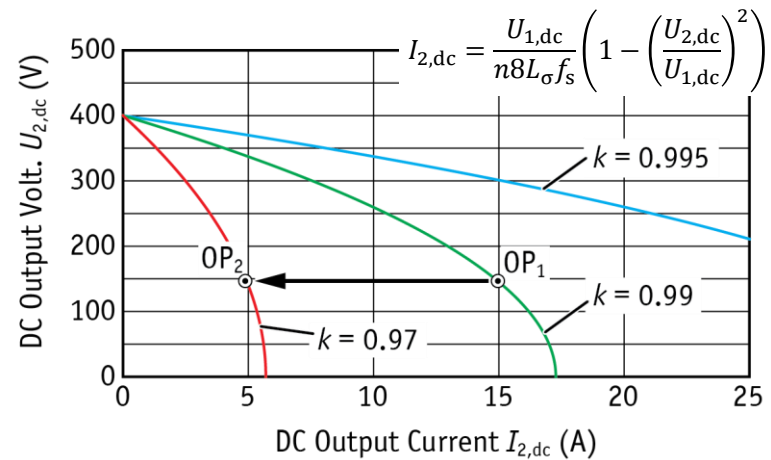
► Transition to IPT System (1)

■ Airgap in the Magnetic Path

- Reduced Primary & Secondary Induct.
- Higher Magnetizing Current
- Reduced Magnetic Coupling k
- Load Dependency of Output Voltage due to Non-Dissipative Inner Resist.



▲ Schematic Converter Waveforms for OP₁ and OP₂ (i_1 - i_2 not to Scale)



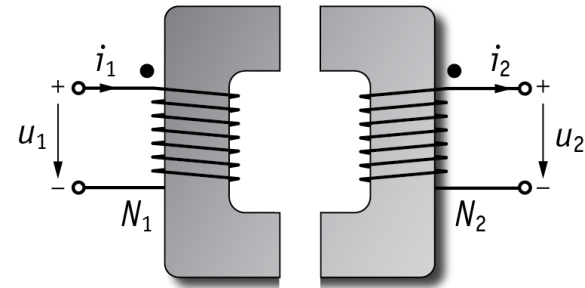
▲ Converter Output Characteristics

► Characterization of the Transformer

■ Transformer Differential Equations

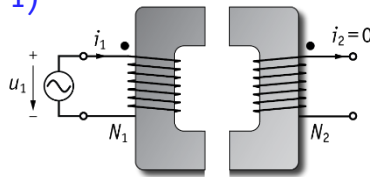
$$\begin{aligned} u_1 &= L_1 \frac{di_1}{dt} - M \frac{di_2}{dt} \\ u_2 &= M \frac{di_1}{dt} - L_2 \frac{di_2}{dt} \end{aligned}$$

Note: No Explicit Dependency on N_1, N_2 (Unknown in General Case)



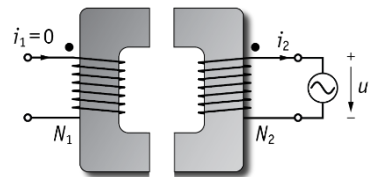
■ Measurement of the Three (!) Parameters L_1 , L_2 and M

1)



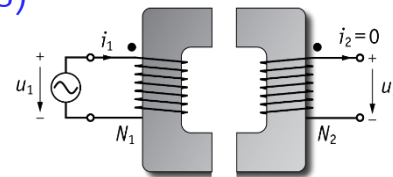
$$L_1 = \frac{1}{\omega} \left(\frac{\partial \hat{U}_1}{\partial \hat{I}_1} \right) \bigg|_{i_2=0}$$

2)



$$L_2 = \frac{1}{\omega} \left(\frac{\partial \hat{U}_2}{\partial \hat{I}_2} \right) \bigg|_{i_1=0}$$

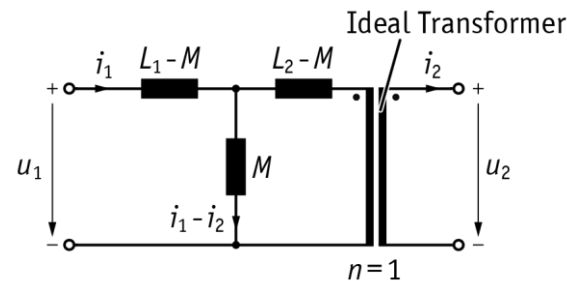
3)



$$M = \frac{1}{\omega} \left(\frac{\partial \hat{U}_2}{\partial \hat{I}_1} \right) \bigg|_{i_2=0}$$

■ General Equivalent Circuit Diagram

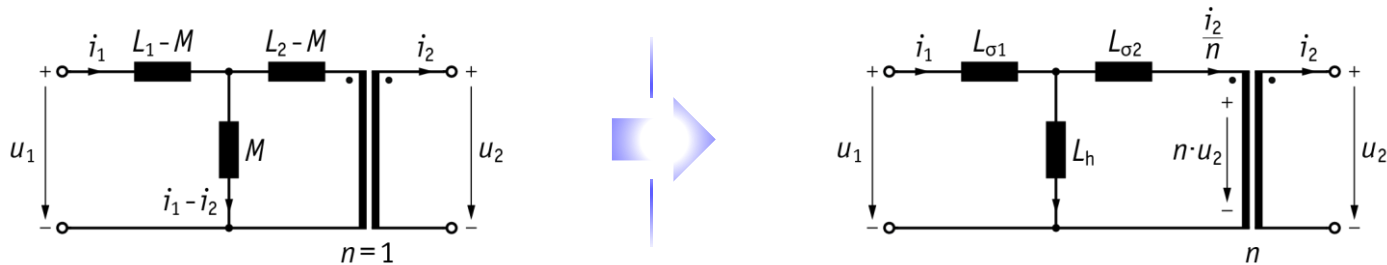
$$\begin{aligned} u_1(t) &= (L_1 - M) \frac{di_1}{dt} + M \frac{d}{dt} (i_1 - i_2) \\ u_2(t) &= M \frac{d}{dt} (i_1 - i_2) - (L_2 - M) \frac{di_2}{dt} \end{aligned}$$



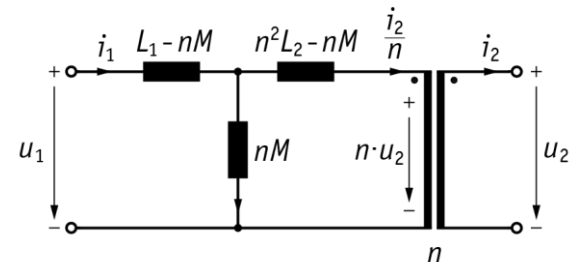
■ Definitions: Coupling Factor $k = \frac{M}{\sqrt{L_1 L_2}}$, Stray Factor $\sigma = 1 - k^2 \rightarrow$ Ideal: $k = 1, \sigma = 0$.

► Transformer Equivalent Circuits (1)

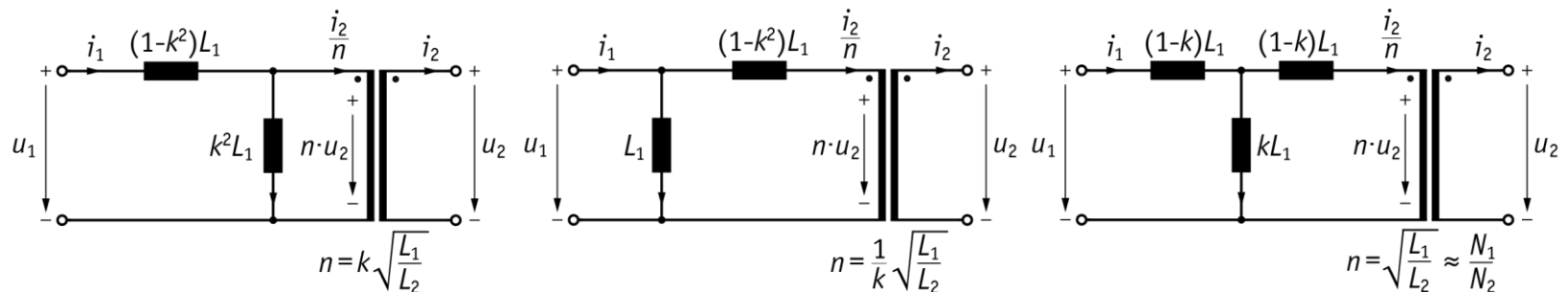
■ Introduction of a General Transformation Ratio n



- 4 Degrees of Freedom ($L_{\sigma 1}$, $L_{\sigma 2}$, L_h , n), but only 3 Transformer Parameters (L_1 , L_2 , M)
- Assume n as given and Calculate Remaining Parameters ($L_{\sigma 1}$, $L_{\sigma 2}$, L_h)



■ Simplified Circuit Diagrams for Specific Values of n

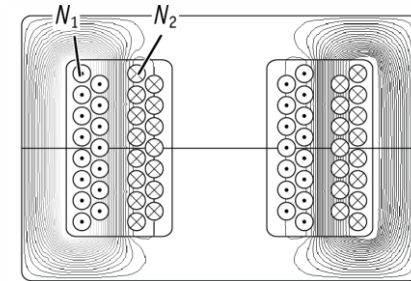
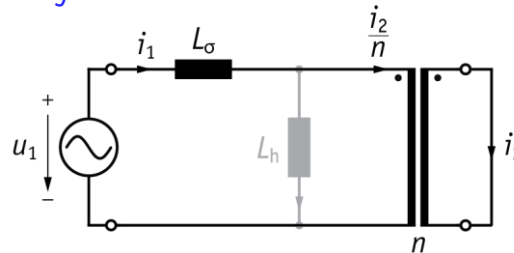


► Transformer Equivalent Circuits (2)

■ Direct Measurement of Transformer Equivalent Circuit Parameters

■ Measurement 1: Secondary-Side Terminals Shorted

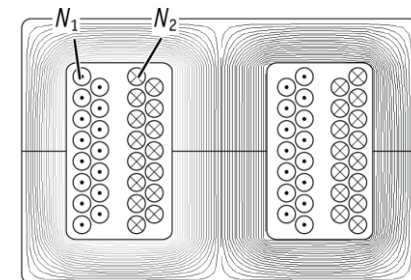
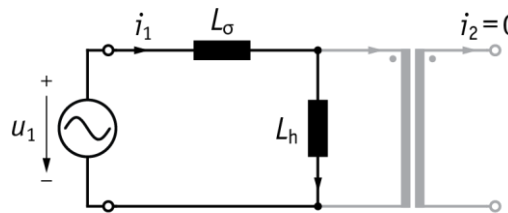
$$L_{\sigma} = \frac{1}{\omega} \left(\frac{\hat{U}_1}{\hat{I}_1} \right) \Big|_{u_2 = 0}$$



■ Measurement 2: Secondary-Side Terminals Open

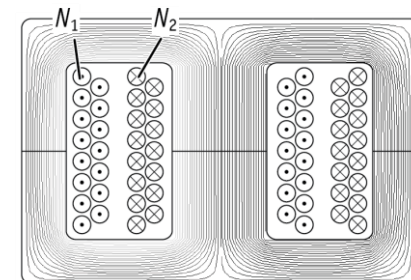
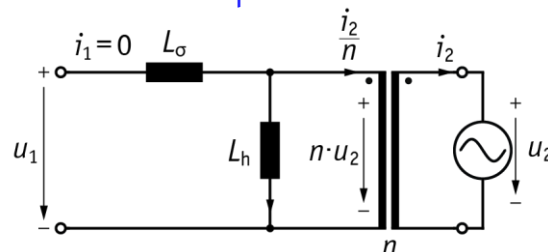
$$L_1 = \frac{1}{\omega} \left(\frac{\hat{U}_1}{\hat{I}_1} \right) \Big|_{i_2 = 0}$$

$$L_h = L_1 - L_{\sigma}$$



■ Measurement 3: Primary-Side Terminals Open

$$n = \left(\frac{\hat{U}_1}{\hat{U}_2} \right) \Big|_{i_1 = 0}$$



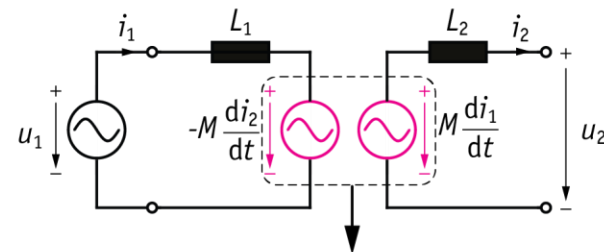
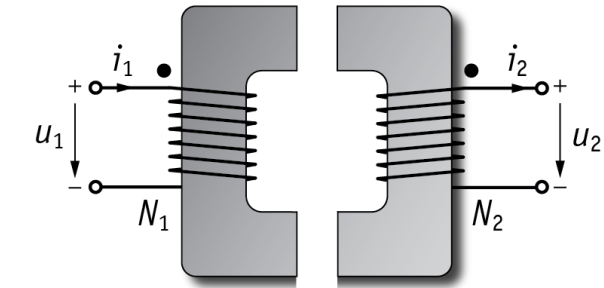
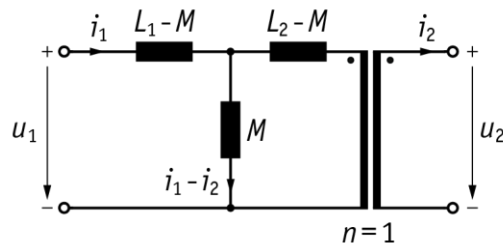
► Transformer Equivalent Circuits (3)

■ Transformer Differential Equations

$$u_1 = L_1 \frac{di_1}{dt} - M \frac{di_2}{dt} = L_1 \frac{di_1}{dt} + u_{1,\text{ind}}$$

$$u_2 = M \frac{di_1}{dt} - L_2 \frac{di_2}{dt} = u_{2,\text{ind}} - L_2 \frac{di_2}{dt}$$

- Equivalent Circuit Representation with Induced Voltages as Voltage Sources:

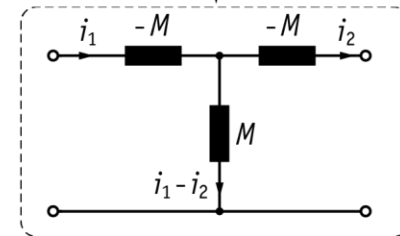


■ Inductive Behavior Partly Hidden in Voltage Sources $u_{1,\text{ind}}$, $u_{2,\text{ind}}$

$$\hat{u}_1 = j\omega L_1 \hat{i}_1 - j\omega M \hat{i}_2 = j\omega L_1 \hat{i}_1 + \hat{u}_{1,\text{ind}}$$

$$\hat{u}_2 = j\omega M \hat{i}_1 - j\omega L_2 \hat{i}_2 = \hat{u}_{2,\text{ind}} - j\omega L_2 \hat{i}_2$$

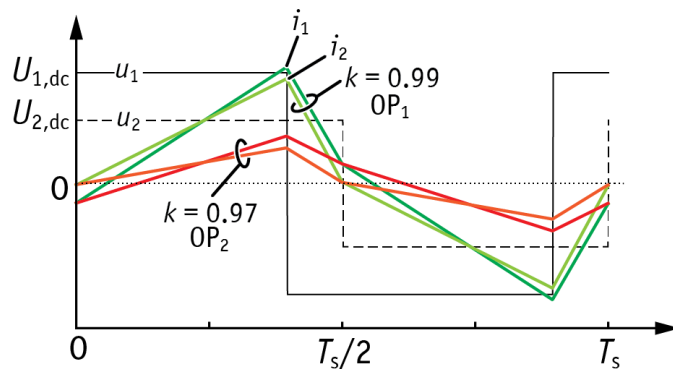
- 90° Phase-Difference between \hat{i}_1 and $\hat{u}_{2,\text{ind}}$ and between \hat{i}_2 and $\hat{u}_{1,\text{ind}}$



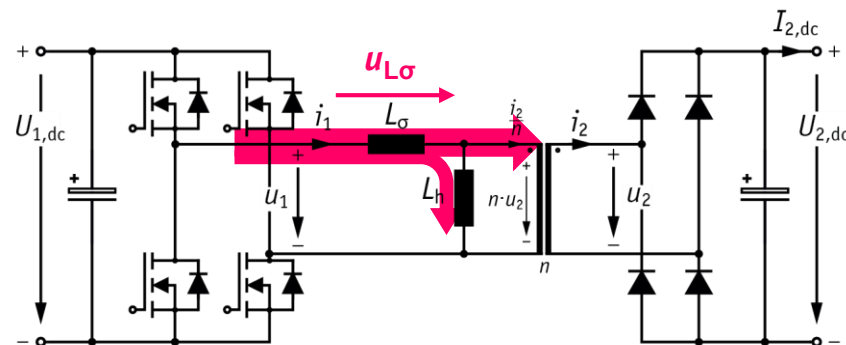
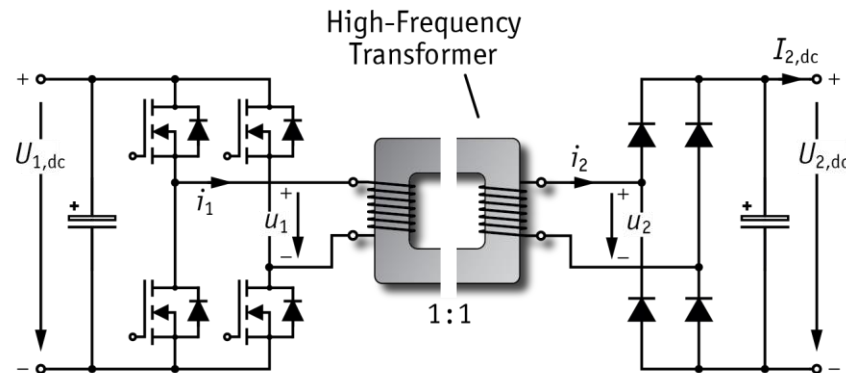
► Transition to IPT System (2)

■ Airgap in the Magnetic Path

- Reduced Primary & Secondary Induct.
- Higher Magnetizing Current
- Reduced Magnetic Coupling k
- Load Dependency of Output Voltage due to Non-Dissipative Inner Resist.



▲ Schematic Converter Waveforms for OP₁ and OP₂ (i_1 - i_2 not to Scale)

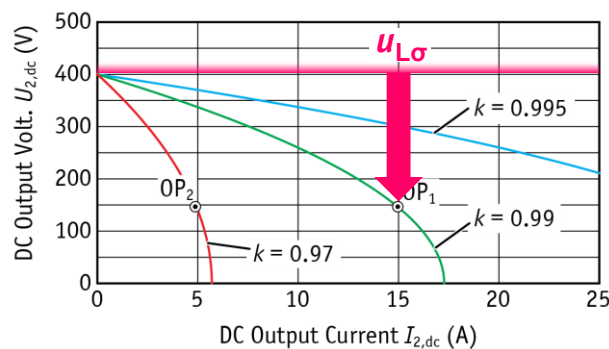


▲ Effects of an Air Gap in the Transformer
 $L_\sigma = (1 - k^2)L_1, L_h = k^2L_1, n = k\sqrt{L_1/L_2}$

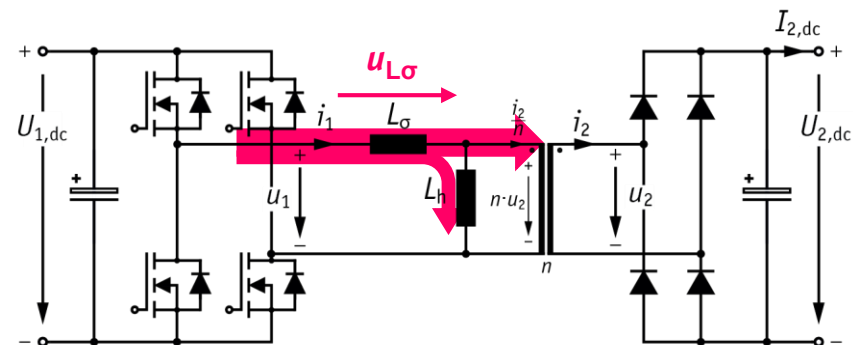
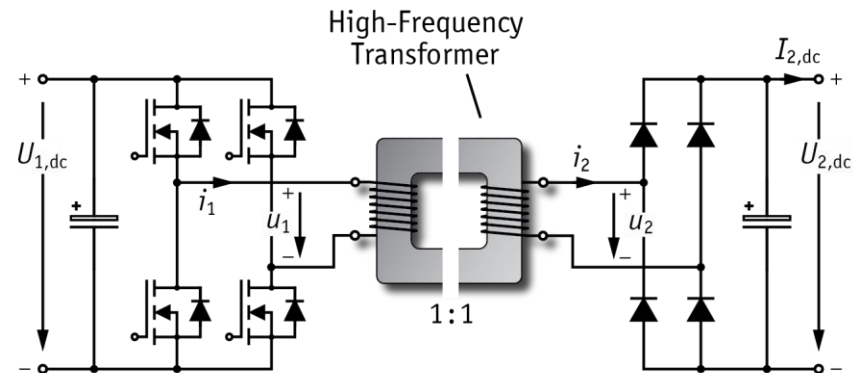
► Transition to IPT System (3)

■ Airgap in the Magnetic Path

- Reduced Primary & Secondary Induct.
- Higher Magnetizing Current
- Reduced Magnetic Coupling k
- Load Dependency of Output Voltage due to Non-Dissipative Inner Resist.



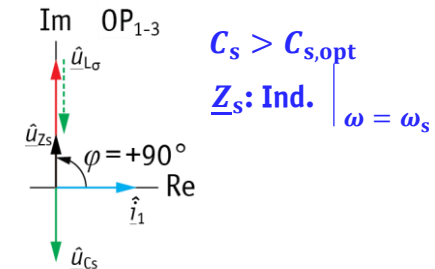
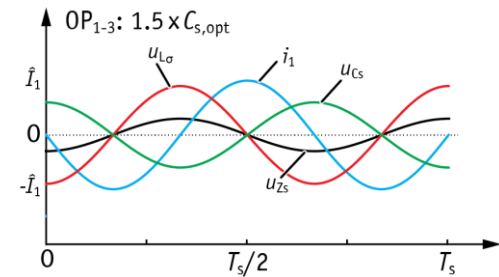
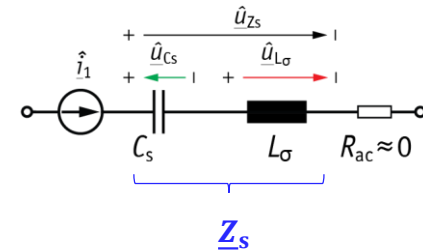
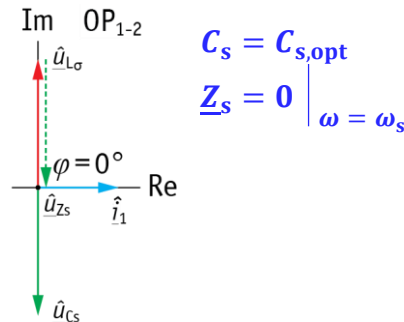
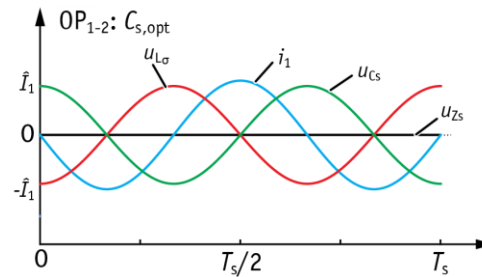
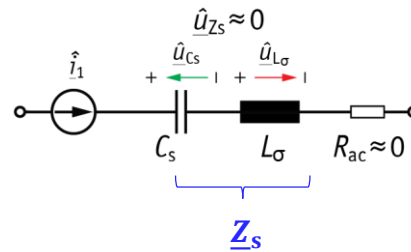
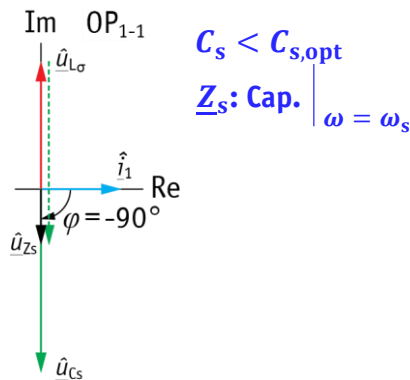
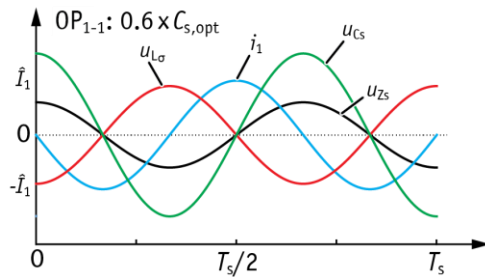
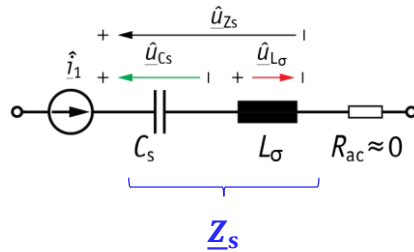
▲ Converter Output Characteristics



▲ Effects of an Air Gap in the Transformer

$$L_\sigma = (1 - k^2)L_1, L_h = k^2L_1, n = k\sqrt{L_1/L_2}$$

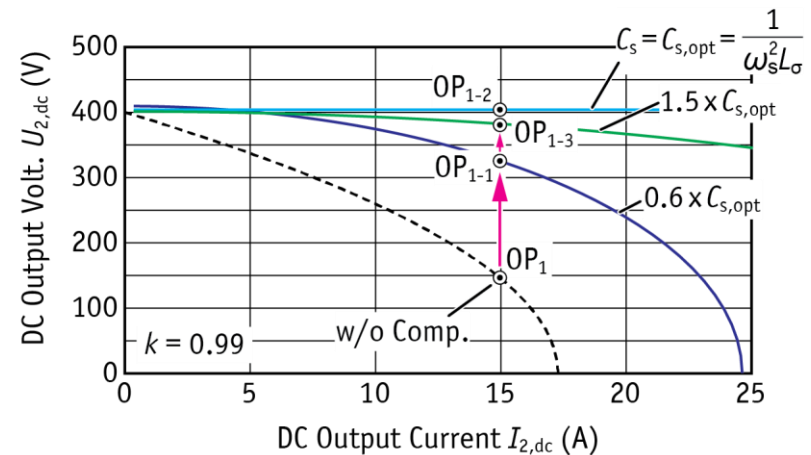
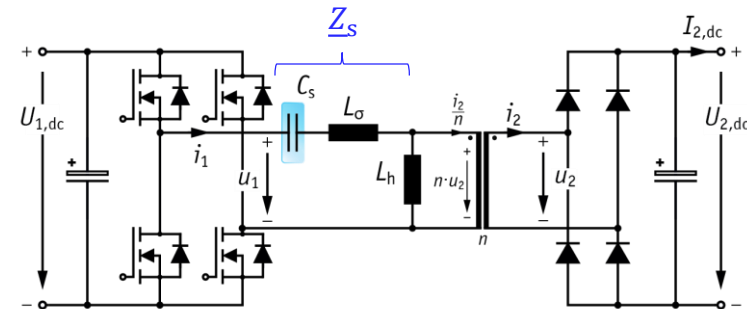
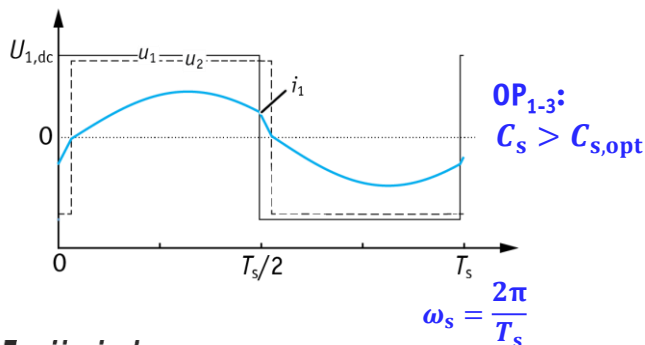
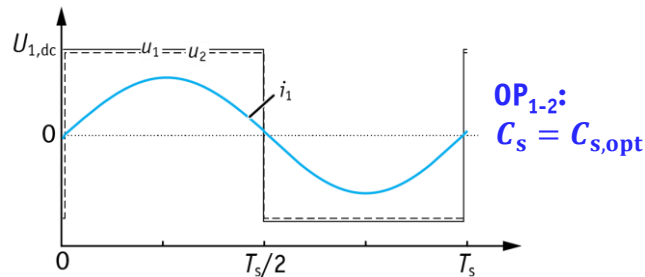
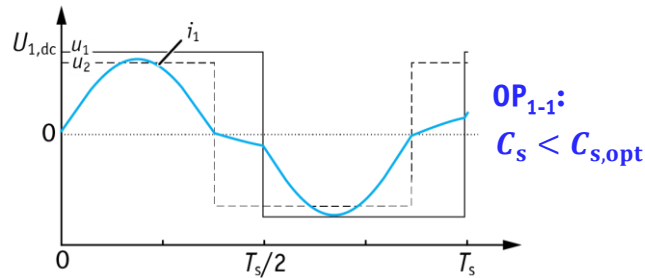
► Resonant Compensation of Stray Inductance (1)



$$\underline{Z}_s = j\omega L_s + \frac{1}{j\omega C_s} + \underbrace{R_{ac}}_{\approx 0} = j(\omega L_s - \frac{1}{\omega C_s}) \rightarrow \omega_s = \frac{1}{\sqrt{L_s C_s}}$$

► Resonant Compensation of Stray Inductance (2)

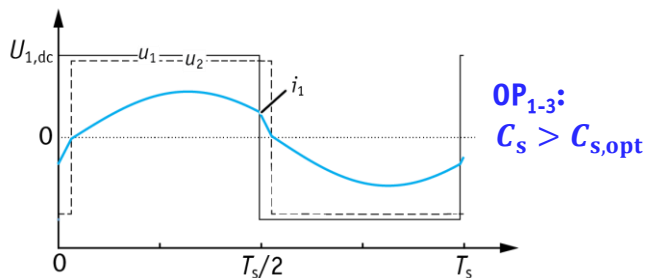
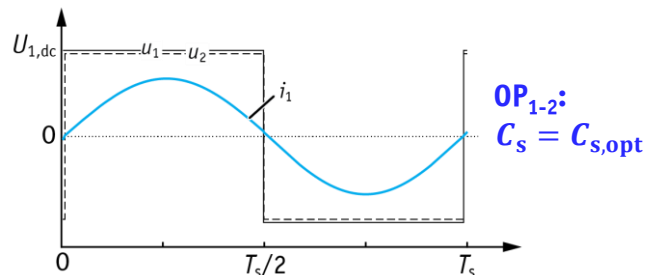
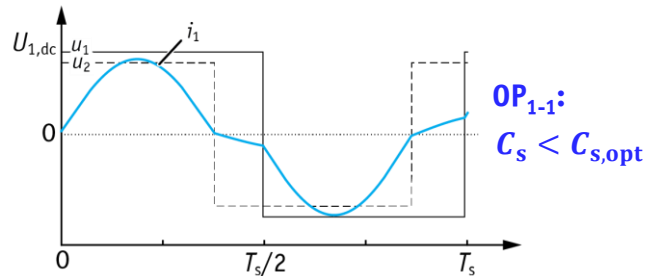
- Insert Capacitor in Series to Transformer Stray Inductance L_σ
- Select Capacitance $C_{s,opt} = 1/(\omega_s^2 L_\sigma)$ to Match Resonance and Inverter Switching Frequency



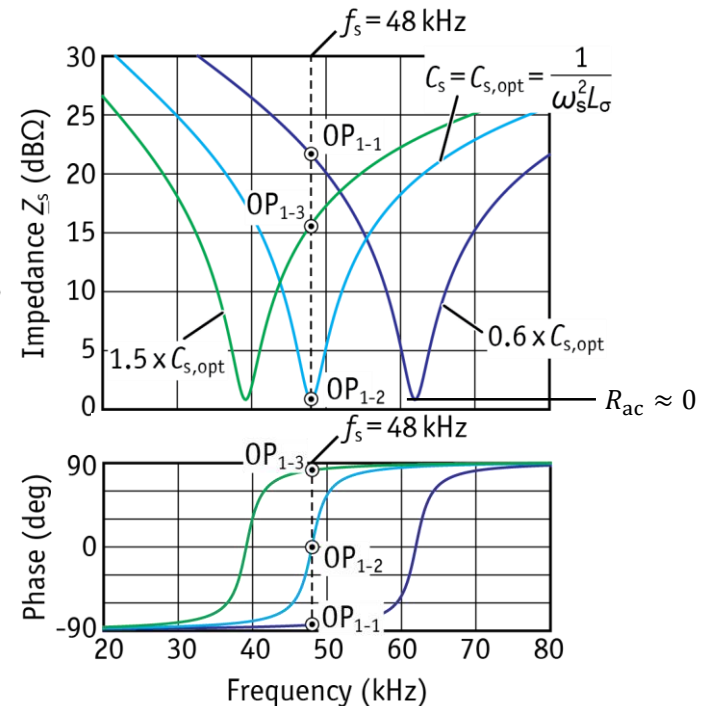
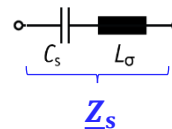
▲ Converter Output Characteristics

► Resonant Compensation of Stray Inductance (3)

- Insert Capacitor in Series to Transformer Stray Inductance L_σ
- Select Capacitance $C_{s,opt} = 1/(\omega_s^2 L_\sigma)$ to Match Resonance and Inverter Switching Frequency



$$\omega_s = \frac{2\pi}{T_s}$$



▲ Bode Diagram for Different Selections of the Compensation Capacitance C_s

► Alternative Compensation Concepts

■ Limitations of Series-Compensation

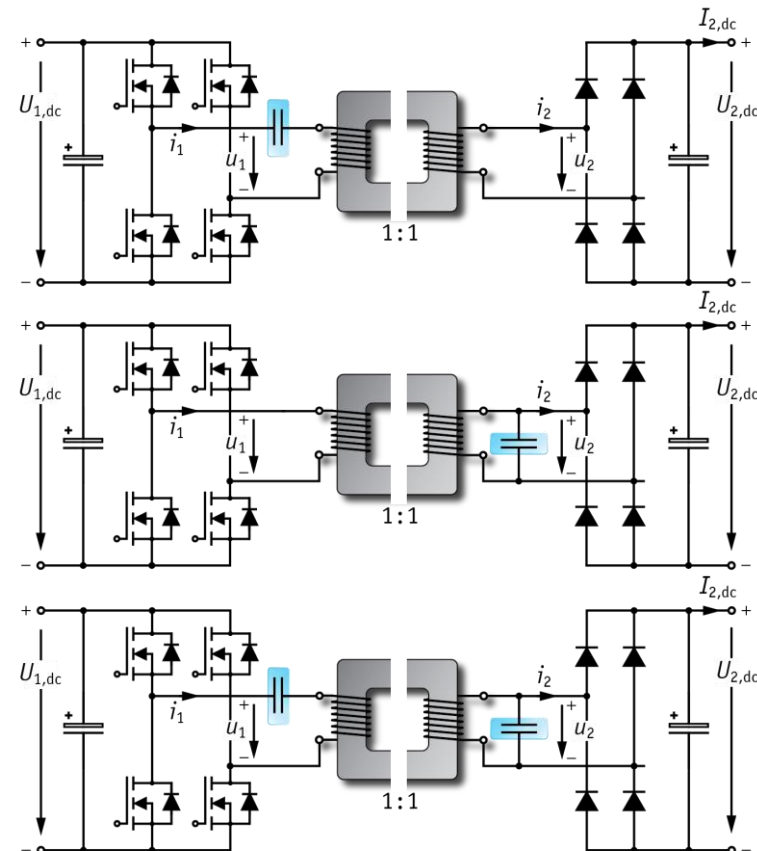
- High Voltages Resonant Elements in High-Power Designs
- Limited to Step-Down Conversion
- No Control of Output at No-Load

■ Alternative Options:

- Parallel Resonant Converter (LLC)
- Series/Parallel Res. Converter (LCC)
- General Matching Networks

■ Limitations of Parallel-Compensation

- Circulating Reactive Current in Parallel Elements also at Low Load
- Potentially Needs Additional Inductors
- Complex Design Process (Selection of Two Capacitor Values for SP-Comp.)

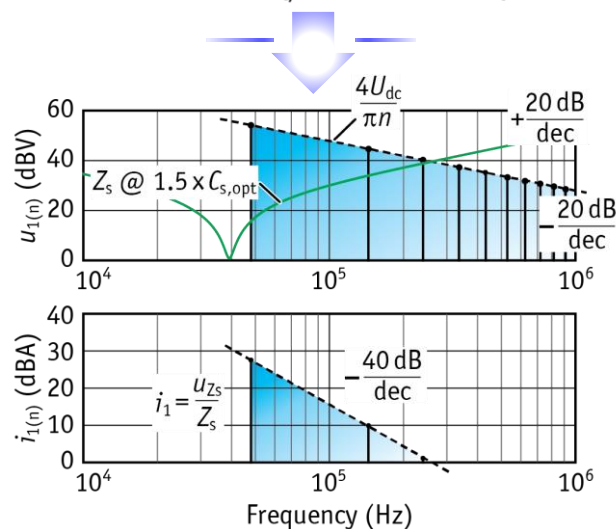
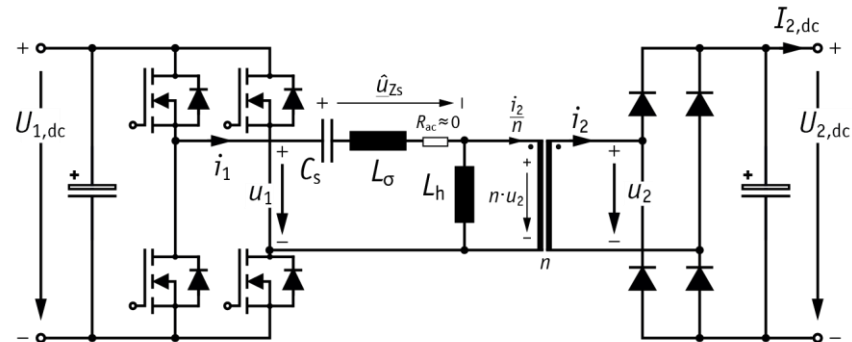
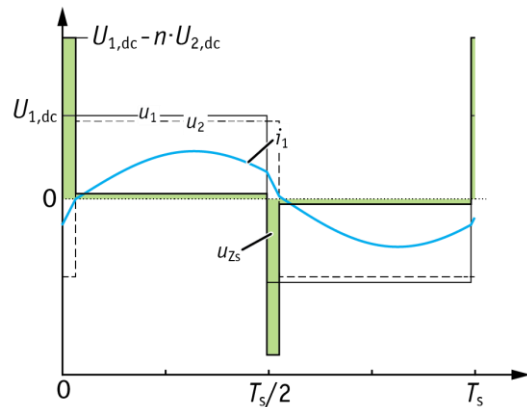


▲ Alternative Compensation Topologies

► Fundamental Frequency Approximation (1)

■ Nearly Sinusoidal Current Shape Despite Rectangular Voltage Waveforms

- Resonant Circuit Acts as Bandpass-Filter on Inverter Output Voltage Spectrum



■ Consider only Switching Frequency Components:

- Fundamentals of u_1, u_2, i_1, i_2
- Power Transfer Modeled with Good Accuracy

as

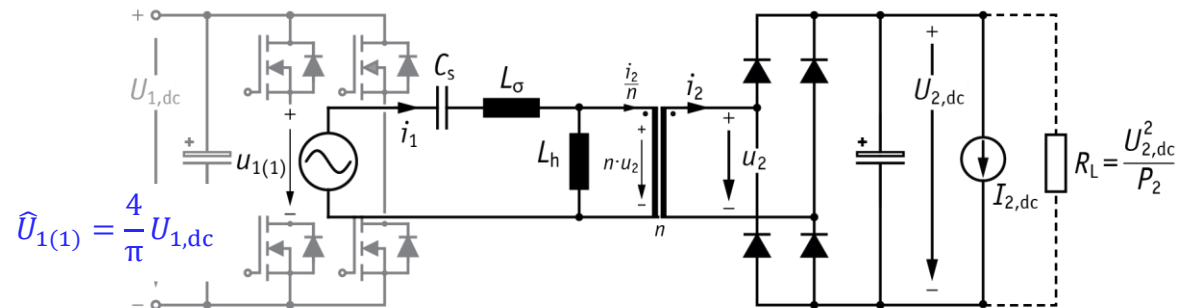
$$P = \sum_{n=1}^{\infty} U_{1(n)} I_{1(n)} \cos(\phi_n) \\ \approx U_{1(1)} I_{1(1)} \cos(\phi_1)$$

→ Fundamental Frequency Model!

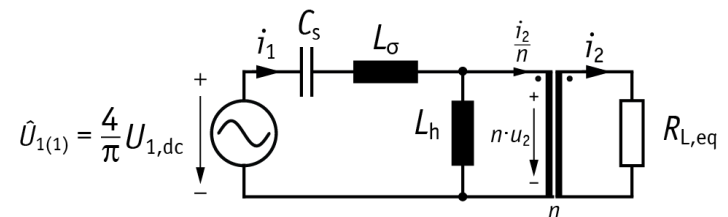
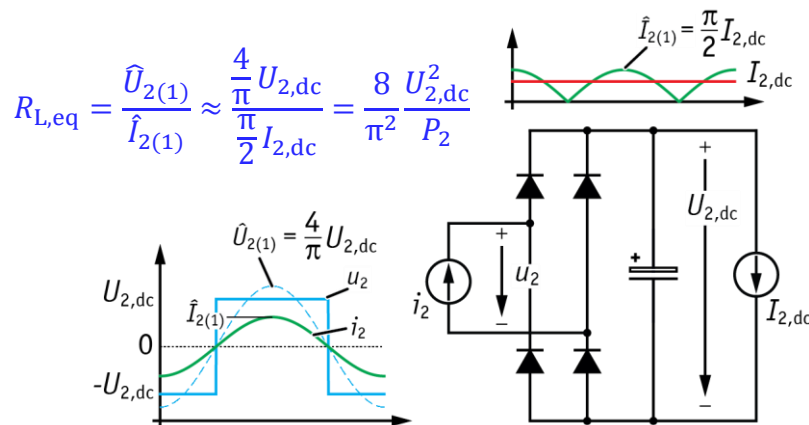
► Fundamental Frequency Approximation (2)

- Replace Rectifier and Load $I_{2,dc}$ by Power Equivalent Resistance $R_{L,eq}$

R. Steigerwald, "A comparison of half-bridge resonant converter topologies," in IEEE Trans. Power Electron., vol. 3, no. 2, 1988.



- Fundamental Frequency Equivalent Circuit

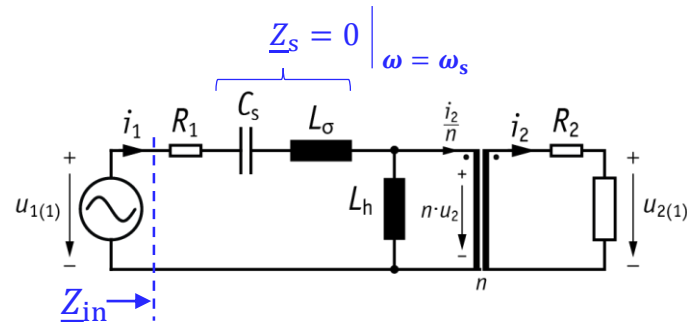


- Simplified Circuit Analysis & Approximate Power Loss Calculations

► Resonant Circuit Transfer Characteristics (1)

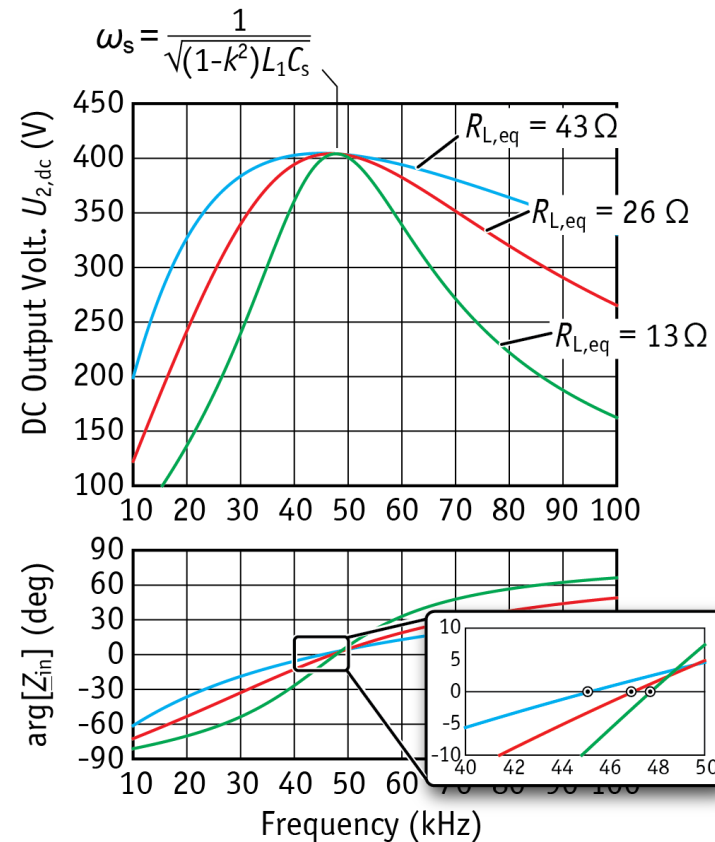
■ Load-Independent Output Voltage due to Series Resonant Compensation

- Except for a (Small) Voltage Drop on Winding Resistances R_1, R_2



■ Close to Ohmic Input Impedance due to Large Mutual Inductance

- Necessary Condition for Minimum Input Current \rightarrow Max. Efficiency!

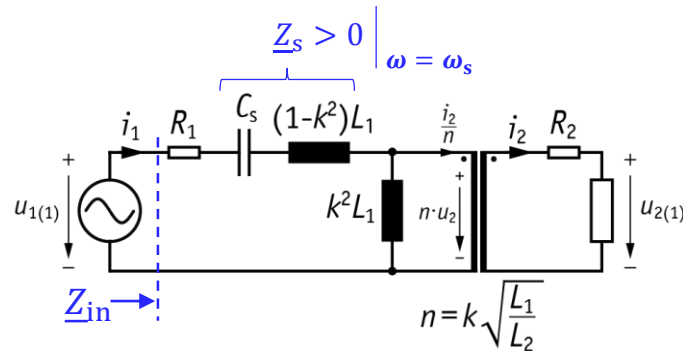


▲ Voltage Transfer Ratio at $k = 0.99$

► Resonant Circuit Transfer Characteristics (2)

■ Strong Coupling Dependency of Output Voltage due to Variation of Series Impedance

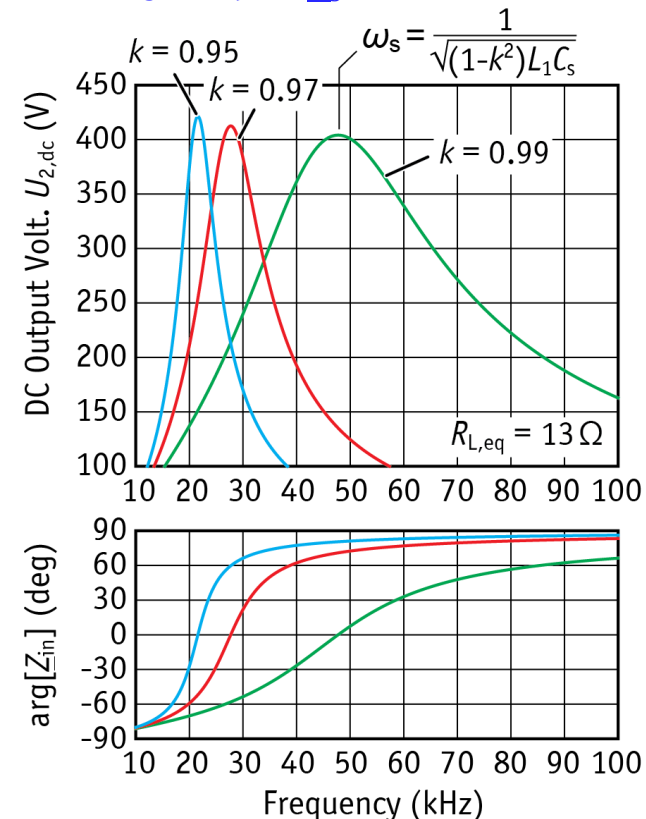
- Variation of Coupling k Changes L_σ which Leads to Series Voltage Drop on $\underline{Z}_s > 0$



■ Large Variation of Resonant Frequency with Changing Magnetic Coupling

- Fixed Frequency Operation Not Possible

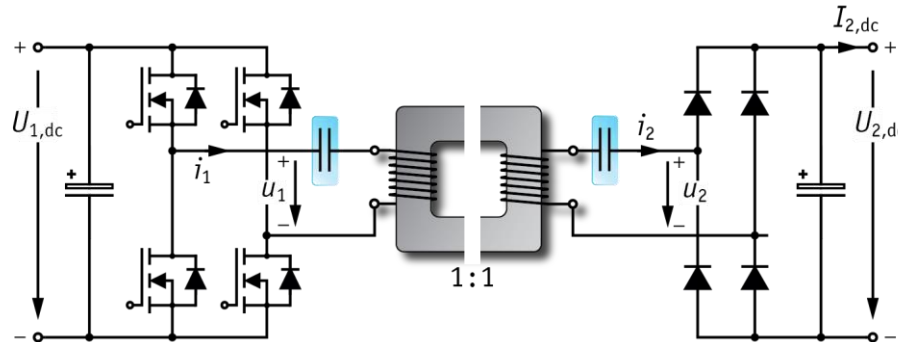
■ Not Practical if Coupling is Variable in the Target Application



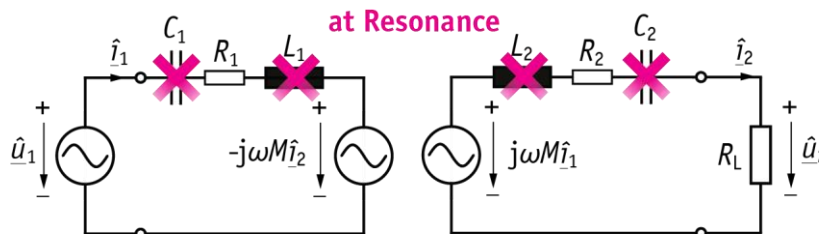
▲ Transfer Characteristics and Phase Angle of Input Impedance for Different Coupling

► Series-Series Compensated IPT System (1)

- Add Second Series Capacitor to Ensure Fixed Resonant Frequency ($\varphi_{Z_{in}} = 0$) for any Value of the Magnetic Coupling k

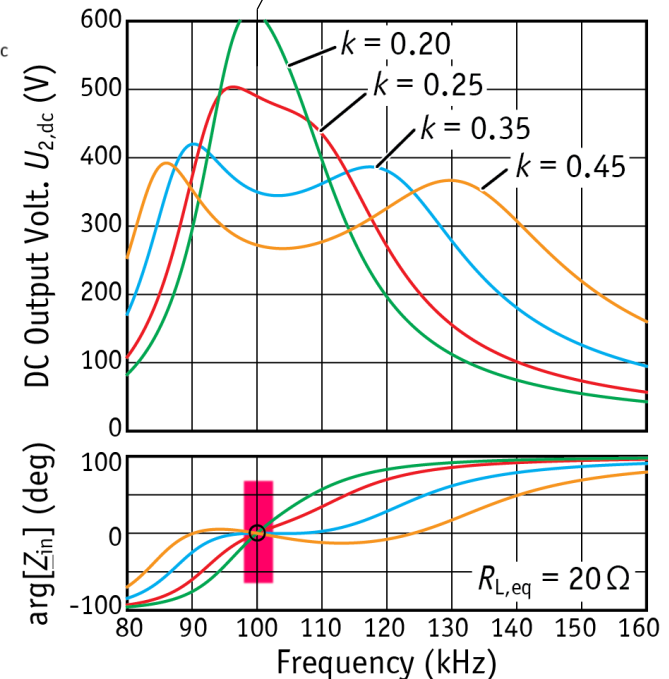


- Resulting Equivalent Circuit @ ω_0
 - Cancel Complete Self-Inductance



- Voltage Gain is Coupling & Load Dependent

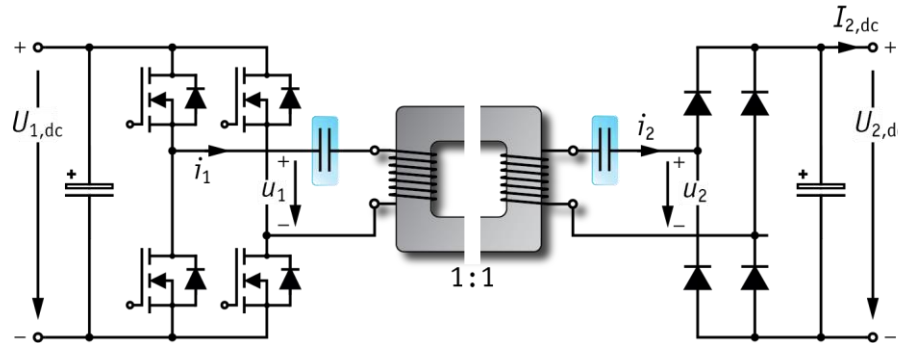
$$\omega_0 = \frac{1}{\sqrt{L_1 C_1}} = \frac{1}{\sqrt{L_2 C_2}}$$



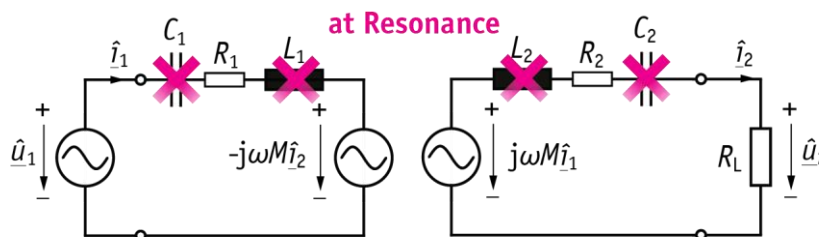
- ▲ Transfer Characteristics and Phase Angle of Input Impedance for Different Coupling

► Series-Series Compensated IPT System (2)

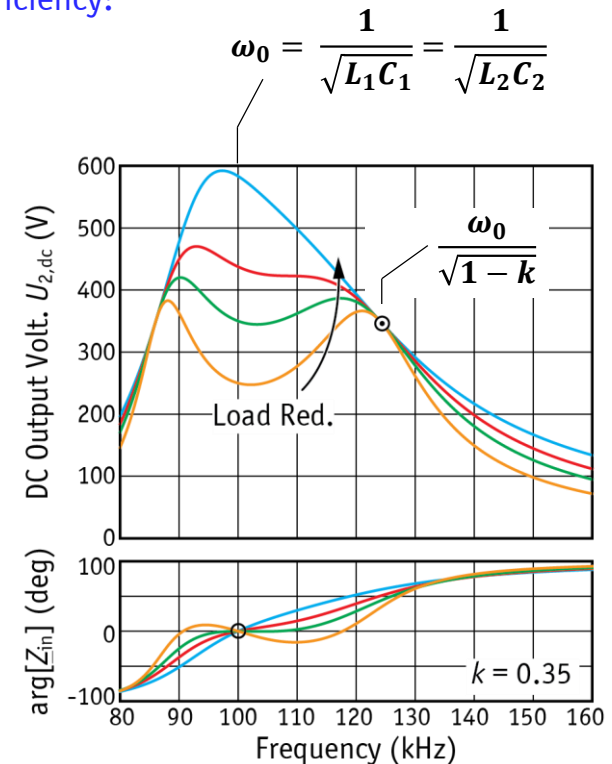
- Resonant Frequency ($\varphi_{Z_{in}} = 0$) is Independent of Magnetic Coupling and of Load
 - Necessary Condition for Minimum Input Current → Max. Efficiency!



- Resulting Equivalent Circuit @ ω_0
 - Cancel Complete Self-Inductance



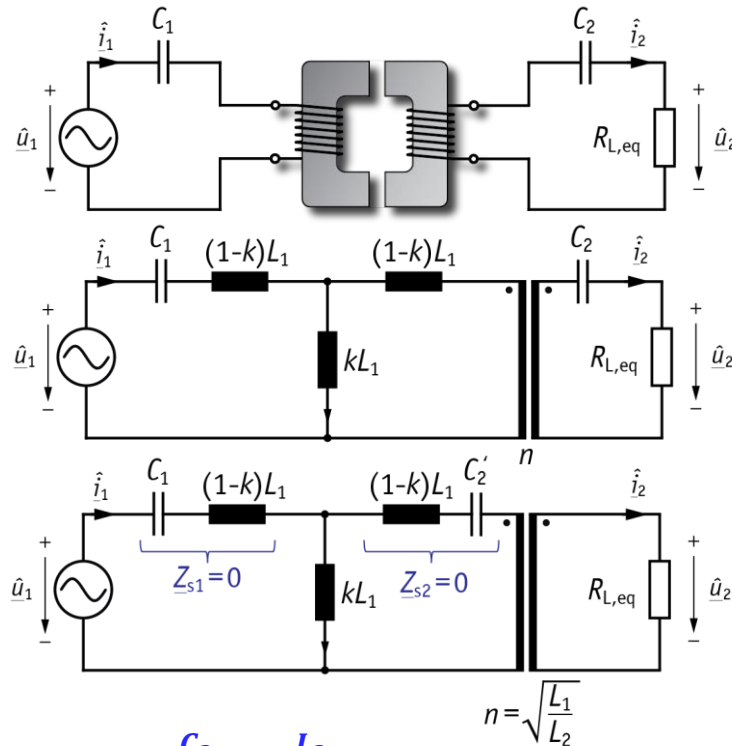
- Voltage Gain is Coupling & Load Dependent



- ▲ Transfer Characteristics and Phase Angle of Input Impedance for Different Loads

► Properties of the Series-Series Compensation (1)

■ Operation at Resonant Frequency $\omega_s = \frac{\omega_0}{\sqrt{1-k}}$



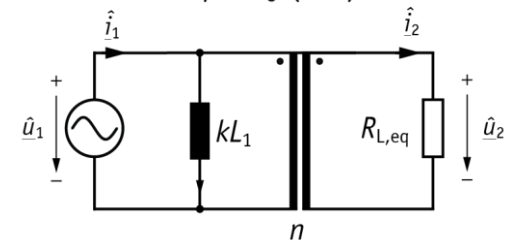
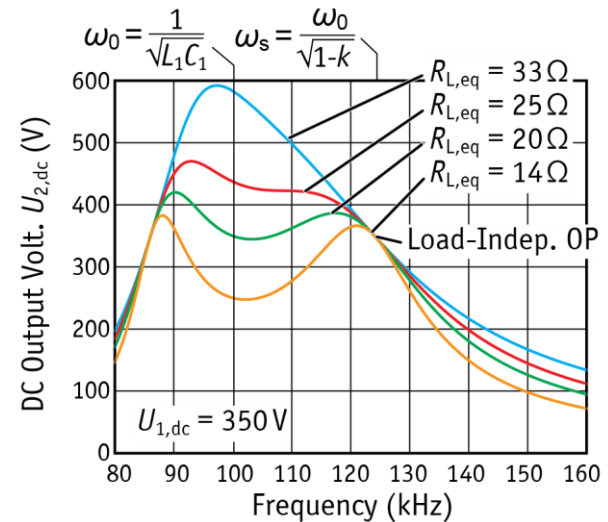
$$C'_2 = \frac{C_2}{n^2} = C_s \frac{L_2}{L_1}$$

$$\omega_{s1}^2 = \frac{1}{C_1 L_1 (1-k)}$$

$$\omega_{s2}^2 = \frac{1}{C_2 L_2 (1-k)}$$

$$\rightarrow \omega_s = \frac{\omega_0}{\sqrt{1-k}}$$

$$\rightarrow \underline{u}_2 = \underline{u}_1 \sqrt{\frac{L_2}{L_1}}$$



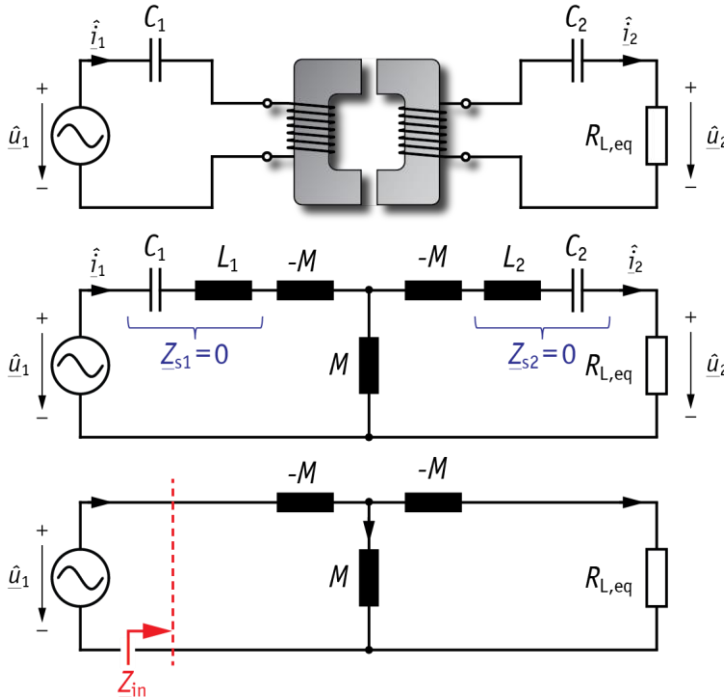
▲ Output Voltage \hat{U}_2 is Independent of Load Resistance at ω_s

■ Load-Independent Output Voltage

- Still Coupling Dependent
- Inductive Input Impedance

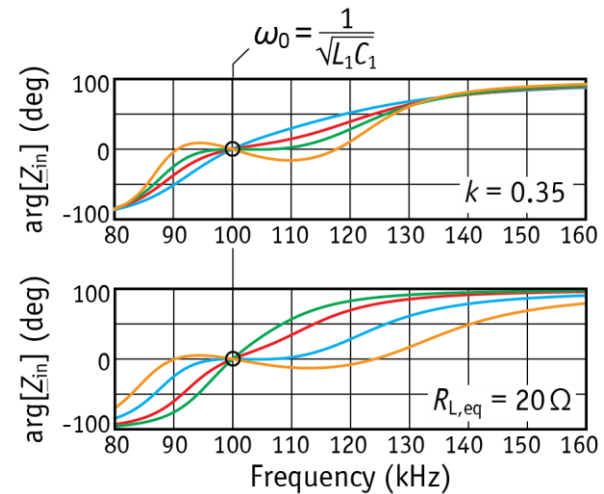
► Properties of the Series-Series Compensation (2)

- Operation at Resonant Frequency $\omega_0 = \frac{1}{\sqrt{L_1 C_1}} = \frac{1}{\sqrt{L_2 C_2}}$



$$\underline{Z}_{in} = -j\omega_0 M + \frac{j\omega_0 M \cdot (R_{L,eq} - j\omega_0 M)}{j\omega_0 M + R_{L,eq} - j\omega_0 M}$$

$$\underline{Z}_{in} = \frac{\omega_0^2 M^2}{R_{L,eq}} \rightarrow \begin{aligned} \arg[\underline{Z}_{in}] &= 0 \\ k &= 0 \rightarrow \underline{Z}_{in} = 0 \\ R_{L,eq} &= 0 \rightarrow \underline{Z}_{in} = \infty \end{aligned}$$

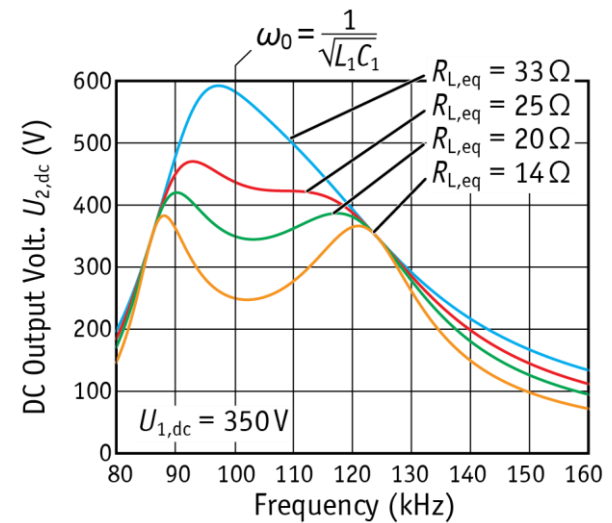
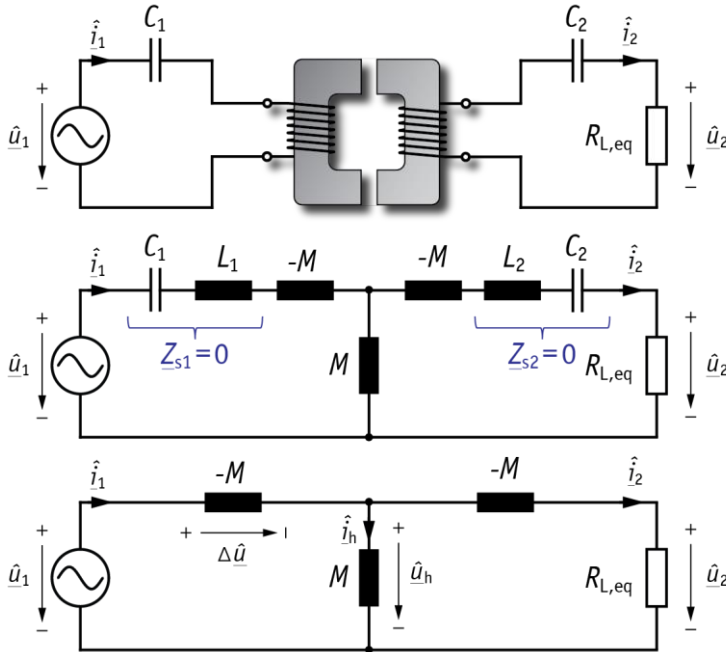


- ▲ Phase Angle of Input Impedance for Varying Load (top) and Coupling (bot.)

- Purely Ohmic Input Impedance For any Load & Coupling

► Properties of the Series-Series Compensation (3)

- Operation at Resonant Frequency $\omega_0 = \frac{1}{\sqrt{L_1 C_1}} = \frac{1}{\sqrt{L_2 C_2}}$



▲ Output Voltage \hat{U}_2 Rises with Load Resistance for Constant \hat{U}_1

$$\hat{u}_h = \hat{i}_2 (R_{L,eq} - j\omega_0 M)$$

$$\hat{i}_h = \frac{\hat{i}_2}{j\omega_0 M} (R_{L,eq} - j\omega_0 M)$$

$$\begin{aligned} \Delta \hat{u} &= -j\omega_0 M (\hat{i}_2 + \hat{i}_h) \\ &= -j\omega_0 M \hat{i}_2 - \hat{i}_2 (R_{L,eq} - j\omega_0 M) \end{aligned}$$

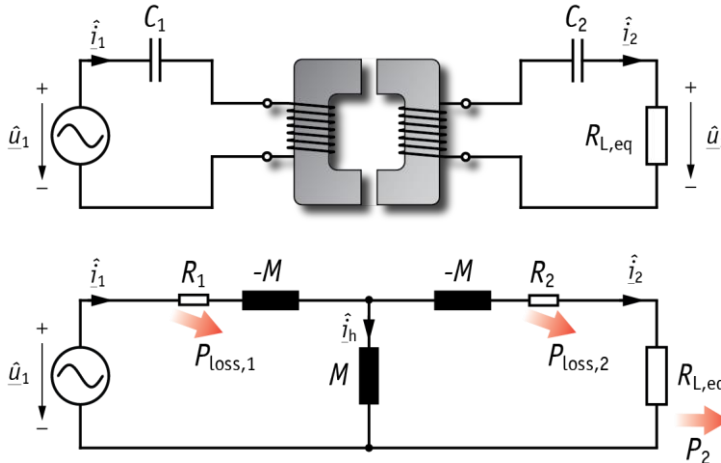
- Output Current Independent of Load Resistance $R_{L,eq}$:

$$\hat{u}_1 = \Delta \hat{u} + \hat{u}_h = -j\omega_0 M \hat{i}_2$$

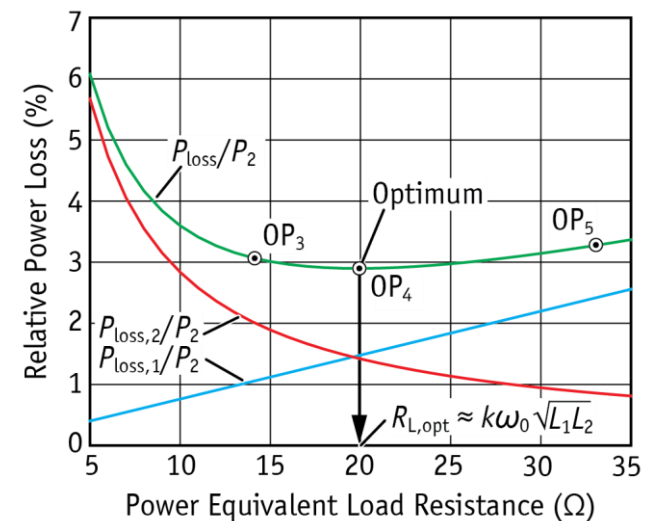
$$\rightarrow \hat{i}_2 = j \frac{\hat{u}_1}{\omega_0 M}$$

► Power Losses of the Series-Series Compensation

- Operation at Resonant Frequency $\omega_0 = \frac{1}{\sqrt{L_1 C_1}} = \frac{1}{\sqrt{L_2 C_2}}$



$$P_{\text{loss},1} = \frac{1}{2} |\hat{i}_1|^2 R_1 \quad P_{\text{loss},2} = \frac{1}{2} |\hat{i}_2|^2 R_2 \quad P_2 = \frac{1}{2} |\hat{i}_2|^2 R_{L,\text{eq}}$$



■ Total Power Losses

- Core Loss Neglected

$$\underbrace{\frac{P_{\text{loss}}}{P_2}}_{\lambda} = \underbrace{\frac{P_{\text{loss},1}}{P_2}}_{\lambda_1} + \underbrace{\frac{P_{\text{loss},2}}{P_2}}_{\lambda_2}$$

■ Minimum Relative Losses

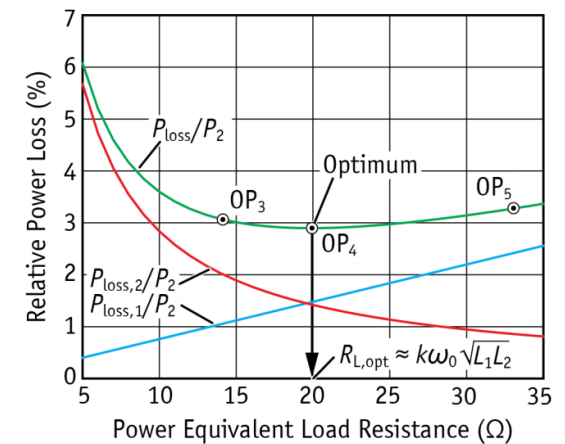
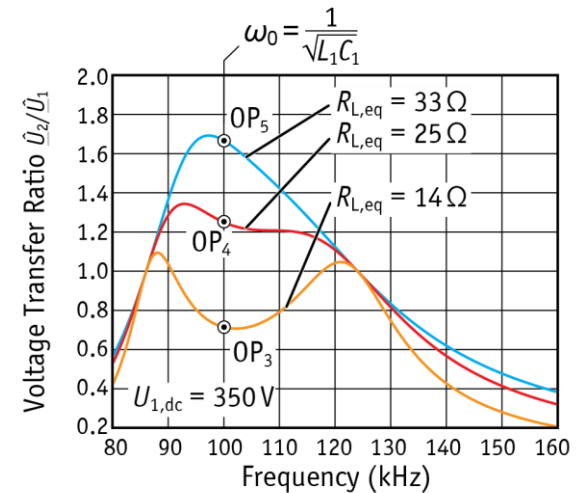
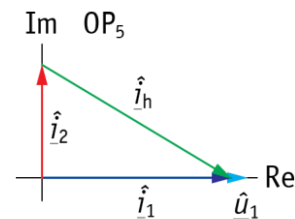
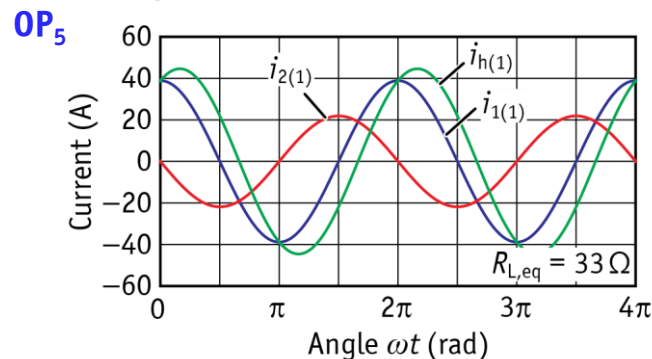
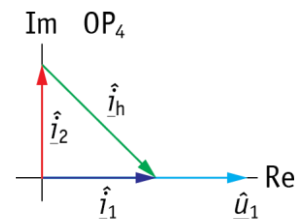
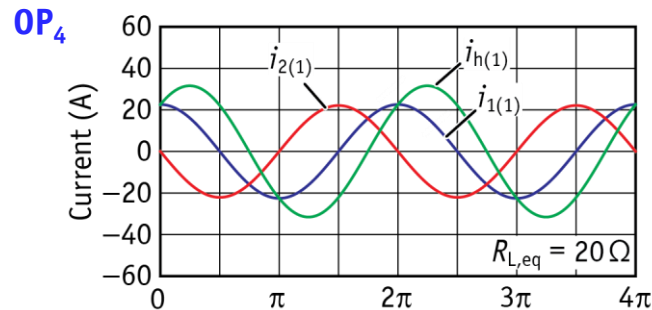
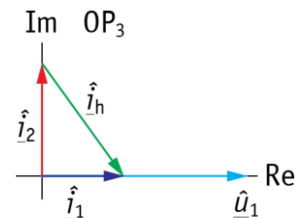
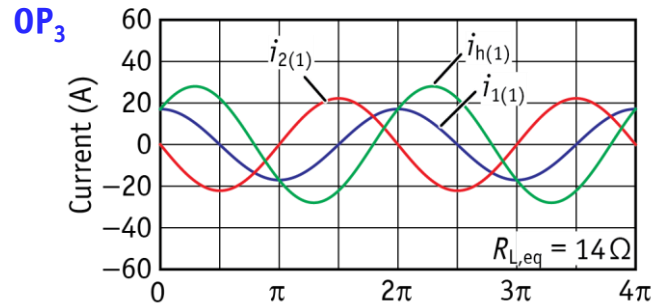
- Minimize Loss Factor λ

$$\frac{d}{dR_{L,\text{eq}}} \left(\underbrace{\frac{P_{\text{loss}}}{P_2}}_{\lambda} \right) = 0 \quad \rightarrow R_{L,\text{opt}} = \sqrt{\omega_0^2 M^2 + \underbrace{R_{\text{ac}}^2}_{R_1 \approx R_2 = R_{\text{ac}} @ \omega_0}} \approx k\omega_0 \sqrt{L_1 L_2}$$

Design Condition for Maximum Efficiency!

► Series-Series Comp. for Maximum Efficiency

■ Current \hat{I}_2 Constant Indep. of $R_{L,eq}$: Current Source Characteristic @ Resonance



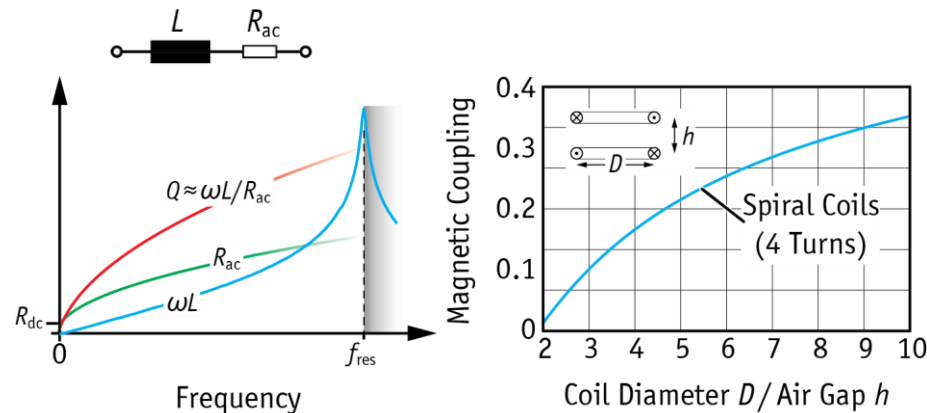
► Efficiency Limit of IPT Systems

■ Condition for Minimum Total Coil Losses: $R_{L,opt} \approx k\omega_0\sqrt{L_1L_2}$

■ Efficiency Limit of IPT Systems

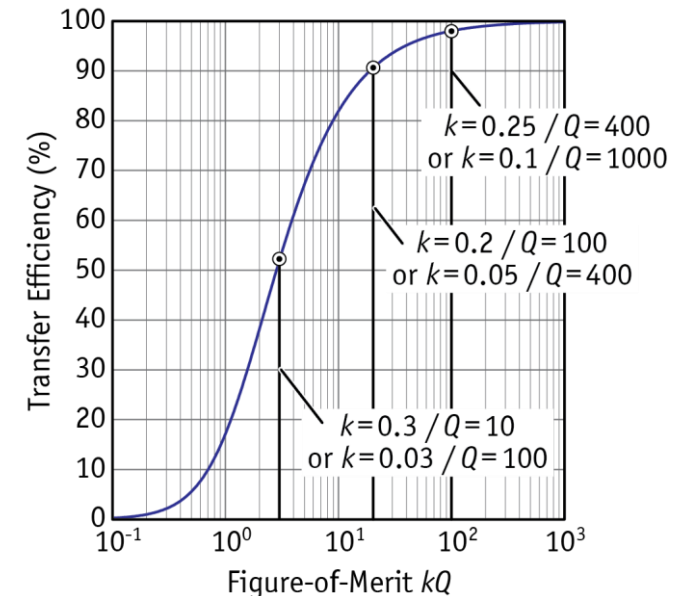
$$\eta_{\max} = \frac{k^2 Q_1 Q_2}{(1 + \sqrt{1 + k^2 Q_1 Q_2})^2}$$

→ Figure-of-Merit = $k\sqrt{Q_1 Q_2} = kQ$



$k = L_h / \sqrt{L_1 L_2}$ Magnetic Coupling
 $Q = \omega L / R_{ac}$ Coil Quality Factor

*K. van Schuylenbergh and
R. Puers, Inductive Powering:
Basic Theory and Application to
Biomedical Systems, 1st ed.,
Springer-Verlag, 2009.*

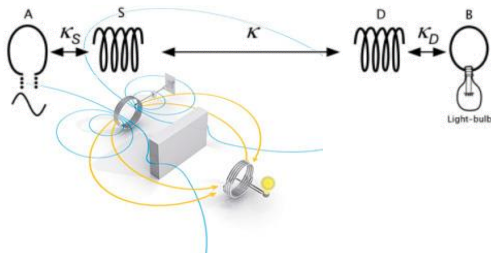


▲ Efficiency Limit of IPT Systems
(Coil Losses Only, Core Neglected)

► $FOM = \text{Quality Factor} \times \text{Magnetic Coupling}$

■ «Highly Resonant Wireless Power Transfer»

- Operation of «High-Q Coils» at Self-Resonance
- Compensation of Low k with High Q :
High Freedom-of-Position
- High Frequency Operation (kHz ... MHz)



WiTricity, www.witricity.com (13.11.2014).

■ Intelligent Parking Assistants for EV

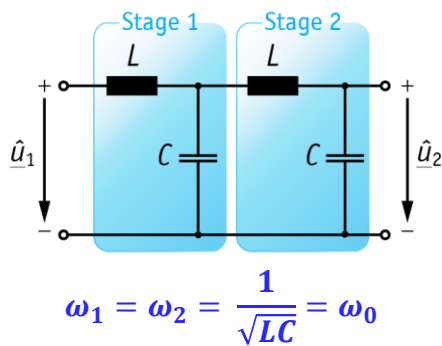
- Maximize k by Perfect Positioning
- Camera-Assisted Positioning Guide
- Achieve up to 5 cm Parking Accuracy



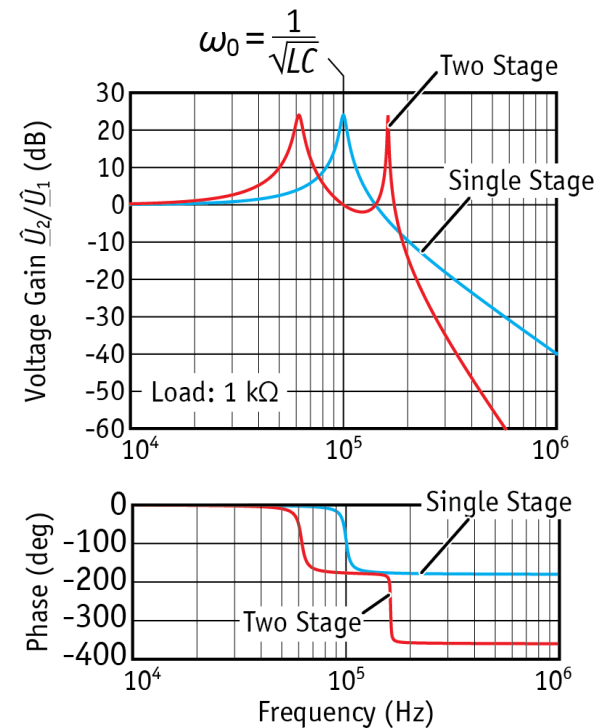
Toyota, www.toyota.com, (18.11.2014).

► Frequency Dependency of Voltage Gain (1)

- Pole-Splitting: Interaction of Coupled Resonant Circuits Tuned to Same Frequency
- Example of a Two-Stage *LC*-Filter



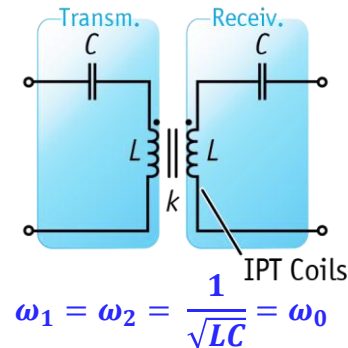
- Both Stages tuned to Same Frequency (100 kHz)
- Pole-Splitting due to Stage-Interaction
- Two Resonant Peaks



▲ Transfer Functions of a Single- and a Two-Stage *LC*-Filter

► Frequency Dependency of Voltage Gain (2)

■ Example of SS-Compensated IPT System



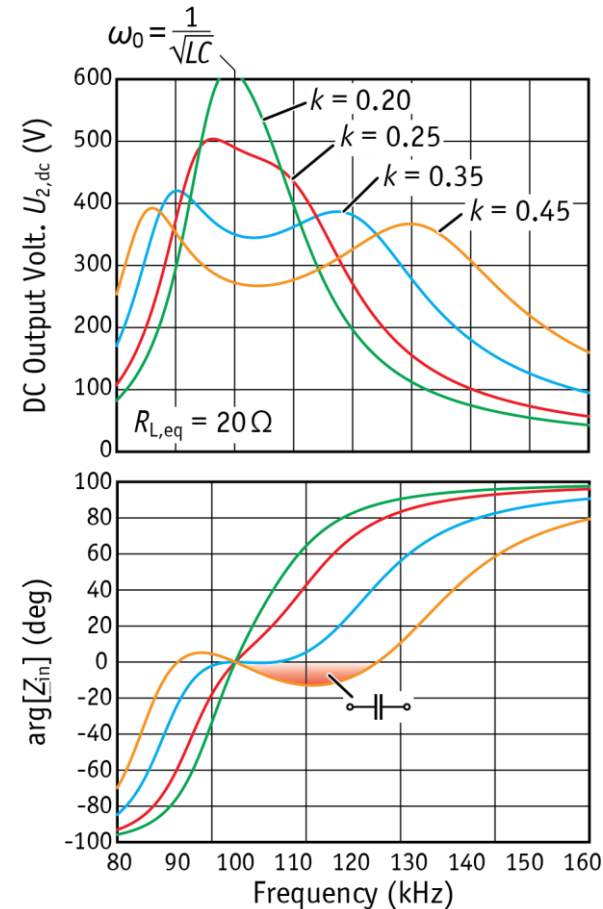
■ Pole Splitting due to Interaction of Transmitter & Receiver Resonant Circuit

- Magnetic Coupling Determines the Strength of Transmitter/Receiver Interaction
- Non-Monotonic Phase Behavior
→ May Lead to Hard-Switching

■ Can be Avoided by Design with Modified Design Rule for Receiver Reactance:

$$\left(\frac{R_L}{\omega_0 \sqrt{L_1 L_2}} \right)_{\text{subopt}} \approx 70..80\% \cdot k_{\text{max}}$$

- Loss-Increase Typically below 5%
- Inductive Behavior Ensured for $\omega_{\text{sw}} > \omega_0$

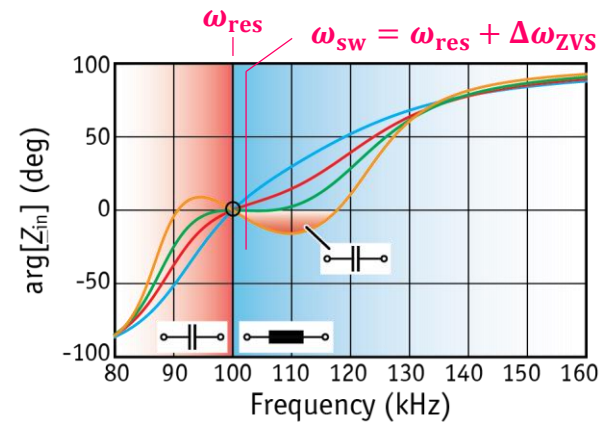
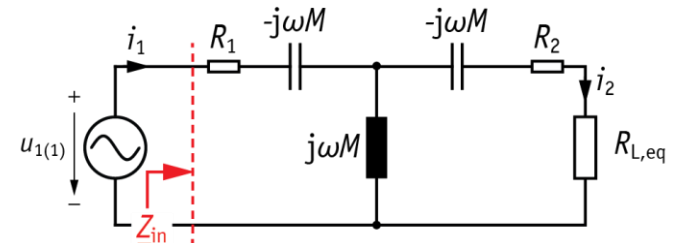
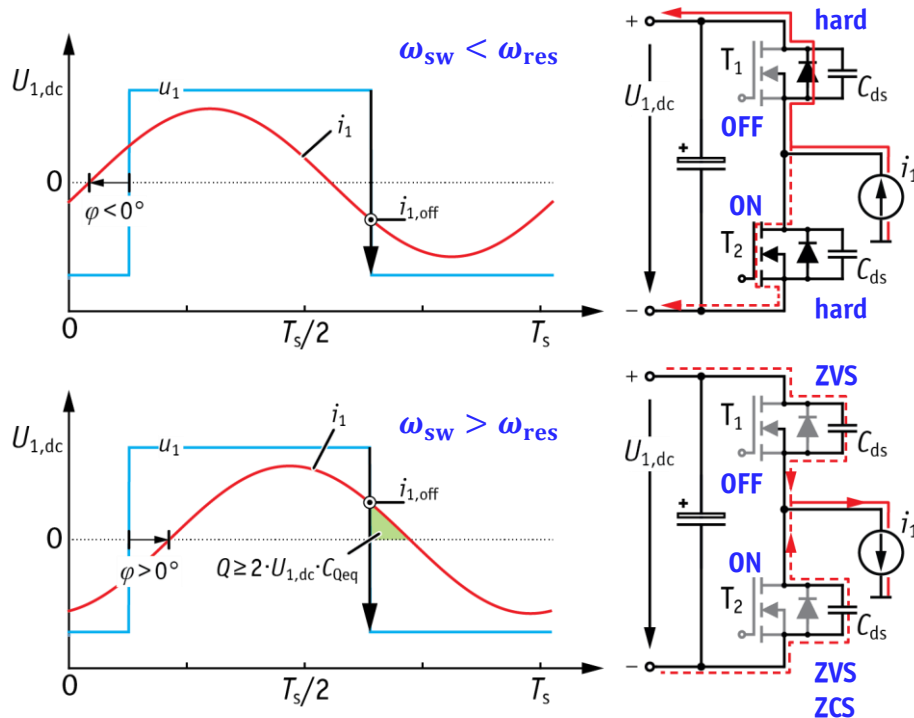


▲ Voltage Transfer Functions and Phase of Input Impedance of an IPT System

► High Efficiency Operation of Inverter Stage (1)

■ Zero-Voltage Switching

- Sufficient Load-Current to (Dis-) Charge Charge-Equivalent MOSFET Capacitance

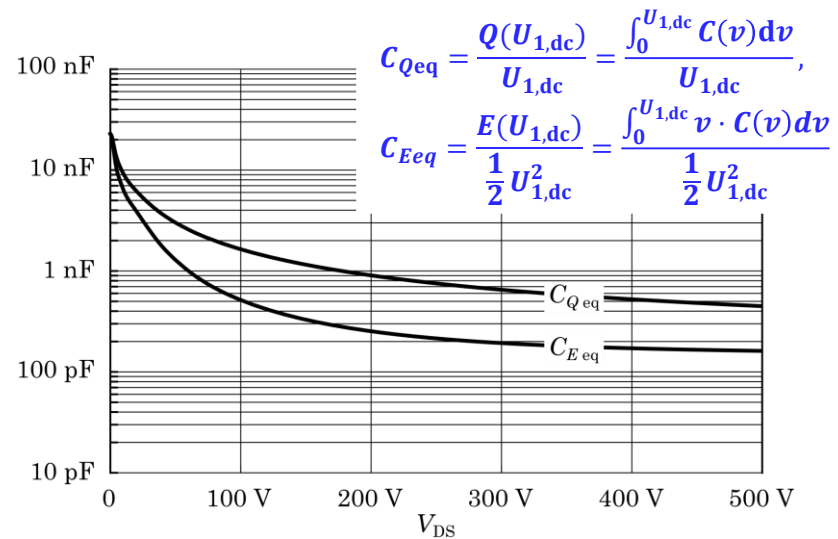
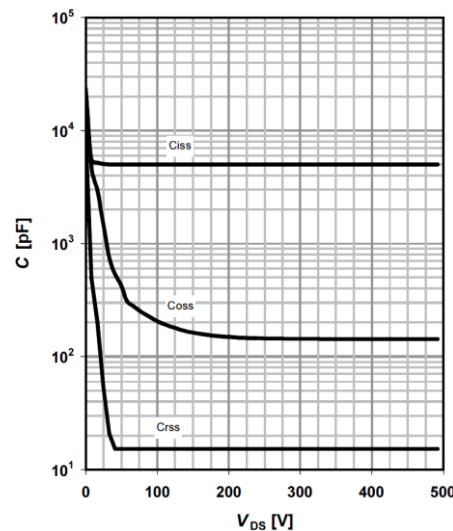
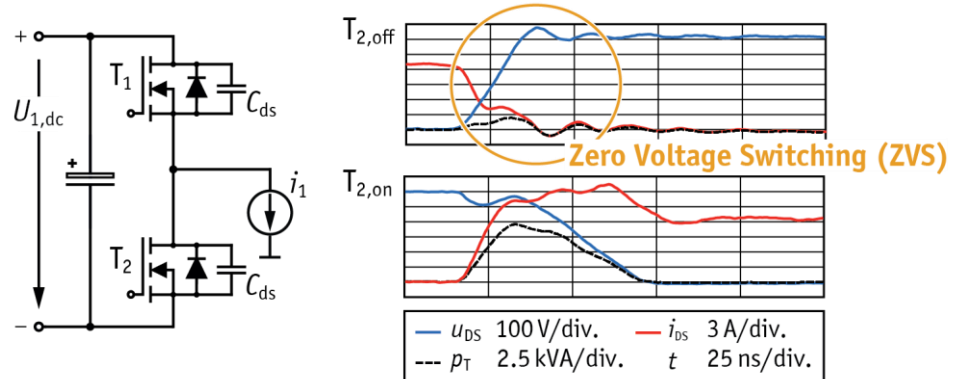


▲ Phase Angle of Input Impedance for Different Loads

► High Efficiency Operation of Inverter Stage (2)

■ Zero-Voltage Switching

- Sufficient Load-Current to (Dis-) Charge Charge-Equivalent MOSFET Capacitance C_{Qeq}
- C_{Qeq} Differs Significantly from Energy Eq. Capacitance C_{Eeq}

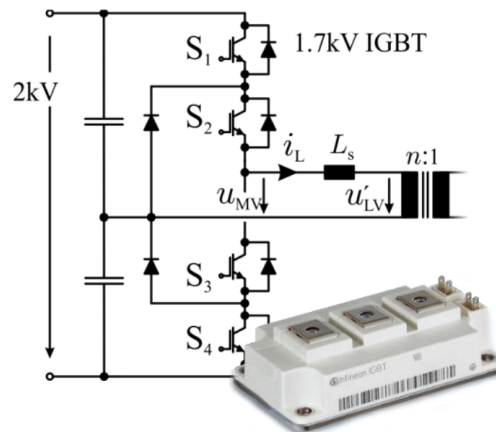


▲ Typical Datasheet Values of a Power MOSFET (Infineon)

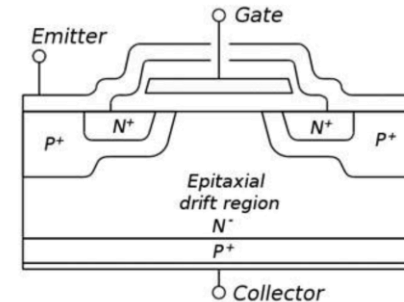
► IGBT Stored Charge Behavior

■ Stored Charge in IGBT Drift Region must be Fully Removed at the Device Turn-Off

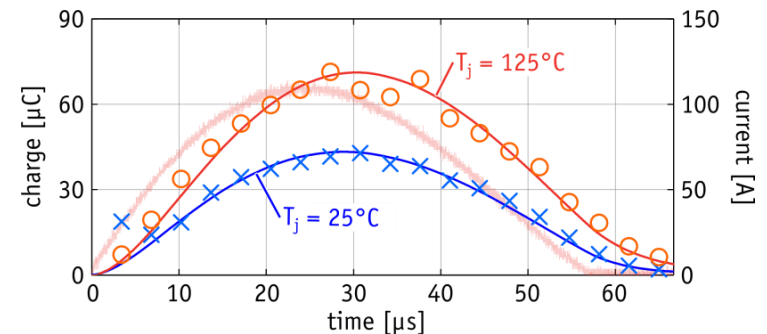
- Phase-Lag between Current and Charge: Residual Charge if Turn-Off at Zero-Current
- Residual Charge causes Turn-On Losses in the Complimentary Device



P. Ranstad and H.-P. Nee, "On dynamic effects influencing IGBT losses in soft-switching converters," IEEE Trans. Power Electron., vol. 26, no. 1, pp. 260–271, 2011.
G. Ortiz, H. Uemura, D. Bortis, J. W. Kolar, and O. Apeldoorn, "Modeling of soft-switching losses of IGBTs in high-power high-efficiency dual-active-bridge dc/dc converters," IEEE Trans. Electron Devices, vol. 60, no. 2, pp. 587–597, 2013.



$$\frac{dQ(t)}{dt} = -\frac{Q(t)}{\tau} + k_s \cdot i_s(t)$$

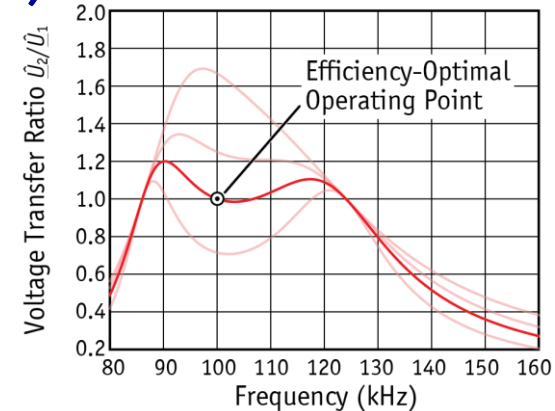


▲ Experimental Stored Charge Dynamic Analysis on 1.7kV FS IGBT and Resonant Sine Pulse

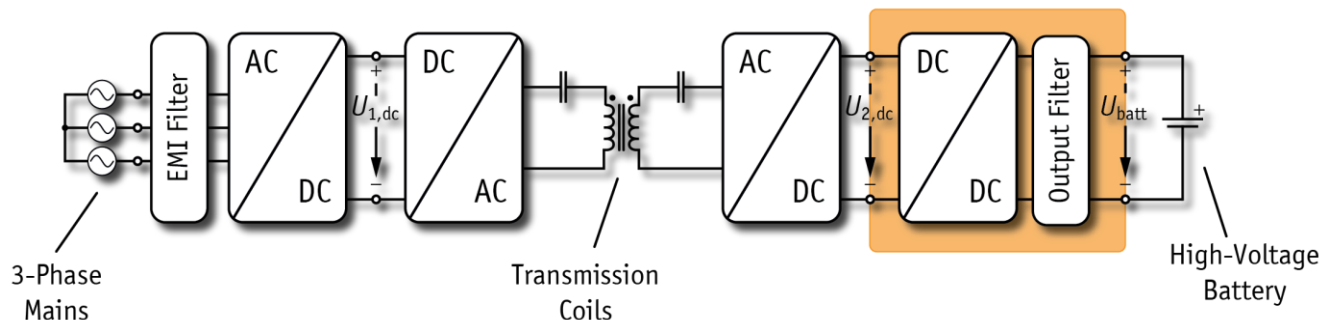
► Efficiency Optimal System Operation (1)

■ Operation of Series-Series Compensated IPT System in Efficiency Optimum

- Given Resonant Circuit
- Given Operating Frequency
- Given Magnetic Coupling
- Given Mains & Battery DC-Voltages

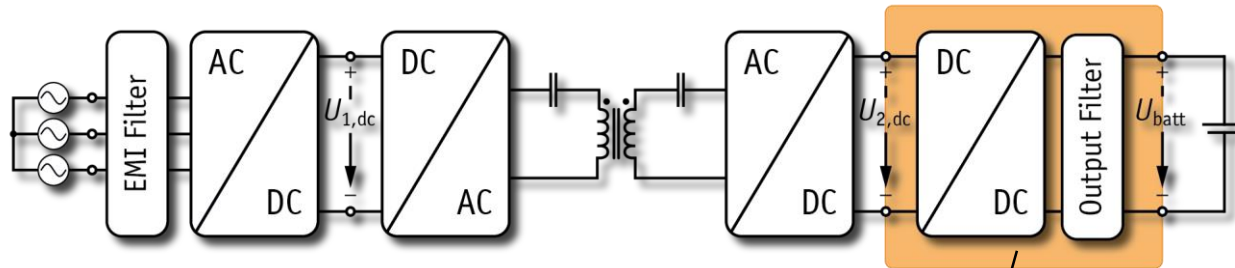


$$\underbrace{\begin{matrix} P_2^* & \dots & \text{reference} \\ \omega_0 & \dots & \text{selected} \\ U_{\text{batt}} & \dots & \text{given} \\ k & \dots & \text{estimated} \end{matrix}}_{\text{Controller Input Variables}} \rightarrow \underbrace{R_L^* \approx k\omega_0 L_2 = \frac{8}{\pi^2} \frac{U_{2,\text{dc}}^2}{P_2^*}}_{\text{Maximum Efficiency Condition}} \rightarrow \underbrace{U_{2,\text{dc}}^* = \sqrt{\frac{\pi^2}{8} P_2^* k \omega_0 L_2}}_{\text{Controller Reference}}$$



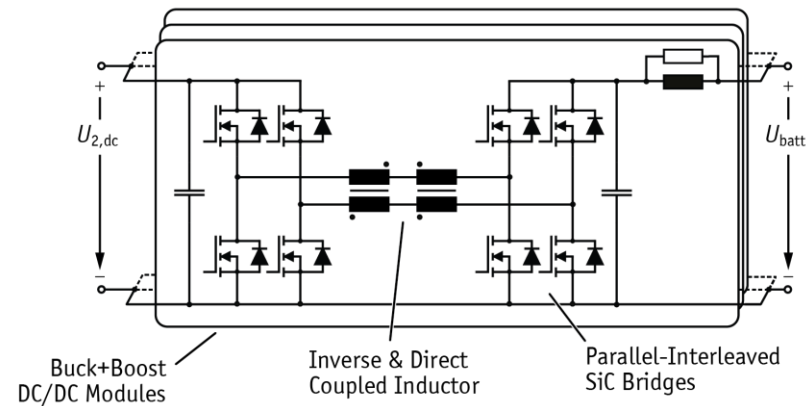
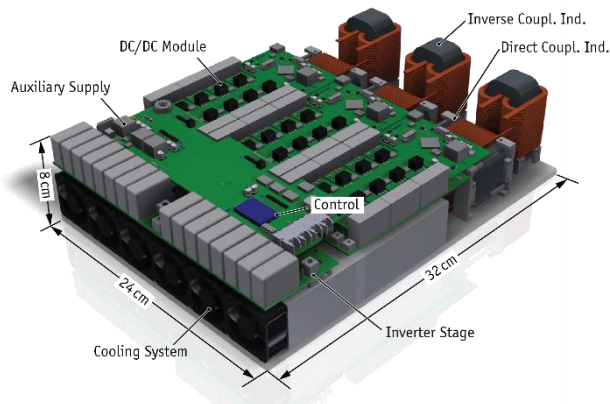
► Receiver Electronics – Potential Solutions (1)

■ Regulation of Receiver-Side DC-Link Voltage with DC/DC Converter



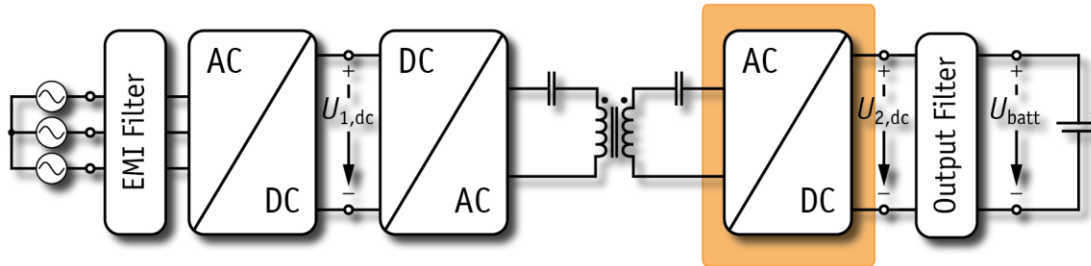
■ Prototype SiC-Converter for 50 kW IPT (Receiver Side)

- Efficiency 98%, 9.2 kW/dm³



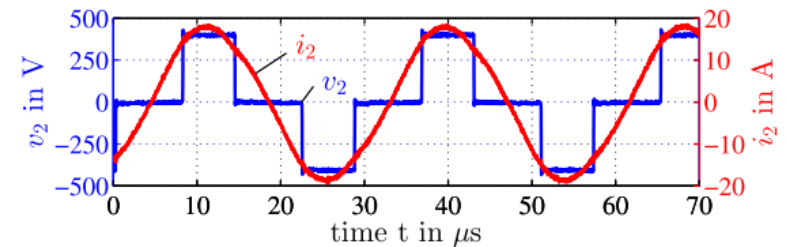
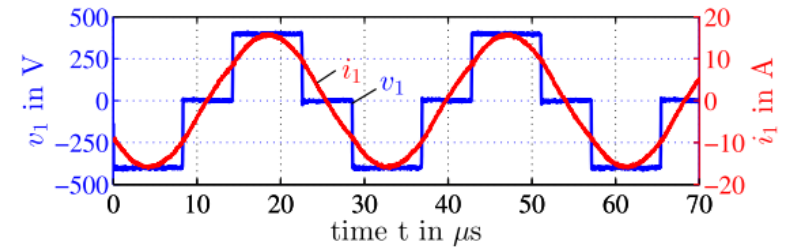
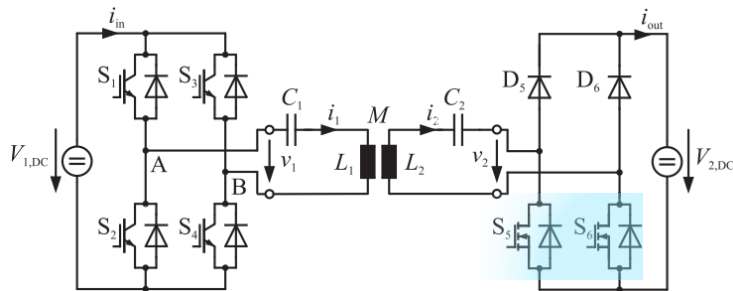
► Receiver Electronics – Potential Solutions (2)

■ Integrated Solution: Regulation of Receiver-Side Voltage with AC/DC Converter

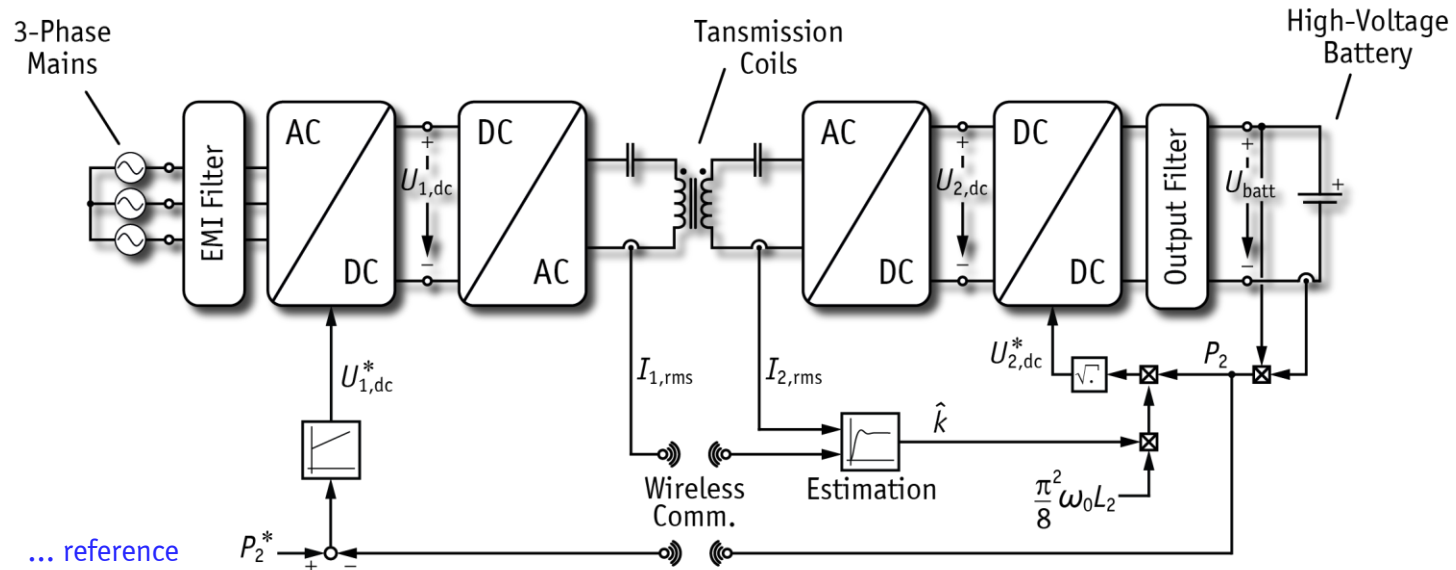


- Utilization of 1- Φ Bridgless-PFC Topology

T. Diekhans, Rik W. De Donker, "A Dual-Side Controlled Inductive Power Transfer System Optimized for Large Coupling Factor Variations," in *Proc. ECCE USA*, 2014.



► Control Diagram for Efficiency Optimal Operation



P_2^* ... reference
 ω_0 ... selected
 U_{batt} ... given
 k ... estimated

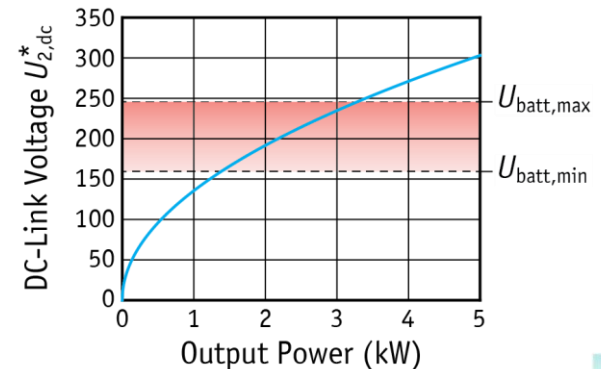
Controller
 Input Variables

$$R_L^* \approx k \omega_0 L_2 = \frac{8}{\pi^2} \frac{U_{2,dc}^2}{P_2^*} \Rightarrow U_{2,dc}^* = \sqrt{\frac{\pi^2}{8} P_2^* k \omega_0 L_2}$$

Maximum
 Efficiency
 Condition

Controller
 Reference

Voltage Step-Up or Step-Down

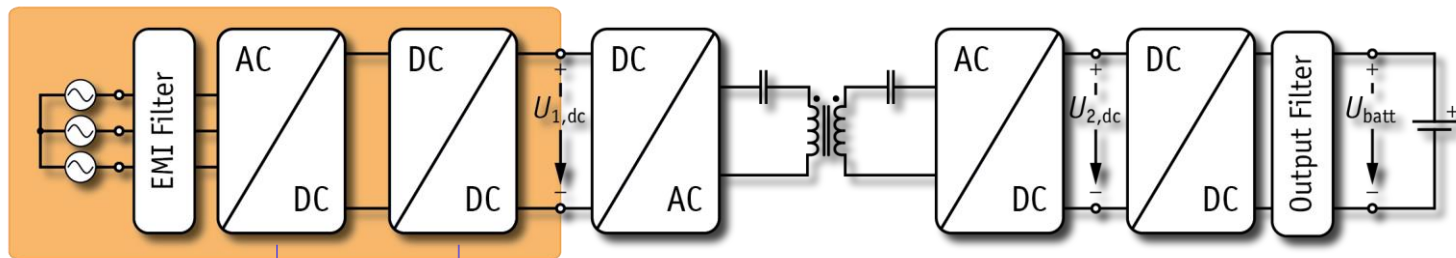


► Transmitter Electronics – Potential Solutions (1)

■ Receiver Voltage $U_{2,dc}$ used for Optimal Load Matching

→ Power Regulation by Adjustment of $U_{1,dc}$ using Characteristic $P_2 = \frac{8}{\pi^2} \frac{U_{1,dc} \cdot U_{2,dc}}{\omega_0 k \sqrt{L_1 L_2}}$

■ 1st Option: **Cascaded AC/DC, DC/DC Conversion**



■ Transmitter-Side DC/DC Converter

- No Isolation Needed
- Identical to Receiver-Side?

■ 3-Phase Mains Interface (Boost-Type)

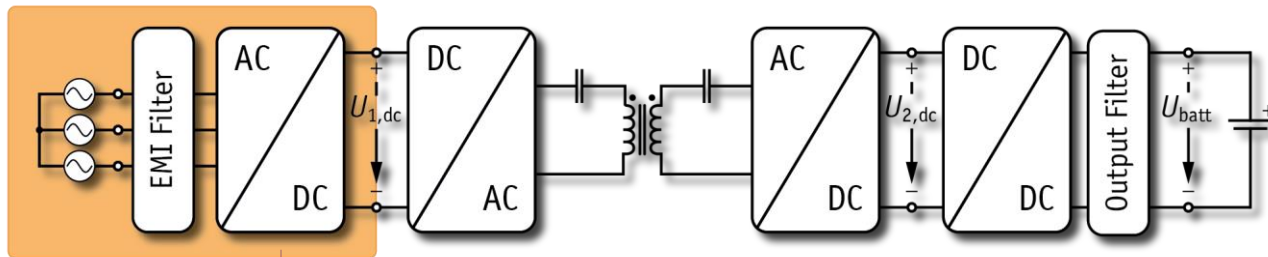
- Power Factor Correction of Phase Current
- Standard Solutions Exist in Industry

► Transmitter Electronics – Potential Solutions (2)

■ Receiver Voltage $U_{2,dc}$ used for Optimal Load Matching

→ Power Regulation by Adjustment of $U_{1,dc}$

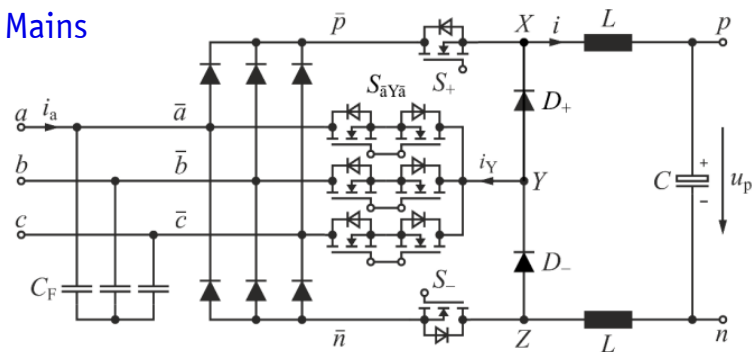
■ 2nd Option: Integrated Rectification and Voltage Controller



■ 3-Phase Buck-Type Mains Interface

- Power Factor Correction of Phase Current
- Regulated Output Voltage below Mains

Example Solution:
SWISS Rectifier



T. B. Soeiro, T. Friedli,
J. W. Kolar, "SWISS
Rectifier – A Novel 3-Phase
Buck-Type PFC Topology for
EV Battery Charging," in
Proc. APEC, 2014.

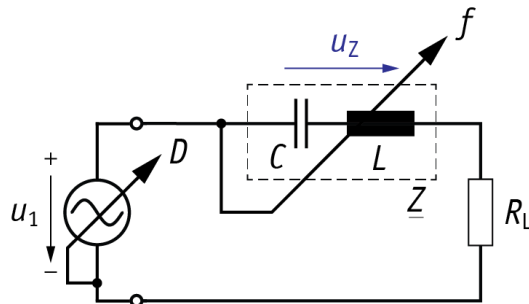
► Alternative Control Concepts for Series Resonant Converters

■ Degrees-of-Freedom for the Control

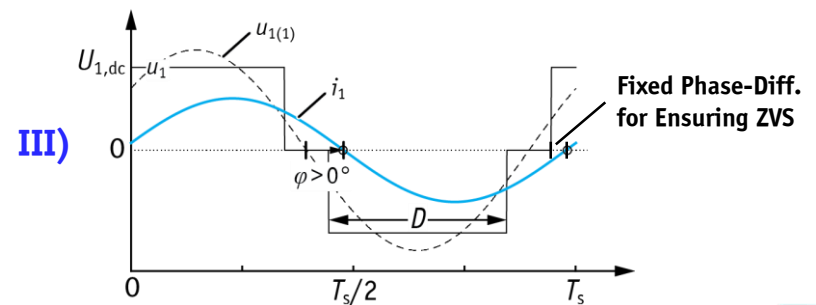
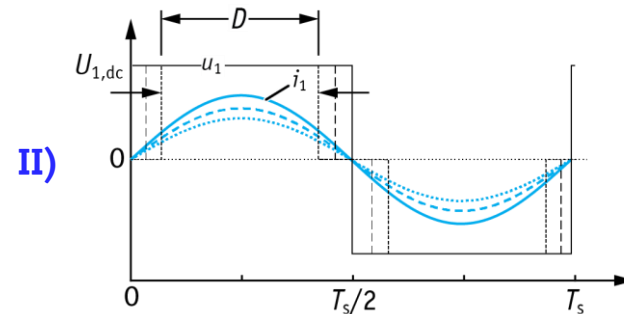
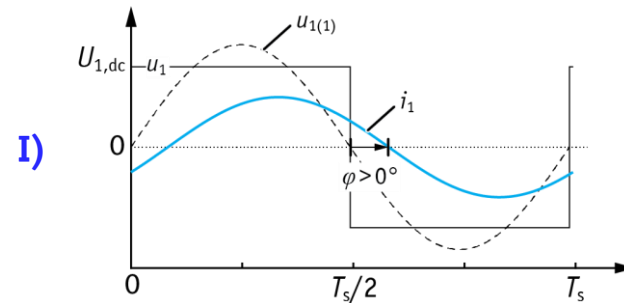
- Inverter Switching Frequency
- Duty Cycle of Inverter Output Voltage
- DC-Link Voltage (with Front-End DC/DC Conv.)

■ Common Control Concepts

- I) Frequency Control @ Fixed Duty Cycle
- II) Duty Cycle Control @ Fixed Frequency
- III) Combined Duty Cycle & Frequency Control



▲ Increase of Switching Frequency Above Resonant Frequency adds Series Voltage Drop



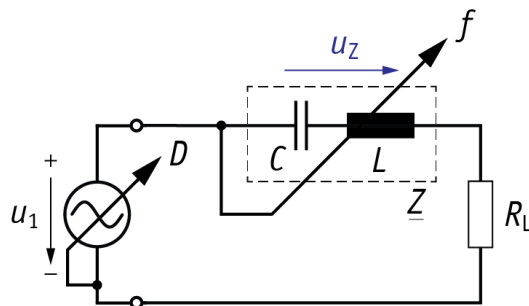
► Frequency Control @ Fixed Duty Cycle

■ Control Switching Frequency of Inverter Stage to Regulate Output Power

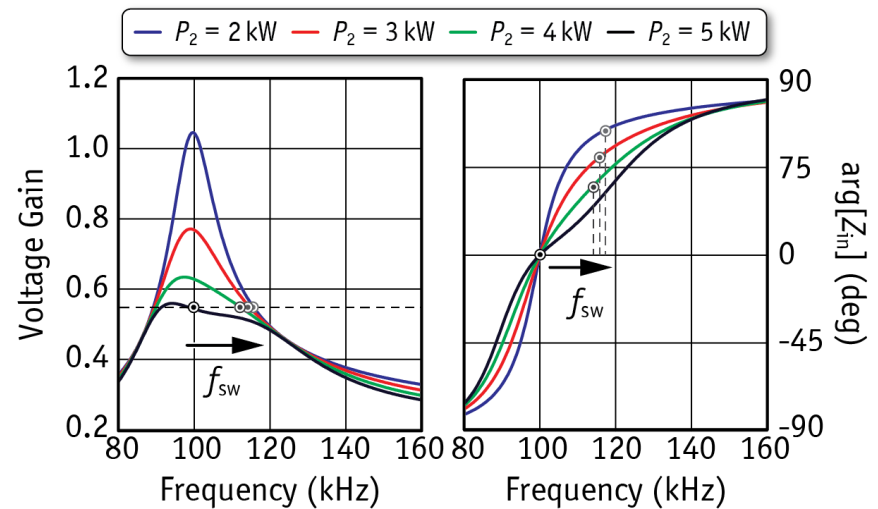
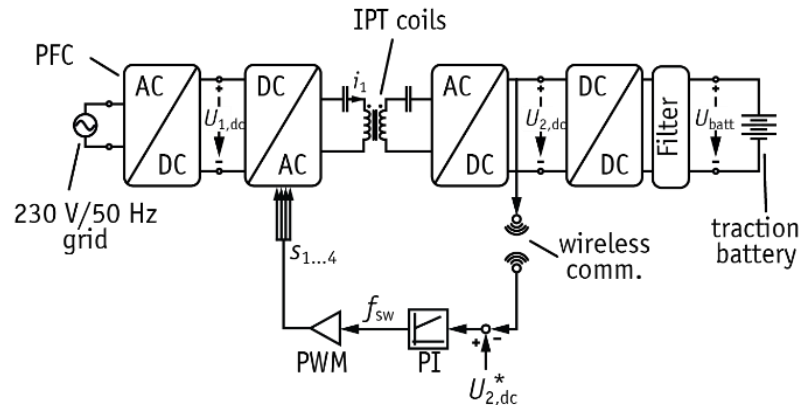
- Switching above Resonant Point Reduces Transmitted Output Power

■ Main Disadvantages:

- Operation Requires Reactive Power
- Increased RMS-Current in Transmitter Coil
- Large Frequency Variation
- Operation at Efficiency Optimum Only at Maximum Output Power



▲ Increase of Switching Frequency Above Resonant Frequency adds Series Voltage Drop



▲ Operating Points shown on Resonant Curves

J. A. Sabate, M. M. Jovanovic, F. C. Lee, and R. T. Gean, "Analysis and design-optimization of LCC resonant inverter for high-frequency AC distributed power system," in *IEEE Trans. Ind. Electron.*, vol. 42, no. 1, pp. 63–71, 1995.

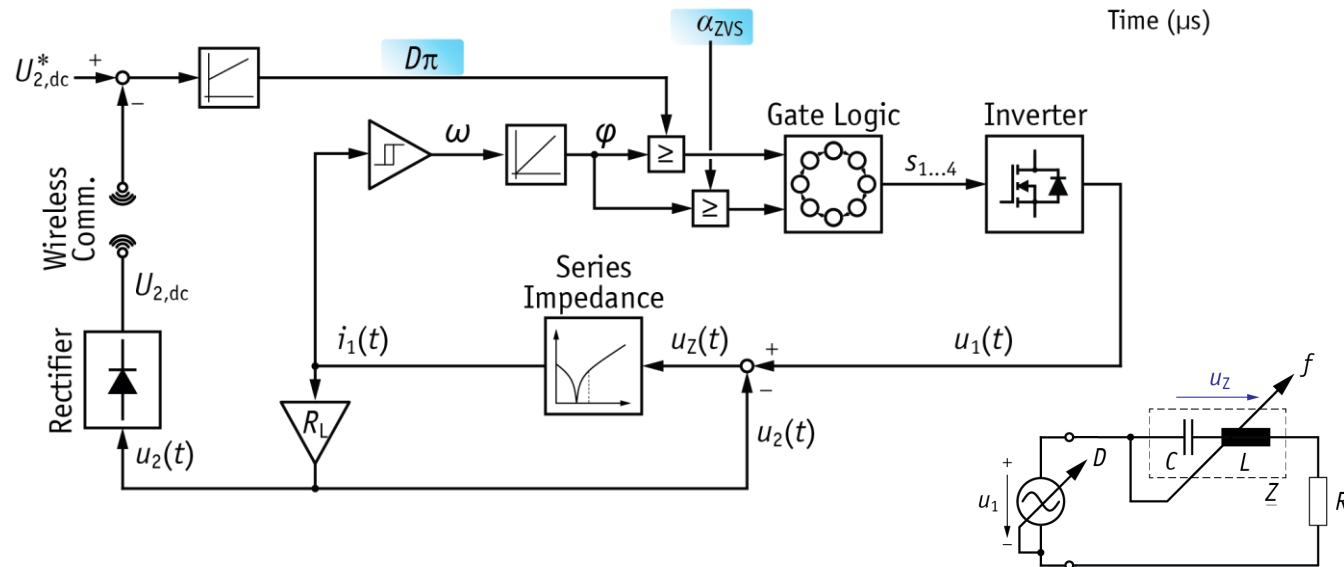
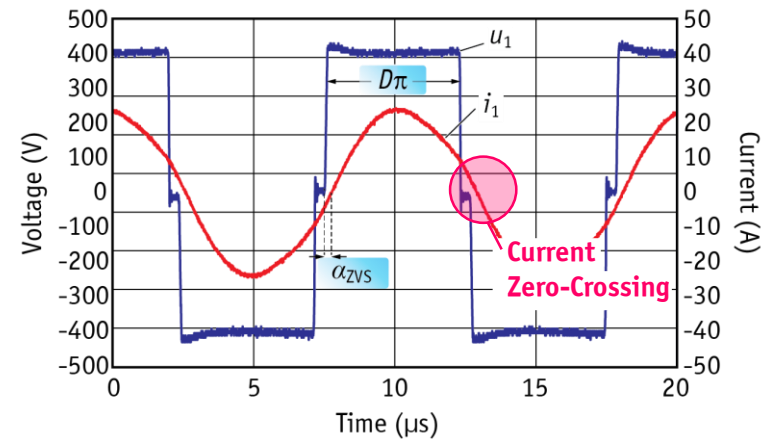
► Self-Oscillating (or Dual) Control Method

■ Dual Control of Phase-Shift and Frequency

- Reduced Amplitude of Voltage Fundamental
- Smaller Frequency Variation
- Guaranteed ZCS/ZVS-Operation with Appropriately Selected α_{ZVS}

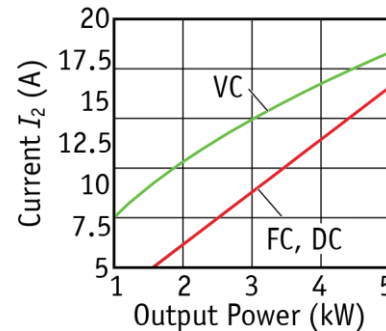
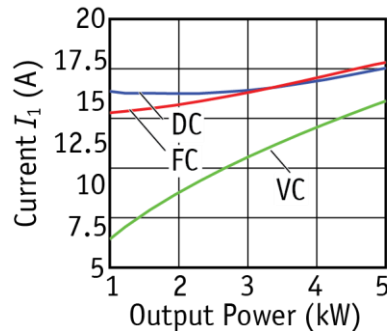
■ Main Disadvantages:

- Operation Requires Reactive Power
- Increased RMS-Current in Transmitter Coil



► Comparison of Control Methods (1)

■ Frequency Control Methods have (almost) Load-Independent Transmitter Current

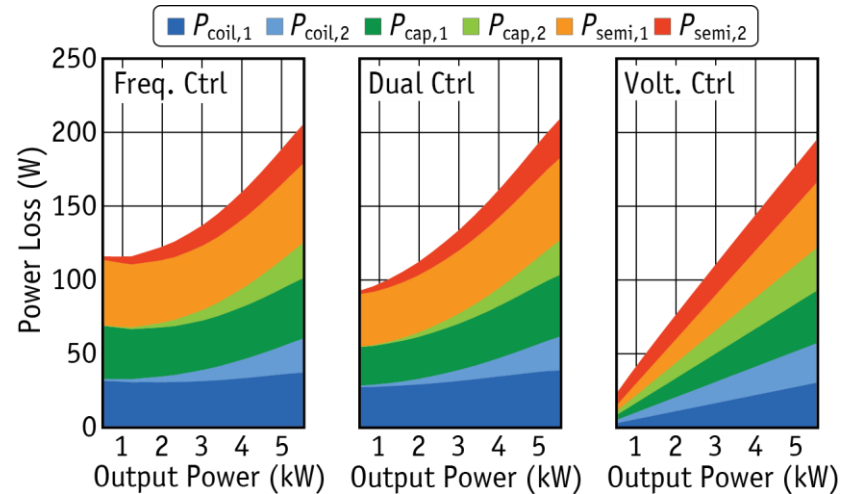


VC ... DC-Link Voltage Control
(Optimal Load Matching)
FC ... Frequency Control
DC ... Dual/Self-Osc. Control

■ Reduction in Transmitter Current I_1 Leads to Over-All Loss Reduction Despite Increased I_2 due to Lower $U_{2,dc}$

■ Large Reduction of Power Losses in Partial-Load Condition with VC

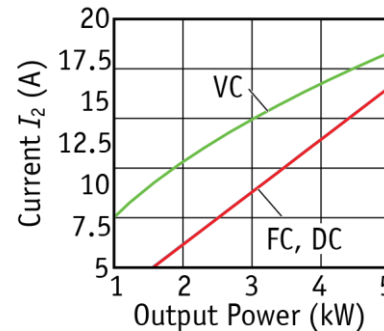
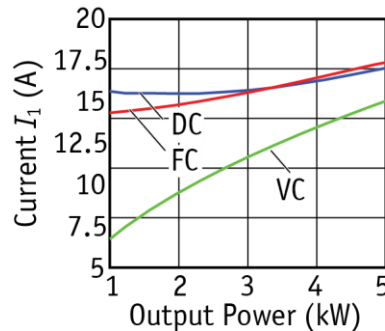
- Reduced Transmitter-Coil RMS-Current
- Decreasing instead of Constant I^2R Losses in Coils/Caps/Switches



▲ For 5 kW IPT Prototype Presented Later

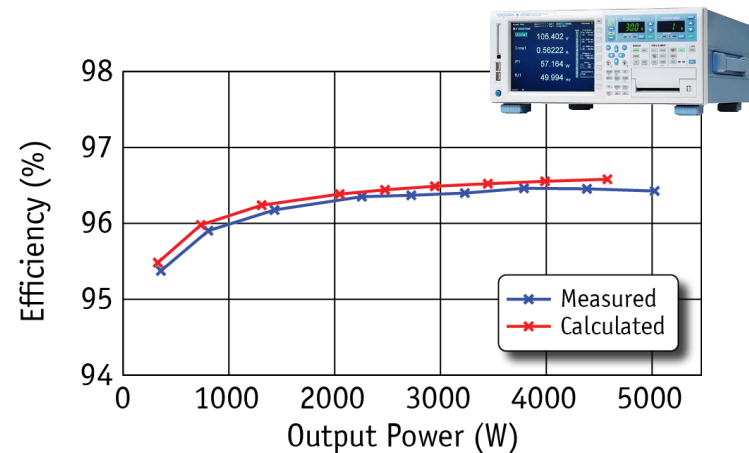
► Comparison of Control Methods (2)

■ Frequency Control Methods have (almost) Load-Independent Transmitter Current



VC ... DC-Link Voltage Control
FC ... Frequency Control
DC ... Dual/Self-Osc. Control

- **Large Reduction of Power Losses in Partial-Load Condition with VC**
 - Reduced Transmitter-Coil RMS-Current
 - Decreasing instead of Constant I^2R Losses in Coils/Caps/Switches
- **Extremely Flat Efficiency Curve even at Low Output Power for Voltage Control Method with Optimum Load Matching**



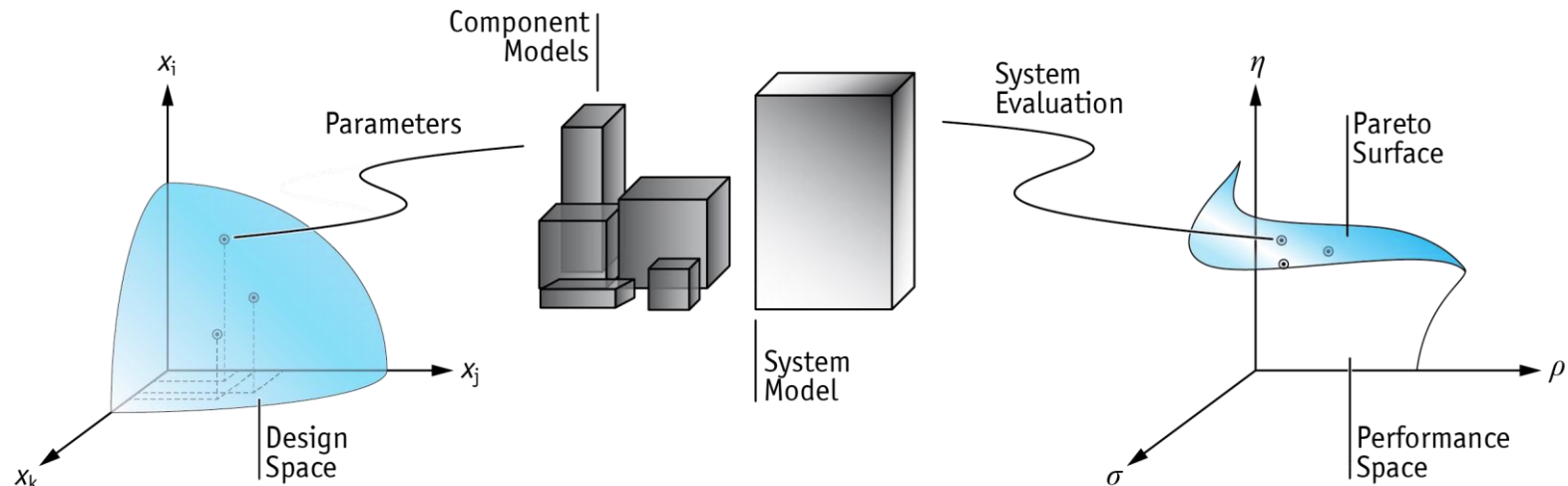
▲ For 5 kW IPT Prototype (Shown in Later Sections)

Components Modeling & Multi-Objective System Optimization

► Multi-Objective System Optimization (2)

■ Mapping of System Design Space into System Performance Space

- Requires Accurate Models for All Main System Components
- Allows Sensitivity & Trade-Off Analysis



- Coil Dimensions
- Winding Scheme
- Number of Turns
- Litz Wire Design
- Core Design
- Core Material

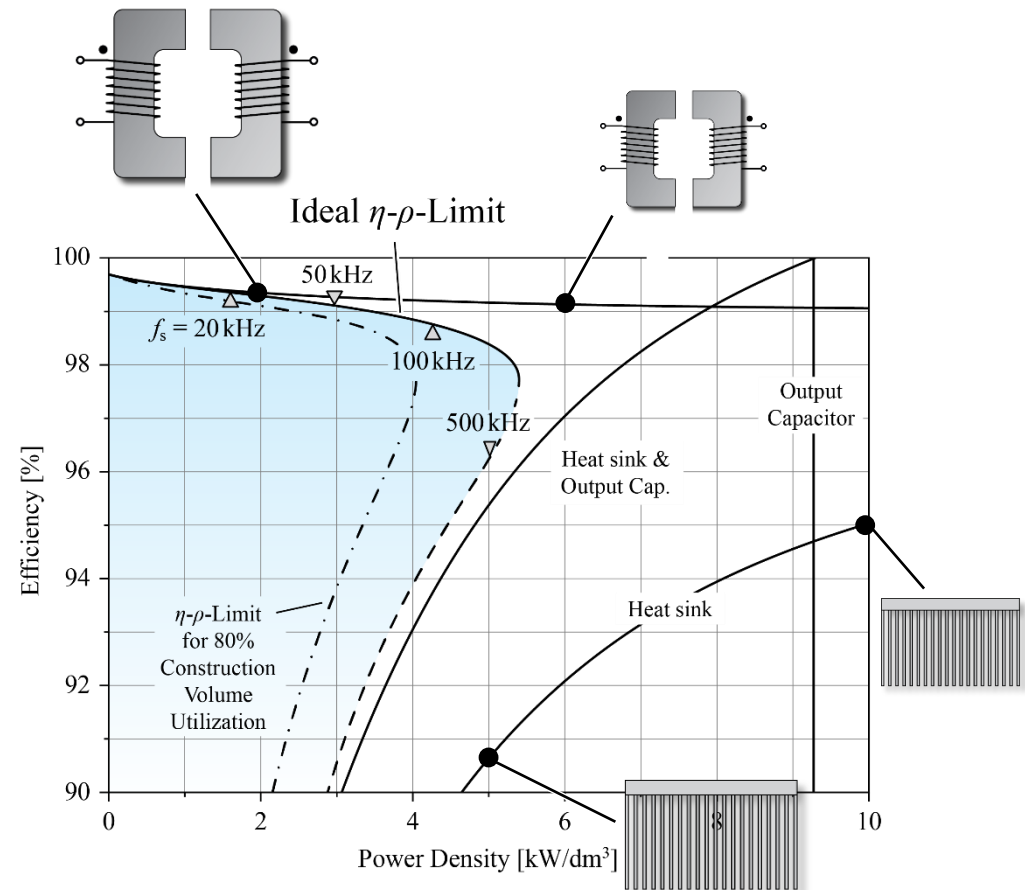
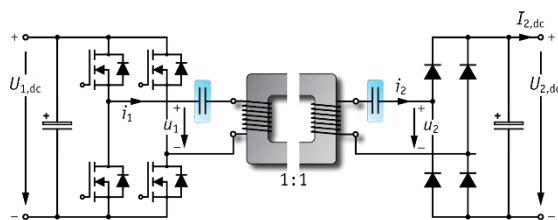
- AC-Losses
- Magnetic Fields
- Capacitor Losses
- Converter Losses
- Component Cost
- Component Size

- Efficiency $\eta = P_{\text{out}}/P_{\text{in}}$ [%]
- Power Density $\rho = P_{\text{out}}/V_{\text{tot}}$ [kW/dm³]
- Stray Field $\beta = B_{\text{max}}/B_{\text{norm}}$ [%]
- Tolerance $\delta = \Delta x/D_{\text{coil}}$ [%]
- Specific Cost $\gamma = C_{\text{tot}}/P_{\text{out}}$ [\$/kW]
- Material Effort $\sigma = \text{kg}_{\text{Cu/Fe}}/P_{\text{out}}$ [kg/kW]

► Multi-Objective System Optimization (2)

- Clarifies Influence of Main Components and Operating Parameters on System Performance

- Analysis of Physical Performance Limits \rightarrow Pareto Front
- Trade-Off between Efficiency and Power Density



System Components and Design Considerations



Coil Modeling
Resonant Capacitors
Magnetic Shielding

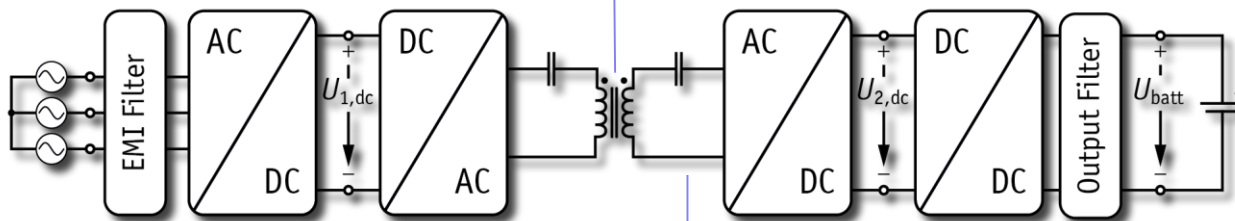
► Main System Components (1)

■ IPT Transmission Coils

- Magnetic Design (using FEM)
- Shielding of Stray Field

■ Receiver-Side Power Electronics

- (Synchronous) Rectification
- Battery Current Regulation



■ Transmitter-Side Power Electronics

- 1/3- Φ Mains Interface
- High-Frequency Inverter Stage

■ Resonant Compensation

- Requirements for Capacitor
- Optimal Component Selection

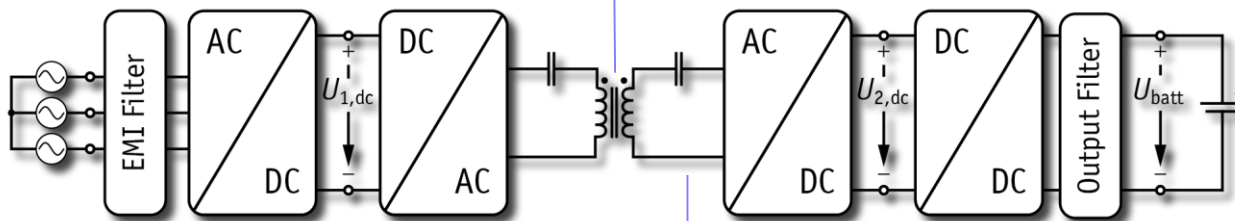
► Main System Components (2)

■ IPT Transmission Coils

- Magnetic Design (using FEM)
- Shielding of Stray Field

■ Receiver-Side Power Electronics

- (Synchronous) Rectification
- Battery Current Regulation



■ Transmitter-Side Power Electronics

- 1/3- Φ Mains Interface
- High-Frequency Inverter Stage

■ Resonant Compensation

- Requirements for Capacitor
- Optimal Component Selection

Transmission Coil: Coil Geometry Options

► Structures of Single-Phase Transformers

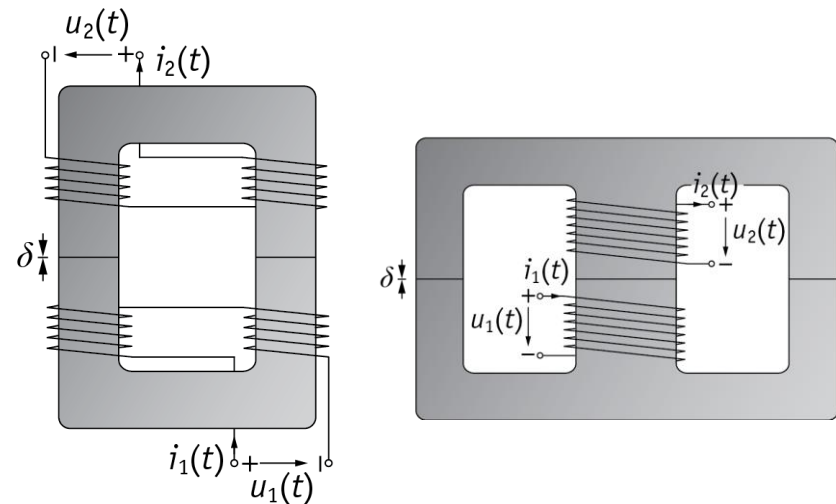
■ Common Transformer Shapes: E- and U-Type

- One or Two Closed Paths for Core-Flux
- Available Ferrite Parts: E-/U-/Pot-/Toroid-Cores



▲ Available Ferrite Parts for Power Transformers

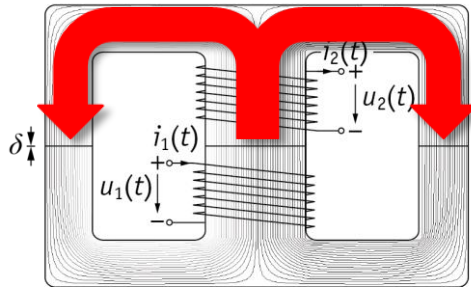
Huigao Megnetics, www.huigao-magnetics.com (18.11.2014).



▲ Common Transformer Structures

► Classification of IPT Coil Geometries (1)

E-Type IPT Coils

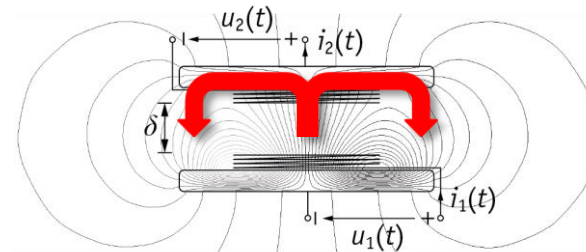
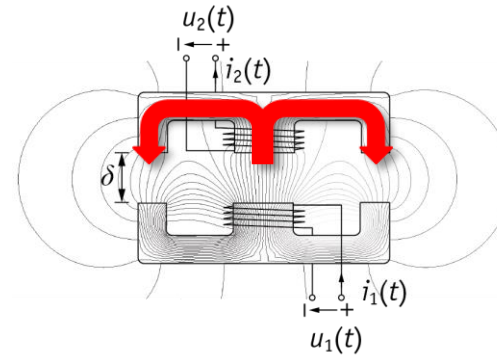


■ E-Core Transformer

- Flux Divided to Two Equal Loops
- 2x Thickness for Central Leg

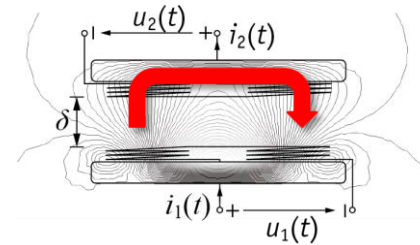
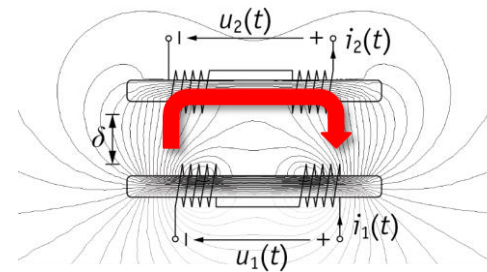
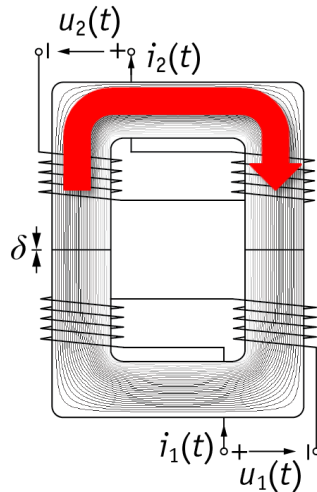
■ E-Type IPT Coil

- Flux Divided to Two Equal Loops
- Max. Coupling for Certain Ratio of Core Size Compared to Winding Diam.



► Classification of IPT Coil Geometries (2)

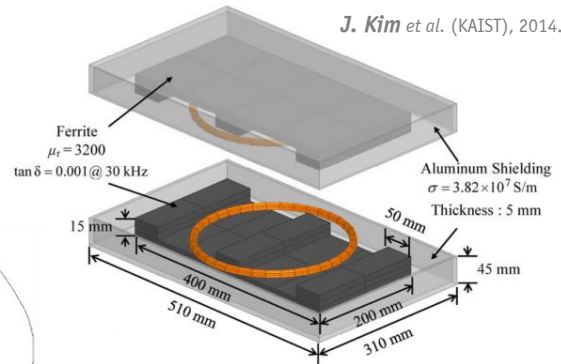
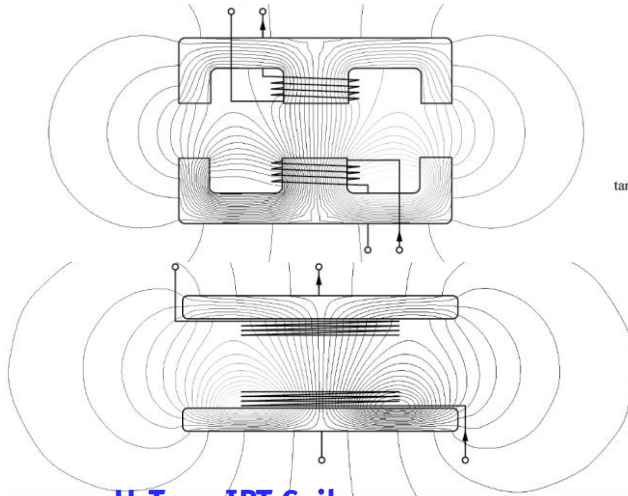
U-Type IPT Coils



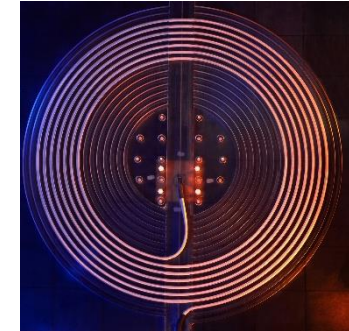
- **U-Core Transformer**
 - Flux on Single Loop
- **U-Type IPT Coil**
 - Single Loop formed by two Windings

► Literature: Realized Example Prototypes

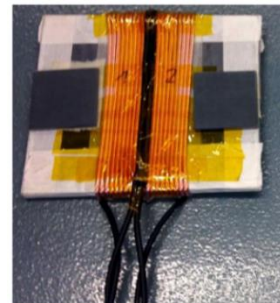
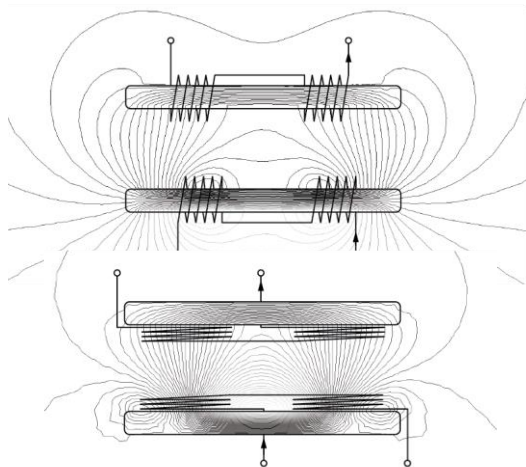
■ E-Type IPT Coils



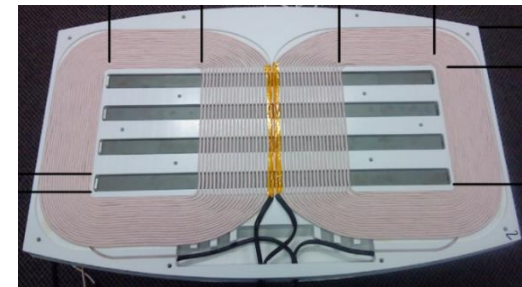
S. Reichert et al. (Fraunhofer ISE), 2013.



■ U-Type IPT Coils



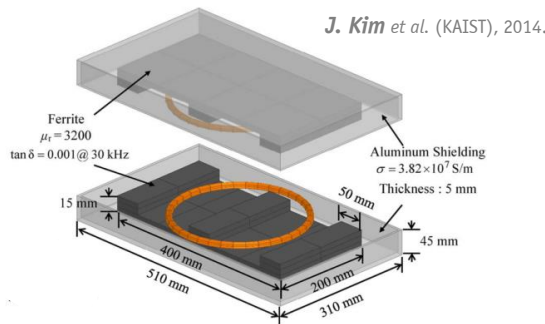
F. Turki et al., PCIM Europe, 2014.



C.-Y. Huang, M. Budhia, G. Covic, T. Boys, 2011-2013.

► Coil Geometry Optimization (1)

■ Conceptual Analysis with Reluctance Model

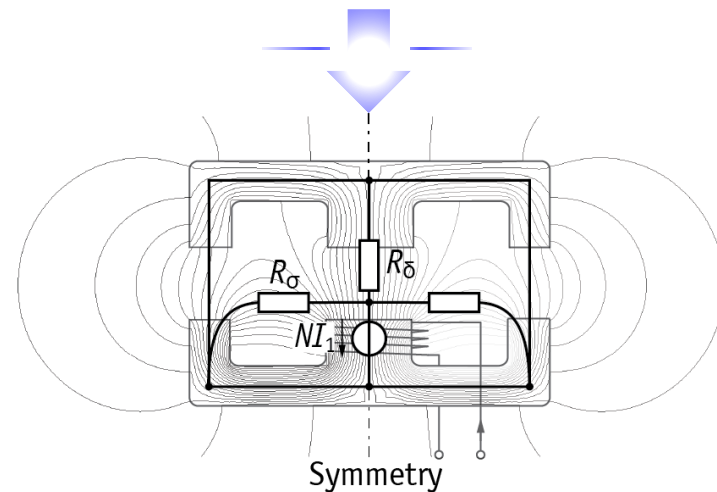
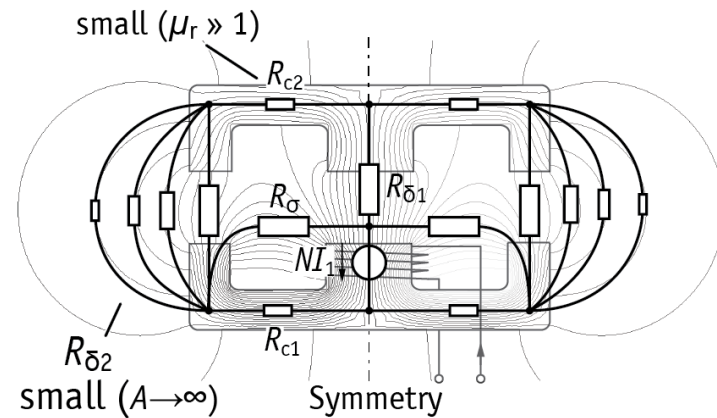


■ Maximize Figure-of-Merit kQ :

$$k = \frac{\psi_h}{\psi_\sigma + \psi_h} \propto \frac{R_\sigma}{R_\delta + R_\sigma}$$

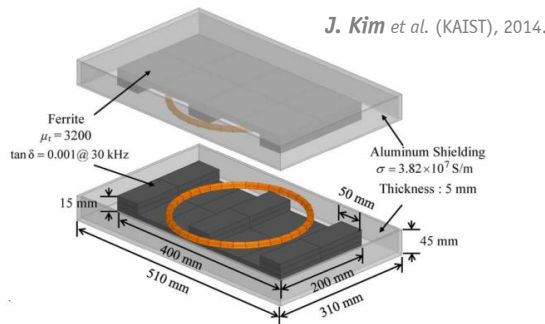
■ Approximations:

- Core Reluctance Small (high Permeability)
- Only Air Gap in Central Leg Considered, Side Legs have small Reluctance (large Area)



► Coil Geometry Optimization (2)

■ Conceptual Analysis with Reluctance Model



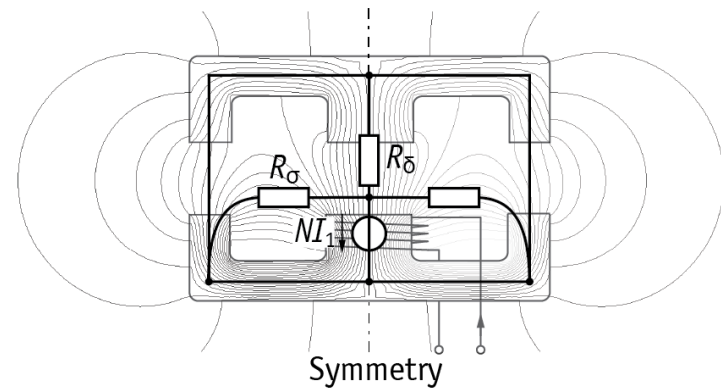
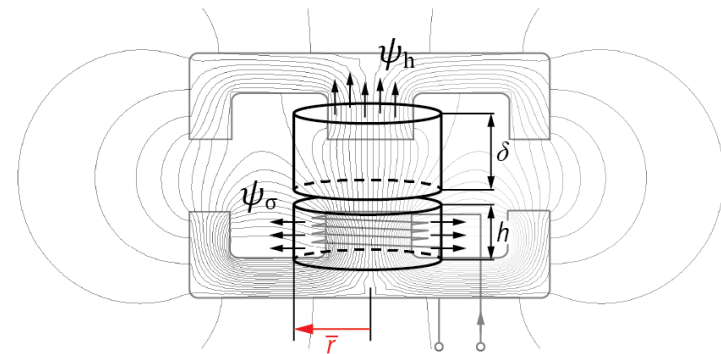
■ Maximize Figure-of-Merit kQ :

$$k = \frac{\psi_h}{\psi_\sigma + \psi_h} \propto \frac{R_\sigma}{R_\delta + R_\sigma}$$

■ Reluctance: Approximate Scaling Law

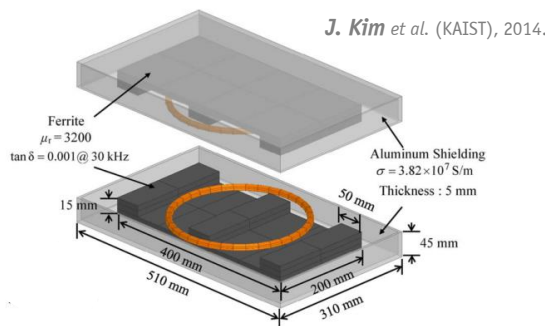
$$R_\sigma \approx \frac{\bar{r}}{\mu_0 \cdot 2\pi \bar{r} h} \approx \text{const.}$$

$$R_\delta \approx \frac{\delta}{\mu_0 A_c} \propto \frac{\delta}{\mu_0 \bar{r}^2}$$



► Coil Geometry Optimization (3)

■ Conceptual Analysis with Reluctance Model



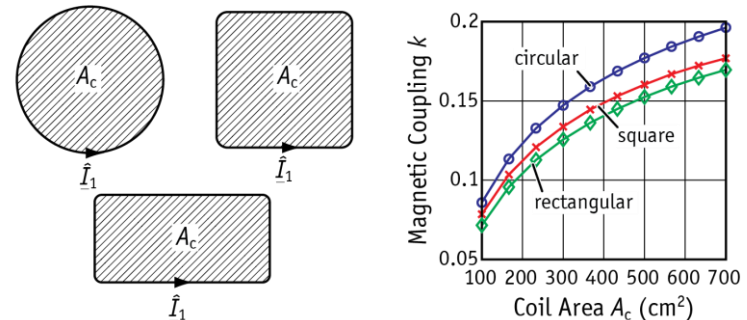
■ Maximize Figure-of-Merit kQ :

$$k = \frac{\psi_h}{\psi_\sigma + \psi_h} \propto \frac{R_\sigma}{R_\delta + R_\sigma}$$

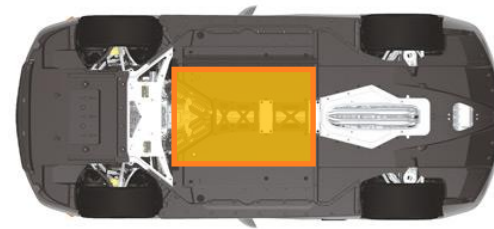
■ Reluctance: Approximate Scaling Law

$$R_\sigma \approx \frac{\bar{r}}{\mu_0 \cdot 2\pi \bar{r} h} \approx \text{const.}$$

$$R_\delta \approx \frac{\delta}{\mu_0 A_c} \propto \frac{\delta}{\mu_0 \bar{r}^2}$$



▲ FEM-Calculated Coupling for Three Exemplary Coil Geometries



→ Maximize Coil Area for High Coupling!

→ Fully Utilize Available Construction Volume

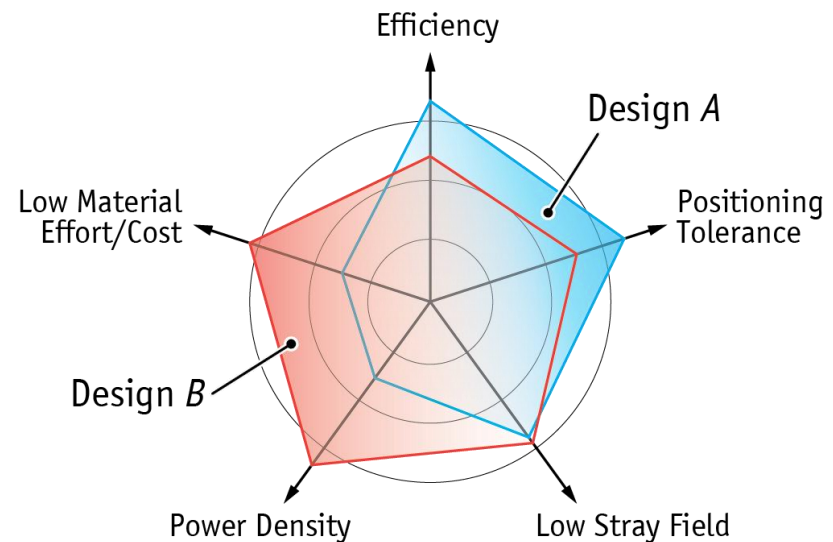
→ Best Choice for Geometry is Application Specific!

► Fair Comparison of IPT Coil Geometries

■ Performance Indicators for IPT Coils

- Efficiency $\eta = P_{\text{out}}/P_{\text{in}}$ [%]
- Power Density $\alpha = P_{\text{out}}/A_{\text{coil}}$ [kW/dm²]
- Stray Field $\beta = B_{\text{max}}/B_{\text{norm}}$ [%]
- Tolerance $\delta = \Delta x/D_{\text{coil}}$ [%]
- Specific Cost $\gamma = C_{\text{tot}}/P_{\text{out}}$ [\$/kW]
- Material Effort $\sigma = \text{kg}_{\text{Cu/Fe}}/P_{\text{out}}$ [kg/kW]

Note: Coupling is Indicative for Efficiency, but does not cover all Loss Components, e.g. Core Losses or Eddy Current Losses.



■ Aspects for a Fair Comparison

- Consider all, not just single Criteria
- Equal Electrical Interfaces
- Designs Optimized for Same Goals with Equal Boundary Conditions

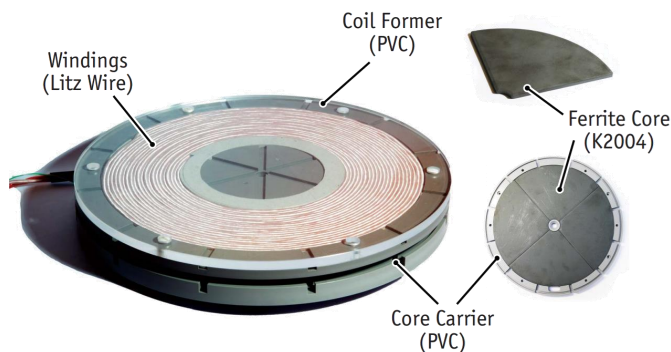
▲ Performance Comparison of two IPT Coil Designs

Designed IPT Demonstrator Systems

► Demonstrator Systems: 5 and 50 kW Output Power (1)

■ 5 kW System for Model Development

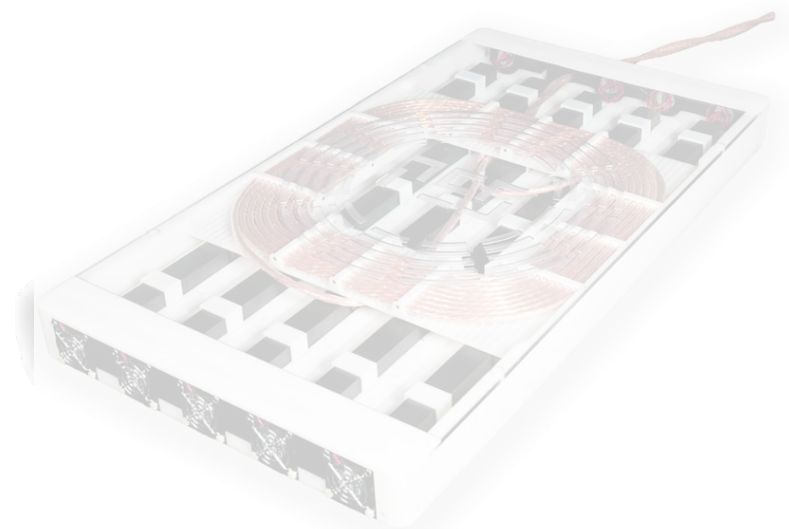
- Output Power 5 kW @ 400V, 100 kHz
- Lab-Scale Coil and Converter Size (210 mm Diameter / 50 mm Air Gap)
- Basic Geometry for Simplified Modeling
- Verification of Calculation & Optimization



R. Bosshard, J. W. Kolar, J. Mühlethaler, I. Stevanovic, B. Wunsch, F. Canales, "Modeling and η - α -Pareto optimization of inductive power transfer coils for electric vehicles," IEEE J. Emerg. Sel. Topics Power Electron., vol. 3, no. 1., pp.50-64, March 2015.

■ 50 kW Prototype System for EV Specs

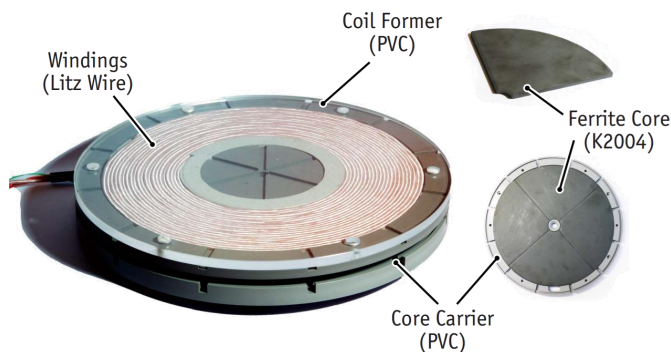
- Output Power 50 kW @ 800V, 85 kHz
- Optimized Geometry for EV Charging (450x750x60 mm, 25 kg)
- Experimental Verification



► Demonstrator Systems: 5 and 50 kW Output Power (2)

■ 5 kW System for Model Development

- Output Power 5 kW @ 400V, 100 kHz
- Lab-Scale Coil and Converter Size (210 mm Diameter / 50 mm Air Gap)
- Basic Geometry for Simplified Modeling
- Verification of Calculation & Optimization



R. Bosshard, J. W. Kolar, J. Mühlethaler, I. Stevanovic, B. Wunsch, F. Canales, "Modeling and η - α -Pareto optimization of inductive power transfer coils for electric vehicles," IEEE J. Emerg. Sel. Topics Power Electron., vol. 3, no. 1., pp.50-64, March 2015.

■ 50 kW Prototype System for EV Specs

- Output Power 50 kW @ 800V, 85 kHz
- Optimized Geometry for EV Charging (450x750x60 mm, 25 kg)
- Experimental Verification

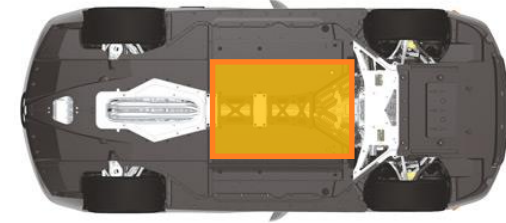


► Comparison: Rectangular vs. DD Coil

■ Which Performance is Achieved within Same Footprint?

- DD Coil Designed to Fit into Housing of Existing Rectangular 50 kW Prototype
- Equal Electrical Interface and Transmission at 85 kHz
- Optimized for Maximum Efficiency

Lexus, www.lexus.com



▲ Realized 50 kW Prototype IPT Coil

VS.

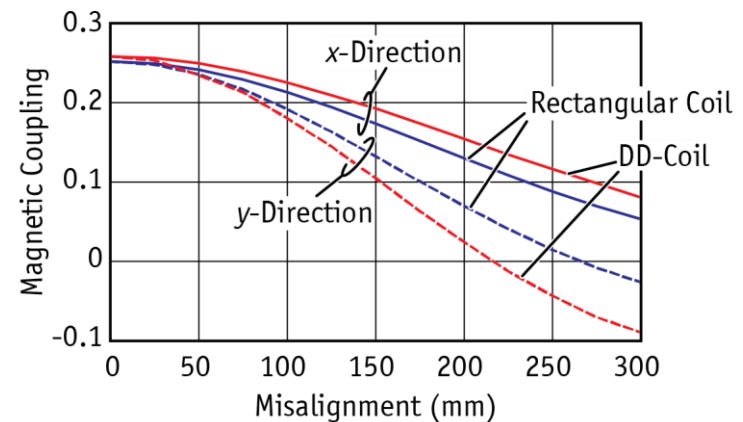
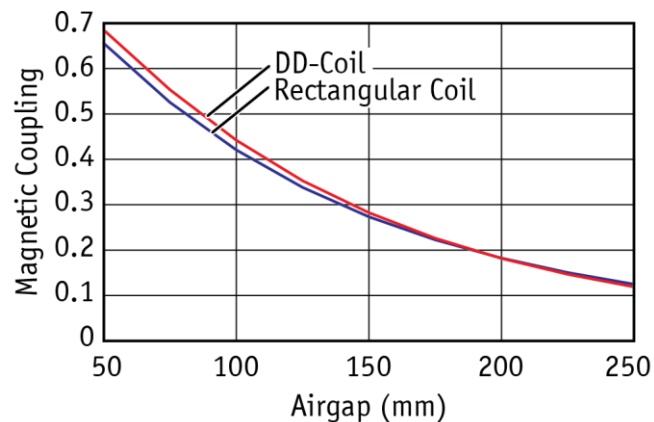


▲ 50 kW DD-Prototype Optimized for same Footprint

► Rectangular vs. DD Coil – Coupling

■ Evaluation of Magnetic Coupling for Ideal and Misaligned Coil Positions

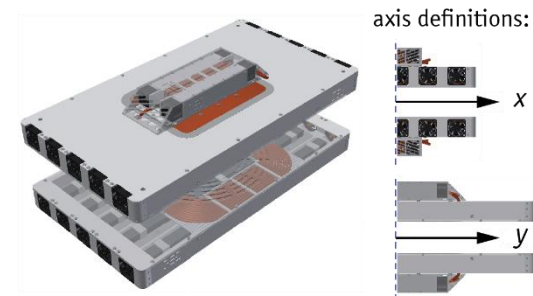
- 3D-FEM Simulation Results in Frequency Domain



■ Rectangular and DD Coil Achieve Equal Coupling at Ideal Positioning

■ Coil Positioning Tolerance:

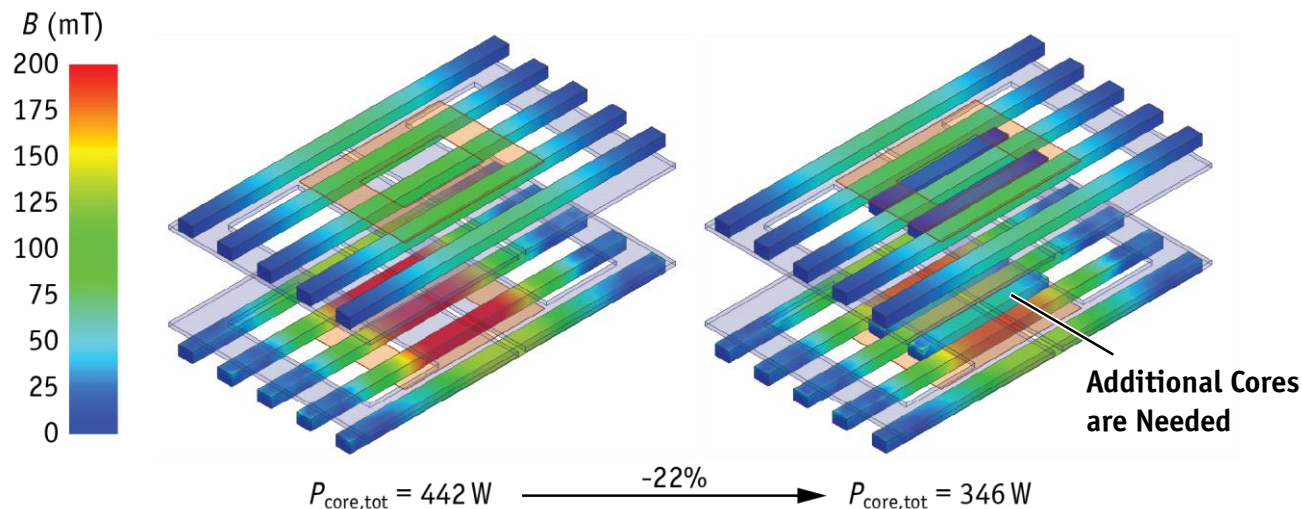
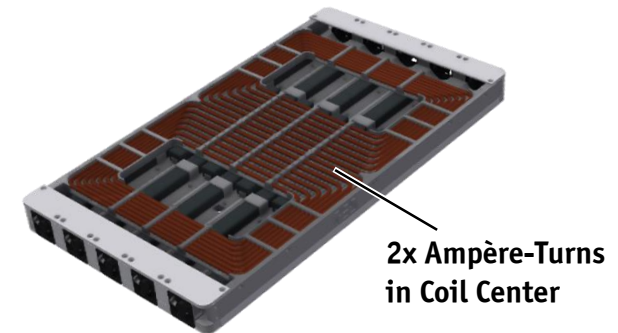
- DD-Coil Better in x-Direction
- Rect.-Coil Better in y-Direction



► Rectangular vs. DD Coil – Core Losses

■ DD has Higher Flux Density in Central Cores

- High Core Losses in Coil Center due to High Ampère-Turns
- Additional Core Elements Required to Reduce Flux Density
- No Additional Eddy-Current Shield on Top/Bottom Needed



▲ FEM Simulation Results without (left) and with (right) additional cores
for flux density / core loss reduction in coil center

► Rectangular vs. DD Coil – Total Losses

■ DD has Higher Core Losses in Central Core Elements due to High Core Flux Density

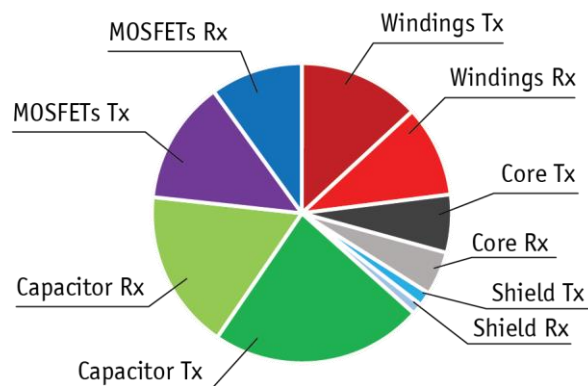
- But does not Require Additional Eddy-Current Shield that is used in Rectangular Design
- Power Losses in Remaining Parts are Comparable, Since Coupling is almost Equal

→ Efficiency of Rectangular and DD Coil is very Similar

→ Additional Cores were needed for DD, Higher Weight: +1.2 kg / +5%

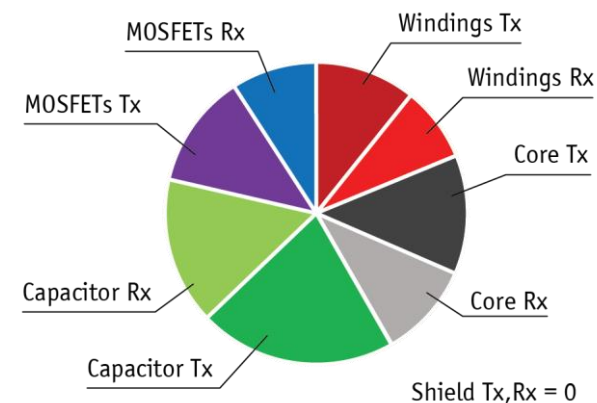
Rectangular Coil Design

Total Losses: 1384 W



Double-D Coil Design

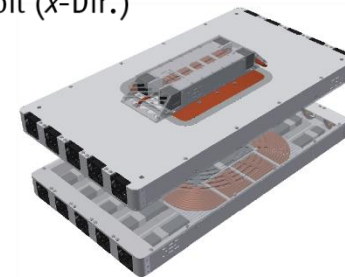
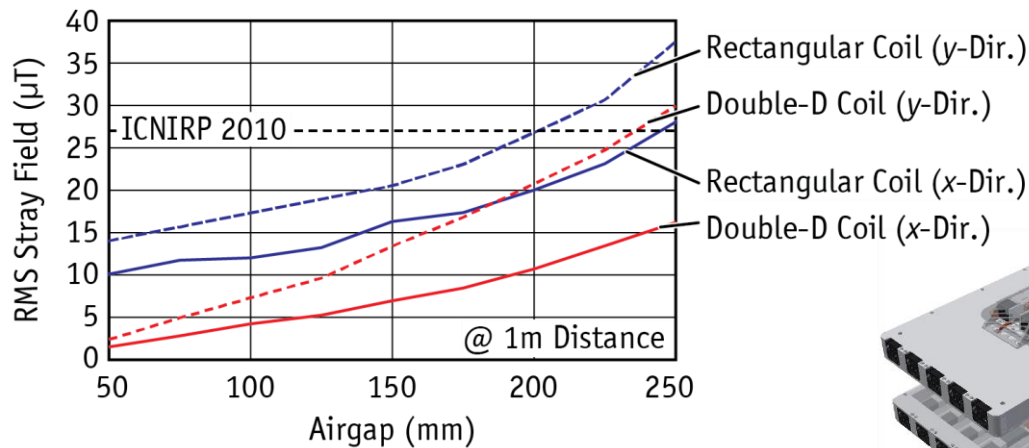
Total Losses: 1511 W



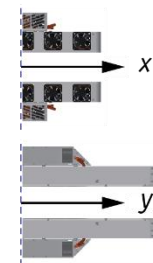
► Rectangular vs. DD Coil – Stray Field

■ Magnetic Stray Field in at Given Reference Position (1 m Distance)

- Note: Coils are Designed for Same Operating Frequency

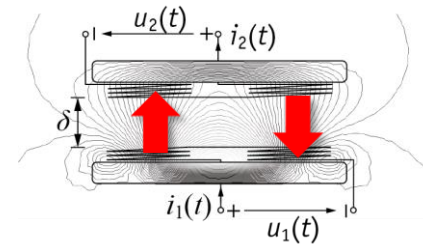
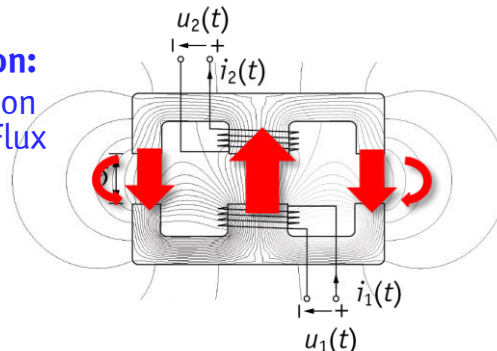


axis definitions:



■ Intuitive Explanation:

- Structural Integration of Return Path for Flux



► Summary of Comparison Results

■ Magnetic Coupling for Equal Coil Size

- Double-D and Rectangular Coil Reach Equal Coupling
- Decrease of Coupling at Misalignment shows no Clear Winner (DD better in x-Direction, Rect. Better in y-Direction)

■ Power Losses and Efficiency

- Power Losses in DD are higher due to Core Losses
- Remaining Loss Components are Similar

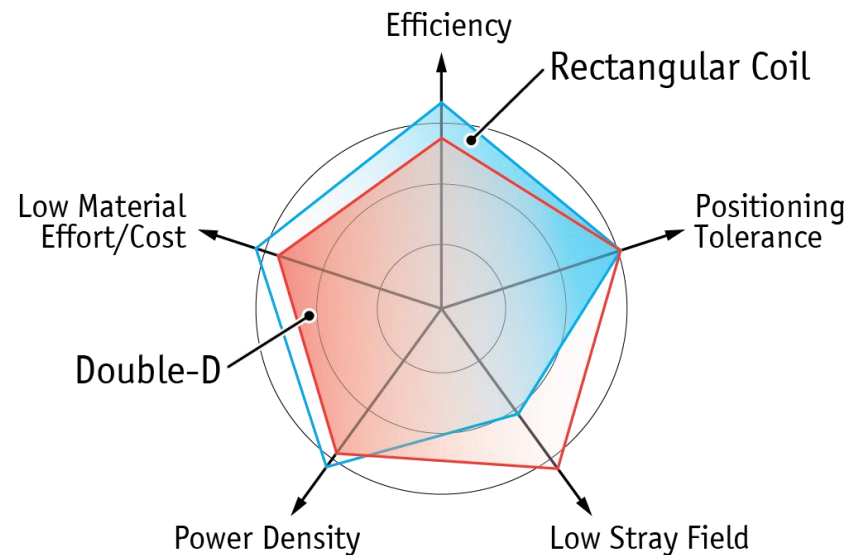
■ Material Effort/Cost

- Additional Cores were Required for DD
- Eddy Current Shield needed for Rect.

■ Stray Field

- Double-D has Lower Stray Field than Rectangular Coil

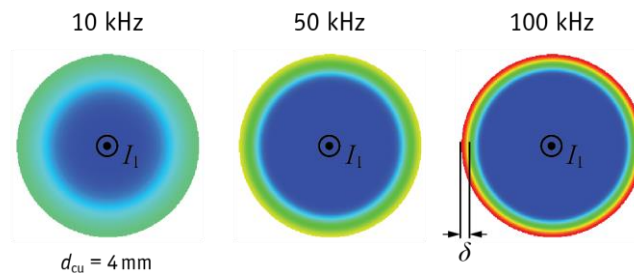
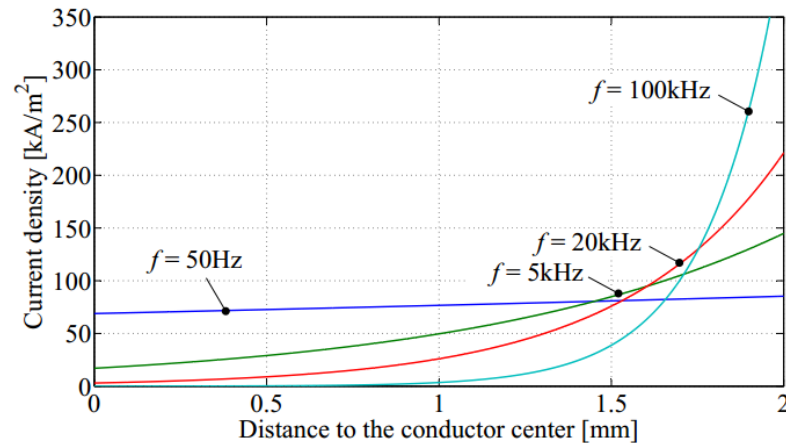
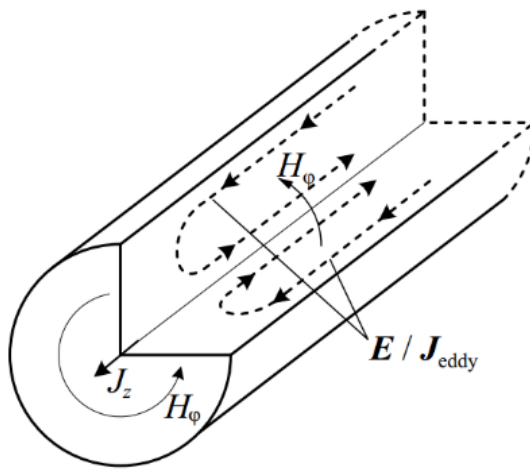
→ Will be Experimentally Verified!



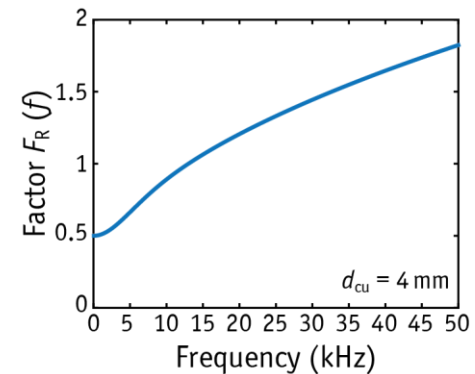
Coil Modeling: High-Frequency Winding Losses

► Winding Loss Calculation – Skin Effect

■ Frequency Dependent Current Distribution in Single Solid Conductor

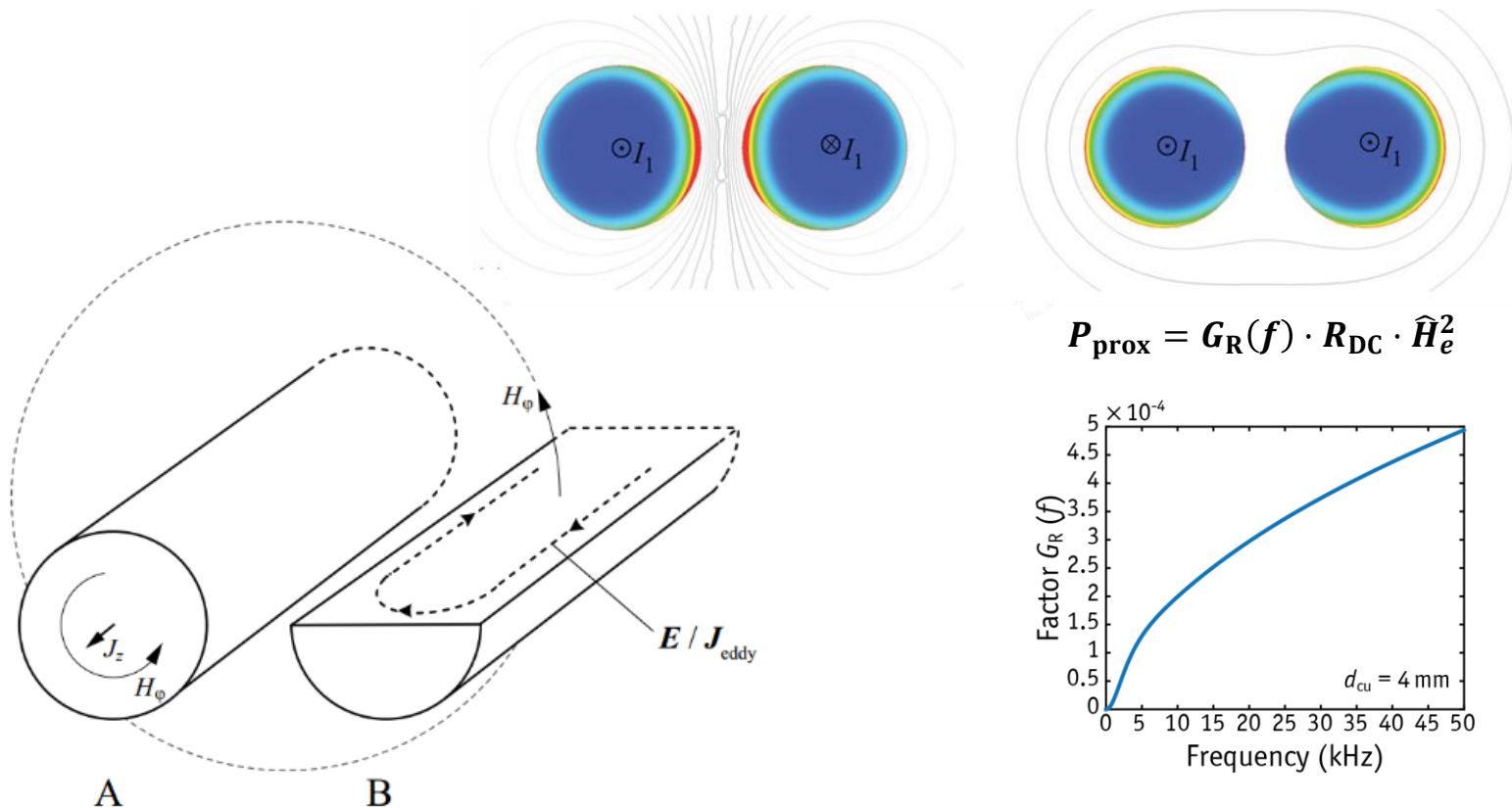


$$P_{\text{skin}} = F_R(f) \cdot R_{\text{DC}} \cdot \hat{I}^2$$



► Winding Loss Calculation – Proximity Effect

■ Frequency Dependent Current Distribution in Neighboring Solid Conductors



J. Mühlethaler, "Modeling and multi-objective optimization of inductive power components," Ph.D. dissertation, Swiss Federal Institute of Technology (ETH) Zurich, 2012.

► Winding Loss Calculation in Litz Wires

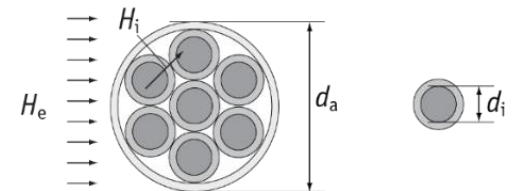
- Calculate Winding Losses in Litz Wire with n Strands, Strand-Diameter d_i & Outer Diameter d_a
 - Skin-Effect Calculated for each Strand Individually and Summed up

$$P_{\text{skin}} = n \cdot F_R(f) \cdot R_{\text{DC}} \cdot \left(\frac{\hat{I}}{n}\right)^2$$

n ... Number of Strands
 R_{dc} ... Strand DC-Resistance
 d_i ... Strand Diameter
 d_a ... Outer Wire Diameter

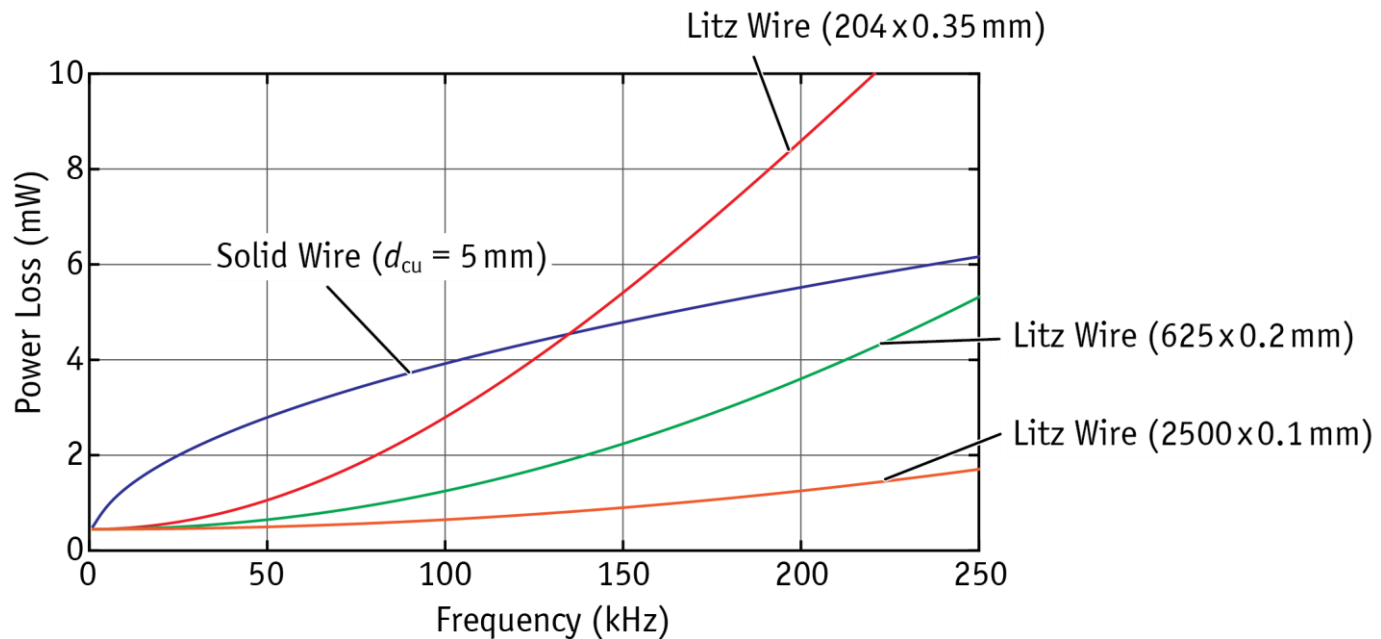
- For Proximity-Effect Bundle-Level Effects must be Included
 - Internal Proximity ... Effect of Currents in other Strands
 - External Proximity ... Effect of External Magnetic Field (e.g. due to Air Gap)

$$P_{\text{prox}} = \underbrace{n \cdot G_R(f) \cdot R_{\text{DC}} \cdot \hat{H}_e^2}_{\text{External Proximity}} + \underbrace{n \cdot G_R(f) \cdot R_{\text{DC}} \cdot \left(\frac{\hat{I}}{\sqrt{2}\pi d_a}\right)^2}_{\text{Internal Proximity}}$$



► Comparison: Solid Wire vs. Litz Wire

- Power Loss per 1 m of Solid or Litz Wire at $\hat{I} = 1$ A with $H_{\text{ext}} = 0$ A/m
 - Only Internal Proximity Effect (no External Field)



- If Litz Wire is Operated far from "intended" Operating Frequency, Solid Wire can become Better Option due to Internal Proximity Effect in Litz Wire Bundles

► Example 1: Transformer Winding Losses

■ Power Loss Calculation for Transformer with Litz Wire Windings

- External Magnetic Field (Simplified):

$$|H_{e,RMS}| \approx \begin{cases} \frac{N_p I_{p,RMS}}{b_c} \cdot \frac{k_p - 1/2}{k_{p,max}} & \dots \text{primary side: } k_p = 1, 2, 3 \\ \frac{N_s I_{s,RMS}}{b_c} \cdot \frac{k_s - 1/2}{k_{s,max}} & \dots \text{secondary side: } k_s = 1, 2 \end{cases}$$

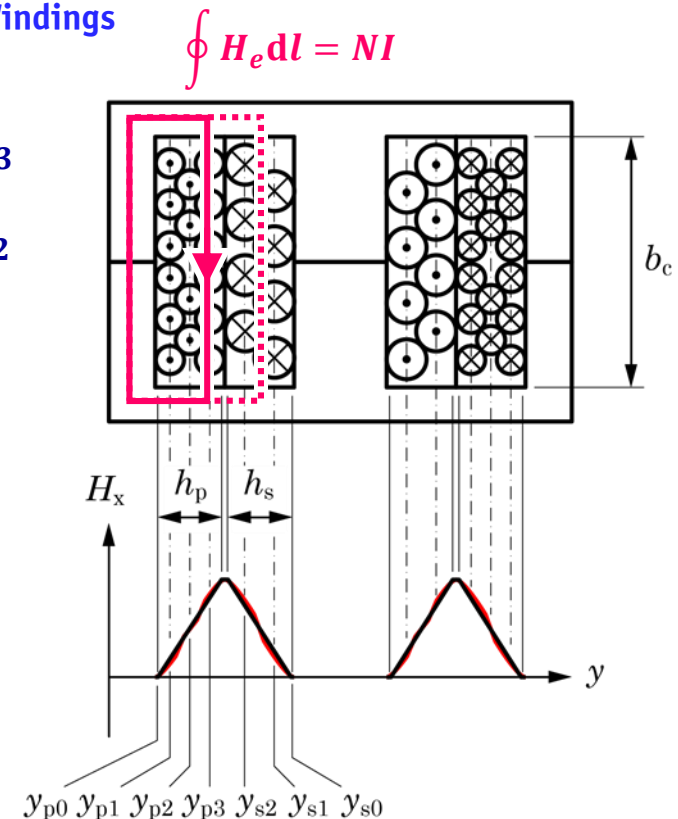
- AC-Resistance of Single Turn of Primary Winding:

$$R_{AC,turn}(k) = \frac{R_{DC}}{N} \cdot \left[2F_R + 2G_R \cdot \left(\frac{N}{b_c} \cdot \frac{2k-1}{2k_{max}} \right)^2 \right]$$

$$R_{DC} \approx \frac{4Nl_{avg}}{\sigma \pi d_{Cu}^2}$$

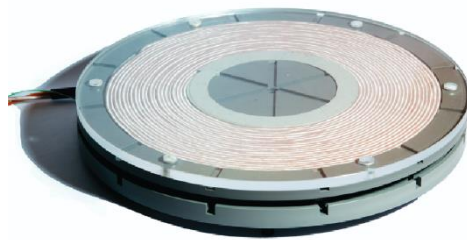
- Equations for F_R and G_R from Literature, e.g.:

J. Mühlethaler, "Modeling and multi-objective optimization of inductive power components," Ph.D. dissertation, Swiss Federal Institute of Technology (ETH) Zurich, 2012.

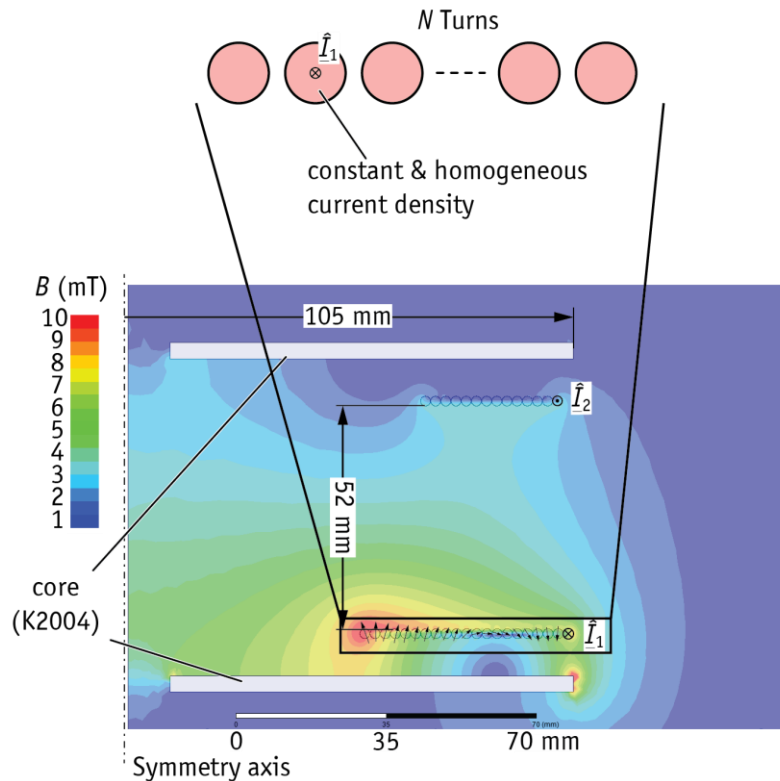


► Example 2: FEM-Based Loss Model of 5 kW Prototype

- **Analytical Field-Calculation not Possible**
 - Core Material / (Asymmetric Geometry)
- **Calculation with Finite Element Method**
 - Extraction of H -Fields for Proximity Losses



▲ 5 kW Prototype IPT Coil



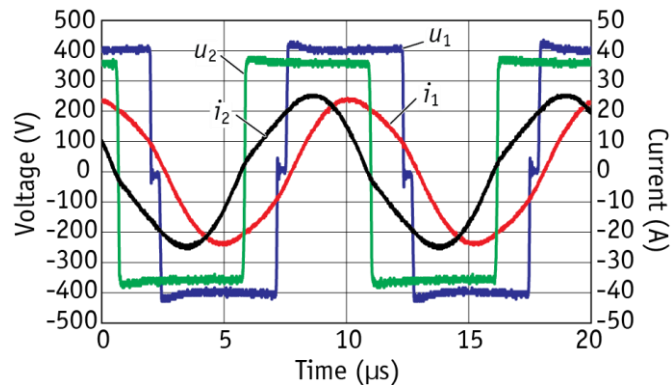
R. Bosshard, J. W. Kolar, J. Mühlethaler, I. Stevanovic, B. Wunsch, F. Canales, "Modeling and η - α -Pareto optimization of inductive power transfer coils for electric vehicles," *IEEE J. Emerg. Sel. Topics Power Electron.*, vol. 3, no. 1., pp.50-64, March 2015.

- **2D-Finite Element Solvers:**
 - FEMM (free, www.femm.info)
 - Ansys Maxwell, COMSOL, ...

► Fundamental Frequency Model

■ Resonant Tank: Highly Selective Bandpass Characteristic

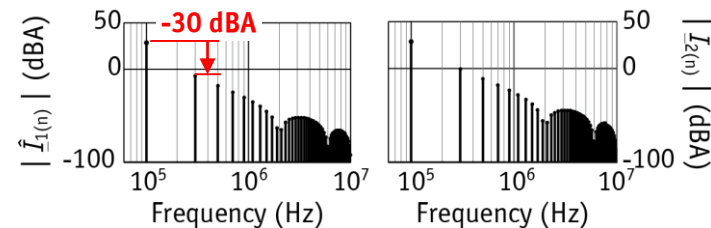
- Filtering Effect on Rectangular Switched Voltage
- Almost Sinusoidal Currents in Transmission Coils



▲ Measured voltage and current waveforms at 5 kW

■ Fundamental Frequency Model Sufficient

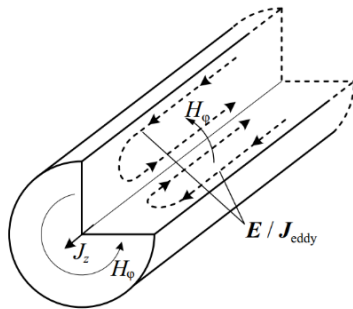
- Frequency Domain FEM
- Simplified Analytical Calculations



▲ Calculated spectra of the coil currents

► High-Frequency Copper Losses in Litz Wire

■ Skin-Effect Calculated Analytically (as for Transformer)

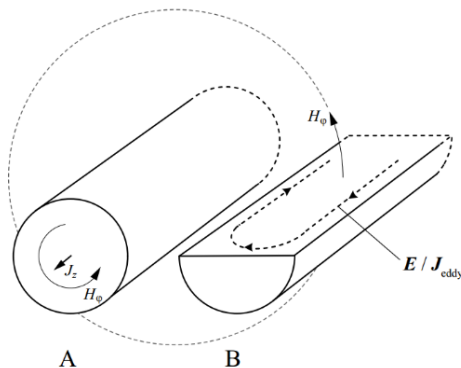


$$P_{\text{skin}} = n \cdot F_R(f) \cdot R_{\text{DC}} \cdot \left(\frac{\hat{I}}{n} \right)^2$$

n ... Number of Strands
 R_{dc} ... Strand DC-Resistance
 d_i ... Strand Diameter
 d_a ... Outer Wire Diameter



■ Proximity-Effect Calculation with External Magnetic Field from FEM Results



■ Extracted from FEM Results

- Evaluation in Center-Point of Each Turn to Isolate External Field

$$P_{\text{prox}} = \underbrace{n \cdot G_R(f) \cdot R_{\text{DC}} \cdot \hat{H}_e^2}_{\text{External Proximity}} + \underbrace{n \cdot G_R(f) \cdot R_{\text{DC}} \cdot \left(\frac{\hat{I}}{\sqrt{2}\pi d_a} \right)^2}_{\text{Internal Proximity}}$$

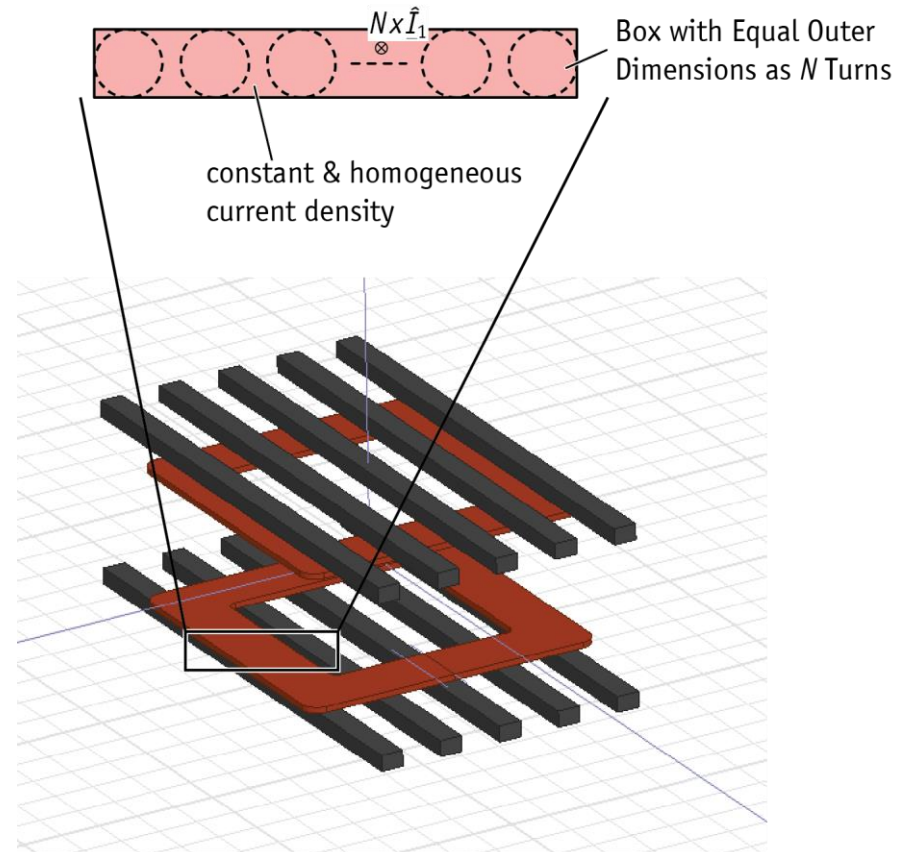
► Example 3: Analytical Loss Model of 50 kW Prototype

■ 3D Coil Design w/o Symmetry

- Resolution of Winding Details requires Long Simulation Time
- Winding Modeled as Box for accurate Field Calculation on Outside (Core Loss, Stray)
- Magnetic Field inside Box Incorrect



▲ 50 kW Prototype IPT Coil



▲ 3D-FEM Model of Tx and Rx Coil

► Measurement of Inductance & Coupling

■ Verification of Inductance Calculation

- Excitation with Linear Amplifier (6 A_{pk}, 85 kHz)
- Inductance Measured with Power Analyzer and with Impedance Analyzer
- Induced Voltage Measured with Diff. Probe

■ Measured: $L_1 = 66.3 \mu\text{H}$, $k = 0.230$

■ Calculated: $L_1 = 67.6 \mu\text{H}$, $k = 0.233$

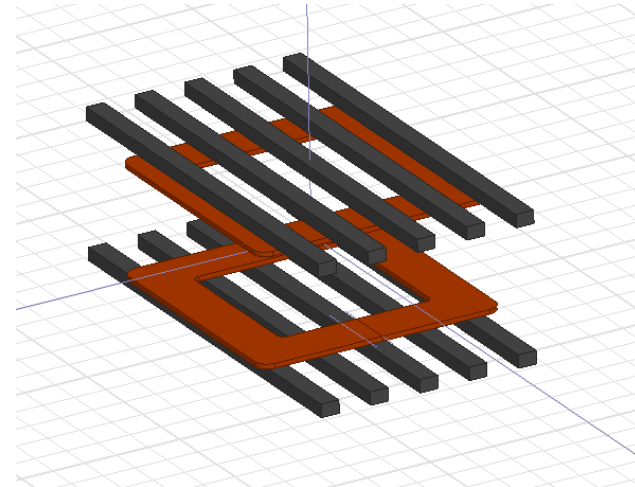
→ High Accuracy Despite Simplifications!



▲ Yokogawa WT3000



▲ 50 kW Prototype IPT Coil



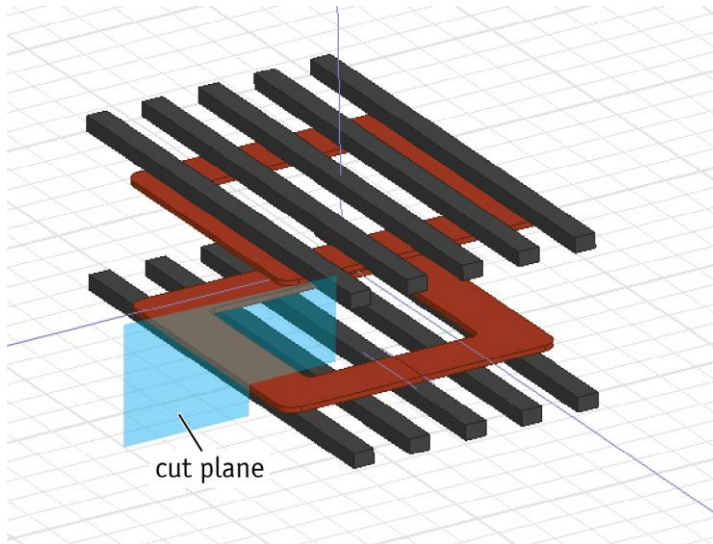
▲ 3D-FEM Model of Tx and Rx Coil

► Estimation of Proximity Effect (1)

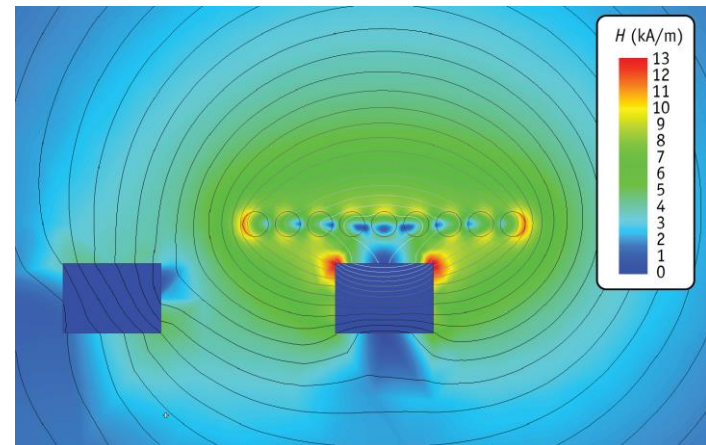
- **H-Field Inside Conductors is Needed to Estimate Proximity Effect**
 - Not Available if Winding Modeled as "Box"

$$P_{\text{prox,ext}} = n \cdot G_R(f) \cdot R_{\text{DC}} \cdot \hat{H}_e^2$$

Unknown!



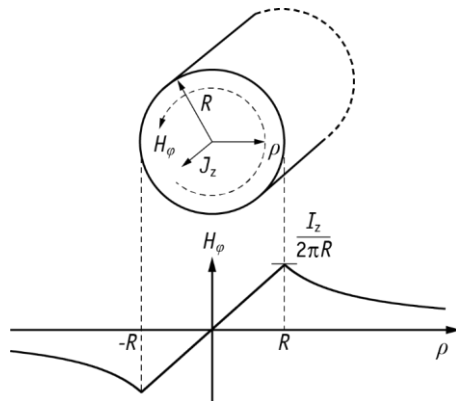
■ Approximation with 2D-Cut Plane



▲ 2D-FE Simulation of Field in Cut Plane

► Estimation of Proximity Effect (2)

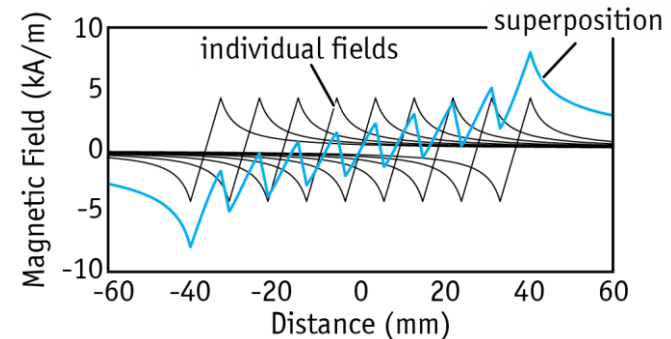
■ Approximation: Analytical Calculation of H -Field in Conductors



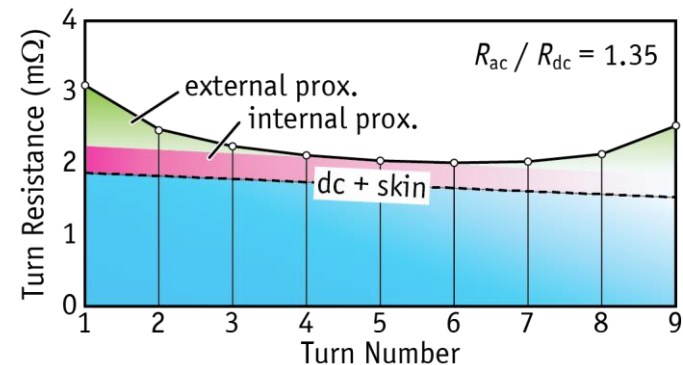
$$H_\phi(\rho) = \begin{cases} \frac{I}{2\pi R^2} \rho, & \text{if } |\rho| \leq R \\ \frac{I}{2\pi \rho}, & \text{if } |\rho| > R \end{cases}$$

■ Assumptions:

- Ferrite Cores are Neglected
- No Losses due to Receiver Coil
- Corner-Effects Neglected
- Ideally Twisted Litz Wire
- DC-Current Distribution only if $R \ll \delta$



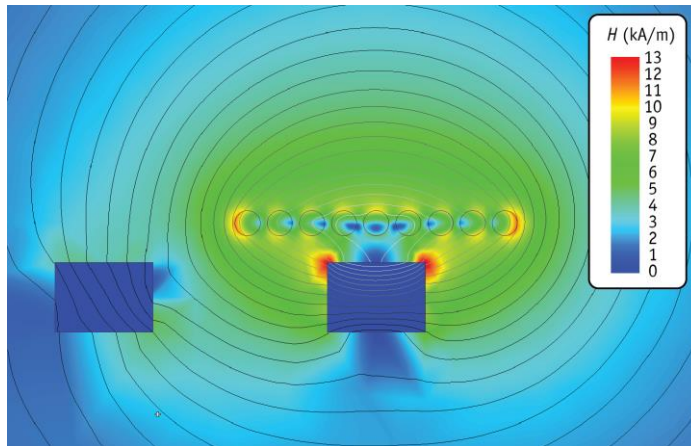
▲ Analytically calculation for 9 conductors



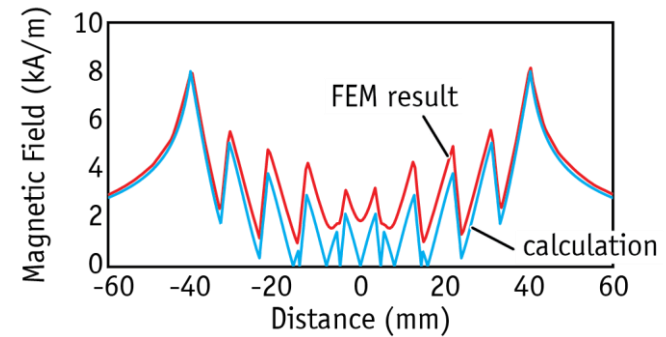
▲ Calculated AC resistance for each turn

► Estimation of Proximity Effect (3)

■ Comparison to 2D-FEM Simulation Including Core



▲ 2D-FE Simulation with Core Rods for Comparison



▲ Comparison of analytical calculation and FEM Simulation

- Core has only Minor Effect on Fields
- Approximation with 2D-Calculation to Estimate External Field

$$P_{\text{prox,ext}} = n \cdot G_R(f) \cdot R_{\text{DC}} \cdot \hat{H}_e^2$$

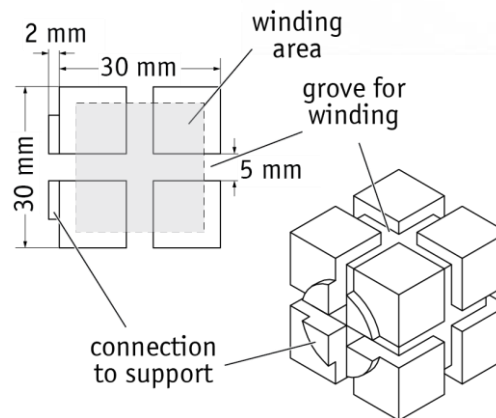
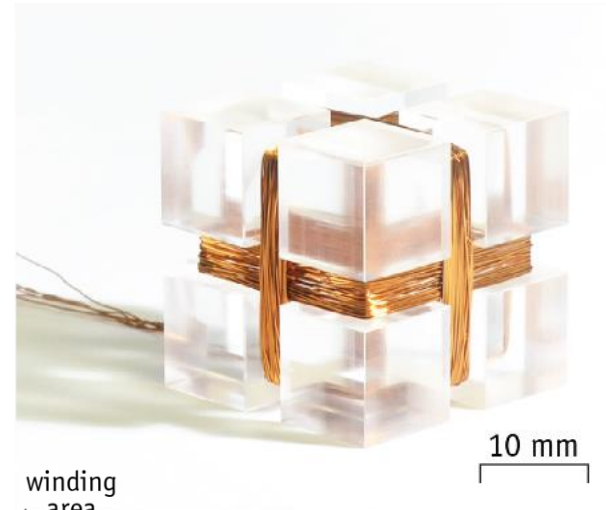
Calculated! —

► Verification of FEM Field Calculations (1)

R. Bosshard, J. W. Kolar, B. Wunsch "Accurate Finite-Element Modeling and Experimental Verification of Inductive Power Transfer Coil Design," Proc. 29th APEC, 2014.



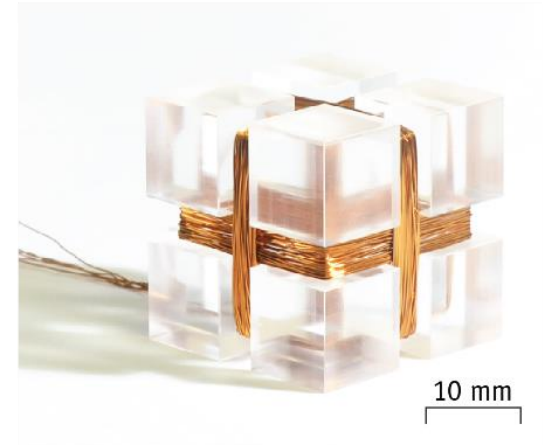
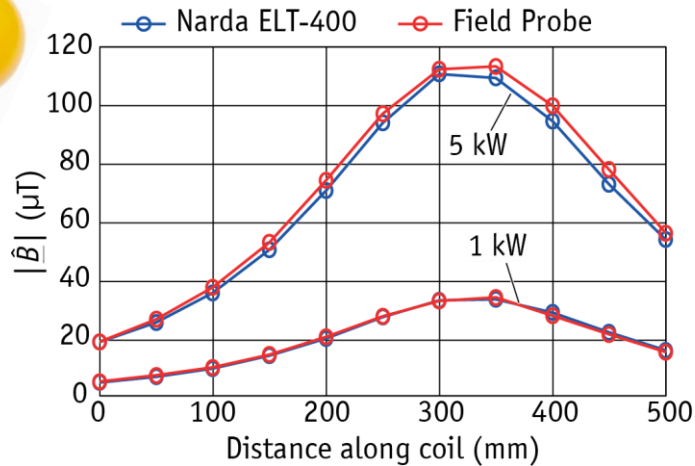
▲ Field probe ELT-400



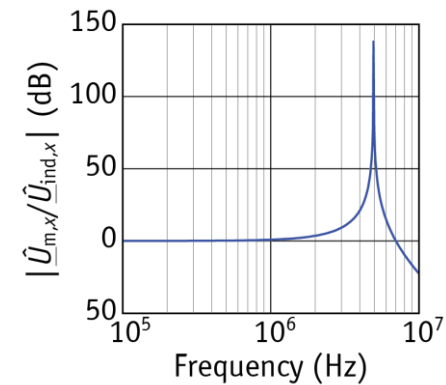
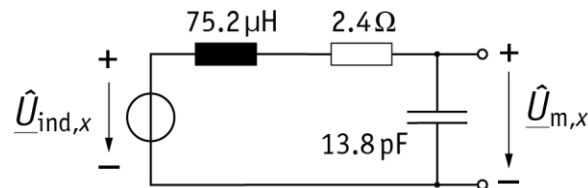
Number of Turns ... 40
Number of Layers ... 2
Wire Diameter ... 0.2 mm
Design Freq. ... 100 kHz
Sensitivity ... 15 mV/uT

► Verification of FEM Field Calculations (2)

R. Bosshard, J. W. Kolar, B. Wunsch "Accurate Finite-Element Modeling and Experimental Verification of Inductive Power Transfer Coil Design," Proc. 29th APEC, 2014.



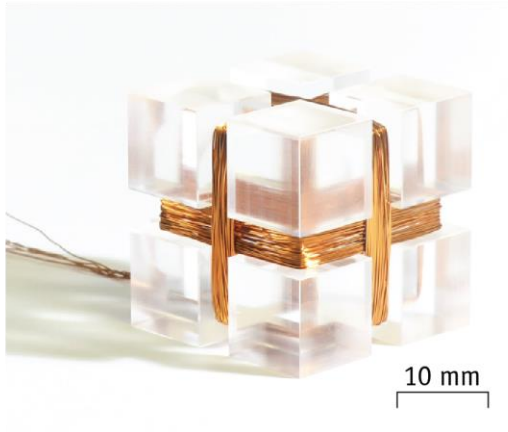
▲ Comparison to Commercial Product



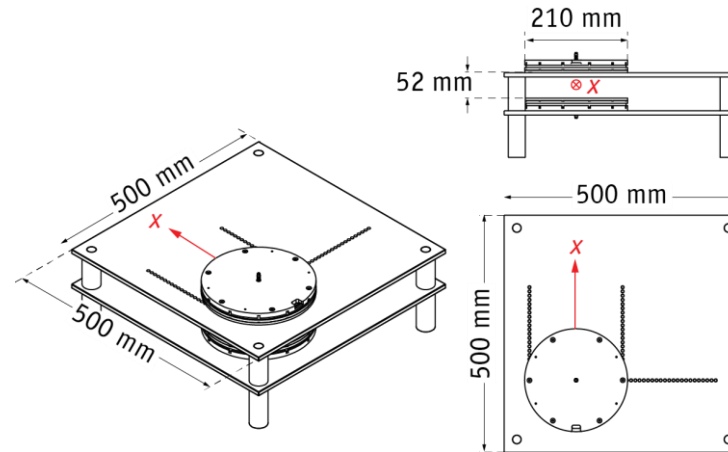
▲ Equivalent Circuit and Transfer-Function with Measured Parameters

R. Bosshard, J. W. Kolar, B. Wunsch "Accurate Finite-Element Modeling and Experimental Verification of Inductive Power Transfer Coil Design," Proc. 29th APEC, 2014.

► Verification of FEM Field Calculations (3)

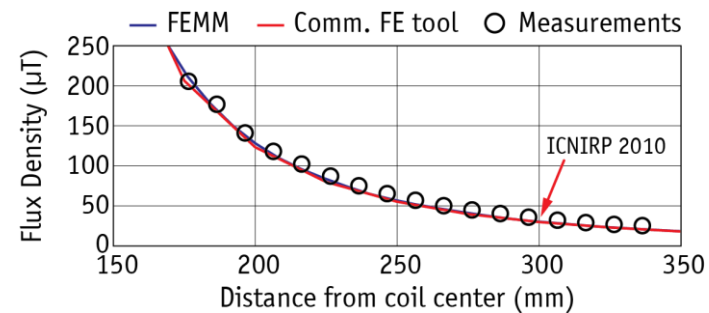


▲ Custom field probe for verification



■ Probe for Magnetic Field Measurements

- Optimized for 100 kHz, High Accuracy
- Sensitivity: 14.5 mV/ μ T @ 100 kHz
- Accuracy: < 5% Error (Comp. to ELT-400)
- Size: 30x30x30 mm

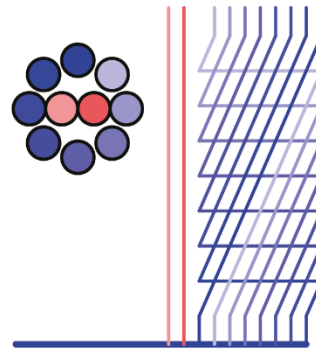
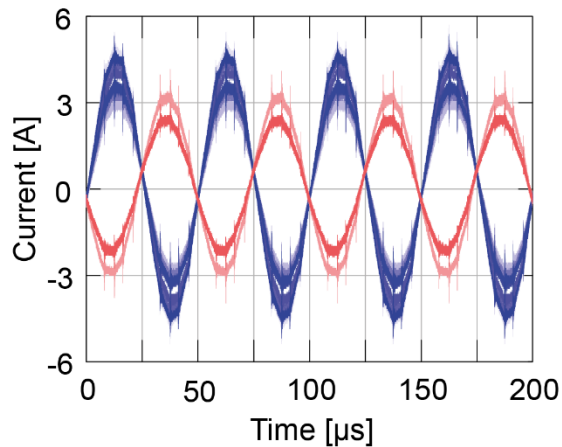


▲ Measured stray field @ 5 kW

Frequency Effects in Non-Ideal Litz Wire

► Copper Losses in Litz Wire – Asymmetric Twisting (1)

- Case study: Litz wire (tot. 9500 strands of 71 μ m each) with 10 sub-bundles
- Current distribution in internal litz wire bundles depends strongly on interchanging strategy



*G. Ortiz, M. Leibl, J. W. Kolar,
"Medium Frequency Transformers
for Solid-State Transformer
Applications — Design and
Experimental Verification", 2013.*

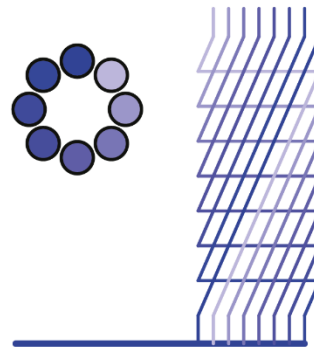
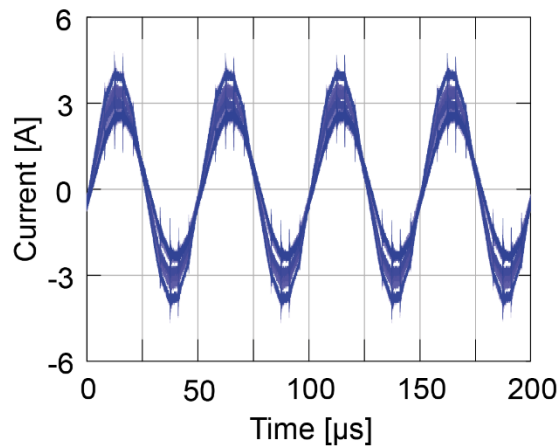


- Total copper losses for 10 bundles: 438W

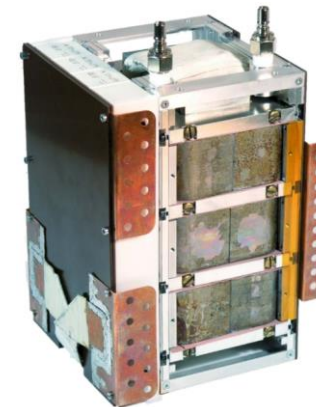
▲ 166 kW/20 kHz Transformer

► Copper Losses in Litz Wire – Asymmetric Twisting (2)

- Case study: Litz wire (tot. 9500 strands of 71 μ m each) with 10 sub-bundles
- Current distribution in internal litz wire bundles depends strongly on interchanging strategy



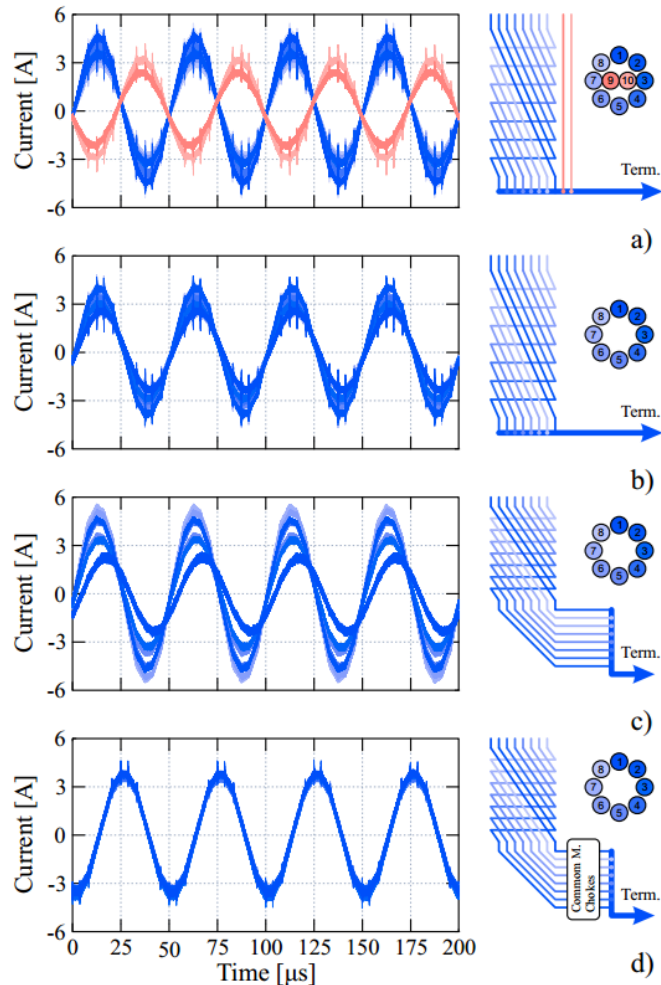
*G. Ortiz, M. Leibl, J. W. Kolar,
“Medium Frequency Transformers
for Solid-State Transformer
Applications — Design and
Experimental Verification”, 2013.*



- Total copper losses for 10 bundles: 438W
- Total copper losses for 8 bundles: 353W

▲ 166 kW/20 kHz Transformer

► Copper Losses in Litz Wire – Termination



Best Option

G. Ortiz, M. Leibl, J. W. Kolar,
“Medium Frequency Transformers
for Solid-State Transformer
Applications — Design and
Experimental Verification”, 2013.

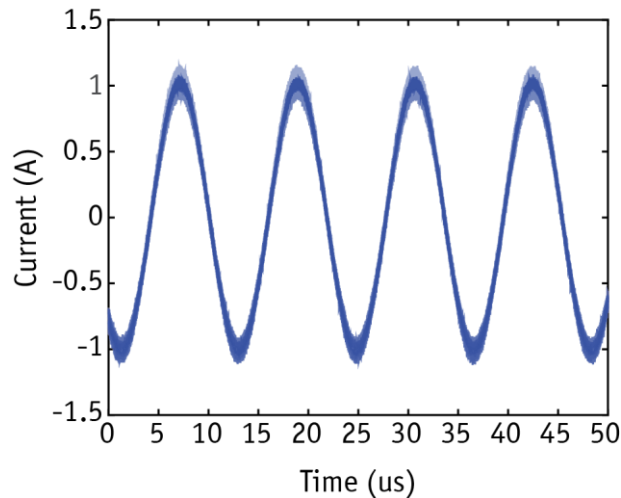


▲ Termination of Litz Wire Bundels
with Common-Mode Chokes

► Copper Losses in Litz Wire – Symmetric Twisting

■ 2nd Example: Measurement of 2500 x 0.1 mm Litz Wire at 85 kHz

- Stranding: 5x5x4x25 Strands of 0.1 mm
- No Common Mode-Chokes are Needed with Symmetric Twisting
- Termination: Standard Cable Shoe (Soldered)



▲ Equal Current Distribution at 85 kHz
Measured in Actual Coil Arrangement

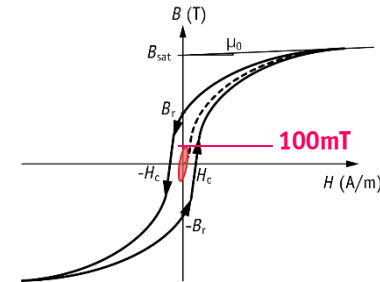


Coil Modeling: High-Frequency Core Losses

► Core Materials for IPT Coils (1)

■ Power Ferrites (e.g. Manganese-Zinc)

- Lowest Core Losses at High-Frequency (20 ... 150 kHz)
- Saturation Typically not Limiting Factor
- Low Specific Weight: 4-5 g/cm³
- Sintering / Tooling: Arbitrary Shape
- Isotropic Material: Flux in any Direction



▲ Schematic drawing of BH-loop

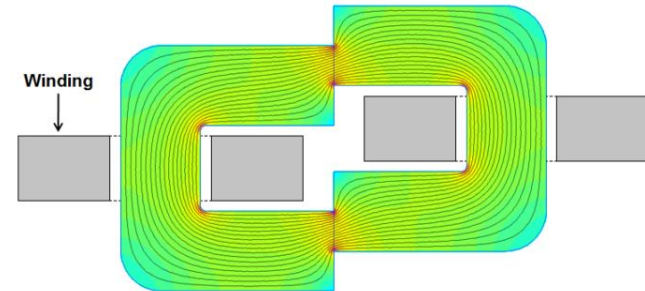


CMI Ferrite, www.cmi-ferrite.com, (6.11.2014).

► Core Materials for IPT Coils (2)

■ Tape Wound Cores

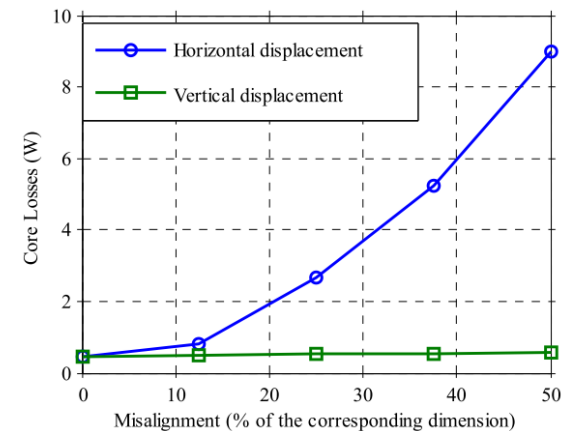
- Custom Shapes with Tape Winding
- High Losses at Frequency $> 20..50$ kHz
- Higher Specific Weight: $7-8 \text{ g/cm}^3$
- **Anisotropic: Orthogonal Flux Causes Losses (Similarly: Litz-Wire and no Foil-Windings!)**



Tape wound core



Ferrite core

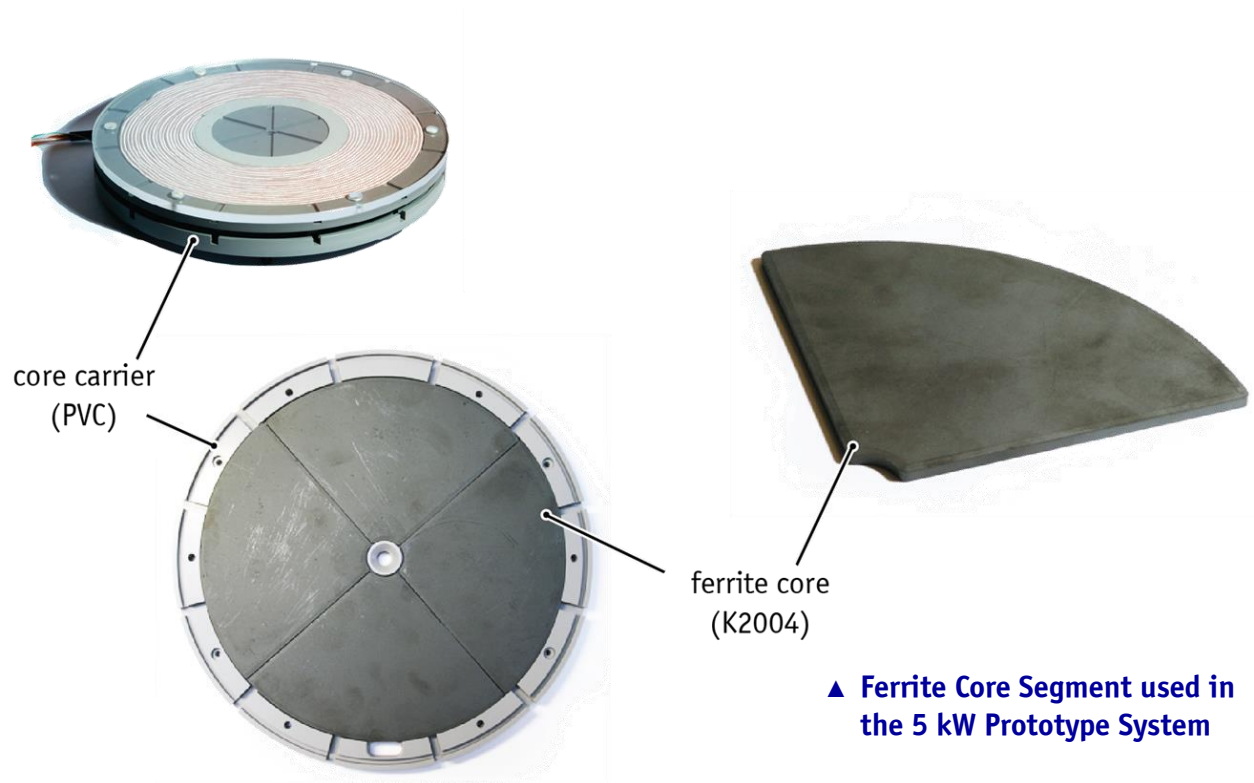


B. Cougo, J. Mühlethaler, J. W. Kolar, "Increase of Tape Wound Core Losses due to Interlamination Short Circuits and Orthogonal Flux Components", 2011.

► Core Segments for Circular Spiral Coil

■ 5 kW Prototype IPT Coil – Core Construction

- MnZn Power Ferrite (K2004: 300 mW/cm^3 , $B_{\text{sat}} = 455 \text{ mT}$, 4.8 g/cm^3)
- Off-the-Shelf 90°-Ferrite Segments
- Typical Application: Induction Cooking

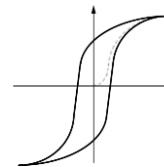
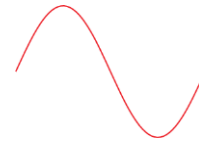


▲ Ferrite Core Segment used in the 5 kW Prototype System

► Core Loss Calculation – General

■ Calculation of Core-Loss Density According to Current Waveform

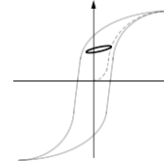
Sinusoidal



Steinmetz Equation

→ Sinusoidal w/o DC-Offset

DC Current +
HF Ripple

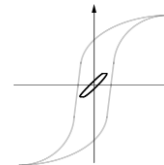
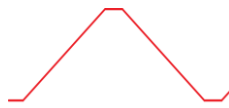


Generalized Versions of the Steinmetz Equation (iGSE, i²GSE)

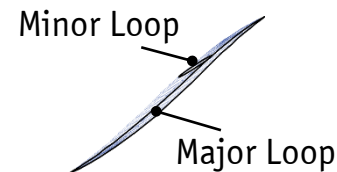
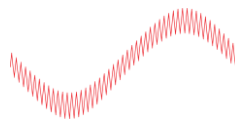
→ Arbitrary Waveform & DC-Offset

→ Relaxation Effects

Non-Sinusoidal
AC Current



Sinusoidal Current +
HF Ripple

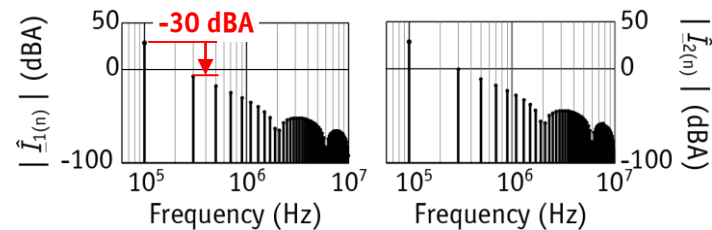


Superposition of Losses due to Minor and Major Loops

► Core Loss Calculation for Sinusoidal Excitation

■ Requirements for Steinmetz Equation

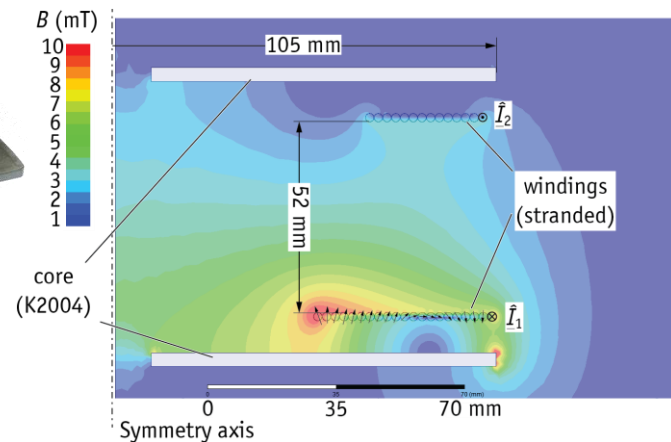
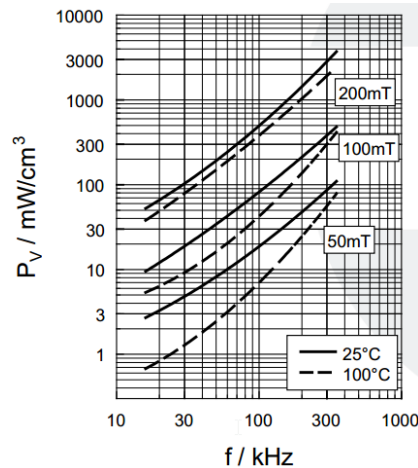
- Sinusoidal Current Excitation
- Parameters Only Valid in Limited Frequency / Flux Density Range!



▲ Calculated spectra of the coil currents

■ Core Loss Calculation with FEM Possible

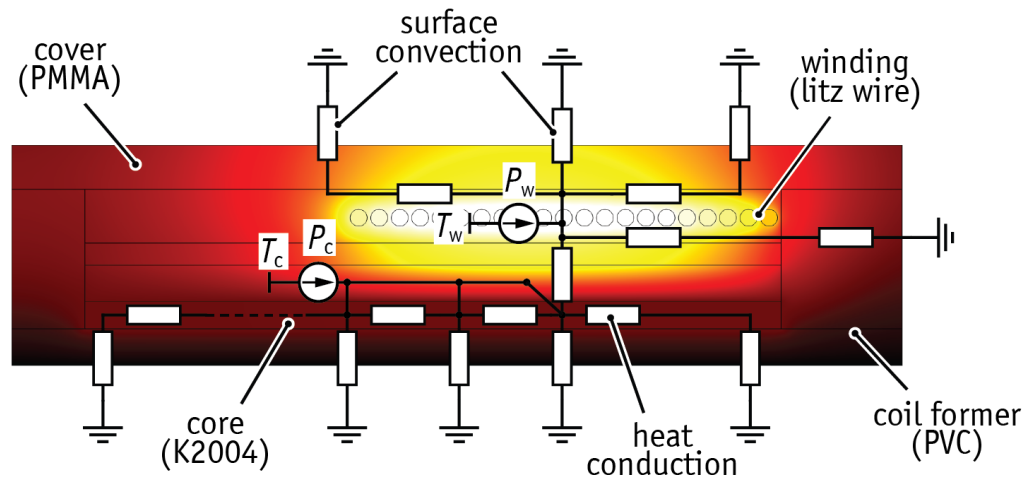
- Integration of Steinmetz Equation over Core Volume Directly within FEM Tool



Thermal Modeling

► Thermal Modeling

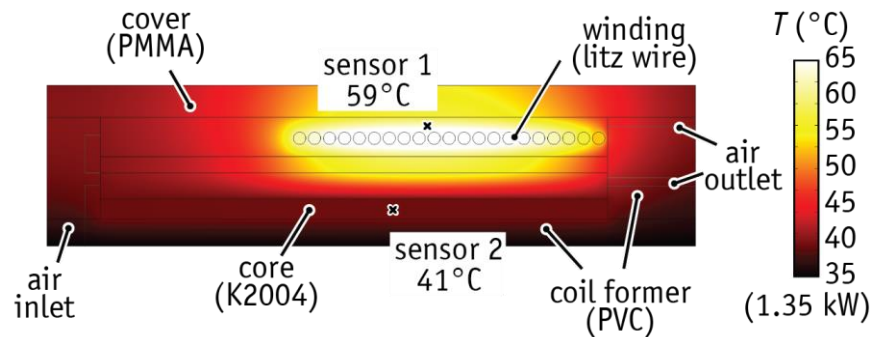
■ Include Thermal Feedback to Model Temperature Effects on Losses



■ Modeling Options:

- Detailed Thermal Network incl. Heat Conduction, Convection at Surfaces
- Simplified Calculations using Surface Heat Transfer Coefficients from Literature
- Thermal Simulations with Thermal FEM Tools

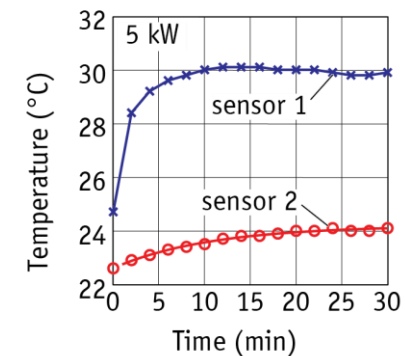
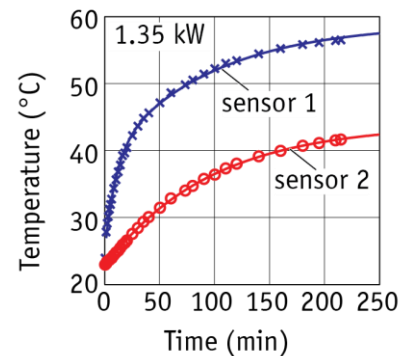
► Experimental Verification for 5 kW Prototype



▲ Thermal Simulation of 5 kW Prototype Coil

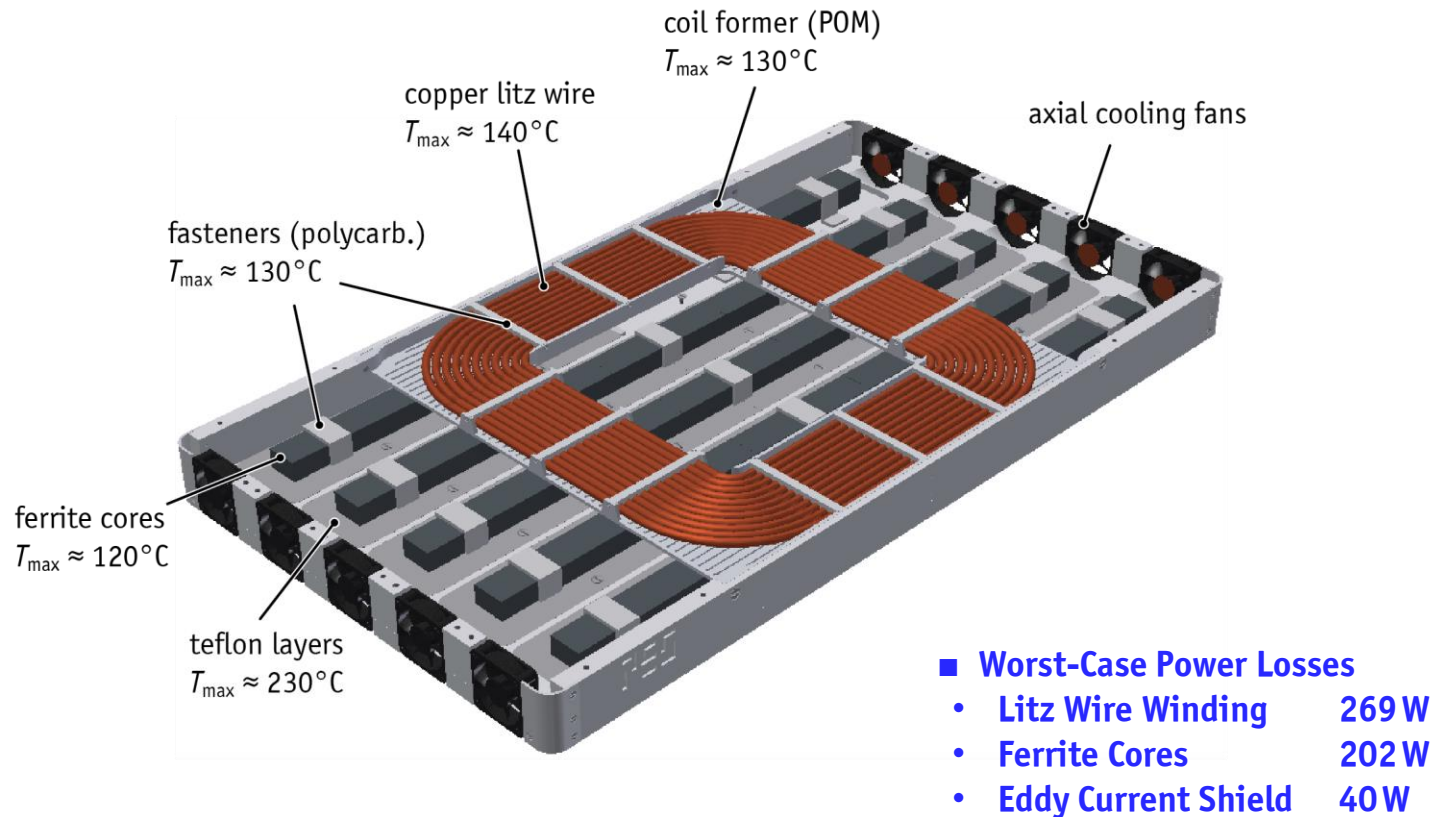
■ Temperature Measurements for Verification of Thermal FEM Results

- Accuracy: < 5% Error of Steady-State Temperature
- Surface-Related Power Losses of up to 0.2 W/cm^2 with Forced Air Cooling



▲ Thermal Measurements with Thermocouples (with/without Forced Air Cooling)

► Forced Air Cooling System of the 50 kW Prototype



*A. Van den Bossche and V. C. Valchev, Inductors
and transformers for power electronics.
New York: Taylor & Francis, 2005.*

► Estimation of Heat Transfer Coefficient



▲ Axial cooling fan for active cooling
of the windings and core elements

■ Empirical Equation for Surface Heat Transfer Coefficient:

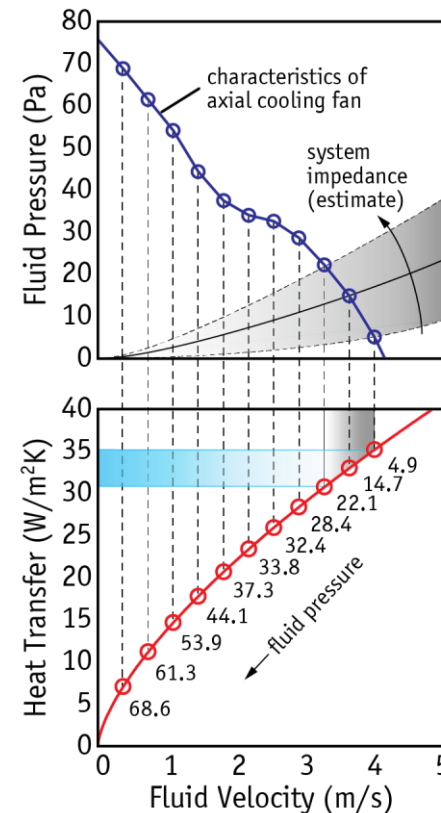
$$h_v \approx C \frac{\lambda_f}{d} \left(\frac{u_\infty d}{v_f} \right)^n Pr_f^{1/3}$$

λ_f, v_f, Pr_f ... conductivity, viscosity, Prantl number

u_∞ ... fluid velocity

d ... component height

C, n ... empirical geometry parameters
($C = 0.102, n = 0.675$)



▲ Heat Transfer Coefficient Estimated from
Fan Characteristics of AUB0524VHD

► Thermal Design with 3D-FEM

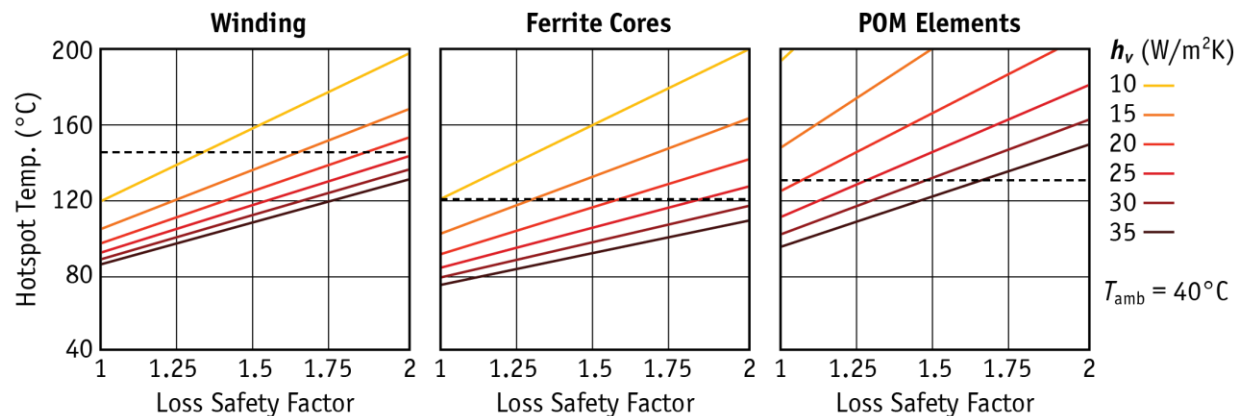
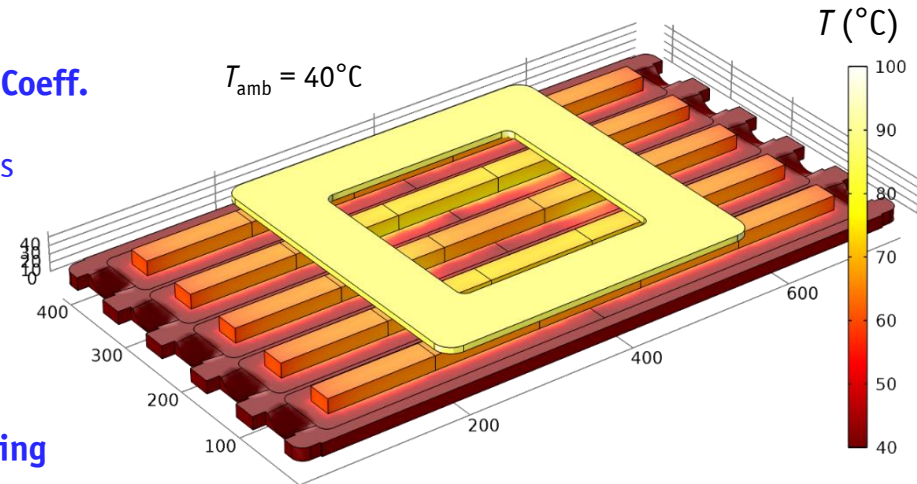
■ Heat Transfer in Solids with Estimated Coeff.

- 30 W/m²K ... active cooled surfaces
- 7.5 W/m²K ... convective cooled surfaces

■ Parameter Sweep in FEM Tool

- Heat Transfer Coefficient
- Loss Safety Factor: $P_{sim} = m_{safety} \cdot P_{calc}$

→ Design is Feasible at Surface-Related
Power Loss **0.2 W/cm²** with Active Cooling



▲ 3D-FEM Thermal Simulation: Results of Parameter Sweep

Resonant Capacitors

► Resonant Capacitors: Component Selection (1)

■ Polypropylene Film Capacitors for Resonant Applications

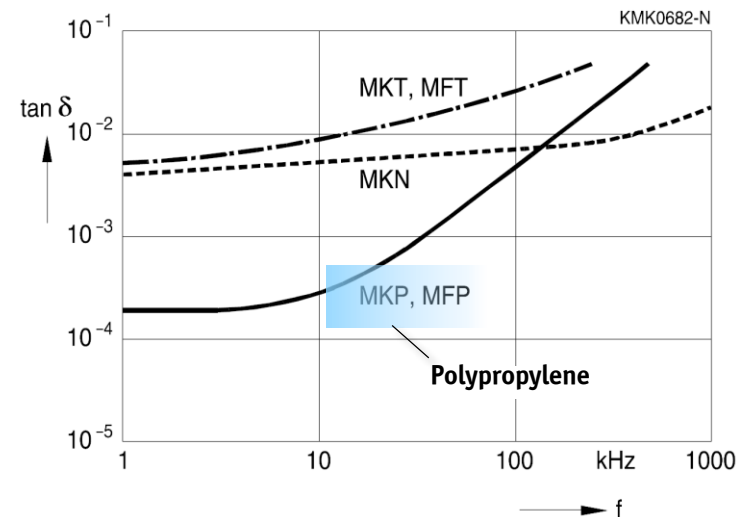
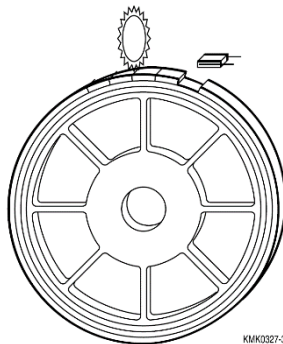
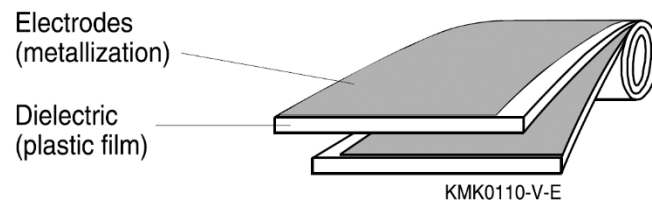
- Low $\tan(\delta) \rightarrow$ Low High-Frequency Losses
- Low Parasitic Inductance and *ESR*
- Least Affected by Temperature/Frequency/Humidity

MK/F * ... Metallized Plastic Film / Metal Foil

***T* ... Polyester

***P* ... Polypropylene

***N* ... Polyethylene Naphthalate



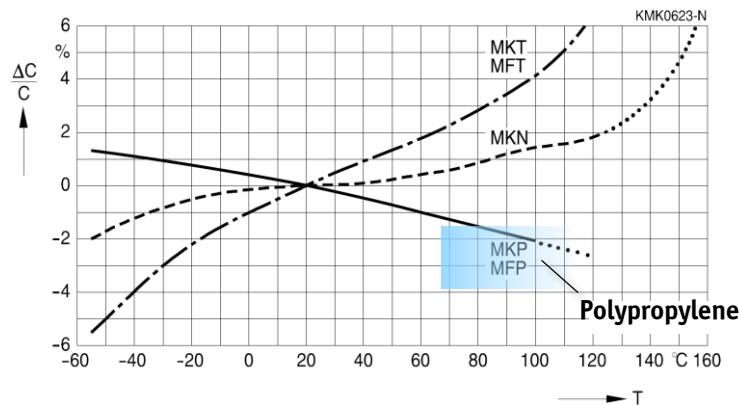
▲ Datasheet Values of $\tan(\delta)$ in Function of Frequency for EPCOS Film Capacitors

EPCOS, Film Capacitors
Data Handbook, 2009.

► Resonant Capacitors: Component Selection (2)

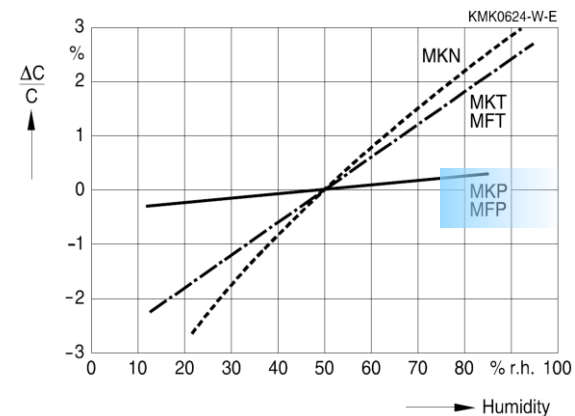
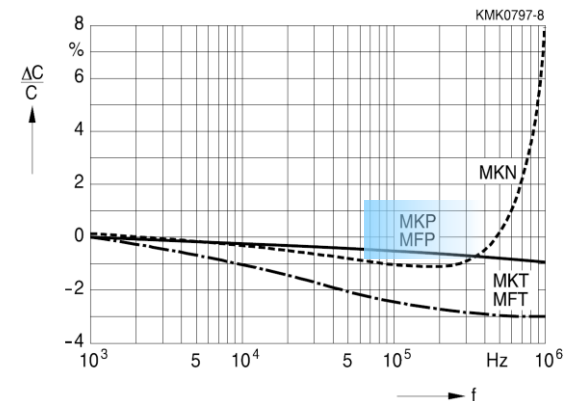
■ Polypropylene Film Capacitors for Resonant Applications

- Low $\tan(\delta) \rightarrow$ Low High-Frequency Losses
- Low Parasitic Inductance and *ESR*
- Least Affected by Temperature/Frequency/Humidity



▲ Typical Material Characteristics for Film Capacitors (EPCOS)

EPCOS, Film Capacitors
Data Handbook, 2009.



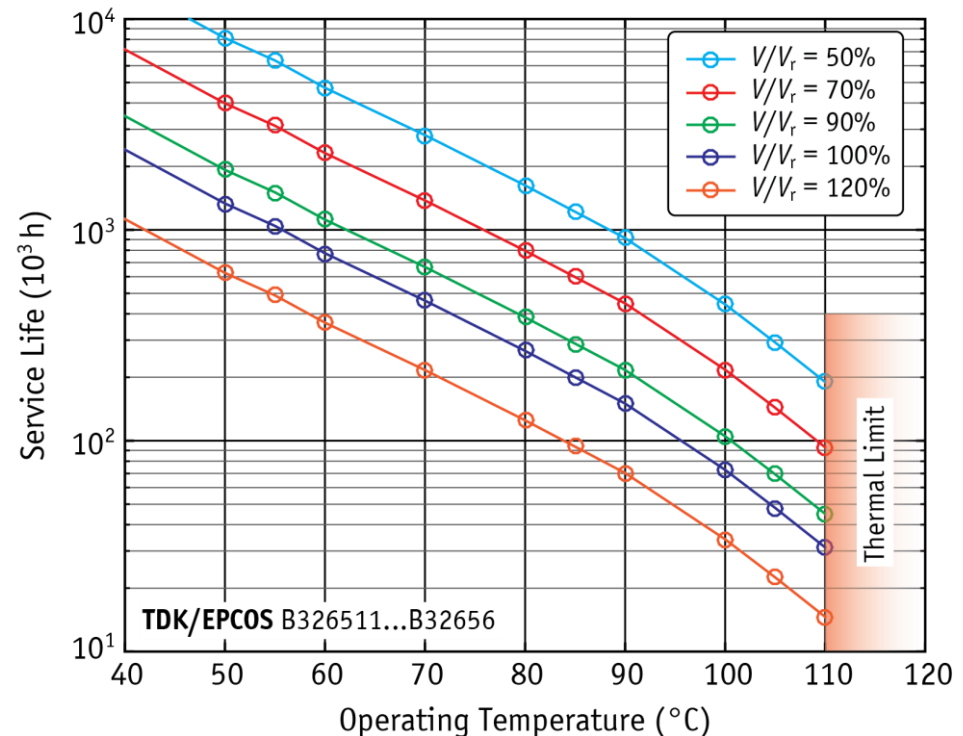
► Capacitor Service Life vs. Temperature & Voltage

■ Service-Life of Film Capacitors Strongly Depends on Operating Temperature and Voltage Utilization

$$t_{\text{life}}(T, V) = t_{\text{life},0} \cdot \frac{1}{\pi_T} \cdot \frac{1}{\pi_V}$$

T (°C)	π_T	V / V _R	π_V
≤ 40	1	10%	0.26
50	1.8	25%	0.42
55	2.3	50%	1.00
60	3.1	60%	1.42
70	5.2	70%	2.04
80	9	80%	2.93
85	12	90%	4.22
90	16	100%	6.09
100	33	110%	9.00
105	50	120%	13.00

▲ Arrhenius Law (Exponential Func.)



TDK/EPCOS Product Profile,
Film Capacitors for Industrial
Applications, 2012.

▲ Service Life vs. Operating Temperature for Different Levels of Voltage Utilization

► High-Power Polypropylene Film Capacitors

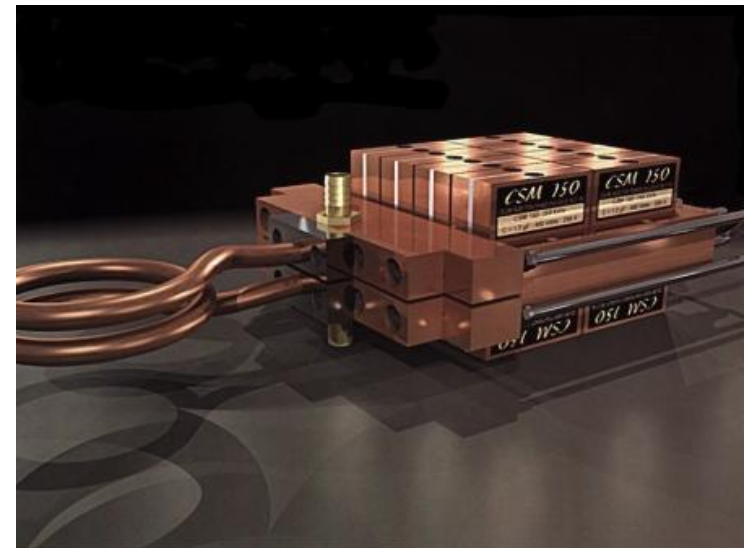
■ 50 kW IPT – Capacitor Requirements

- $> 100 A_{rms} / 3..4 kV_{rms} / 20..150 kHz$



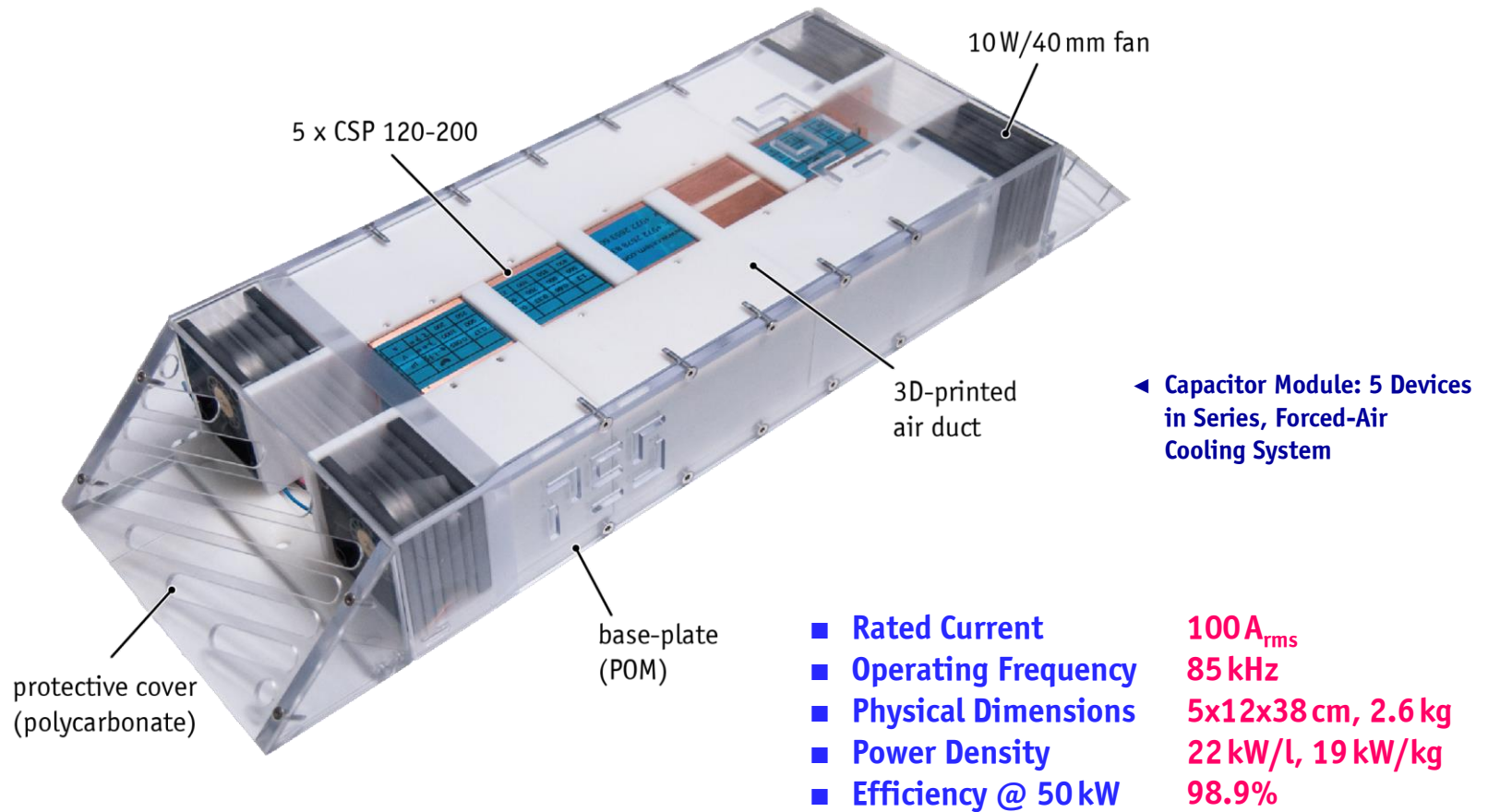
▲ CSP 120-200 Polypropylene Film Capacitor
(1.1 kV_{pk} / 100 A_{rms} / 1 MHz @ full power)

- Tangent-Delta: 1/1000 - 1/700
- High Power Density: 5.95 kVar/cm³
- Active Cooling: Water / Air @ 35% Power
- Typical Application: Induction Heating



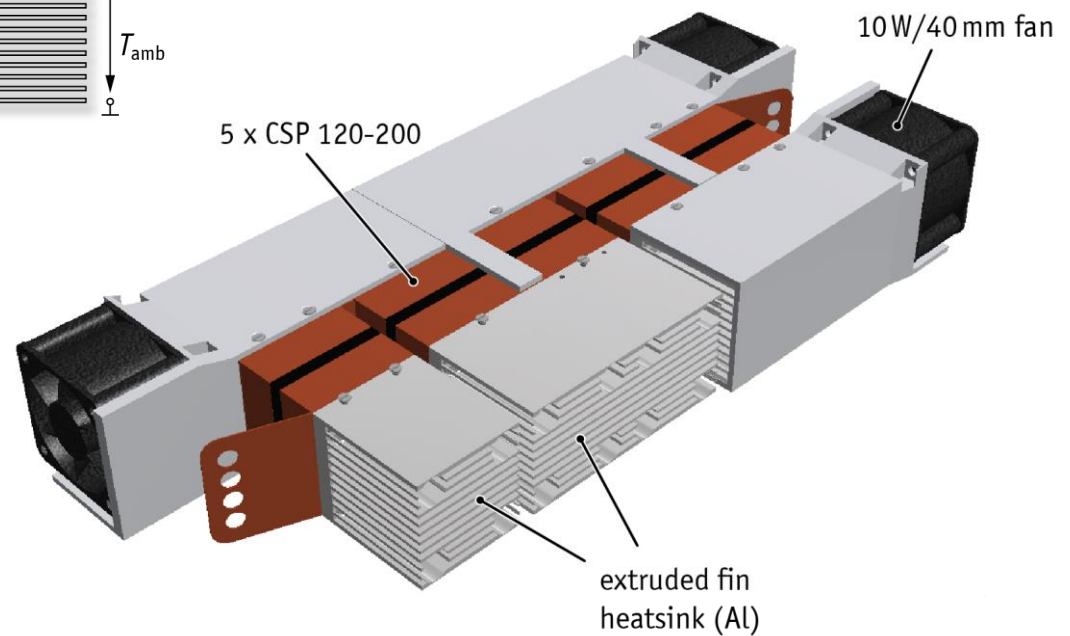
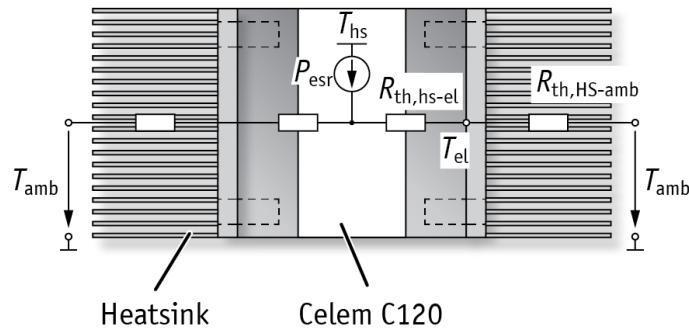
▲ Induction Heating System (www.celem.com)

► Resonant Capacitor Module for 50 kW



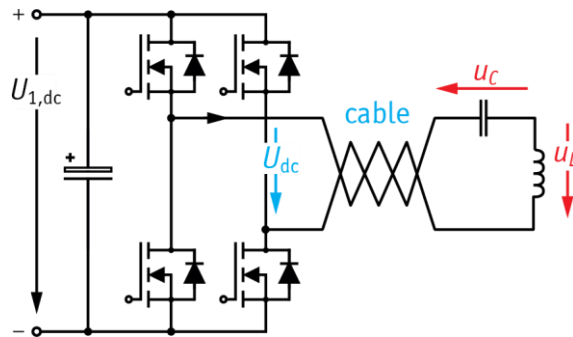
► Capacitor Module Cooling System

- **Forced-Air Cooling Required for Resonant Capacitors at 50 kW Operation**
 - Aluminum Extrudend Fin Heatsink Mounted to Capacitor Terminals

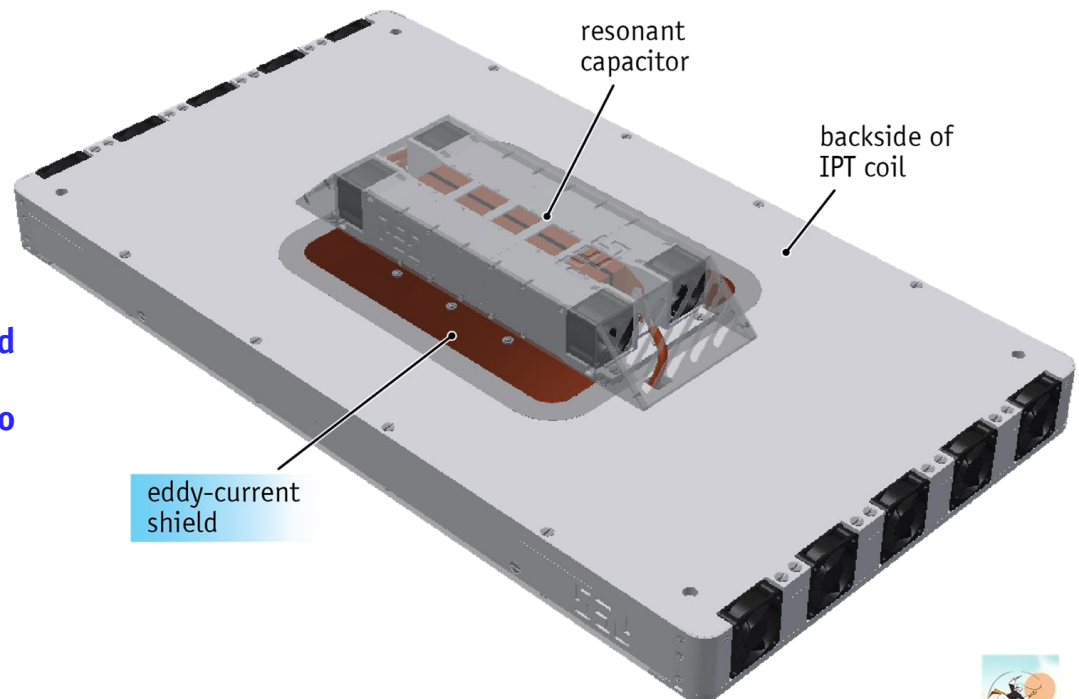


- **Rated Current** $100 A_{rms}$
- **Operating Frequency** $85 kHz$
- **Tangent-Delta** 1.5%
- **Power Losses** $314 W$

► Mounting of Capacitor Module on IPT Coil



- Compact Realization as Integrated IPT Coil & Capacitor Module
- Close Placement of Components to Limit EMI due to HF-Coil Current

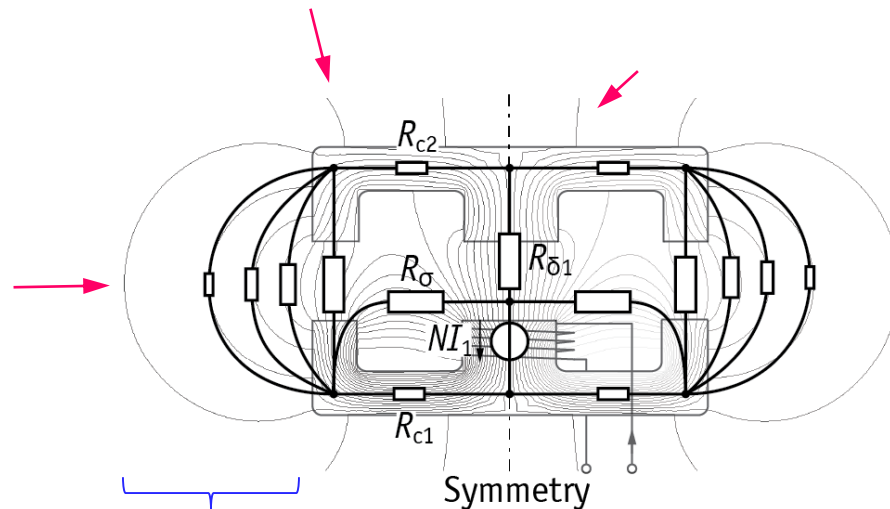


Magnetic Shielding

► Magnetic Shielding with *Magnetic Materials* (1)

■ Low Reluctance Path (=Core) Allows Guiding Magnetic Flux

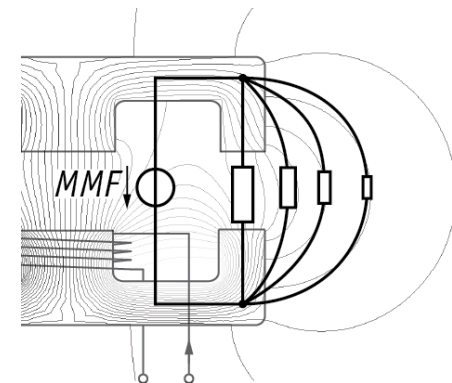
- Some Stray Field Remains due to Low Air Gap Reluctance, even at the Backside of the Coil
- "Complete" Shielding Requires kg's of Core Material



Magnetic Flux Follows
Low Reluctance Path:

$$R_{\delta 2} = \frac{l}{\mu_0 A}$$

■ MMF Across Air Gap is not influenced by the core

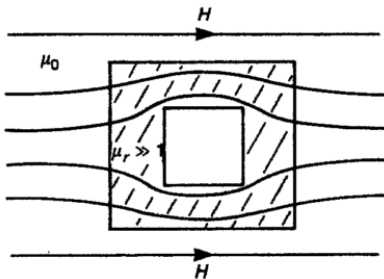


→ Core has no Effect on Stray Field
Horizontally Outside the Coil Area

► Magnetic Shielding with *Magnetic Materials* (2)

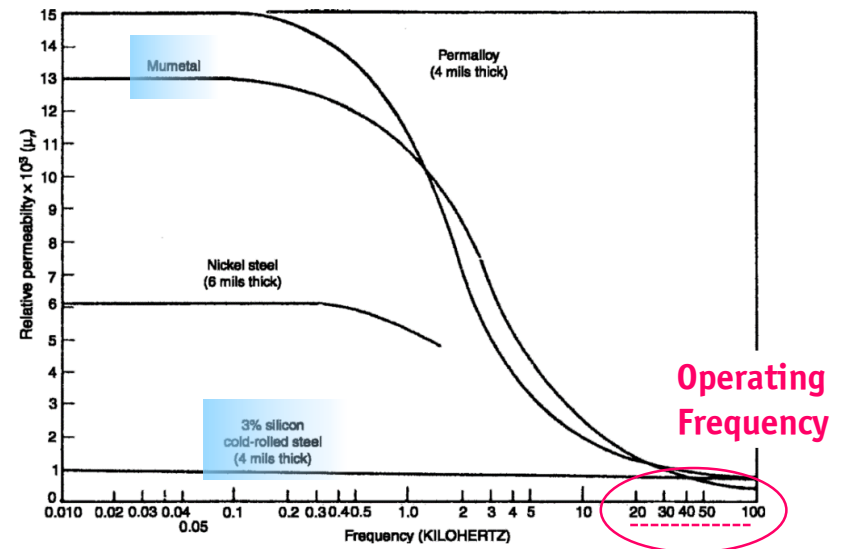
■ Save Weight, Use High Permeability Material ($\mu_r > 10'000$)?

- Machine Steel & Amorphous Iron: High Frequency Losses
- Permalloy: Strong Frequency Dependency and Low Saturation



▲ High-Permeability Material Attracts Magnetic Field

C. Paul, "Shielding," in *Introduction to Electromagnetic Compatibility*, 2nd ed., Jon Wiley & Sons, Hoboken, 2006, ch. 10, sec. 4, pp. 742-749.



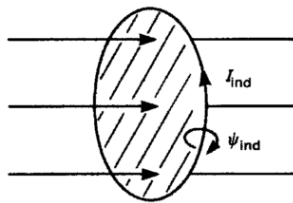
▲ Frequency dependency of ferromagnetic materials

H. W. Ott, *Noise Reduction Techniques in Electronic Systems*, 2nd ed., Wiley- Interscience, New York, 1988.

► Magnetic Shielding with *Conductive* Materials (1)

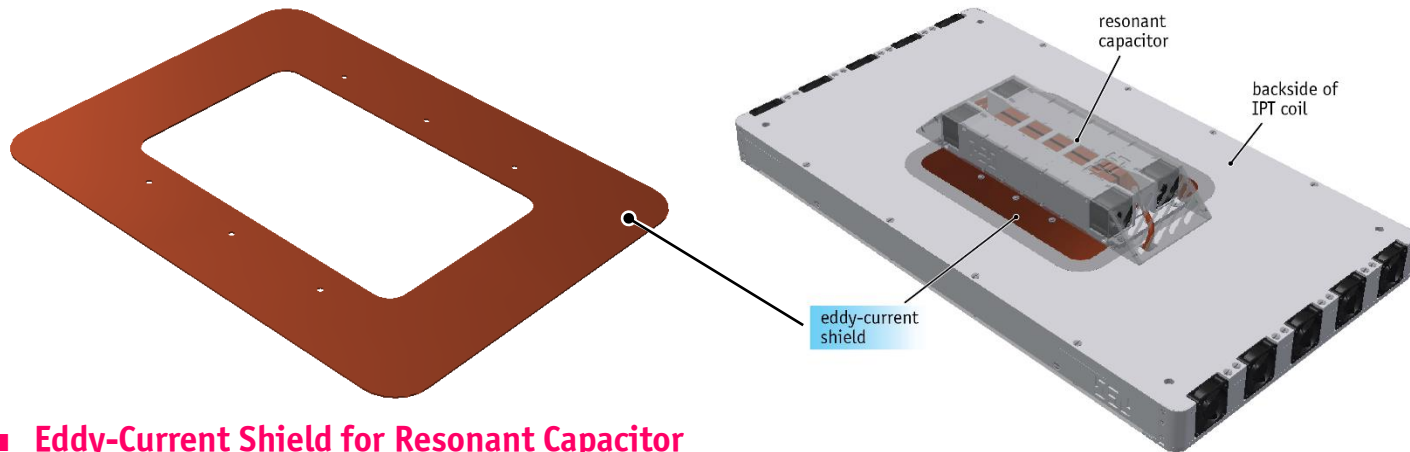
■ Magnetic Flux Diversion with Eddy Current Shield

- Circulating Eddy Current Produces Opposing Magnetic Field



◀ Current in Conductor Produces
Opposing Magnetic Field

C. Paul, "Shielding," in *Introduction to Electromagnetic Compatibility*, 2nd ed., Jon Wiley & Sons, Hoboken, 2006, ch. 10, sec. 4, pp. 742-749.

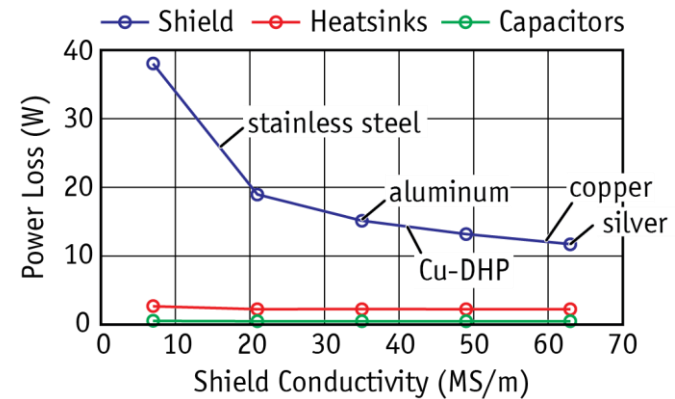
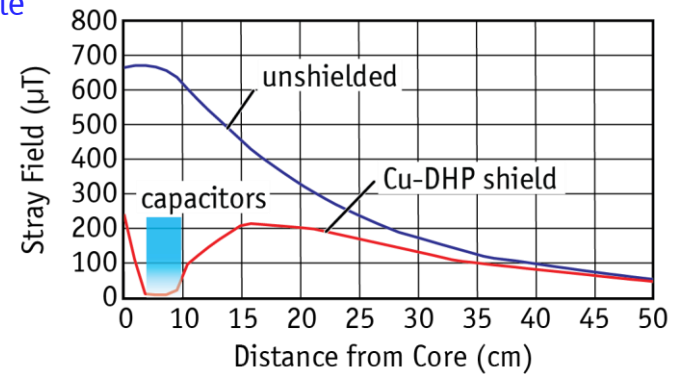
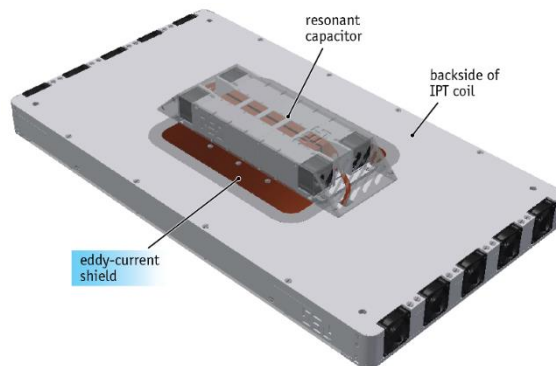
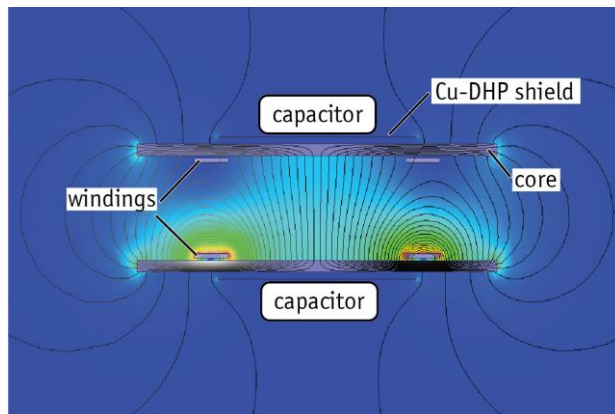


■ Eddy-Current Shield for Resonant Capacitor Module incl. Heatsink & Fans

▲ Passive shielding of resonant capacitor module
with a copper shielding ring

► Magnetic Shielding with *Conductive Materials* (2)

- Magnetic Flux Diversion with Eddy Current Shield
 - Create a Field-Free Space Around Capacitor Module



▲ FE-Calculated Field and Power Loss at 50 kW

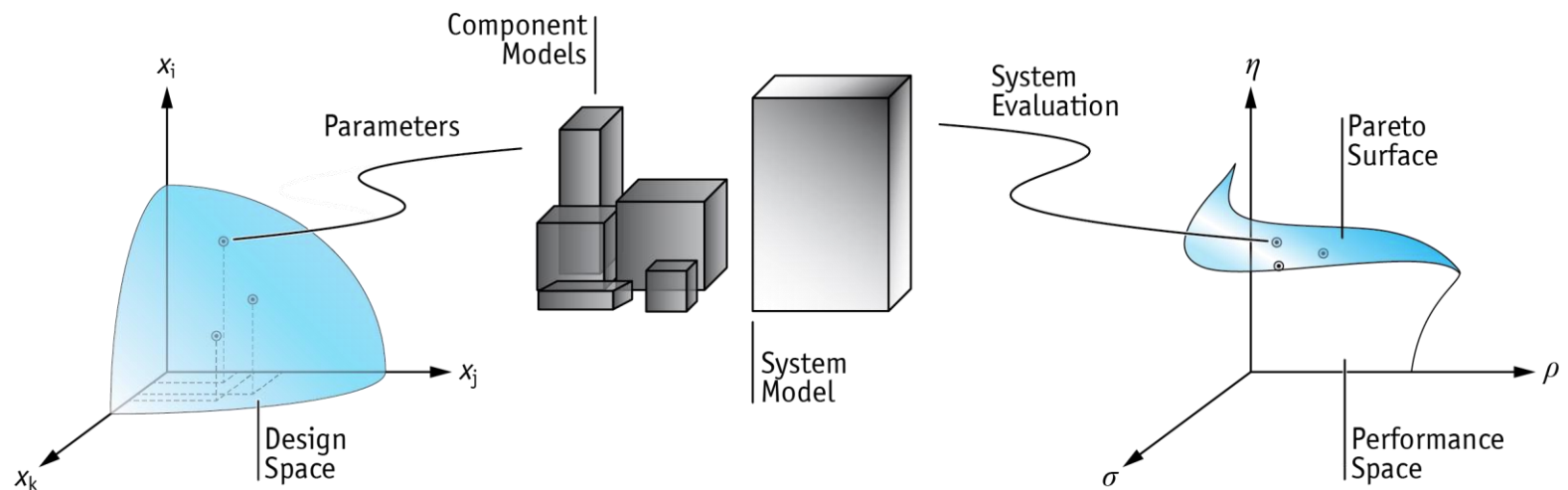
Requirements & Limits
Optimization Method
Trade-Off Analysis



► Multi-Objective Optimization of 5 kW Prototype (1)

■ Design of a 5 kW Prototype System with Maximum Possible Performance

- Use Component Models to Analyze Mapping from Design Space into Performance Space



- Coil Dimensions
- Winding Scheme
- Number of Turns
- Litz Wire Design
- Core Design
- Core Material

- AC-Losses
- Magnetic Fields
- Capacitor Losses
- Converter Losses
- Component Cost
- Component Size

- Efficiency $\eta = P_{\text{out}}/P_{\text{in}}$ [%]
- Power Density $\rho = P_{\text{out}}/V_{\text{tot}}$ [kW/dm³]
- Stray Field $\beta = B_{\text{max}}/B_{\text{norm}}$ [%]
- Tolerance $\delta = \Delta x/D_{\text{coil}}$ [%]
- Specific Cost $\gamma = C_{\text{tot}}/P_{\text{out}}$ [\$/kW]
- Material Effort $\sigma = \text{kg}_{\text{Cu/Fe}}/P_{\text{out}}$ [kg/kW]

► Multi-Objective Optimization of 5 kW Prototype (2)

■ Design Process Taking All Performance Aspects into Account

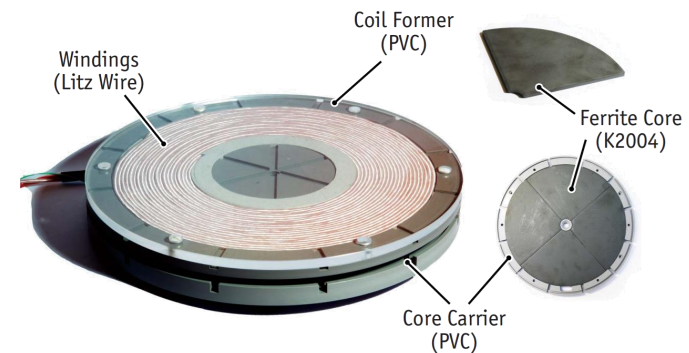
■ System Specification

- Input Voltage 400 V
- Battery Voltage 350 V
- Output Power 5 kW
- Air Gap 50 mm

■ Constraints / Side Conditions

- Thermal Limitations [°C]
- Stray Field Limitations [μ T]
- Max. Construction Vol. [m^3]
- Switching Frequency [kHz]

R. Bosshard, J. W. Kolar, J. Mühlethaler, I. Stevanovic, B. Wunsch, F. Canales, "Modeling and η - α -Pareto optimization of inductive power transfer coils for electric vehicles," *IEEE J. Emerg. Sel. Topics Power Electron.*, vol. 3, no. 1., pp.50-64, March 2015.



■ System Performance

- Efficiency $\eta = P_{\text{out}}/P_{\text{in}}$ [%]
- Power Density $\alpha = P_{\text{out}}/A_{\text{coil}}$ [kW/dm²]
- Stray Field $\beta = B_{\text{max}}/B_{\text{norm}}$ [%]

η - α -Pareto Optimization

► η - α -Pareto Optimization – Results (1)

■ Evaluation of Design Options in an Iterative Procedure

- Evaluation of FEM/Analytical Models for Power Losses, Thermal Constraints, Stray Fields, etc.
- Iterative Parameter / Grid Search for a Given Design Space

■ Degrees-of-Freedom:

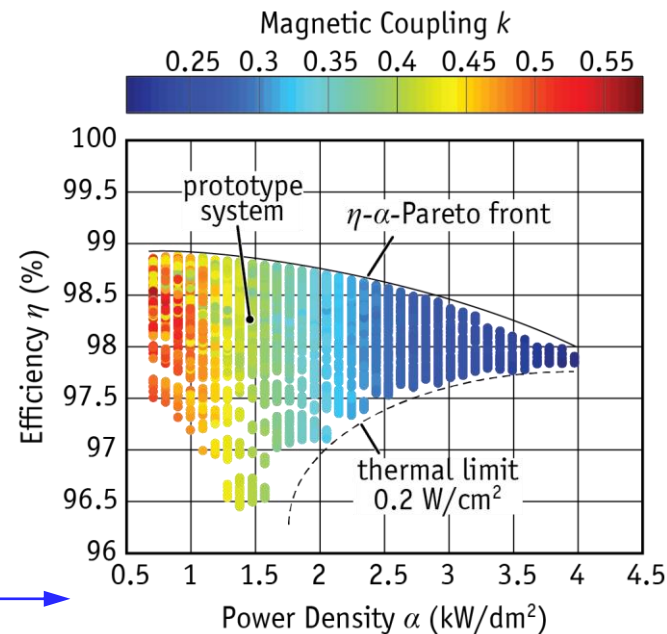
- Coil Dimensions
- Litz Wire Dimensions
- Number of Turns
- Operating Frequency

Design Space

Component Models

System Model

Performance

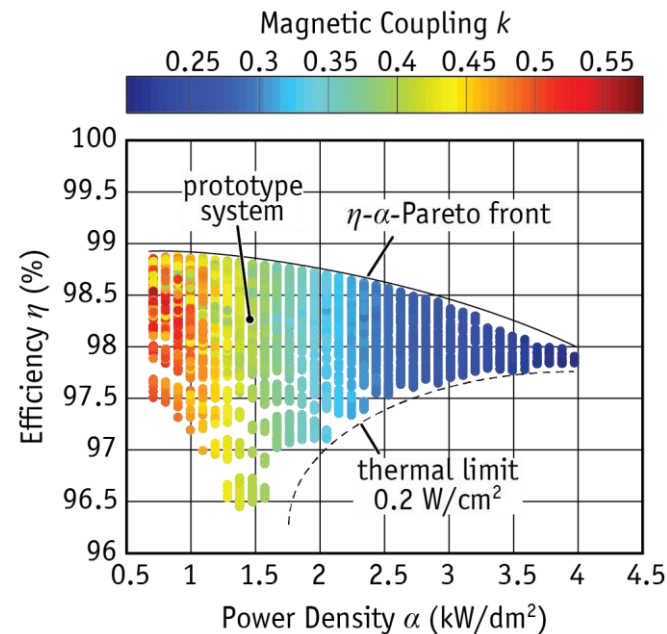
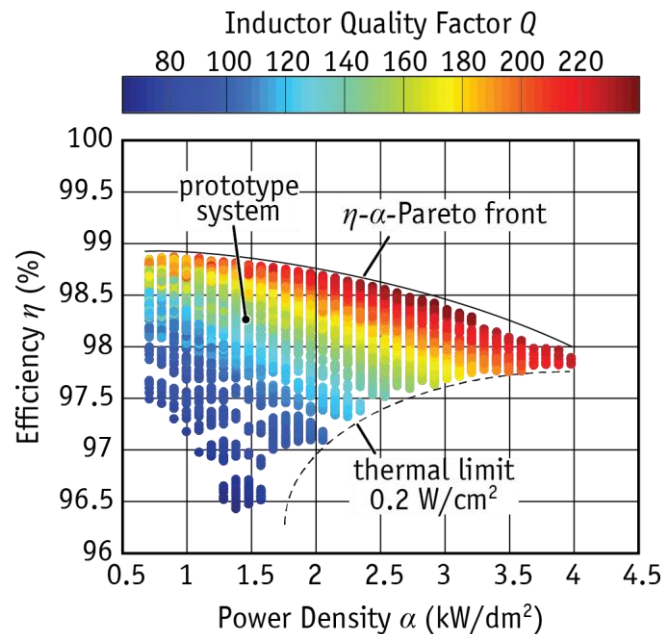


▲ Efficiency vs. Power Density of >12k
IPT Coils with 5 kW Output Power

► η - α -Pareto Optimization – Results (2)

■ Analysis of Result Data to Understand Relevant Design Trade-Offs

- Confirm Predictions of Analytical Models and Estimations → $FOM = kQ$
- Identify Key-Parameters that Impact System Performance → High Frequency

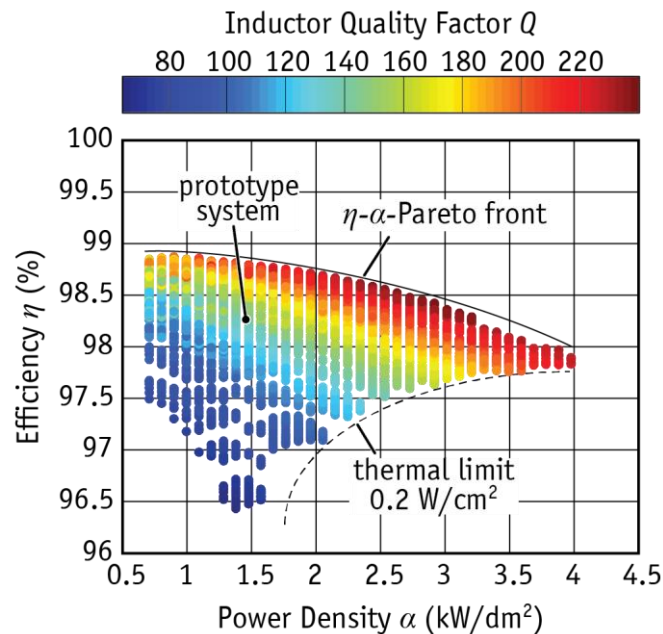


▲ Trade-Off Analysis with Result Data: Effect of Quality Factor and Magnetic Coupling

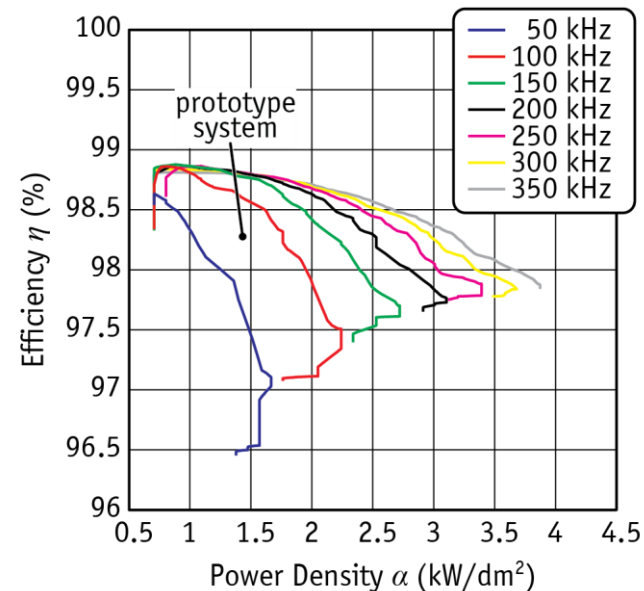
► η - α -Pareto Optimization – Results (3)

■ Analysis of Result Data to Understand Relevant Design Trade-Offs

- Confirm Predictions of Analytical Models and Estimations → $FOM = kQ$
- Identify Key-Parameters that Impact System Performance → High Frequency



▲ Calculated efficiency vs. power density, colored by Inductor Quality Factor

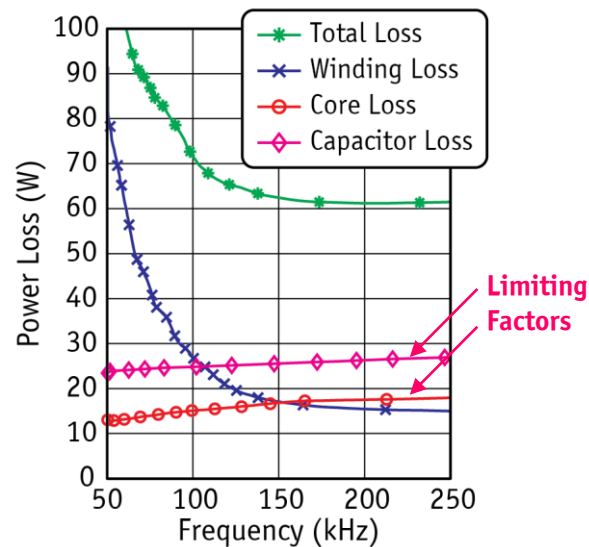


▲ Calculated Efficiency vs. Power Density, divided by Transmission Frequency

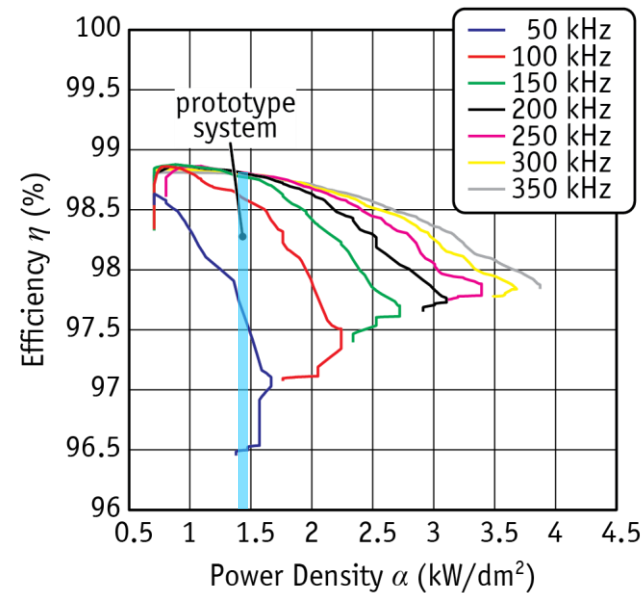
► Efficiency at High-Frequency Transmission

■ Reduced Winding Losses due to Lower Number of Turns in Transmission Coils

- Matching Condition allows Lower Inductance at Higher Frequency
- Reduction of Flux leads to Slower Increase of Core Losses



▲ Power Loss Breakdown at **1.47 kW/dm²**
(Power Density of 5 kW Prototype)

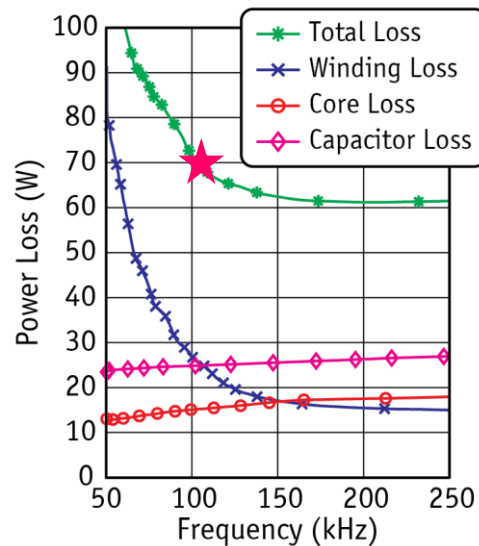


▲ Calculated Efficiency vs. Power Density,
divided by Transmission Frequency

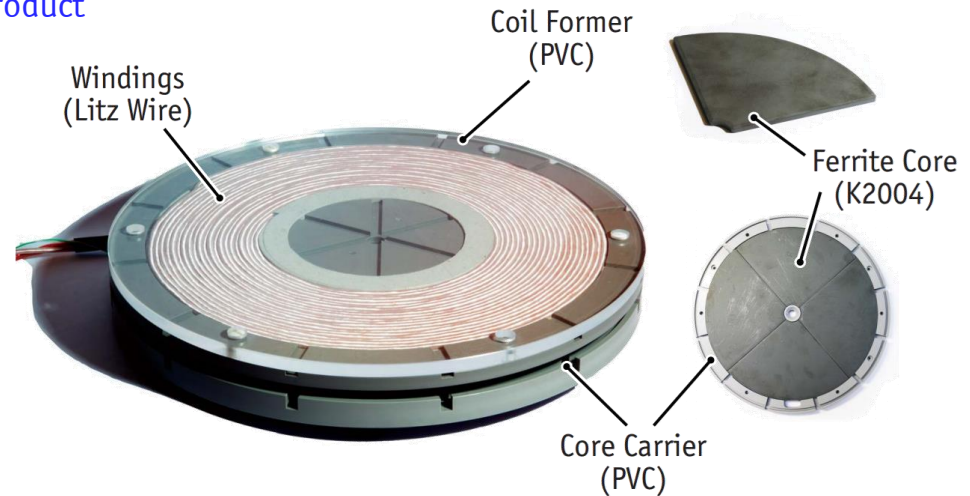
► Selected Design for 5 kW Prototype System

■ Selection of Transmission Frequency

- Significant Improvements up to 100 kHz
- Standard Power Electronics Design (5 kW)
- Litz Wire (630 x 71 μm) is Standard Product



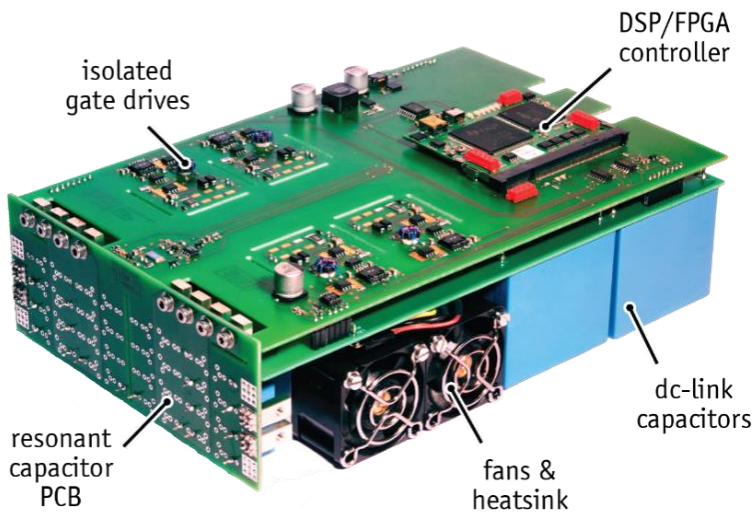
▲ Power Loss Breakdown at 1.47 kW/dm²
(Power Density of 5 kW Prototype)



■ 5 kW Prototype IPT System

- Coil Diameter **210 mm**
- Trans. Frequency **100 kHz**
- Trans. Efficiency **98.25% @ 52 mm Air Gap**
- Power Density **1.47 kW/dm²**
- Stray Field **26.16 μT**

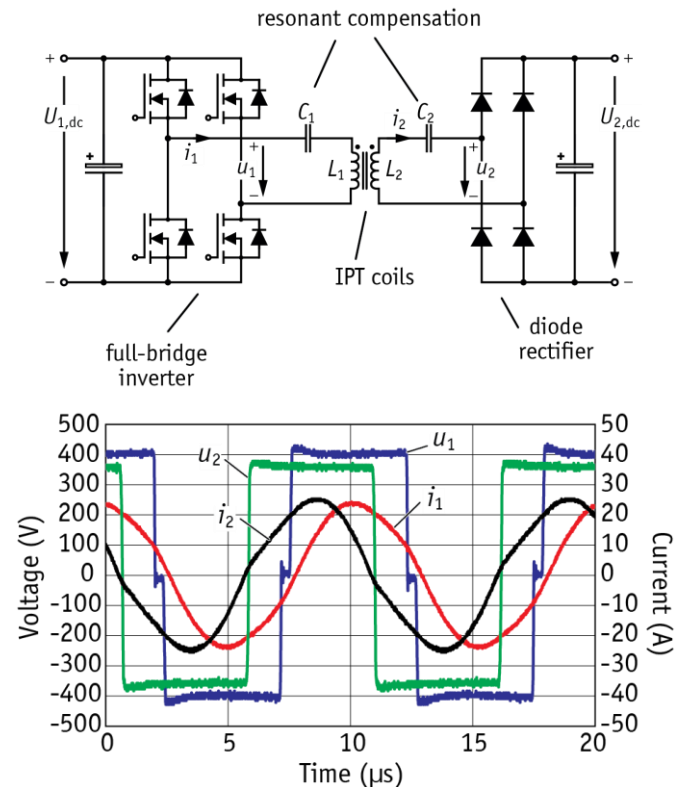
► Resonant Converter for 5 kW Testing



▲ 5 kW Prototype Power Converter

■ Full-Bridge Test-Inverter 5 kW @ 400-800 V

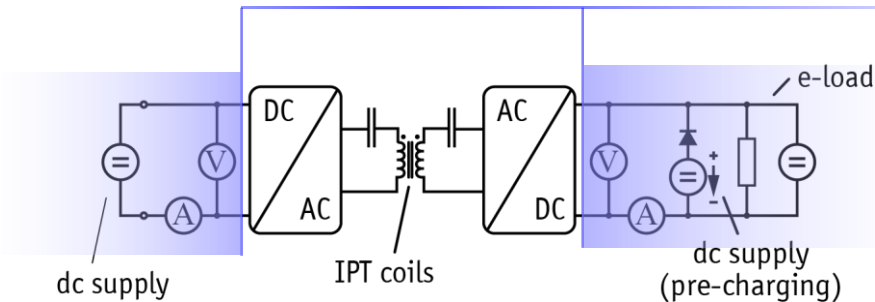
- Cree 1.2 kV SiC MOSFETs (42 A, 100 kHz)
- DSP/FPGA-based Control
- Film Capacitors for DC-Link



▲ Measured Waveforms at 5 kW / 400 V

► DC-to-DC Power Loss Measurement

- **Difficult to Measure V/I-Phase Shift at High Frequency (100 kHz)**
 - Indirect Measurement of DC Input and Output Power



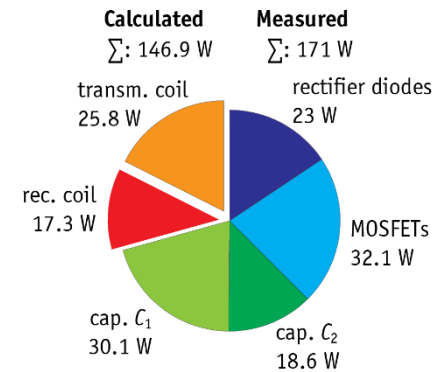
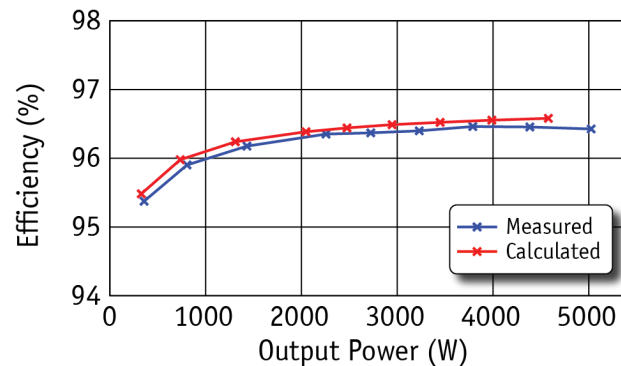
▲ Efficiency Measurement Setup



▲ Yokogawa WT3000

■ Efficiency Measurement

- Maximum Efficiency of 96.5%
- Higher than 96% down to 1 kW
- Flat Efficiency-Curve because of DC-Link Voltage Control



► High-Frequency Transmission & Stray Field

■ Higher Transmission Frequency Leads to Lower Stray Field

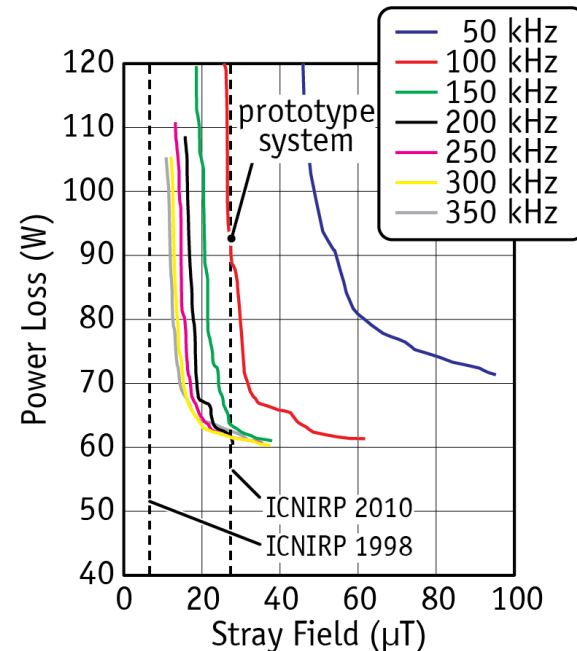
- Higher Frequency → Lower Energy per Cycle

- Scaling Law: $U_L = N \frac{d\phi}{dt} = N\omega\hat{\phi} \propto \omega\hat{B}$

→ Trade-Off: Frequency vs. Stray Field

■ Alternatives for Lower Stray Field:

- Smaller Coils: “Shielding by Distance” (but: Losses, Misalignment)
- Shielding of Coils & of Objects/People in Environment of Transmission System



▲ Calculated efficiency vs. stray field
at 30 cm distance from coil center

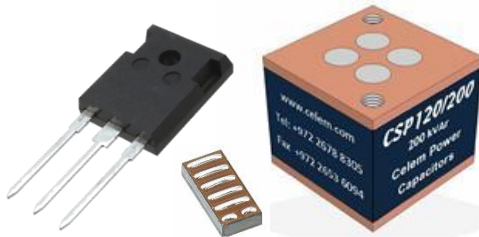
► Limiting Factors for High-Frequency Design

■ Litz Wires



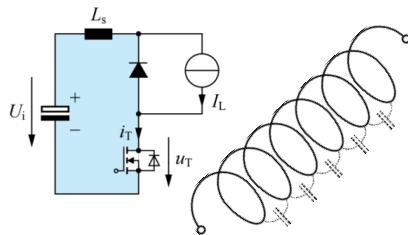
- High Manufacturing Cost of Litz Wire
- Difficult Handling and Reliability of very Thin Strands under Mechanical Stress
- Decreasing Copper Filling-Factor

■ Power Electronics



- Low-ESR / High-Power Resonant Capacitors
- Low-Loss (Wide Bandgap) Semiconductors
- Fast Switching for Low (ZVS) Losses

■ Converter & Coil Parasitics



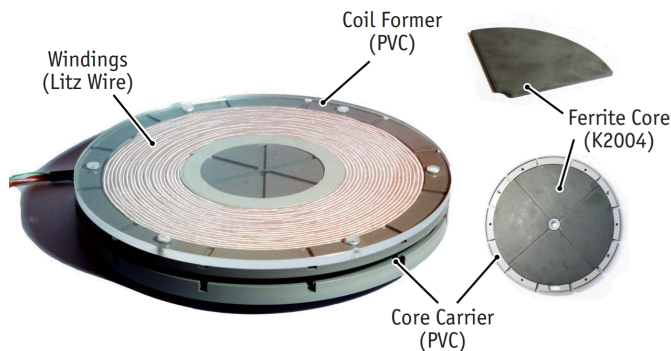
- Stray Inductance of Layout & Device Packages
- Coil Self-Capacitance (→ Include in Models)
- Sensitive Tuning of Resonant Circuit

Application to Design of 50 kW Prototype System

► Demonstrator Systems: 5 and 50 kW Output Power

■ 5 kW System for Model Development

- Output Power 5 kW @ 400V, 100 kHz
- Lab-Scale Coil and Converter Size (210 mm Diameter / 50 mm Air Gap)
- Basic Geometry for Simplified Modeling
- Verification of Calculation & Optimization



R. Bosshard, J. W. Kolar, J. Mühlethaler, I. Stevanovic, B. Wunsch, F. Canales, "Modeling and η - α -Pareto optimization of inductive power transfer coils for electric vehicles," IEEE J. Emerg. Sel. Topics Power Electron., vol. 3, no. 1., pp.50-64, March 2015.

■ 50 kW Prototype System for EV Specs

- Output Power 50 kW @ 800V, 85 kHz
- Optimized Geometry for EV Charging (450x750x60 mm, 25 kg)
- Experimental Verification



► Optimization of the 50 kW Prototype System

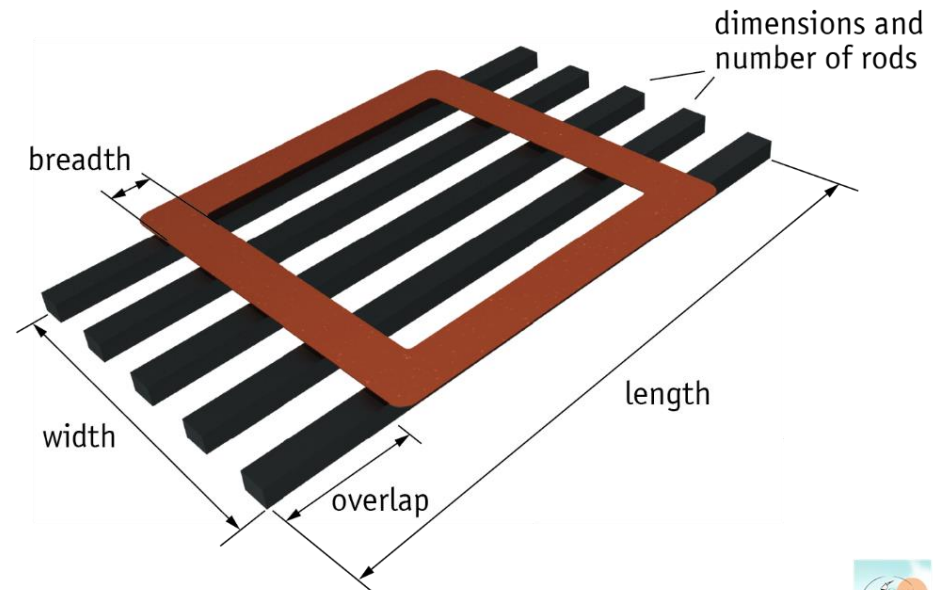
■ Selection of Coil Geometry

- Rectangular Coil Shape given by EV Application
- Size Chosen to Fully Utilize Available Coil Area
- E-Type Coil Geometry for Low Stray Field

■ Optimization Problem:

3D-FEM Simulations take 10x Longer than 2D-FEM

- Simulation Time up to 30mins (96GB RAM, 16 CPUs)
- «Brute-Force» Parameter Sweeps no Longer Useful



► Iterative IPT Coil Optimization

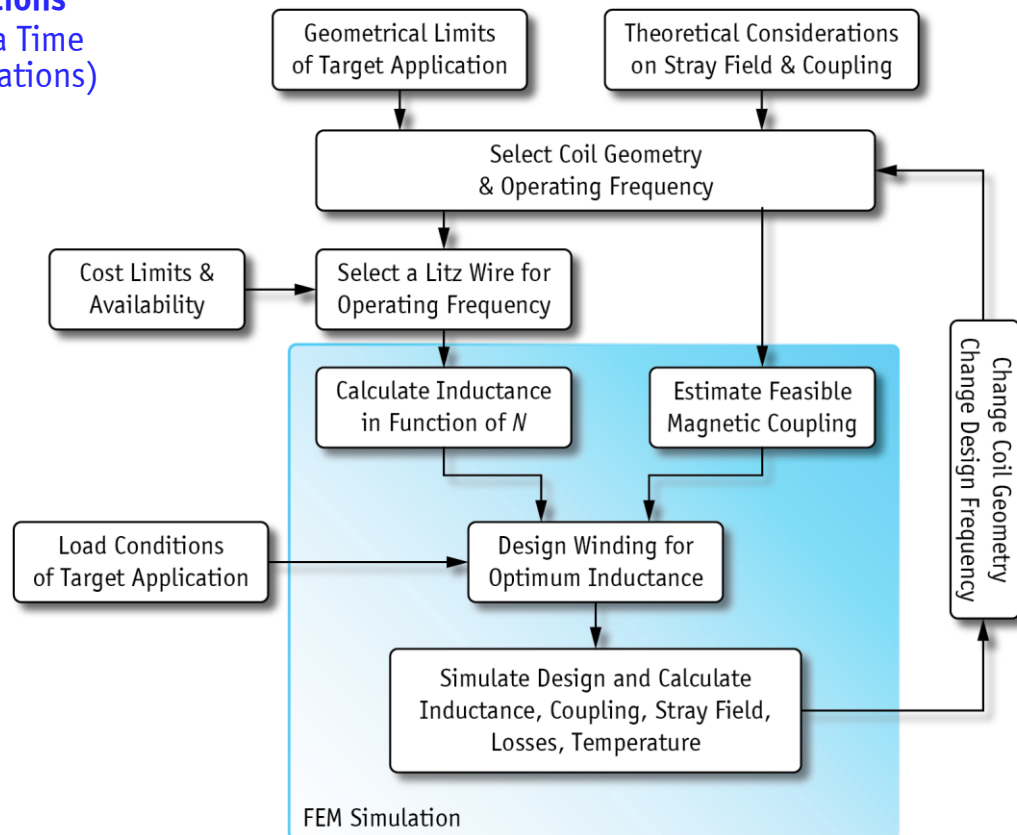
■ Iterative Procedure with Reduced Number of Evaluated Design Configurations

- Change only one Parameter at a Time (Instead of all Possible Combinations)

■ Exploit Condition for Pareto-Optimal Designs:

$$R_L^* = \frac{8}{\pi^2} \frac{U_{2,dc}^2}{P_2} \approx k\omega_0 L_2$$

Maximum
Efficiency
Condition



► Parameter Optimization

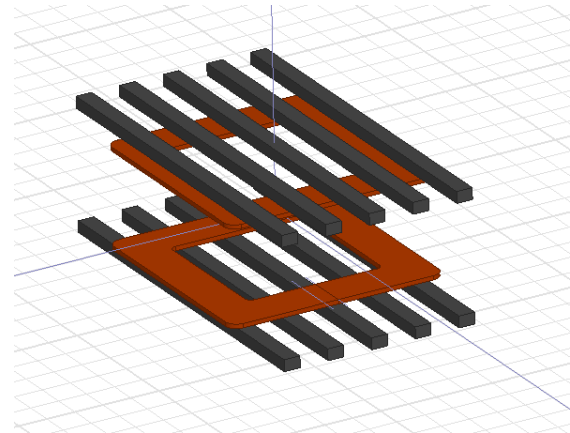
■ List of Parameter Variations

- Coil Dimensions
- Type of I-Cores
- Etc.



■ Fully Parameterized 3D-FEM Model

- All Geometry Variables can be Accessed and Changed via Software Interface



Software
Interfaces

- ### ■ Calculation of Actual Coil Currents & Number of Turns for 50 kW @ 800 V and 85 kHz



- ### ■ Calculation of Coupling & Inductance (Simulation with prelim. Test Currents)

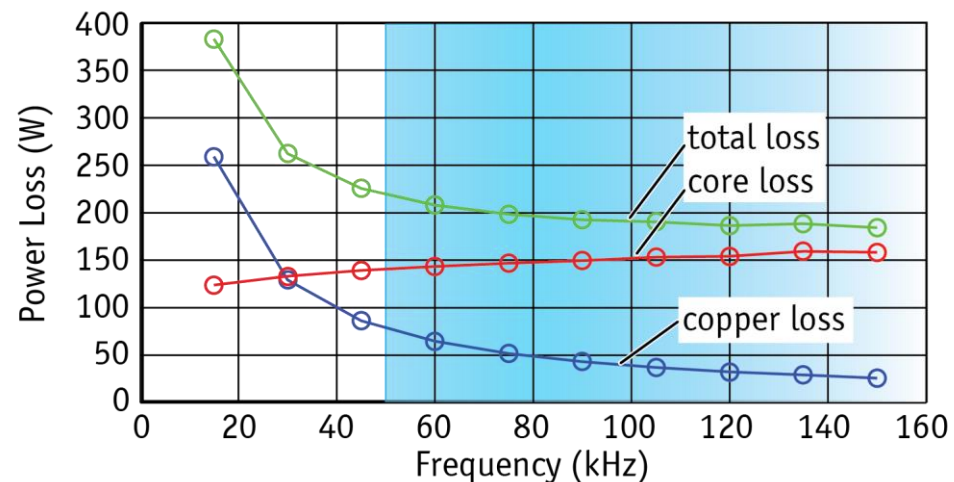


- ### ■ Calculation Fields and Power Losses at Actual Operating Point

► Effect of the Transmission Frequency (1)

■ Parameter Sweep Over Transmission Frequency

- Decreasing Power Losses in the Transmission Coils
- Reasons: Lower Inductance & Flux, Fewer Turns/Shorter Wires
- Significant Improvements up to approx. 50 kHz

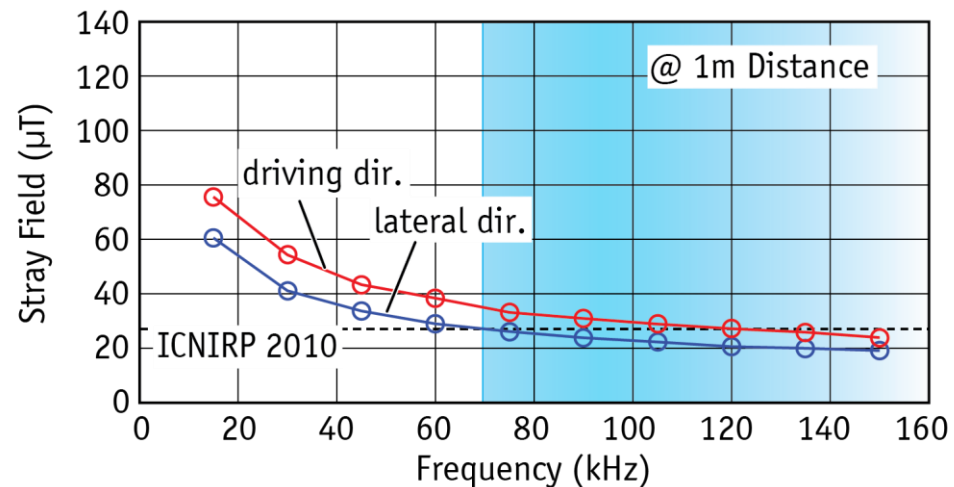
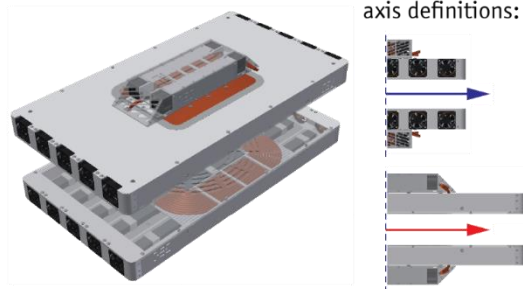


▲ Calculated Coil Losses in Function of the Transmission Frequency of the Designs

► Effect of the Transmission Frequency (2)

■ Parameter Sweep Over Transmission Frequency

- Decreasing Stray Field at Higher Frequency
- Reasons: Reduced Flux for Equal Output Power
- Stray Field Norm @ 1 m from Coil Center above 70 kHz



▲ Calculated Stray Field in Function of the Transmission Frequency of the Designs

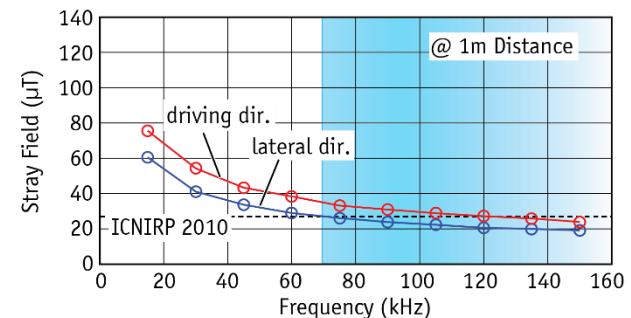
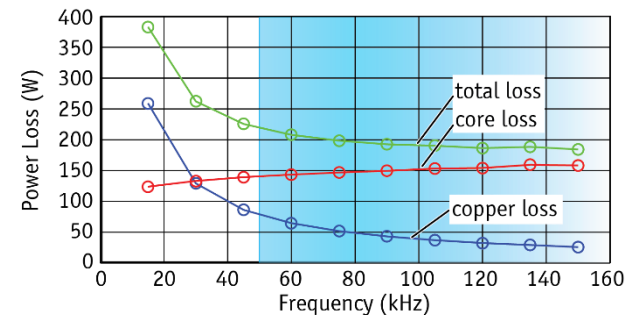
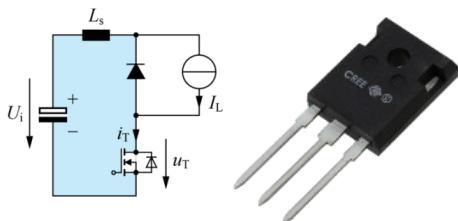
► Selected Transmission Frequency

- Decreasing Losses (Significant up to 50 kHz)
- Stray Field Norm met above 70 kHz
- Up-Coming SAE Standard J2954 Suggests 85 kHz

→ Selected Frequency: 85 kHz

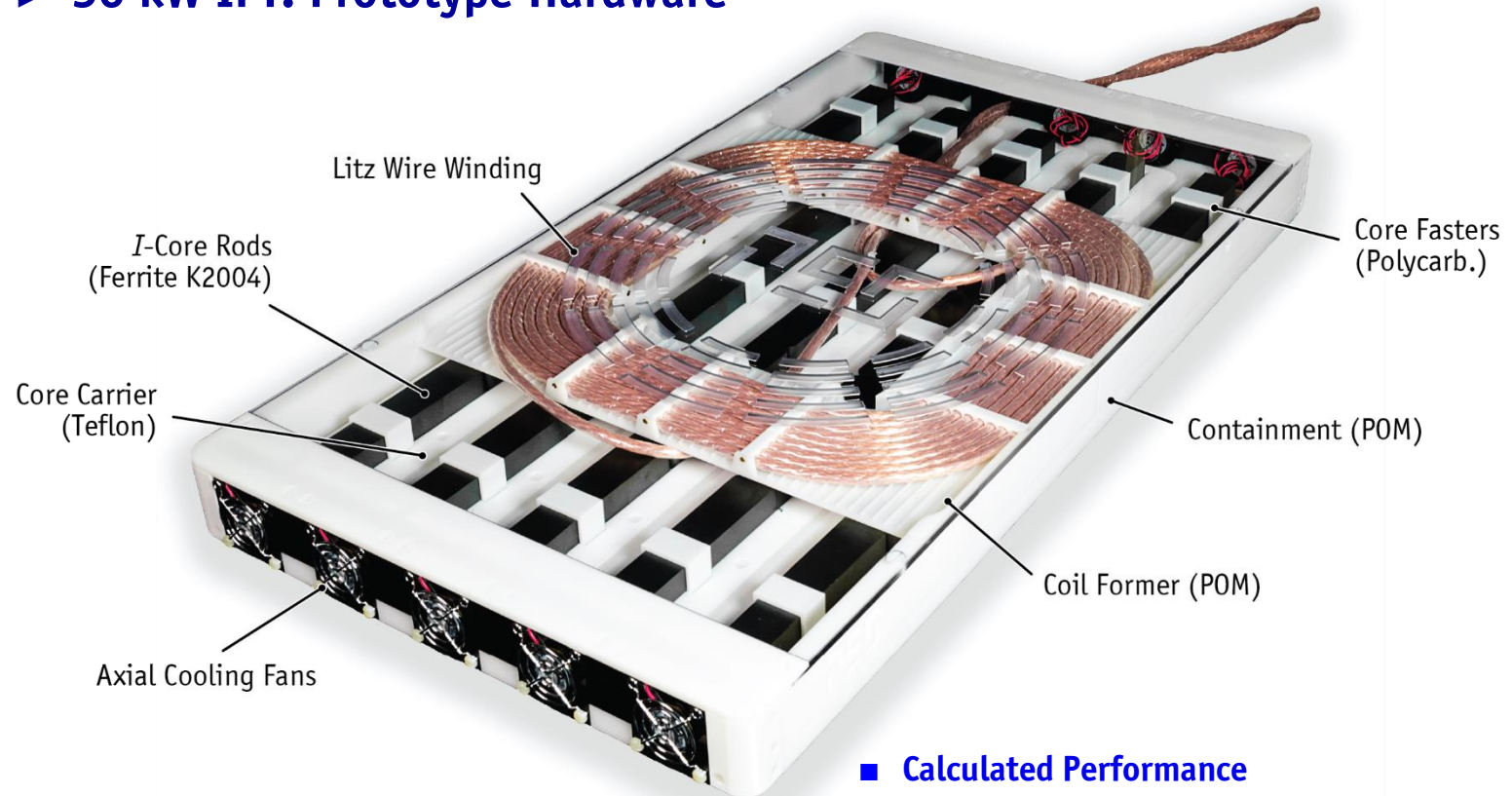
■ Immediate Implication:

- Use Latest SiC-MOSFET Technology for the Inverter-Stage
- Design and Layout of Power Electronics is Crucial for the IPT System



▲ FEM Calculation Results

► 50 kW IPT: Prototype Hardware



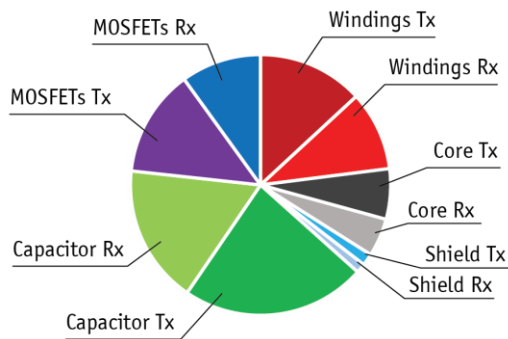
■ Calculated Performance

- Output Power 50 kW @ 800V, 85 kHz
- Max. DC/DC-Efficiency 96.5%
- Coil Dimensions 41 x 76 x 6 cm
- Coil + Cap. Weight 24.6 kg

► Estimated DC-to-DC Performance

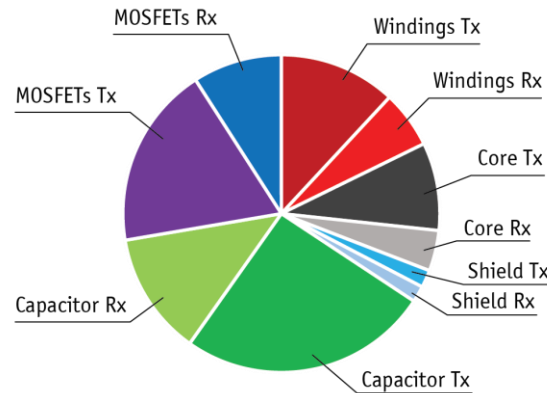
Nominal Position

Total Losses: 1384 W



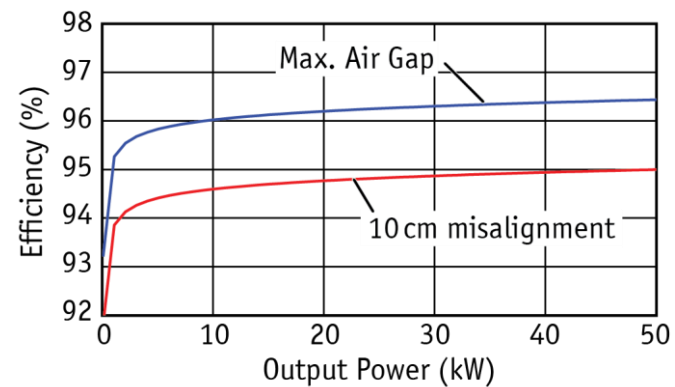
10 cm Misalignment

Total Losses: 2254 W



■ Calculated Performance

- Output Power 50 kW
- Maximum Efficiency 95.2% ... 96.5 %
- Coil Dimensions 41x76x6 cm
- Weight (Coil + Cap) 25.7 kg
- Power Density 2.7 kW/l, 1.9 kW/kg



▲ Calculated efficiency over output power for control with variable DC-link voltage

Power Electronics Concept for 50 kW

System Topology
IPT Coil Interface
3- Φ PFC Rectifiers

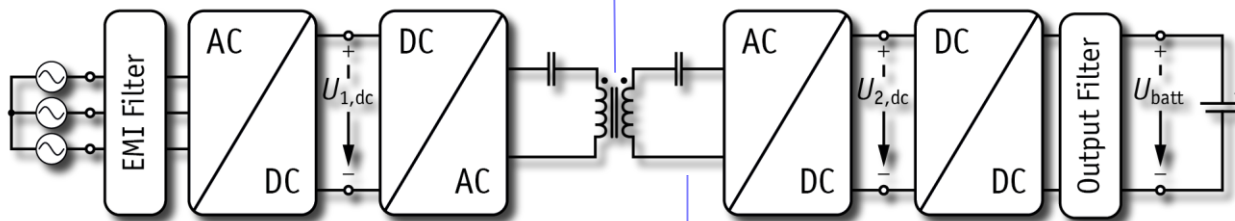
► Main System Components

■ IPT Transmission Coils

- Magnetic Design (using FEM)
- Shielding of Stray Field

■ Receiver-Side Power Electronics

- (Synchronous) Rectification
- Battery Current Regulation



■ Transmitter-Side Power Electronics

- 1/3- Φ Mains Interface
- High-Frequency Inverter Stage

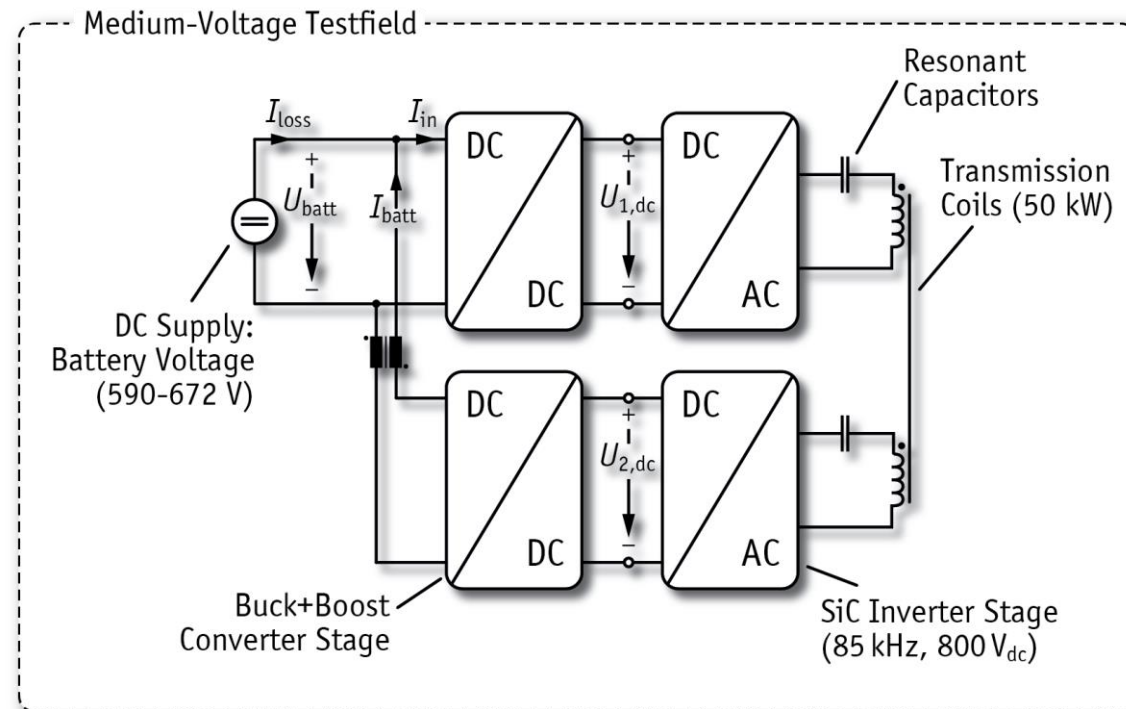
■ Resonant Compensation

- Requirements for Capacitor
- Optimal Component Selection

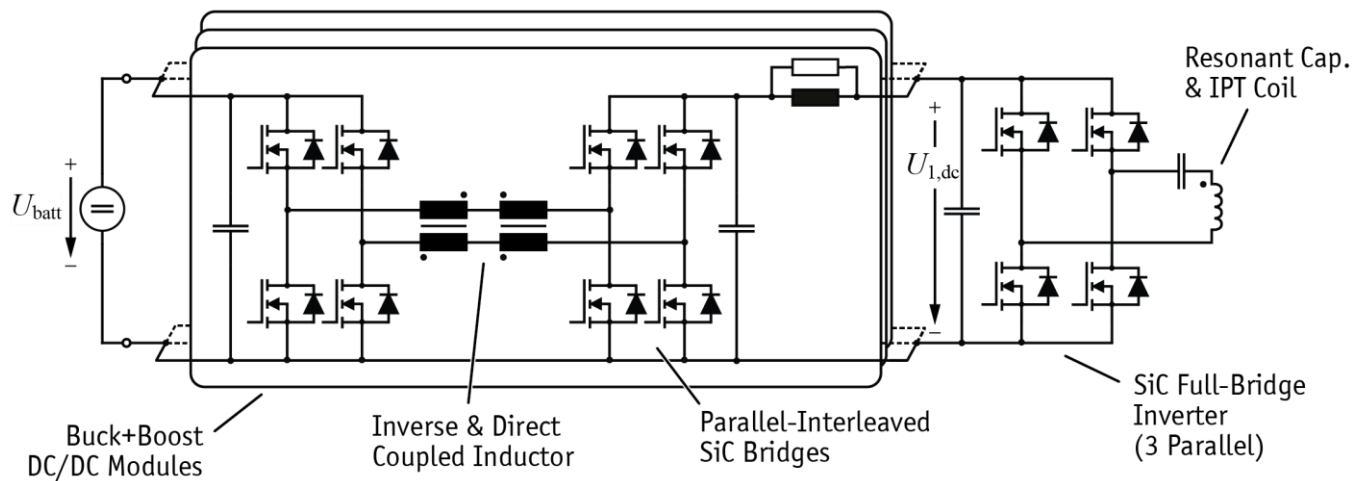
► Back-to-Back IPT Test Bench

■ Test Setup for High-Power Back-to-Back 50 kW Operation

- Direct DC-to-DC Power Loss Measurements at DC Power-Supply
- Experimental Evaluation of Different Control Options
- Design & Evaluation of Different Coil Designs



► Design Concept for 50 kW Prototype System

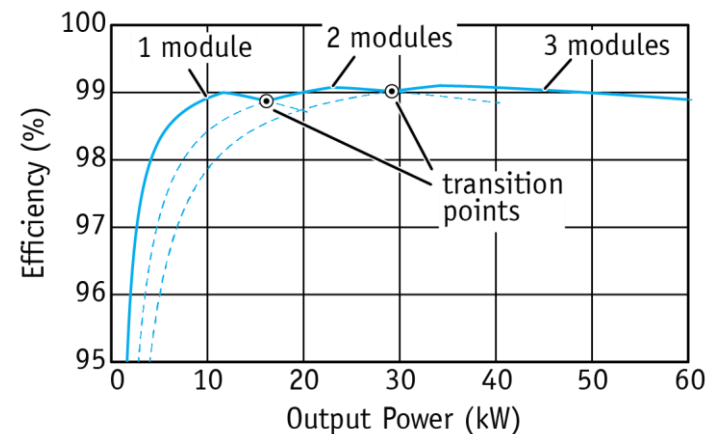


■ Ripple Cancellation by Parallel Interleaving

- 3 x 20 kW DC/DC-Converter Modules
- Each Module has 2 Interleaved and Magnetically Coupled Stages

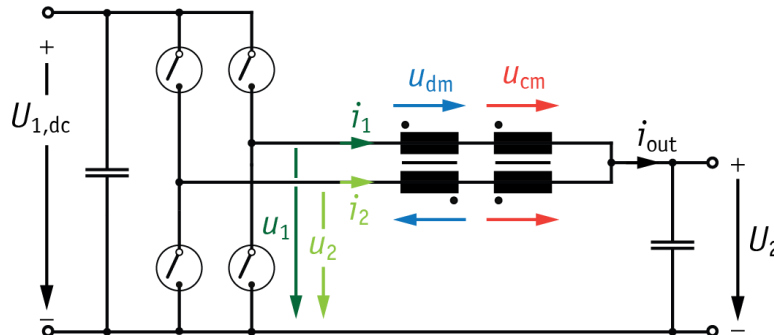
■ Modular Design allows Disabling Stages at Low Output Power

→ Fully Benefit from High Partial-Load Efficient IPT Concept



► Interleaved DC/DC-Converter with Coupled Inductors

■ 180°-Interleaved Switching (shown for Buck-Mode)

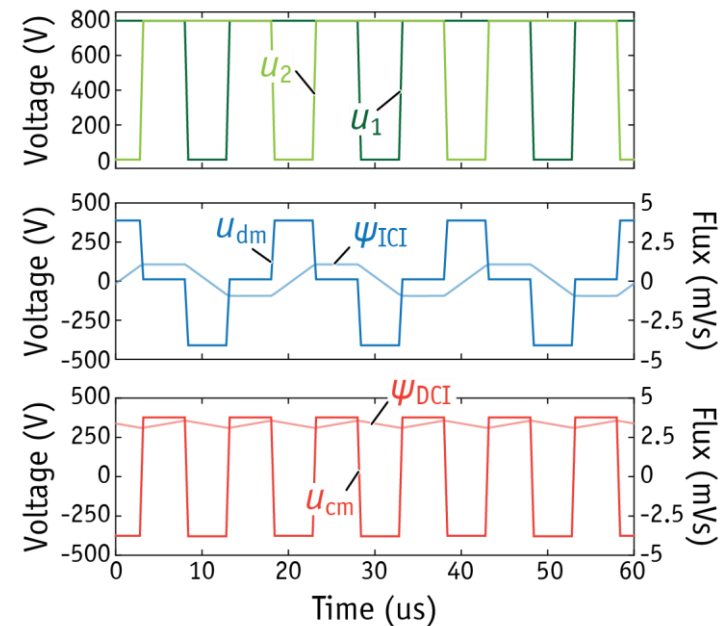


■ Direct Coupled Inductor

- Flux due to Common-Mode Voltage
- DC-Flux \rightarrow Energy Storage
- Reduction of Current-Ripple Requires More Stored Magnetic Energy

■ Inverse Coupled Inductor

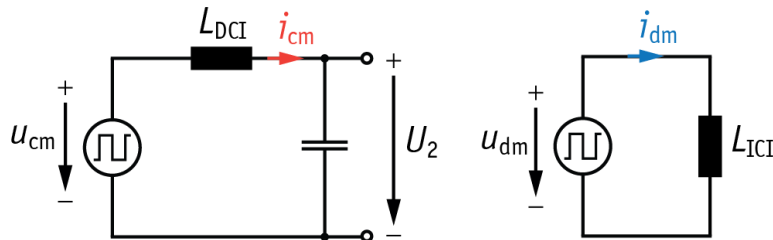
- Flux due to Differential-Mode Voltage
- No DC-Flux \rightarrow No Stored Energy
- Reduction of Current-Ripple does not Require Net Energy Storage



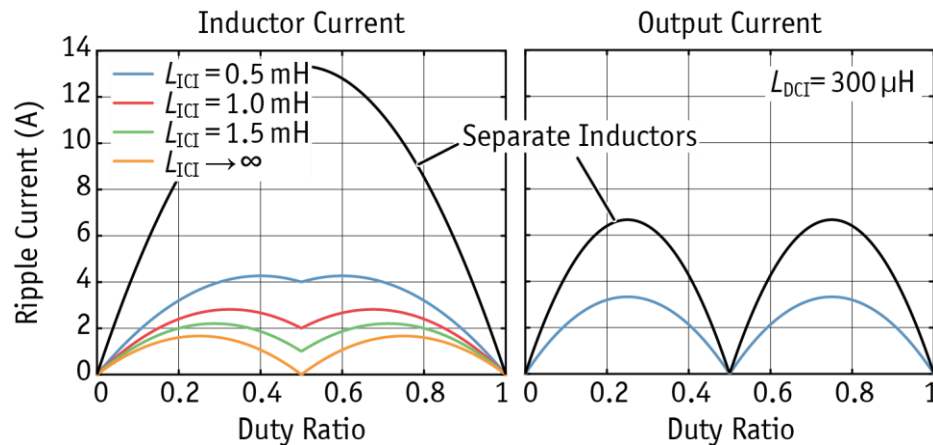
▲ Simulated Voltage and Flux Waveforms

► Separation of CM/DM Current Ripples

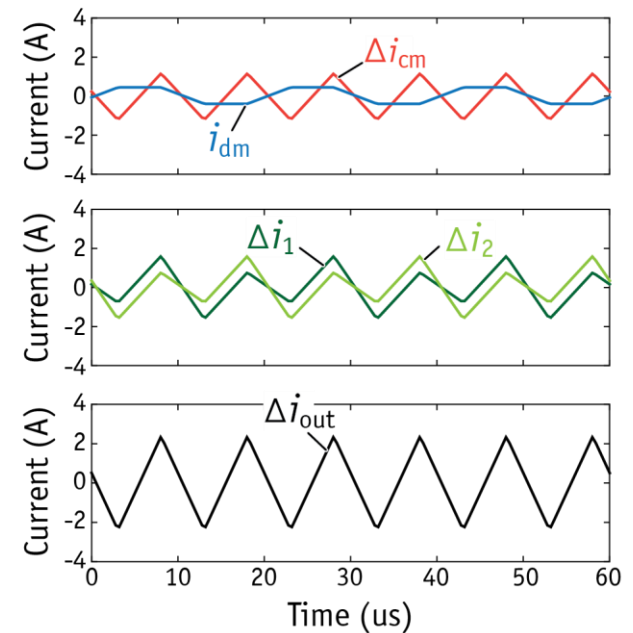
■ Common-/Differential-Mode Equivalent Circuits



■ Separate Design of CM/DM Current Ripples using Dedicated Magnetic Devices



▲ Calculated Inductor/Output Current Ripple



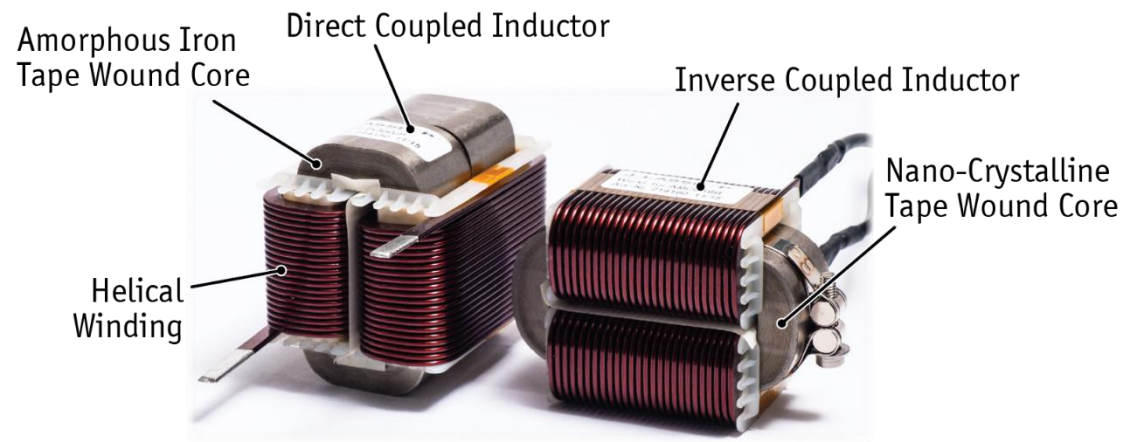
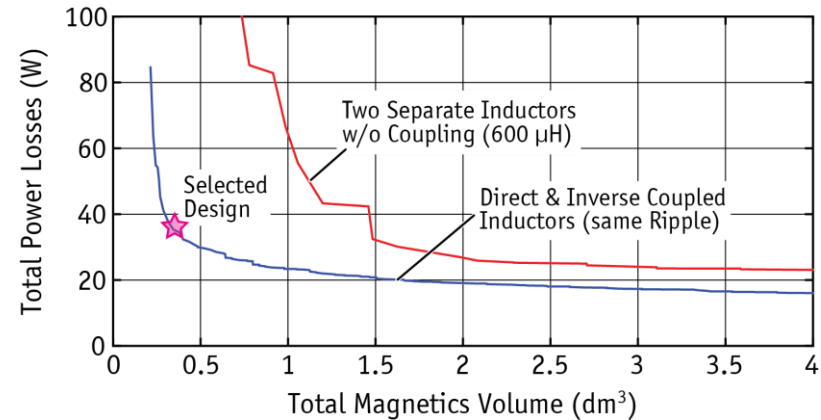
▲ Simulated Inductor/Output Current

► Component Volume and Power Losses

■ Compact Design of the Inductors

- Helical Winding for High Filling Factor
- Amorphous Iron Core with Gap for DCI
- Nano-Crystalline Core w/o Gap for ICI
- Switching Frequency 50 kHz,
10% Output Current Ripple
→ 300 μH vs. 600 μH

■ Significantly Reduced Total Magnetics Volume (DCI+ICI) in Comparison to Two Separate, Uncoupled Inductors



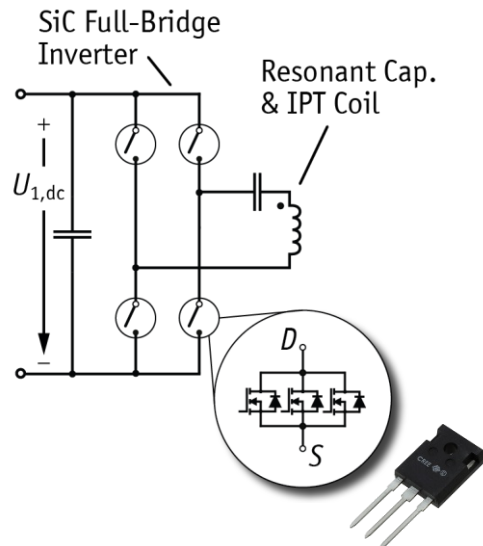
► Inverter-Stage Using Parallel-Connected SiC-Devices

■ Mainly Conduction Losses in Inverter Stage due to ZVS

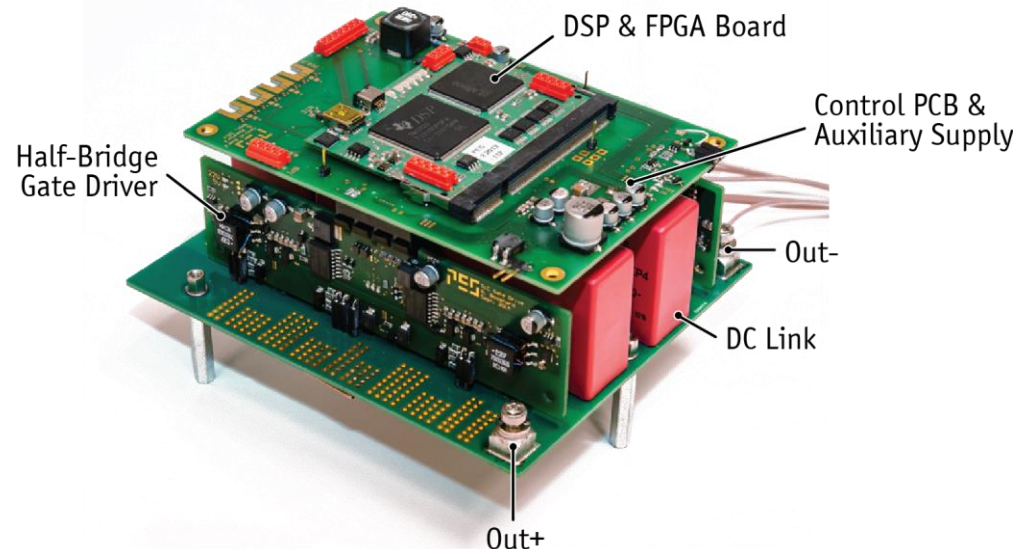
- Multiple SiC-Devices in Parallel for $R_{ds(on)}$ -Reduction
- Single Gate-Drive for all Devices for Minimum Complexity

■ Test-Bench for Evaluation of

- Switching Performance of Paralleled Devices
- HF-Design of Power PCB and Device-Current Sharing



▲ Bridge Topology with 3 SiC MOSFET Devices Connected in Parallel

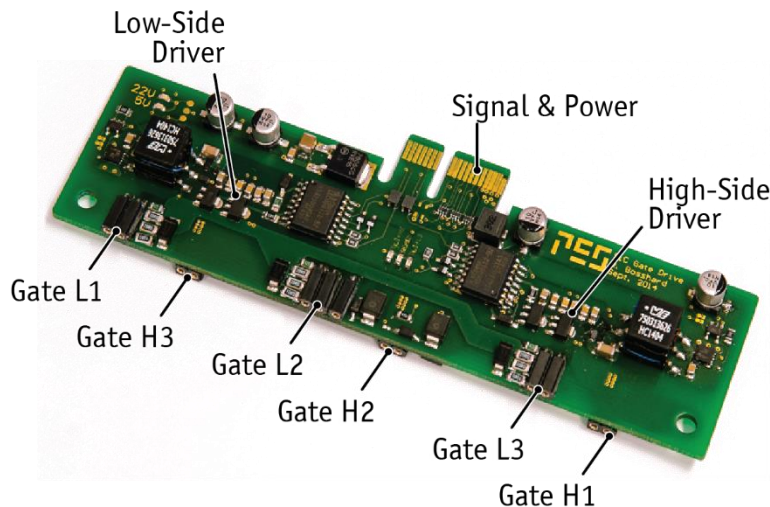


▲ 85 kHz Switching Test Bench (SiC Full-Bridge)

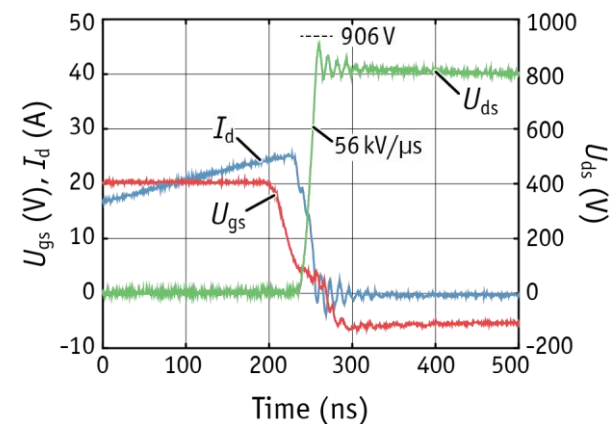
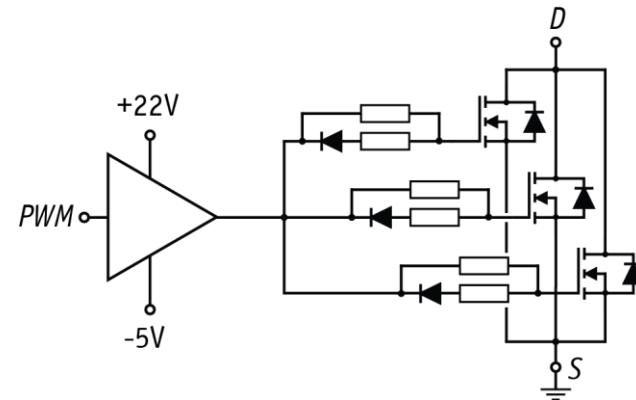
► Gate-Drive Concept for 3 Parallel-Connected Devices

■ Half-Bridge SiC-Driver PCB

- One Driver IC for all 3 Parallel Devices,
Separate Gate Resistors for each Device
- Synchronous Turn-On w/o Gate-Oscillation



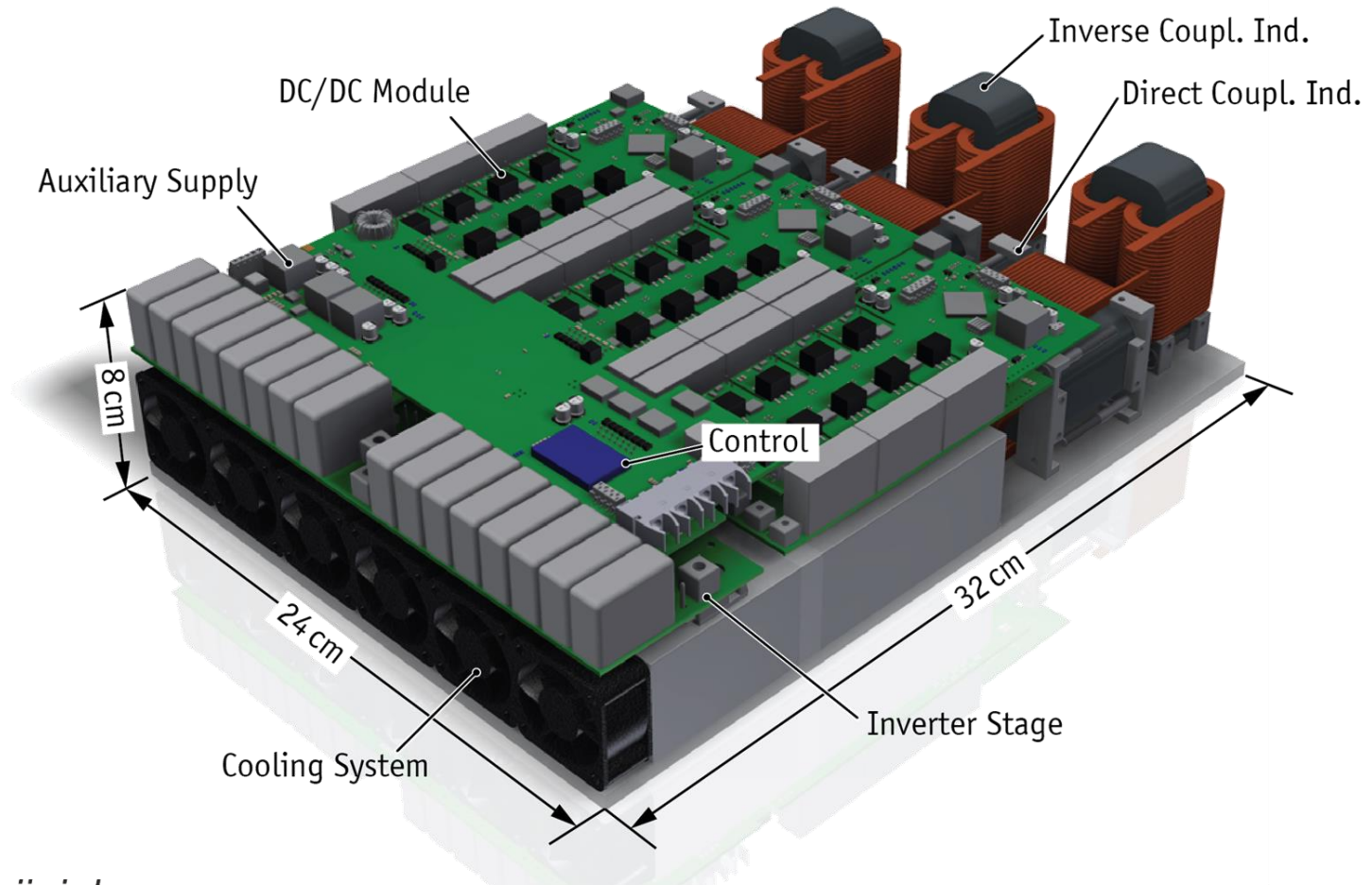
▲ Half-Bridge Gate Driver PCB for 3 Parallel MOSFETs on each Gate



▲ Zero-Voltage Turn-Off Transition

► 60 kW SiC Power Converter

- Efficiency 98%, Power Density 9.2 kW/l, Forced-Air Cooled



3- Φ PFC Rectifier Systems

J. W. Kolar, T. Friedli,
The Essence of Three-Phase PFC Rectifier Systems - Part I, IEEE Transactions on Power Electronics, Vol. 28, No. 1, pp. 176-198, January 2013.

T. Friedli, M. Hartmann, J. W. Kolar, *The Essence of Three-Phase PFC Rectifier Systems - Part II,* IEEE Transactions on Power Electronics, Vol. 29, No. 2, February 2014.

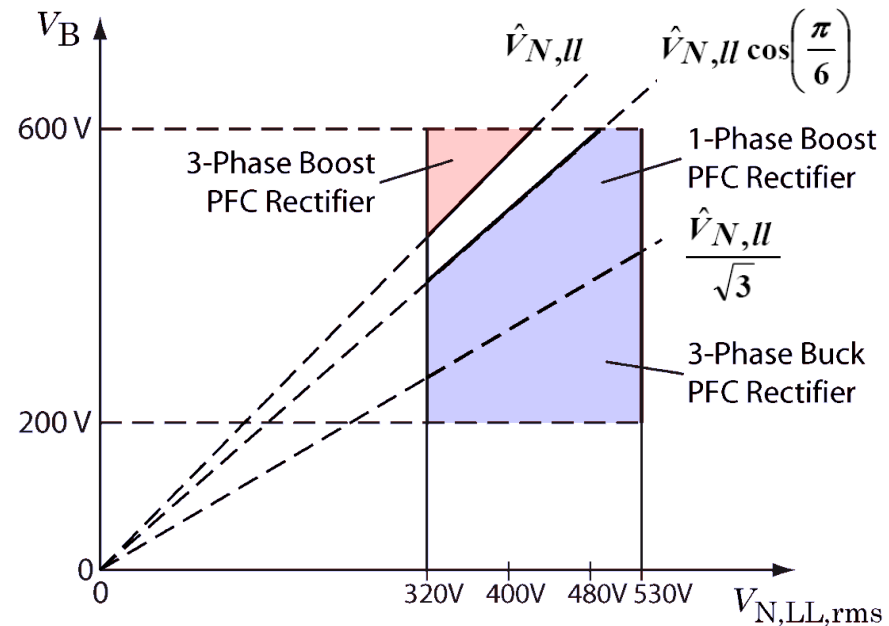
3- Φ AC/DC Power Conversion

■ Basis Requirement for EV Charging / IPT Front End Converter Stages

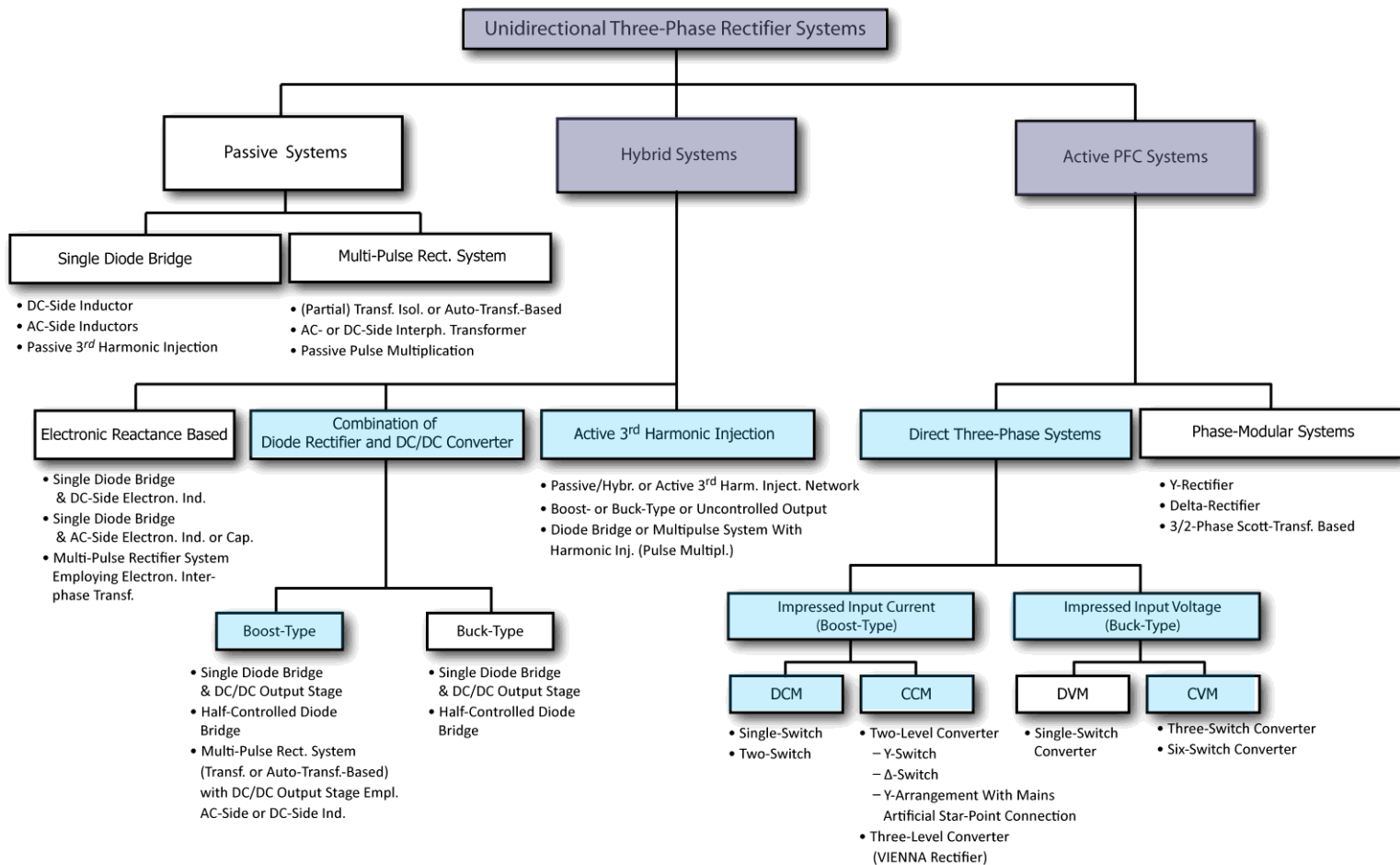
- Wide Input/Output Voltage Range – Voltage Adaption
- Mains Side Sinusoidal Current Shaping / Power Factor Correction

- **Boost Type**
- **Buck Type**

V_B Output Voltage
 $V_{N,ll,rms}$... RMS Value of
 Mains Line-to-
 Line Voltage



► Classification of General Unidirectional 3- Φ Rectifier Systems



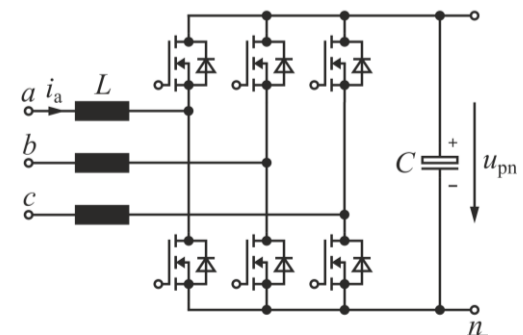
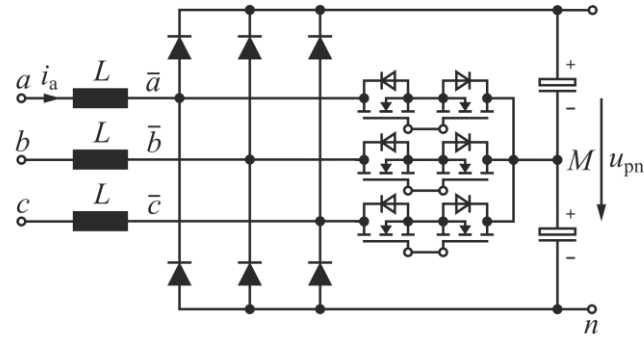
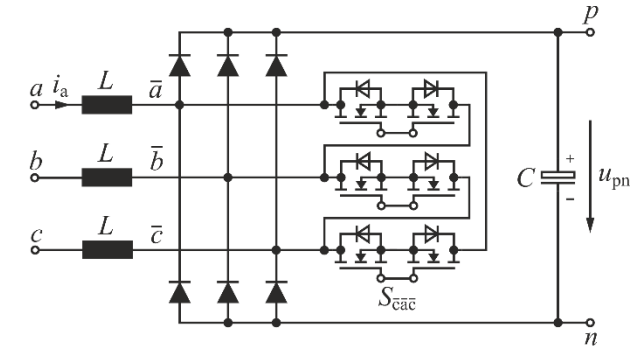
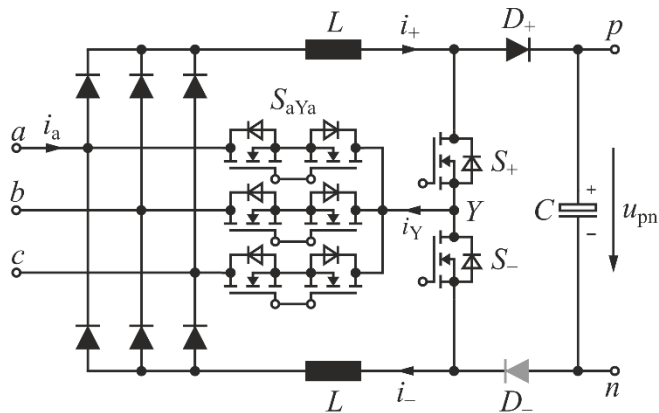
► Classification of Unidirectional Rectifier Systems

- **Passive Rectifier Systems**
 - Line Commutated Diode Bridge/Thyristor Bridge - Full/Half Controlled
 - Low Frequency Output Capacitor for DC Voltage Smoothing
 - Only Low Frequency Passive Components Employed for Current Shaping, No Active Current Control
 - No Active Output Voltage Control
- **Hybrid Rectifier Systems**
 - Low Frequency and Switching Frequency Passive Components and/or
 - Mains Commutation (Diode/Thyristor Bridge - Full/Half Controlled) and/or Forced Commutation
 - Partly Only Current Shaping/Control and/or Only Output Voltage Control
 - Partly Featuring Purely Sinusoidal Mains Current
- **Active Rectifier Systems**
 - Controlled Output Voltage
 - Controlled (Sinusoidal) Input Current
 - Only Forced Commutations / Switching Frequ. Passive Components
- **Phase-Modular Systems**
 - Phase Rectifier Modules of Identical Structure
 - Phase Modules connected in Star or in Delta
 - Formation of Three Independent Controlled DC Output Voltages
- **Direct Three-Phase Syst.**
 - Only One Common Output Voltage for All Phases
 - Symmetrical Structure of the Phase Legs
 - Phase (and/or Bridge-) Legs Connected either in Star or Delta

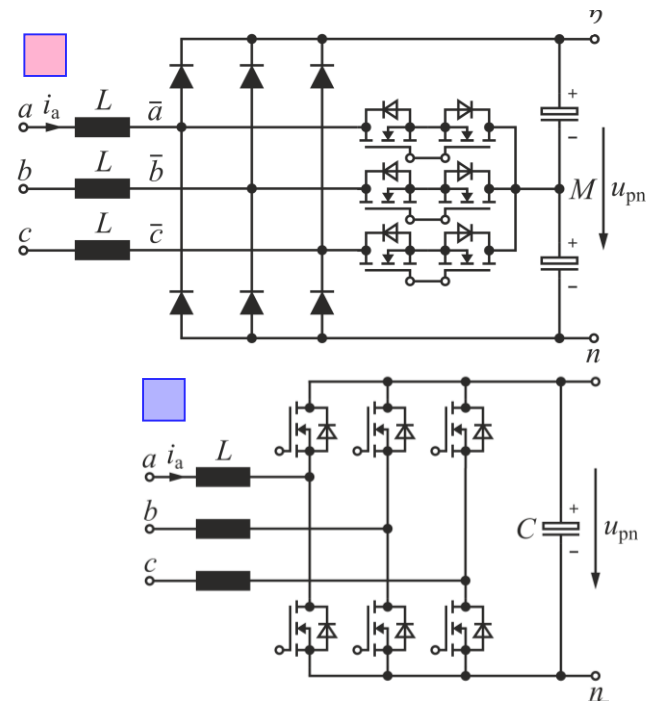
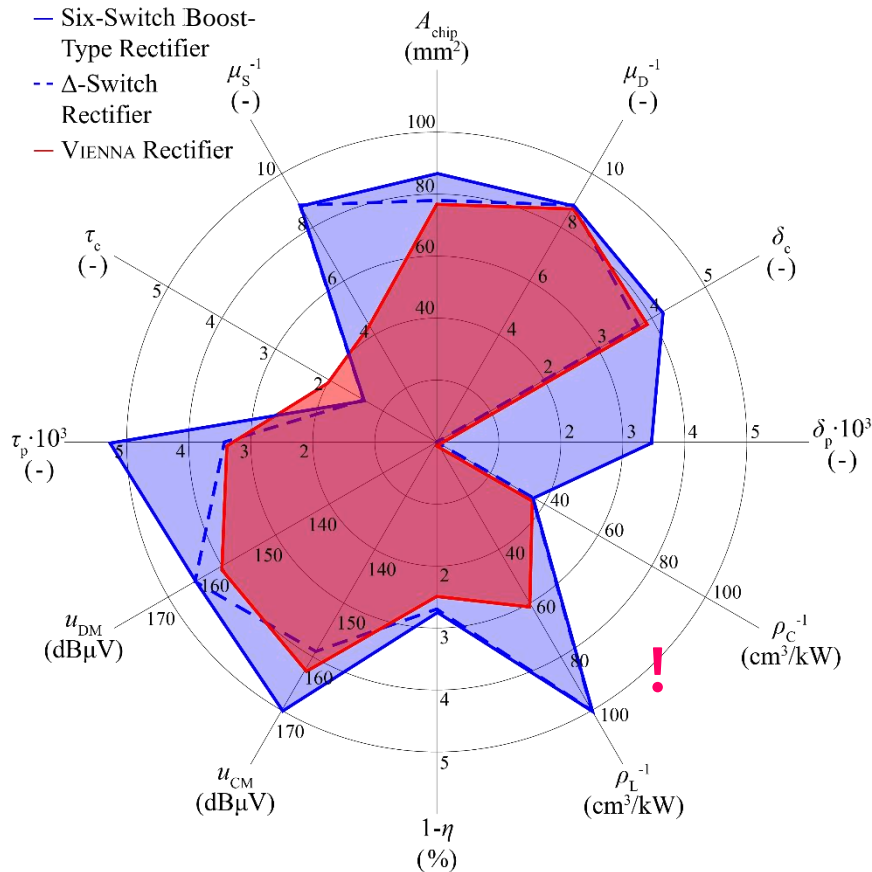
Evaluation of Boost-Type Systems

Boost-Type PFC Rectifiers

- 3rd Harmonic Inj. Type
- Diode Bridge Conduction Modulation

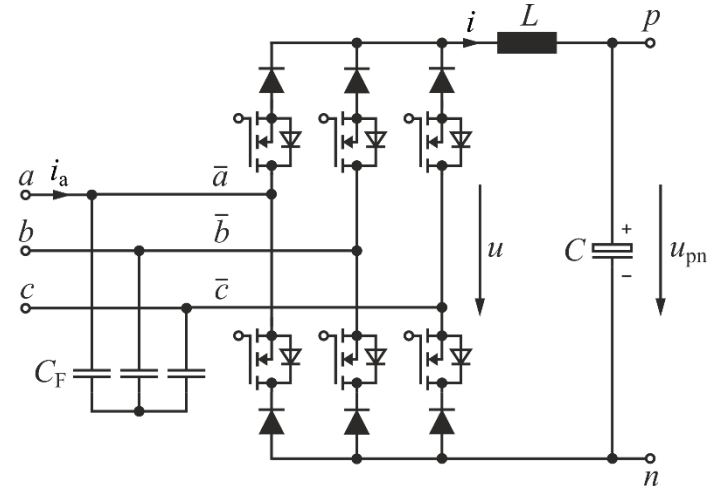
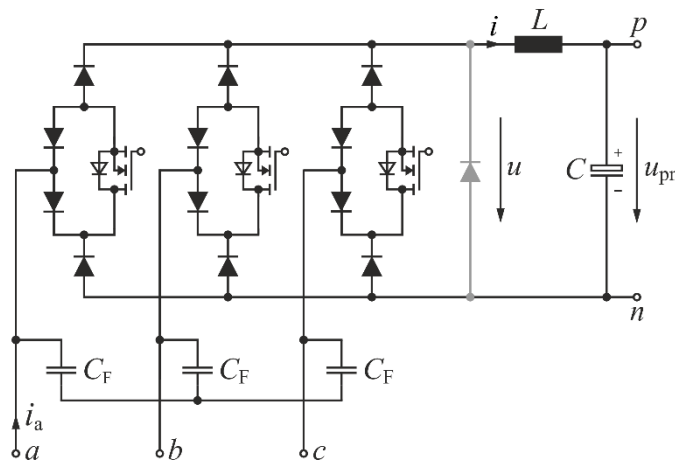


Vienna Rectifier vs. Six-Switch Rectifier

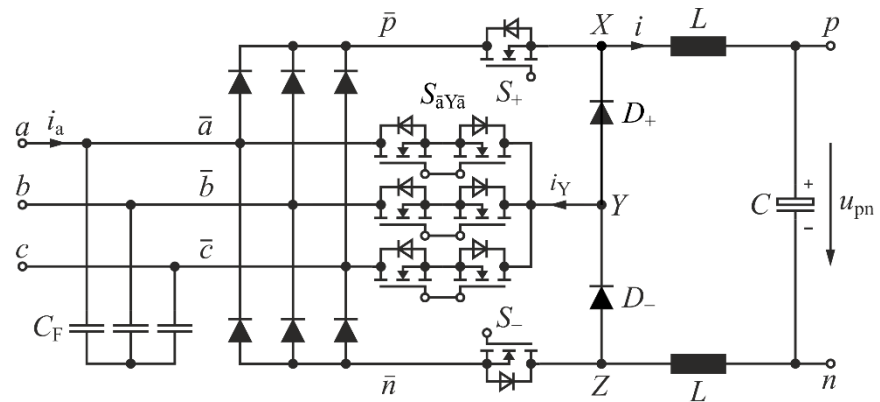


Comparison of Buck-Type Systems

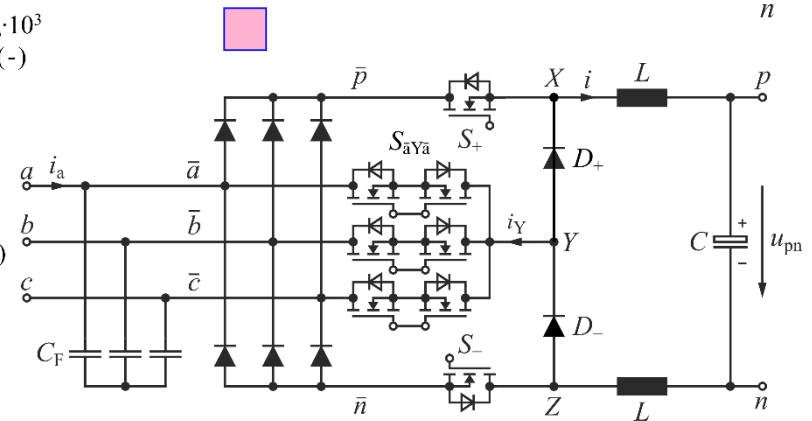
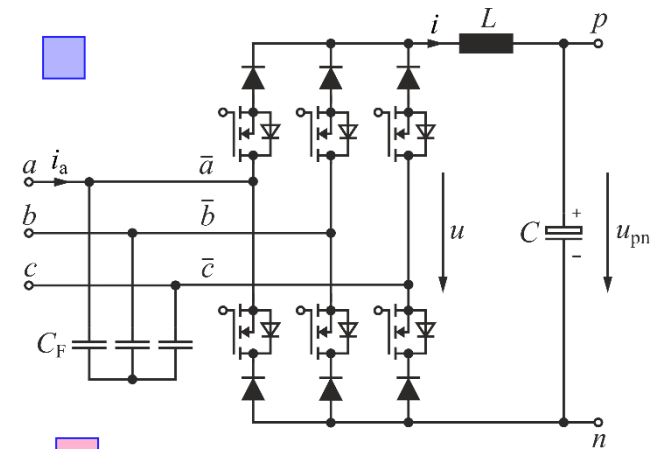
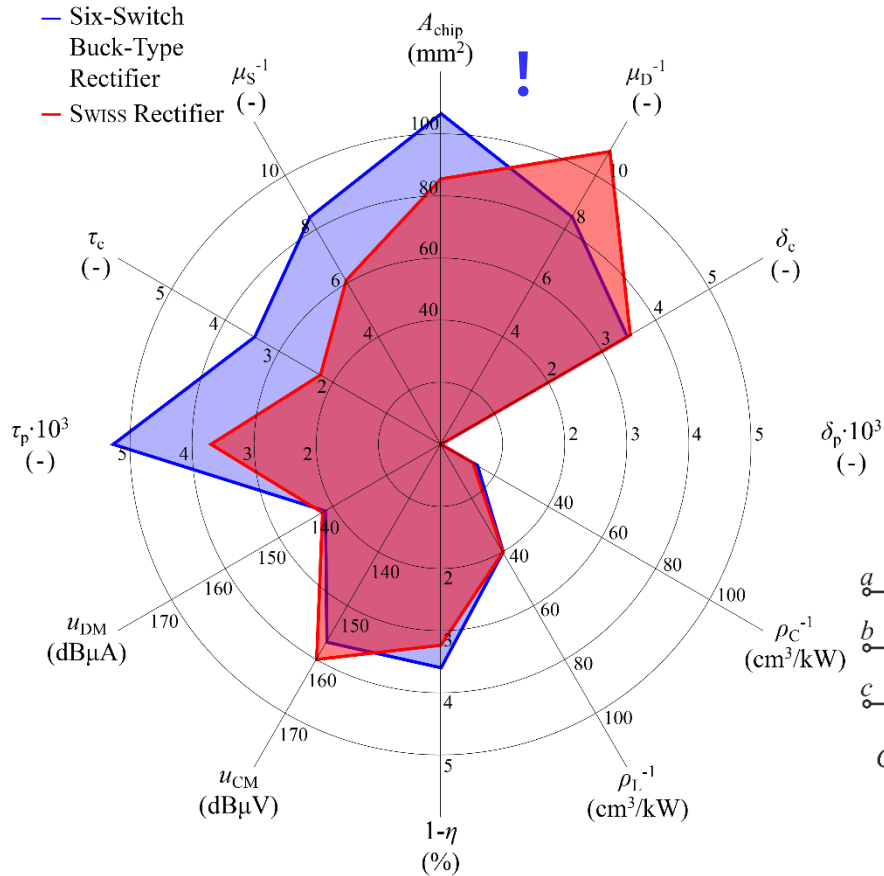
Buck-Type PFC Rectifiers



- 3rd Harmonic Inj. Type
- Diode Bridge Cond. Modulation



SWISS Rectifier vs. Six-Switch Rectifier

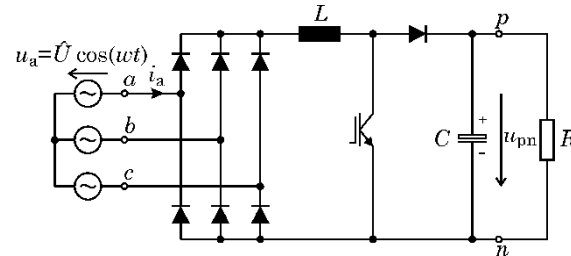
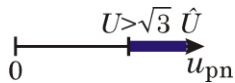


Summary: Unidirectional PFC Rectifier Systems

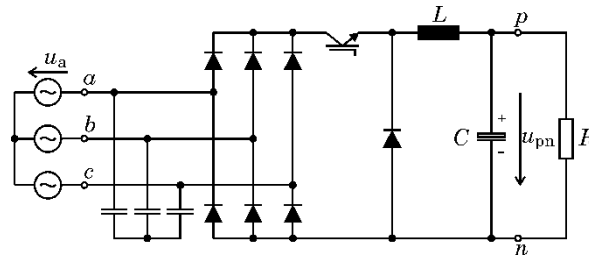
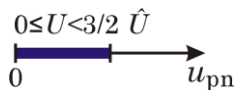
► Block Shaped Input Current Rectifier Systems

- + Controlled Output Voltage
- + Low Complexity
- + High Semicond. Utilization
- + Total Power Factor $\lambda \approx 0.95$
- $\text{THD}_I \approx 30\%$

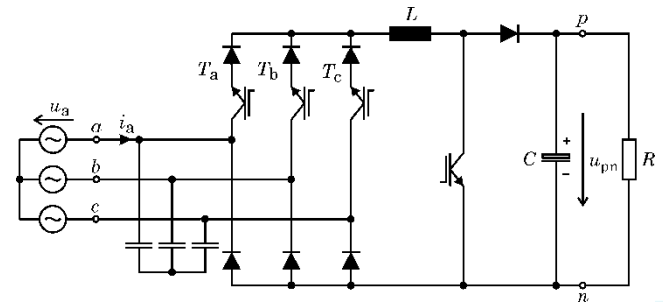
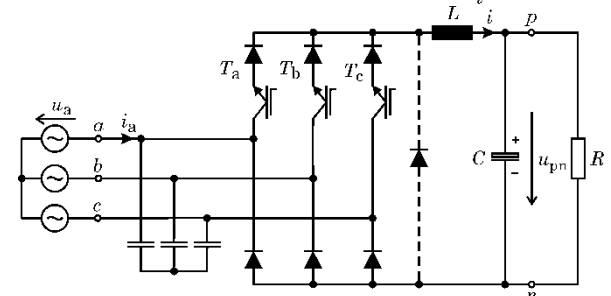
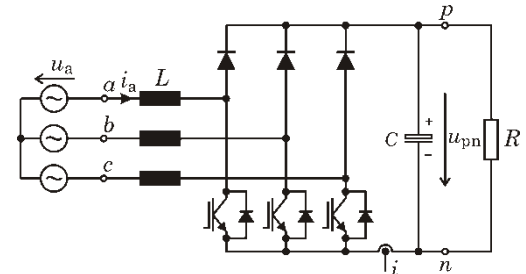
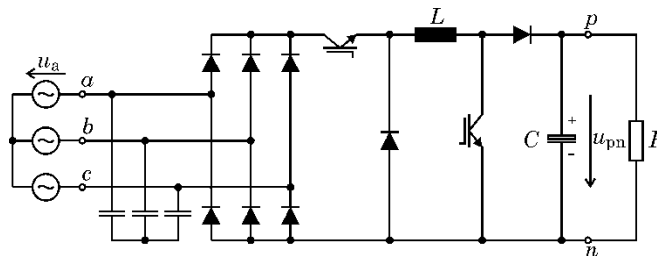
Boost-Type



Buck-Type



Buck+Boost-Type



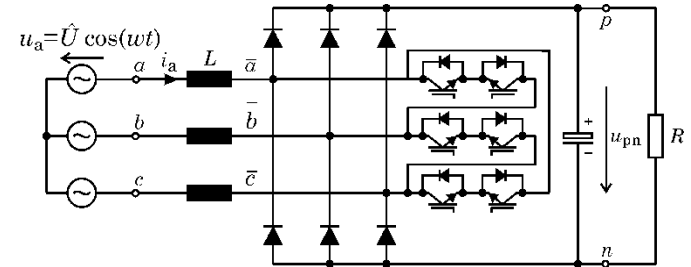
► Sinusoidal Input Current Rectifier Systems (1)

- + Controlled Output Voltage
- + Relatively Low Control Complexity
- + Tolerates Mains Phase Loss
- 2-Level Characteristic
- Power Semiconductors Stressed with Full Output Voltage

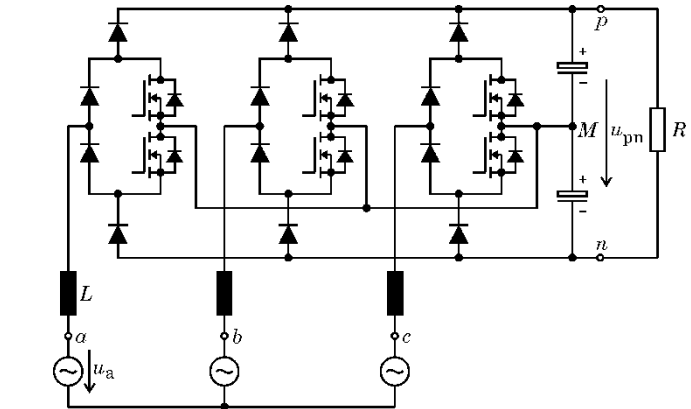
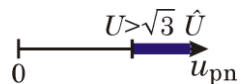
- + Controlled Output Voltage
- + 3-Level Characteristic
- + Tolerates Mains Phase Loss
- + Power Semicond. Stressed with Half Output Voltage
- Higher Control Complexity

- + Low Current Stress on Power Semicond.
- + In Principal No DC-Link Cap. Required
- + Control Shows Low Complexity
- Sinusoidal Mains Current Only for Const. Power Load
- Power Semicond. Stressed with Full Output Voltage
- Does Not Tolerate Loss of a Mains Phase

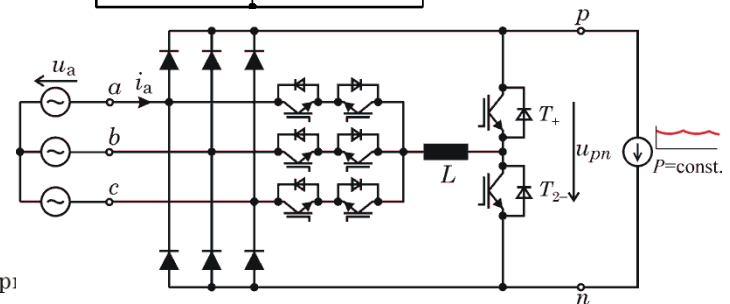
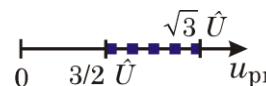
Boost-Type



Boost-Type

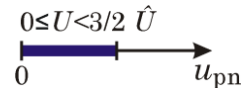


Unregulated Output

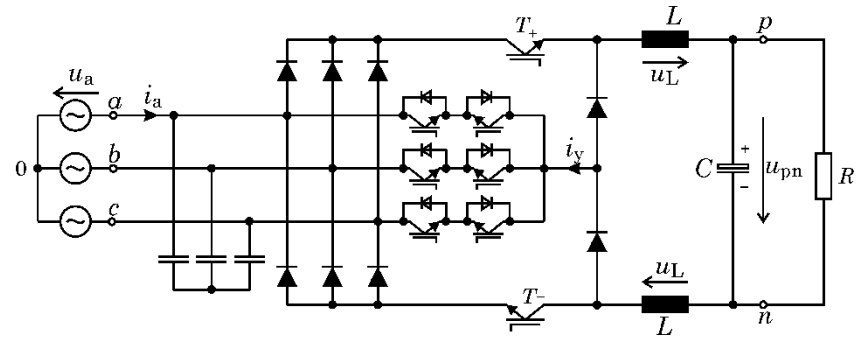


► Sinusoidal Input Current Rectifier Systems (2)

Buck-Type



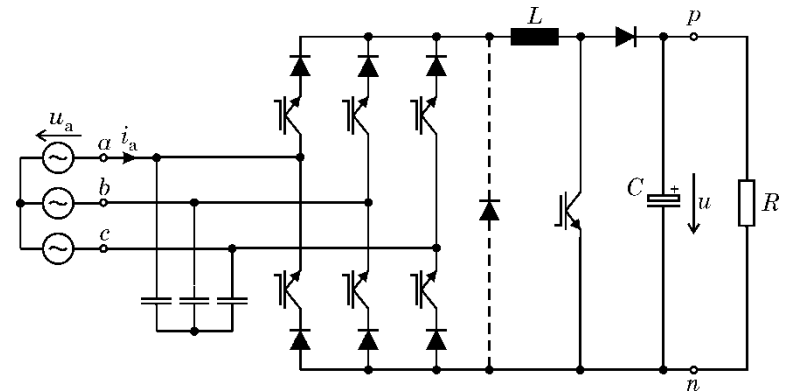
- + Allows to Generate Low Output Voltages
- + Short Circuit Current Limiting Capability
- Power Semicond. Stressed with LL-Voltages
- AC-Side Filter Capacitors / Fundamental Reactive Power Consumption



Buck+Boost-Type



- + See Buck-Type Converter
- + Wide Output Voltage Range
- + Tolerates Mains Phase Loss, i.e. Sinusoidal Mains Current also for 2-Phase Operation
- See Buck-Type Converter (6-Switch Version of Buck Stage Enables Compensation of AC-Side Filter Cap. Reactive Power)



Conclusions & Outlook

Summary of Key Results
Advantageous Applications
Key Challenge



► Key Figures of Designed Transmission Systems

■ 5 kW Prototype System

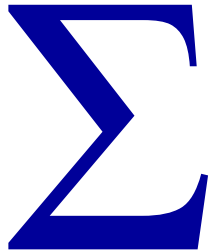


- Output Power 5 kW @ 400 V, 100 kHz
- DC/DC-Efficiency 96.5% @ 52 mm (measured)
- Coil Dimensions 210 mm x 30 mm
- Weight Coil + Cap. 2.3 kg
- Spec. Weight 2.2 kW/kg
- Area-Rel. Power Dens. 1.47 kW/dm²
- Power Density 4.8 kW/dm³
- Spec. Copper Weight 43 g/kW
- Spec. Ferrite Weight 112 g/kW

■ 50 kW Prototype System



- Output Power 50 kW @ 800 V, 85 kHz
- DC/DC-Efficiency 96.5% (calculated)
- Coil Dimensions 41 x 76 x 6 cm
- Weight Coil + Cap. 24.6 kg
- Spec. Weight 2.0 kW/kg
- Area-Rel. Power Dens. 1.6 kW/dm²
- Power Density 2.7 kW/dm³
- Spec. Copper Weight 52 g/kW
- Spec. Ferrite Weight 160 g/kW
- Spec. SiC-Chip Area 9.4 mm²/kW



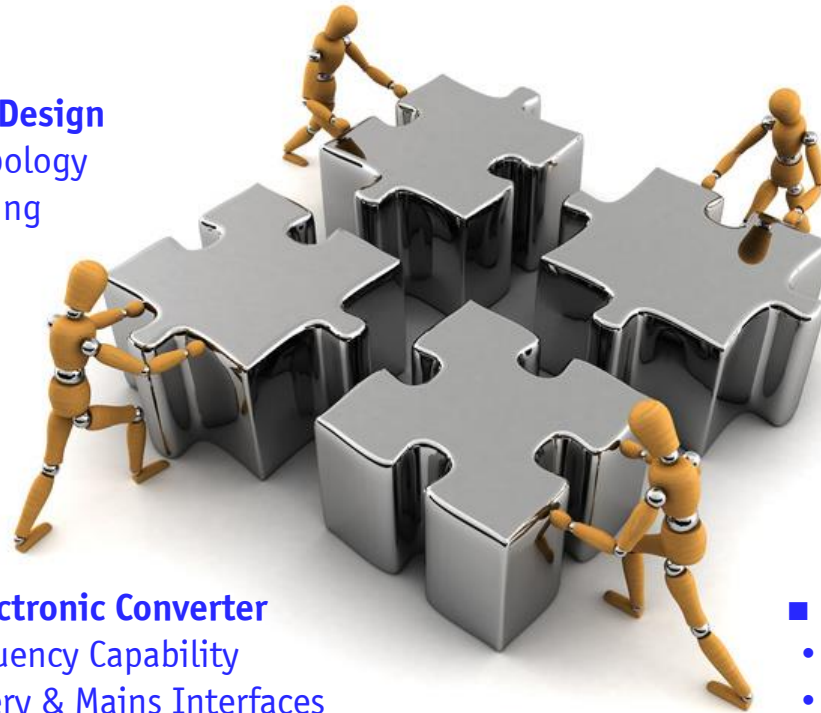
Inductive Power Transfer for EV Charging

■ Resonant Circuit Design

- Compensation Topology
- Impedance Matching

■ Coil Design & Optimization

- Magnetic Modeling & Design
- Multi-Objective Optimization



■ Power Electronic Converter

- High Frequency Capability
- Coil, Battery & Mains Interfaces

■ Modulation & Control Scheme

- Active Load Matching
- High Partial-Load Efficiency

Inductive Power Transfer

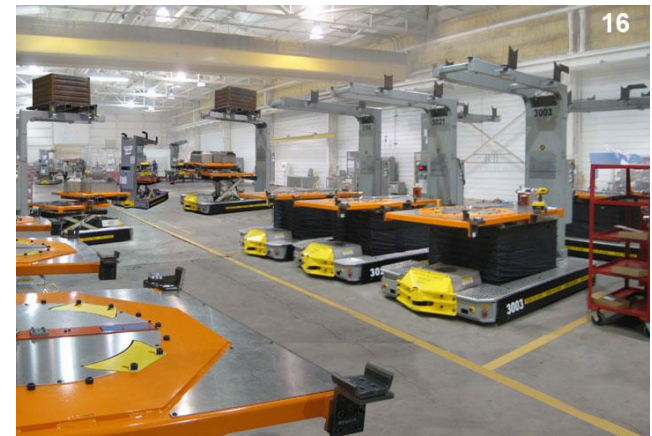
Potential Application Areas

■ Industrial Environments with Power < 50 kW

- Conveyor Vehicles at Industrial Sites / Airports / Hospitals
- Controlled Environment / Autonomous Vehicles
- Reduced Battery Volume & Weight → Lower Cost

■ Power Supply with High Insulation

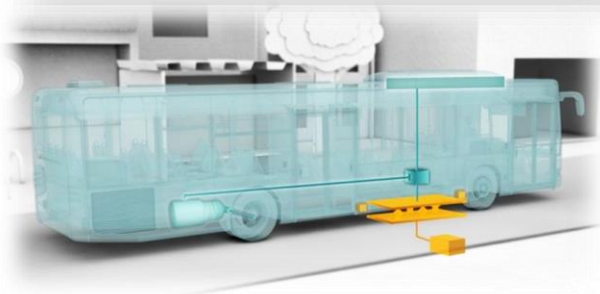
- Auxiliary Supply with High Insulation Strength, e.g. for Gate Drives, Modular Multi-Level, ...



Inductive Power Transfer for Stationary EV Charging

- **Domestic EV Charging form Household Supply**
 - Lower Power Level Simplifies Design
- **Stationary EV Charging for Public Transportation**
 - Simplified Quick-Charging at Bus Stops
 - Reduced Battery Volume/Weight/Cost
 - Reduced Number of Fleet Vehicles

→ **Reduced Operating Costs!**



Evatran PLUGLESS, <http://pluglesspower.com> (6.11.2014).

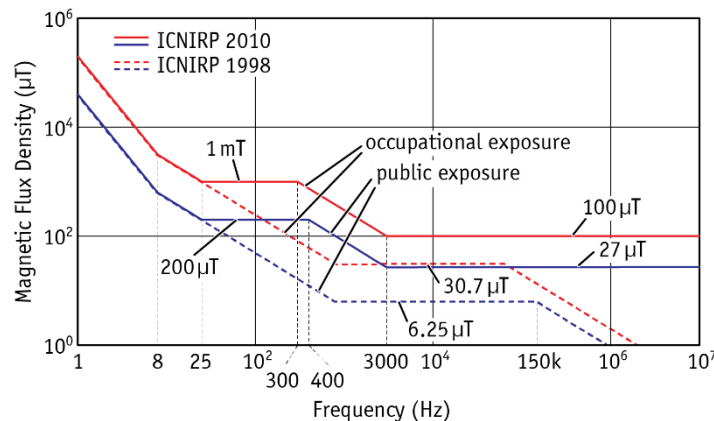
Bombardier PRIMOVE, <http://primove.bombardier.com>.

Inductive Power Transfer

Key Challenge

■ Compliance with Field-Exposure Standards at High Power Levels

- High Frequency for High Power Transfer → Where is the Limit?
- Include Modifications on Vehicle Chassis?
- Positioning of the Coil: On the Floor / the Roof?

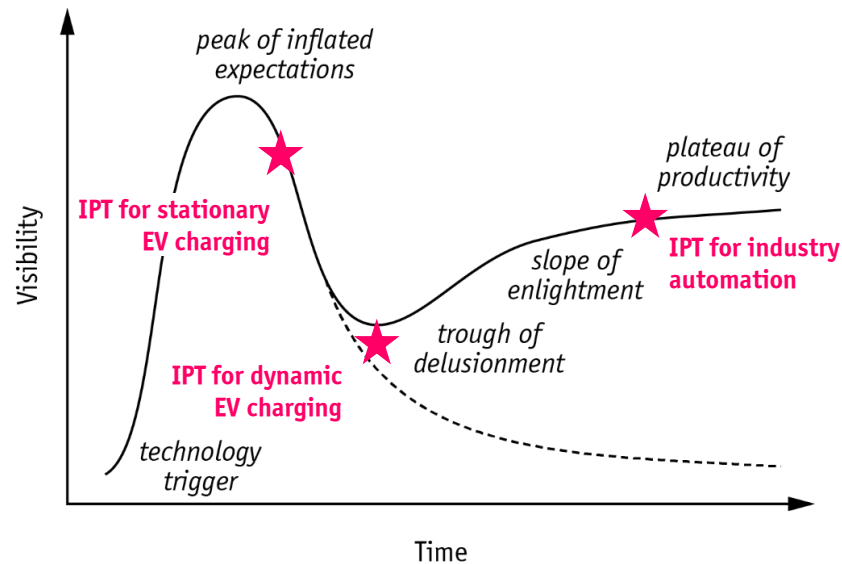


▲ Field Values are Limiting Factor at High Power



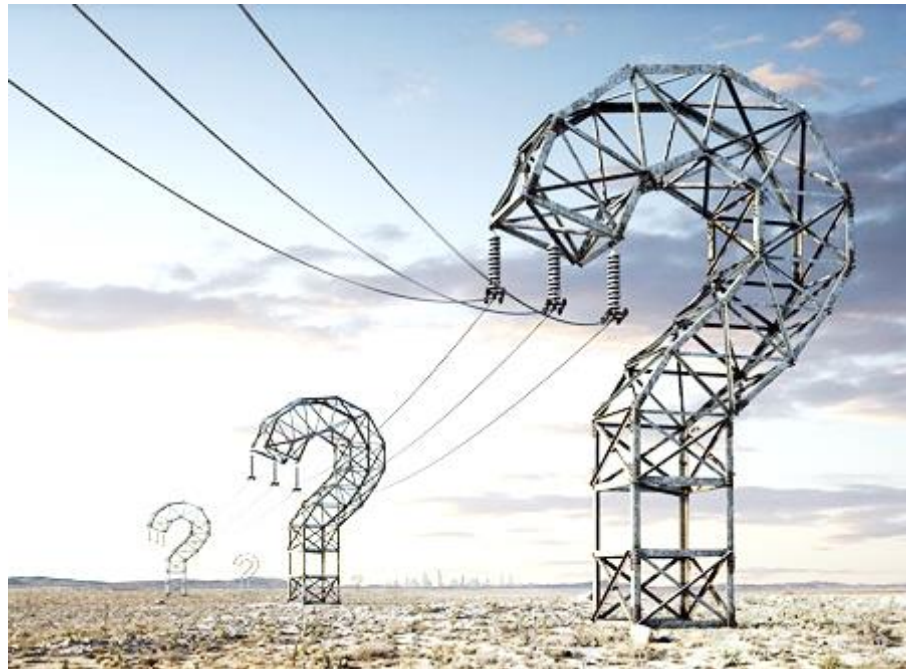
▲ Include Chassis Modifications in Design
& Re-Consider Coil Positioning

Inductive Power Transfer Applications ... the Hype Cycle



Thank You!

Questions?



► Further Information

- **Appendix 1:** Comments on Dynamic IPT Charging
- **Appendix 2:** 3- Φ PFC Rectifier Systems

■ List of Key Publications (click title to view online)

- **R. Bosshard, J. W. Kolar, J. W. Mühlethaler, I. Stevanovic, B. Wunsch, F. Canales**, “Modeling and η - α -Pareto optimization of inductive power transfer coils for electric vehicles,” *IEEE J. Emerg. Sel. Topics Power Electron.*, vol. 3, no. 1., pp.50-64, March 2015.
- **R. Bosshard, J. W. Kolar, B. Wunsch**, “Control Method for Inductive Power Transfer with High Partial-Load Efficiency and Resonance Tracking,” *Proc. Int. Power Electron. Conf. - ECCE Asia (IPEC 2014)*, May 2014.
- **R. Bosshard, J. W. Kolar, B. Wunsch**, “Accurate Finite-Element Modeling and Experimental Verification of Inductive Power Transfer Coil Design,” *Proc. 29th Appl. Power Electron. Conf. and Expo. (APEC 2014)*, March 2014.
- **R. Bosshard, J. Mühlethaler, J. W. Kolar, I. Stevanovic**, “Optimized Magnetic Design for Inductive Power Transfer Coils,” *Proc. 28th Appl. Power Electron. Conf. and Expo. (APEC 2013)*, March 2013.
- **R. Bosshard, U. Badstübner, J. W. Kolar, I. Stevanovic**, “Comparative Evaluation of Control Methods for Inductive Power Transfer,” *Proc. Int. Conf. on Renewable Energy Research and Appl. (ICRERA 2012)*, November 2012.
- **R. Bosshard, J. Mühlethaler, J. W. Kolar, I. Stevanovic**, “The η - α -Pareto Front of Inductive Power Transfer Coils,” *Proc. Annu. Conf. IEEE Ind. Electron. Soc. (IECON 2012)*, October 2012.
- **J. W. Kolar, T. Friedli**, “The Essence of Three-Phase PFC Rectifier Systems - Part I,” *IEEE Trans. Power Electron.*, vol. 28, no. 1, pp. 176-198, January 2013.
- **T. Friedli, M. Hartmann, J. W. Kolar**, “The Essence of Three-Phase PFC Rectifier Systems - Part II”, *IEEE Trans. Power Electron.*, vol. 29, no. 2, February 2014.

■ Contact Information

- Roman Bosshard: bosshard@lem.ee.ethz.ch
- Johann W. Kolar: kolar@lem.ee.ethz.ch

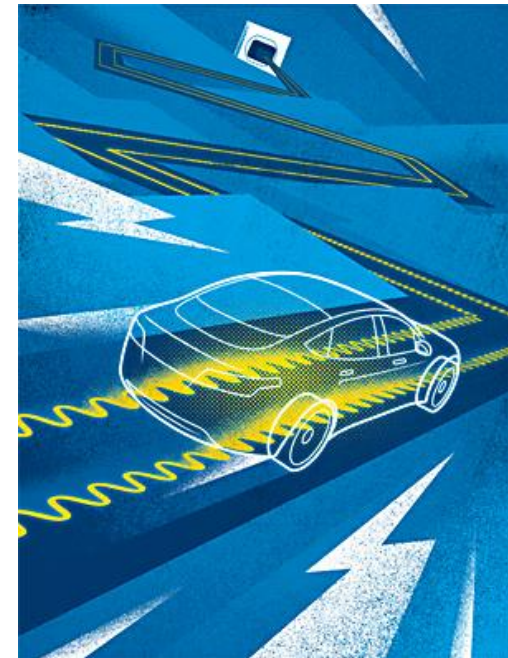
Appendix 1: Comments on Dynamic IPT Charging

Inductive Power Transfer for Dynamic EV Charging

Simplified Calculation

- **20 km of Highway @ avg. 25 kW¹, 120 km/h**
 - $20/120 \text{ h} \times 25 \text{ kW} = 4.2 \text{ kWh}$ used
- **200 m IPT-Lane per 20 km of Highway**
 - Electrification of 1%
- **Speed while Charging 50 km/h**
 - 14 s for Charging of 4.2 kWh
- **1 MW / Vehicle Required Charging Power**
 - High Cost for Medium Voltage Infrastructure
 - Battery that Handles 1 MW?
 - Slowing Down to 50 km/h every 20 km?
- **Stationary: 10 min \times 1 MW = 167 kWh \rightarrow 6.6 h Driving!**

James Provost for IEEE Spectrum



¹ T. Bütler and H. Winkler, «Energy consumption of battery electric vehicles (BEV),» EMPA, Dübendorf, Switzerland, 2013.

Inductive Power Transfer for Dynamic EV Charging

- **Large & Expensive Installation**
vs. Improving Battery Technology
- **Medium-Voltage Supply & Distribution of**
Power along 1% of all Highways
- **Efficiency of Dynamic IPT**
vs. Increasing Energy Cost?
- **Possible Applications:**
 - Electrification @ Traffic Lights, Bus Stops, ...
 - Transportation Vehicles @ Industrial Sites



Appendix 2: 3- Φ PFC Rectifier Systems

J. W. Kolar, T. Friedli,

*The Essence of Three-Phase PFC Rectifier
Systems - Part I*, IEEE Transactions on
Power Electronics, Vol. 28, No. 1, pp.
176-198, January 2013.

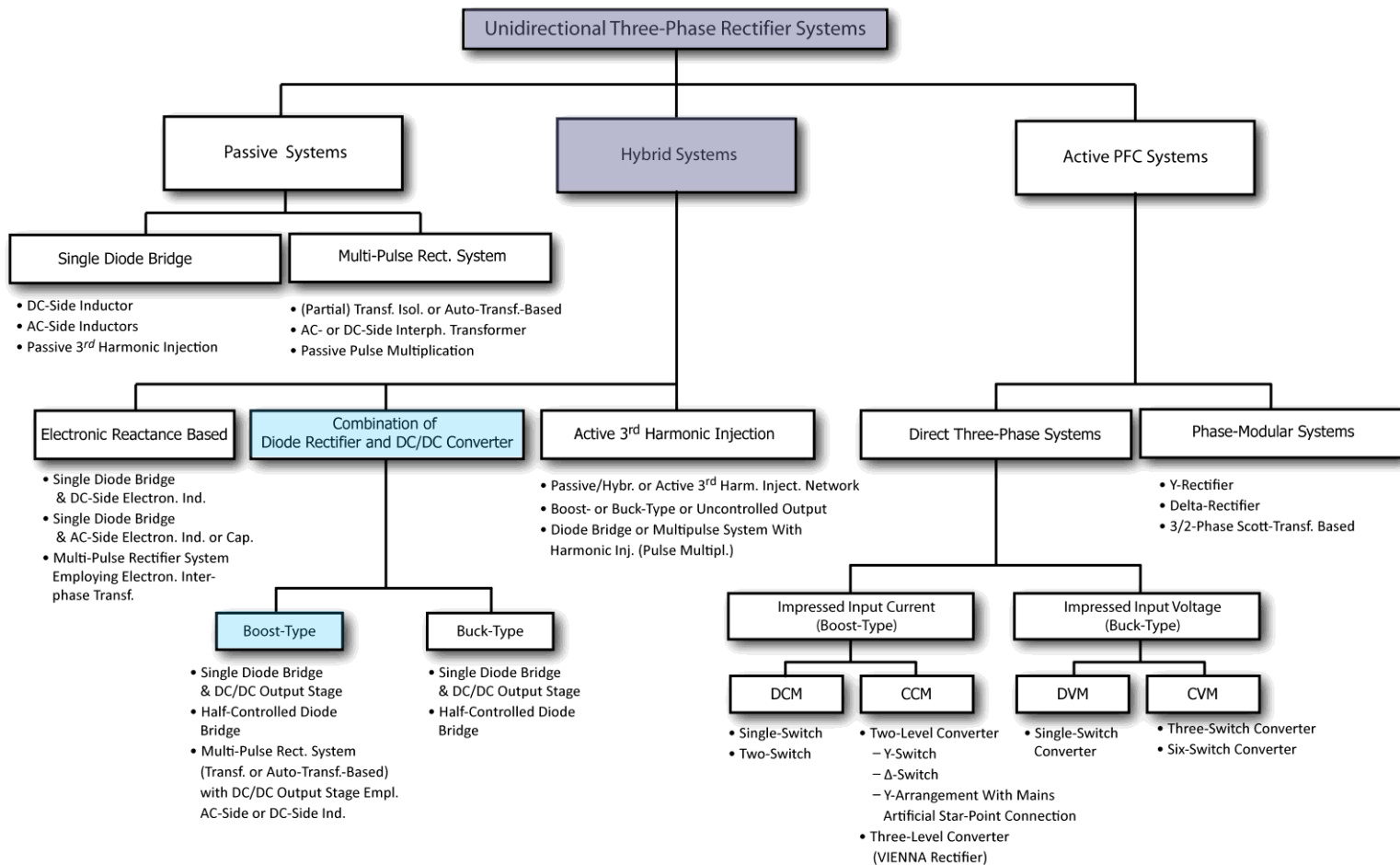
T. Friedli, M. Hartmann, J. W. Kolar,

*The Essence of Three-Phase PFC Rectifier
Systems - Part II*, IEEE Transactions on
Power Electronics, Vol. 29, No. 2,
February 2014.

Hybrid 3- Φ Boost-Type PFC Rectifier Systems

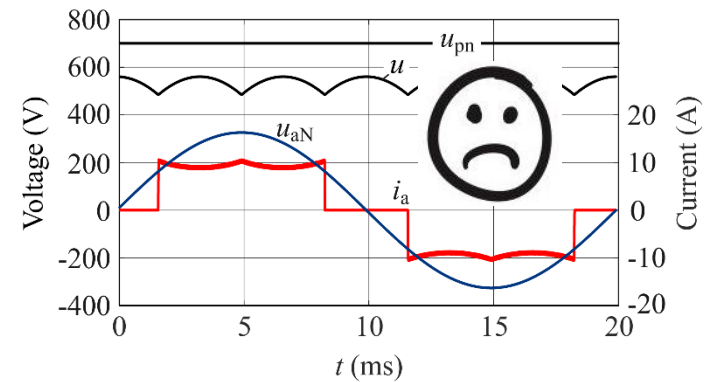
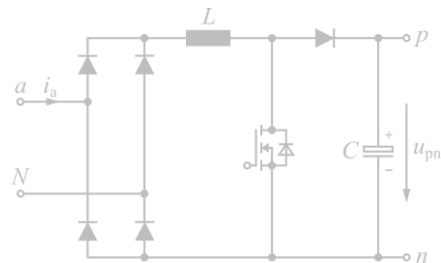
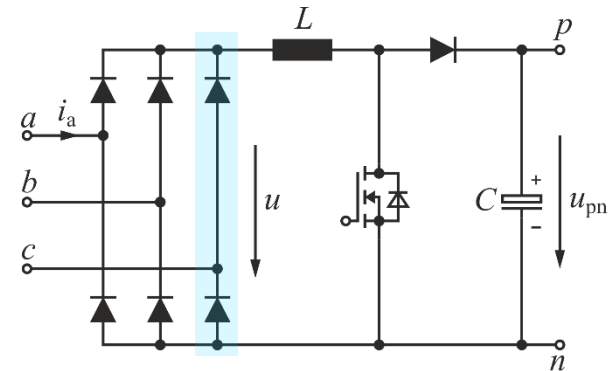
3rd Harmonic Injection Rectifier

► Classification of Unidirectional Rectifier Systems



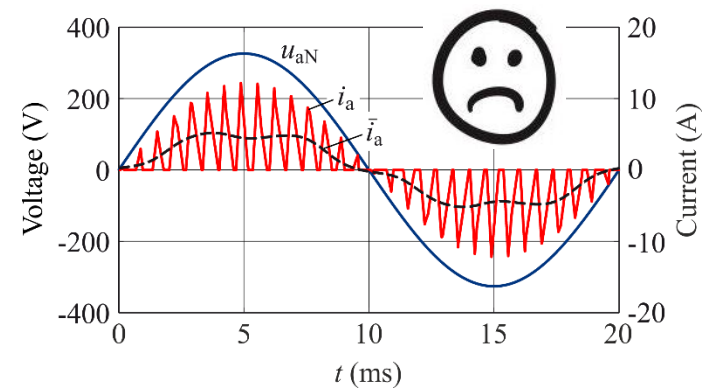
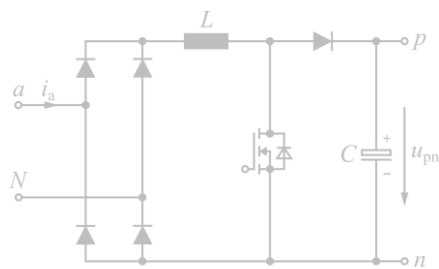
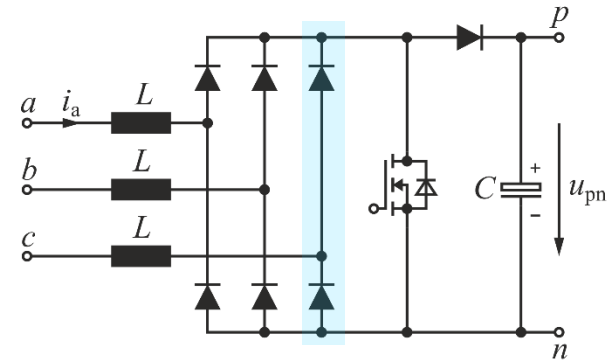
Diode Bridge + DC/DC Boost Converter

- Controllable Output Voltage
- Low-Frequency Mains Current Distortion

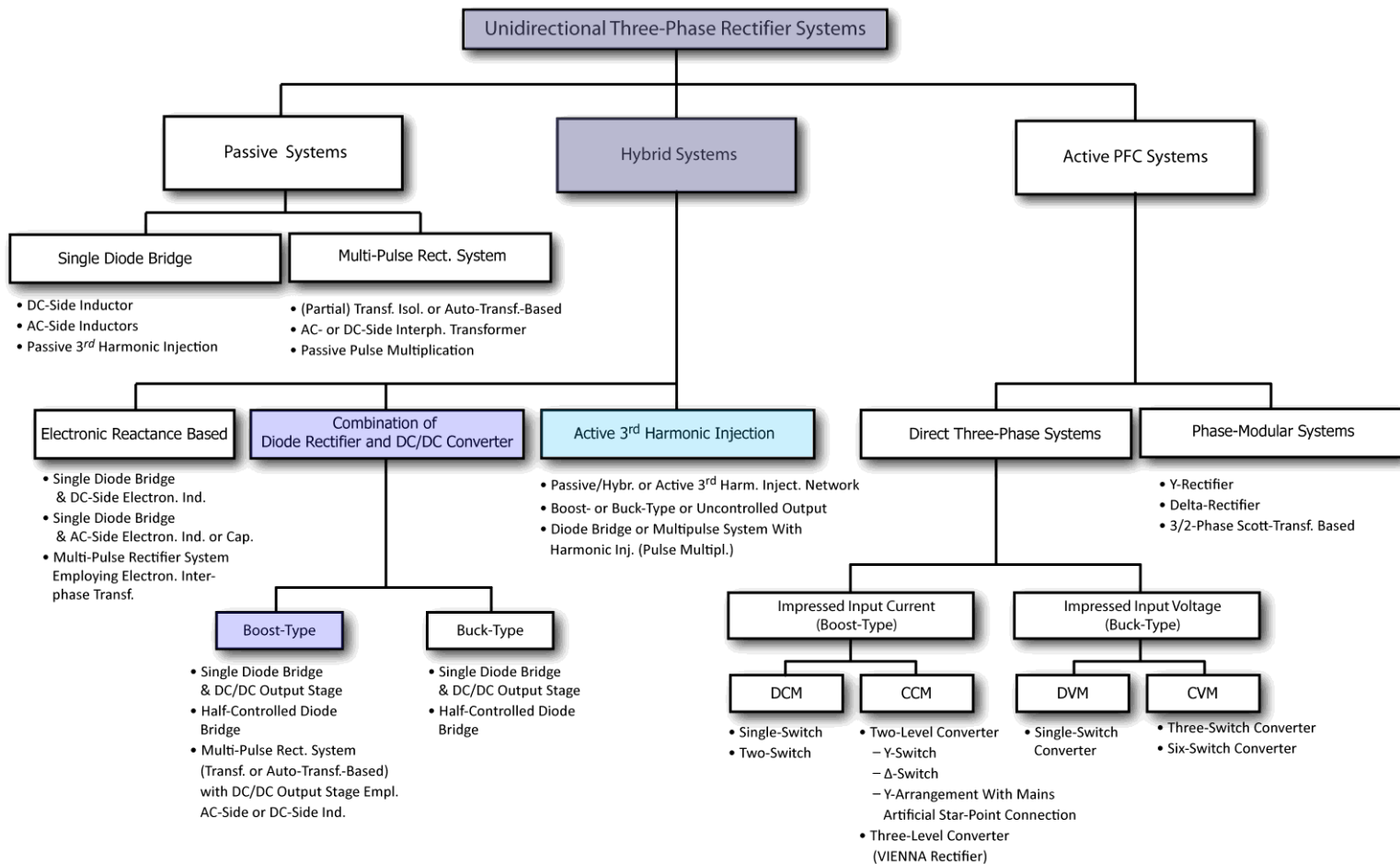


3- Φ DCM (PFC) Boost Rectifier

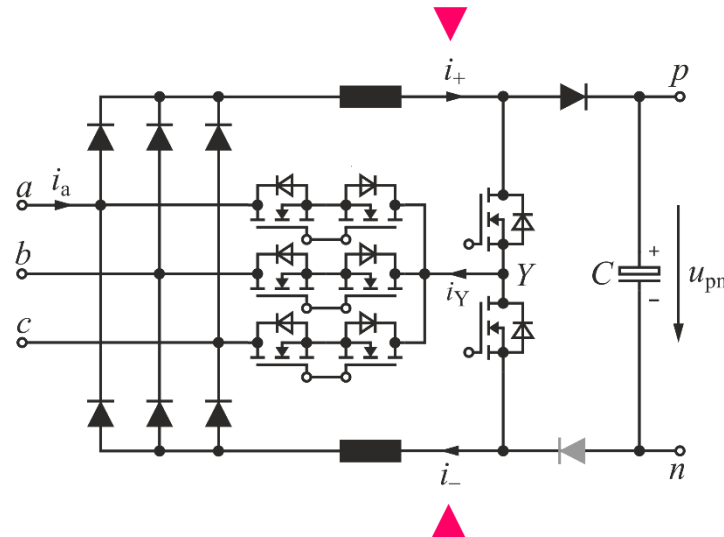
- Controllable Output Voltage
- Low-Frequency Mains Current Distortion



► Classification of Unidirectional Rectifier Systems

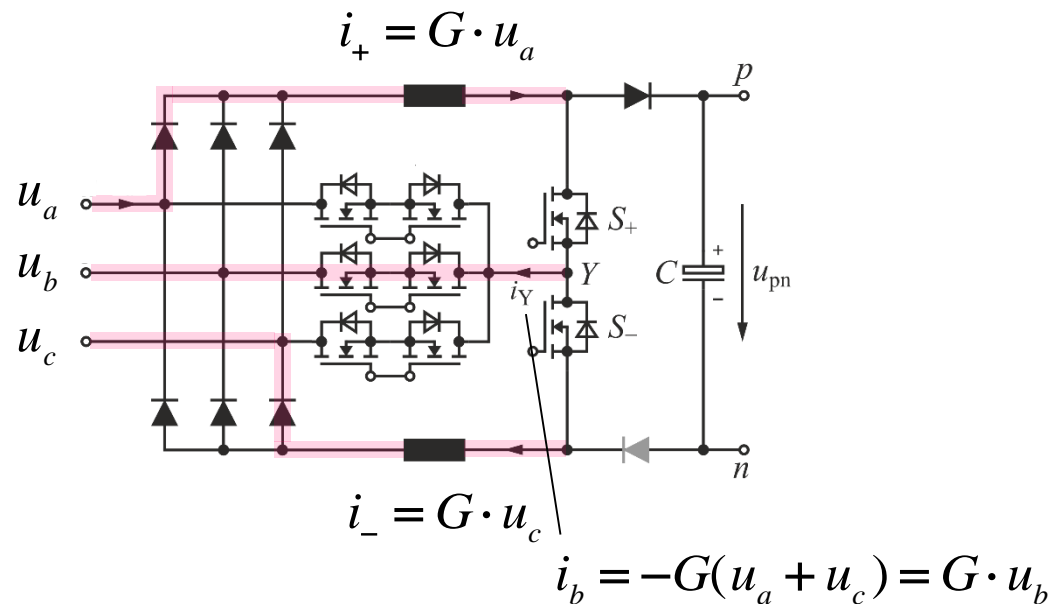


3- Φ Hybrid 3rd Harmonic Inj. PFC Boost-Rectifier

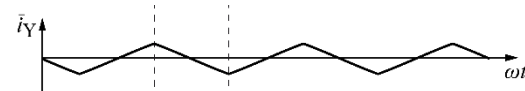


- Independent Control of i_+ and i_-

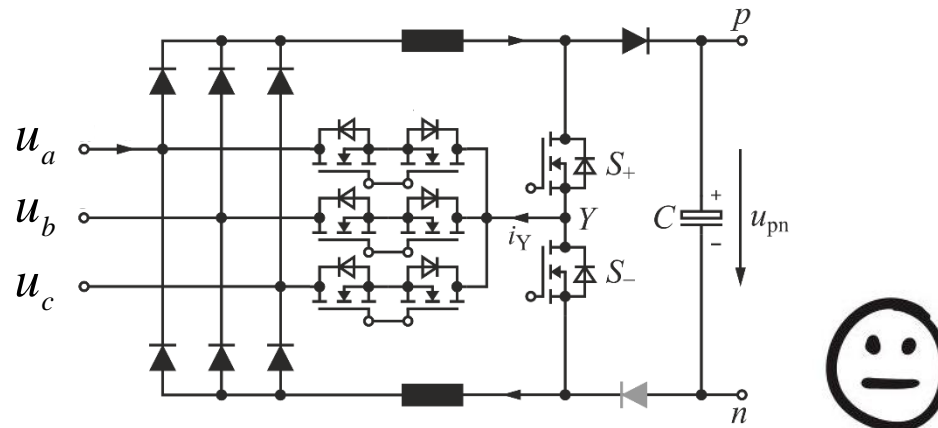
3- Φ Hybrid 3rd Harmonic Inj. PFC Boost-Rectifier



■ Sinusoidal Control of i_+ and i_- and i_Y



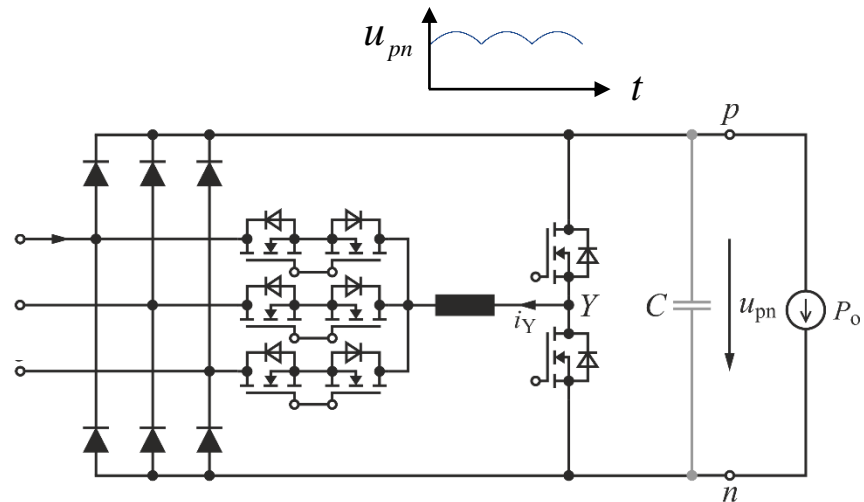
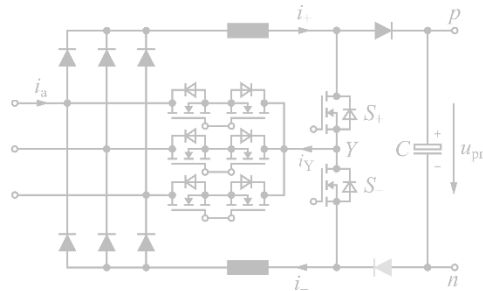
3- Φ Hybrid 3rd Harmonic Inj. PFC Boost-Rectifier



- Sinusoidal Mains Current Control
- Output Voltage Control

- Limited to Ohmic Mains Behavior
- High Minimum Output Voltage Level

3- Φ Active Filter Type PFC Rectifier



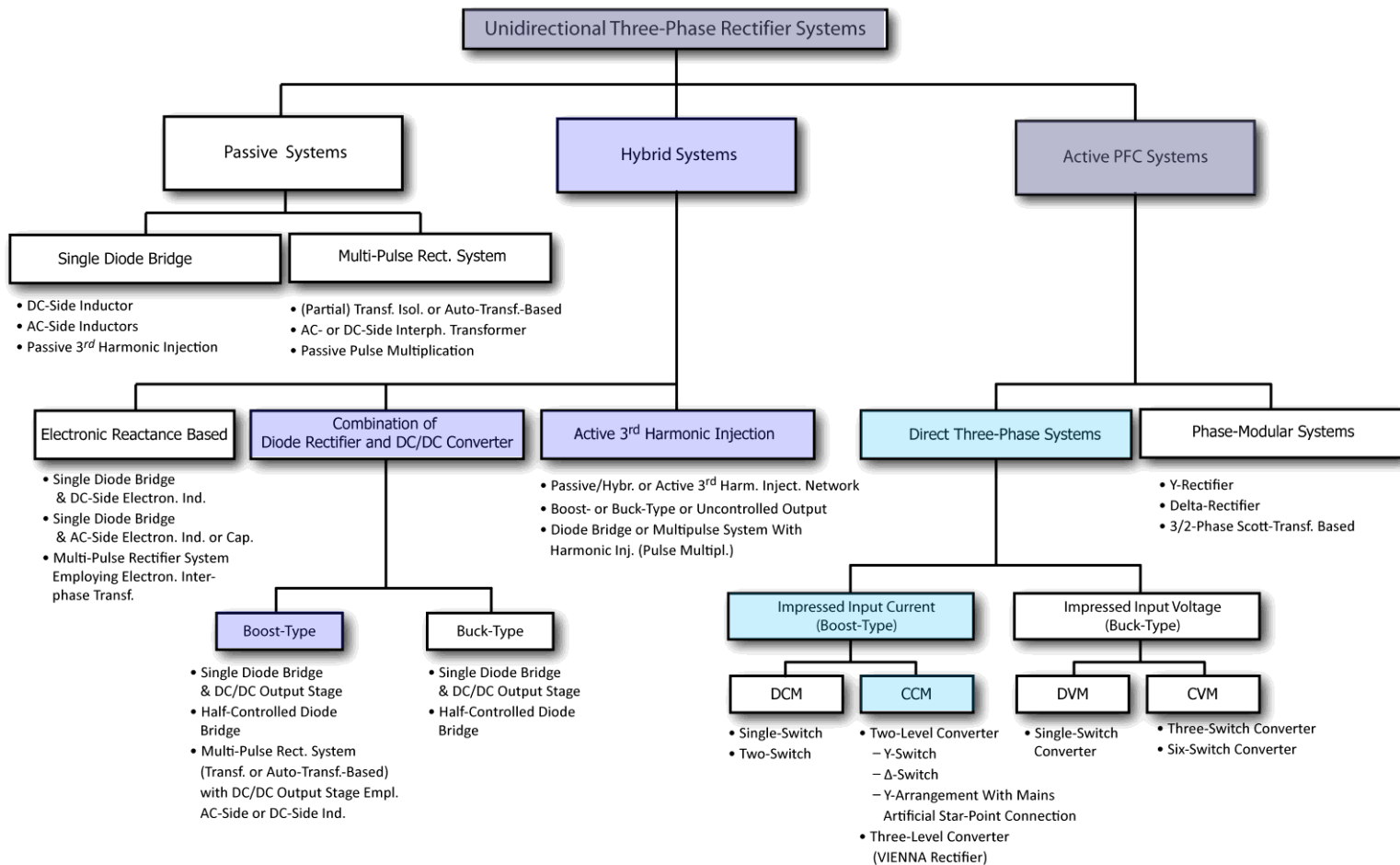
■ Sinusoidal Mains Current

→ Requires Constant Power Load $P_o = \text{const.}$
→ NO (!) Output Voltage Control

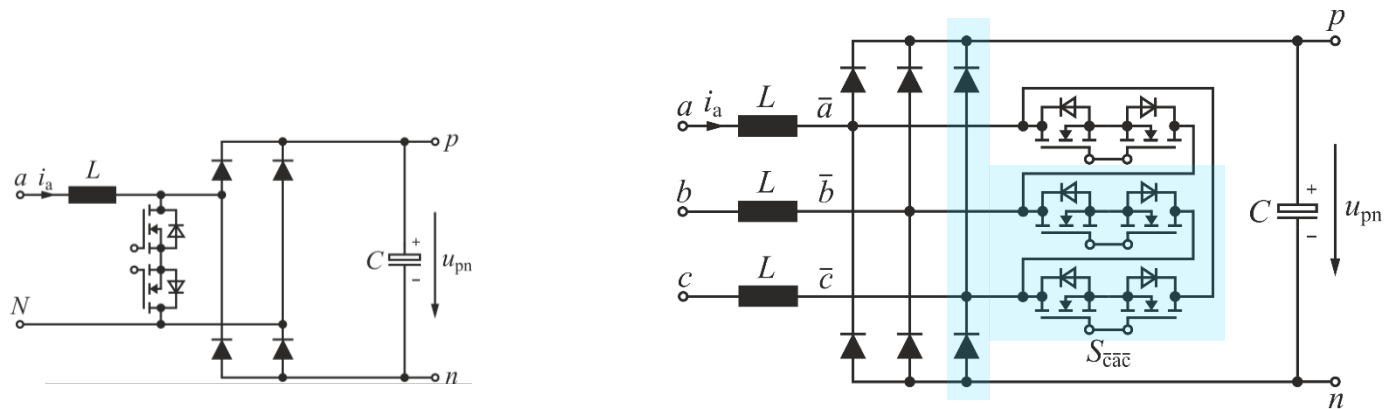
Active 3- Φ Boost-Type PFC Rectifier Systems

*Δ -Switch Rectifier
Vienna-Rectifier
Six-Switch Rectifier*

► Classification of Unidirectional Rectifier Systems

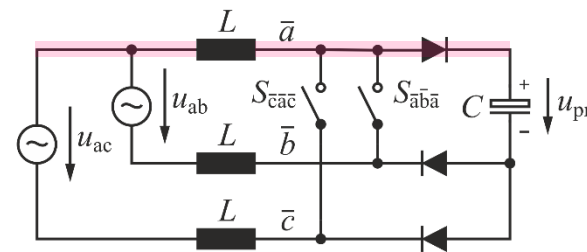
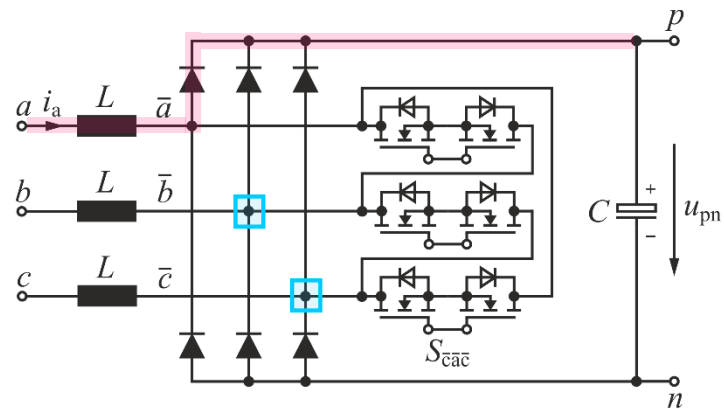
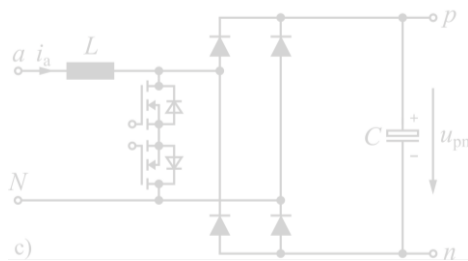


Δ -Switch Rectifier



- Modulation of Diode Bridge Input Voltages / Conduction States
- Derivation of 3- Φ Topology \rightarrow Phase-Symmetry / Bridge-Symmetry

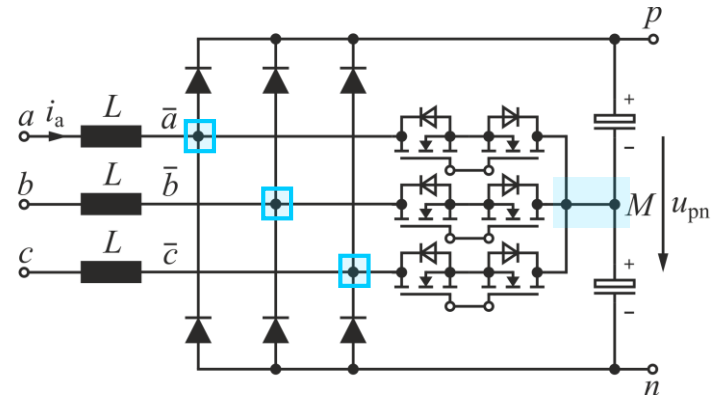
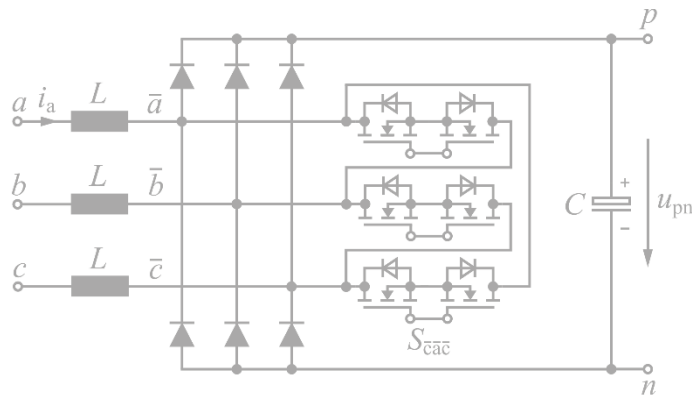
Δ -Switch Rectifier



- Output Voltage Control
- Sinusoidal Mains Current Control
- $\Phi = (-30^\circ, +30^\circ)$



Vienna Rectifier

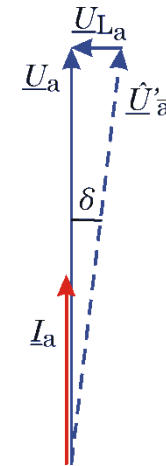
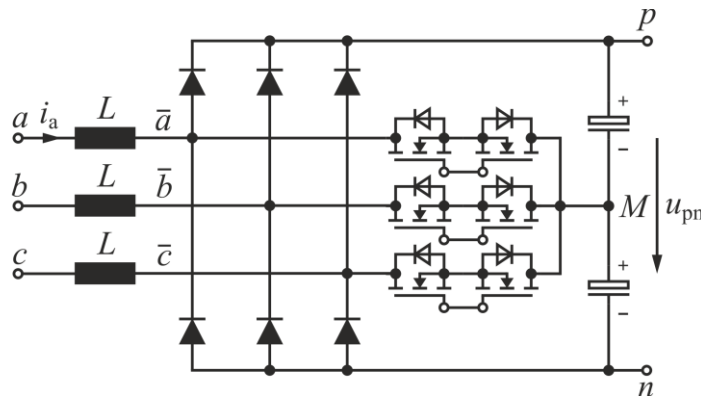


- Replace Δ -Switch by Y-Switch
- Connect Y-Switch to Output Center Point
- Maximum Phase/Bridge Symmetry

- Output Voltage Control
- Sinusoidal Mains Current Control
- $\Phi = (-30^\circ, +30^\circ)$

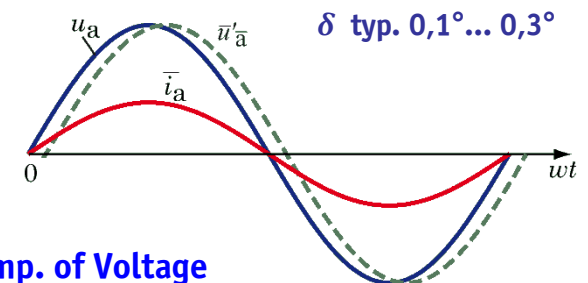
Vienna Rectifier

► Three-Level Characteristic

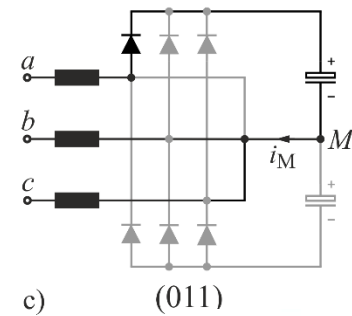
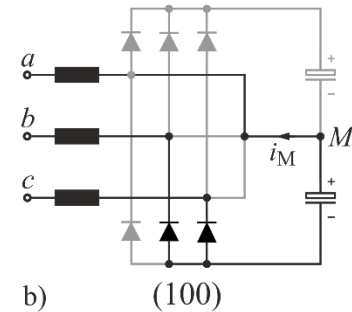
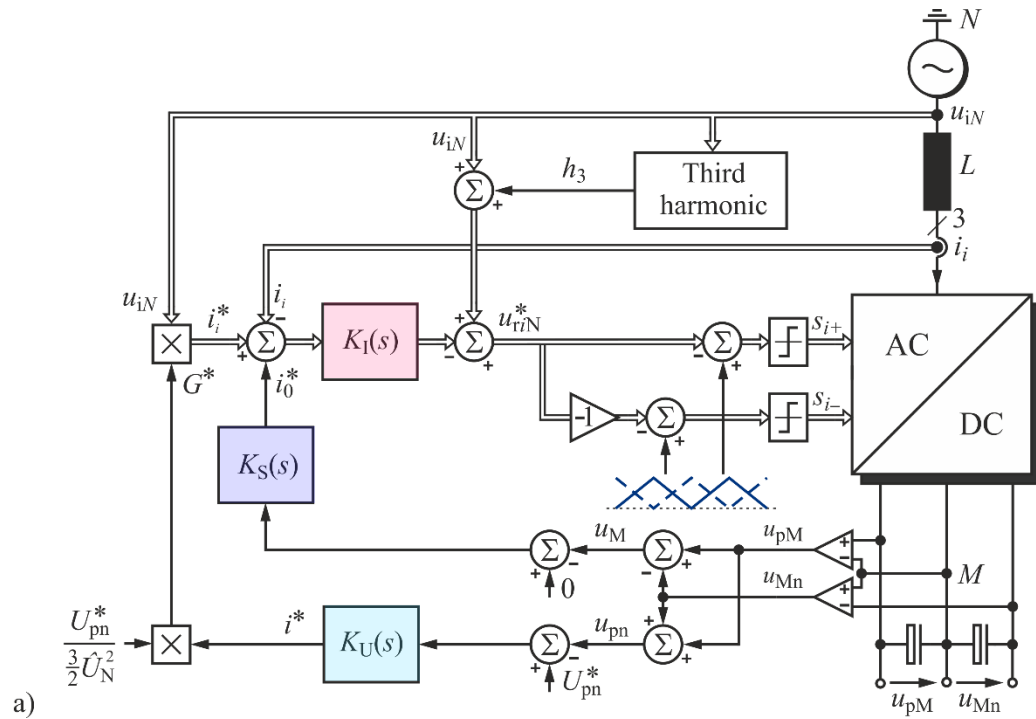


- + Low Input Inductance Requ.
- + Low Switching Losses,
- + Low EMI
- Higher Circuit Complexity
- Control of Output Voltage Center Point Required

► Difference of Mains Voltage (e.g. u_a) and Mains Frequency Comp. of Voltage Formed at Rectifier Bridge Input (e.g. \bar{u}'_a) Impresses Mains Current (e.g. i_a)



Control Structure

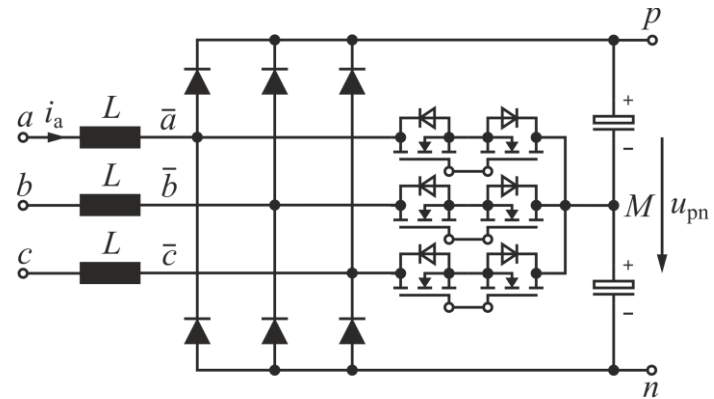


- ## ■ Output Voltage Control & Inner Mains Current Control & *NPP* Control

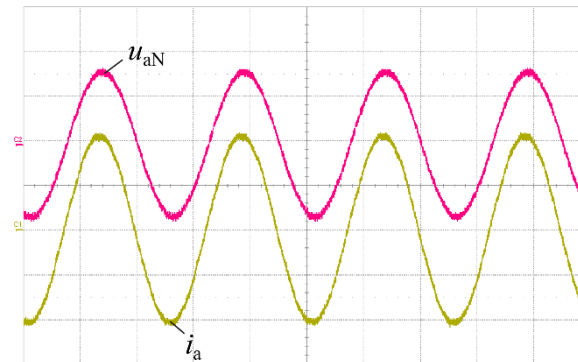
Experimental Results

$P_o = 10\text{kW}$
 $U_N = 230\text{V}$
 $f_N = 800\text{Hz}$
 $U_o = 800\text{V}$
 $THD_i = 1.6\%$

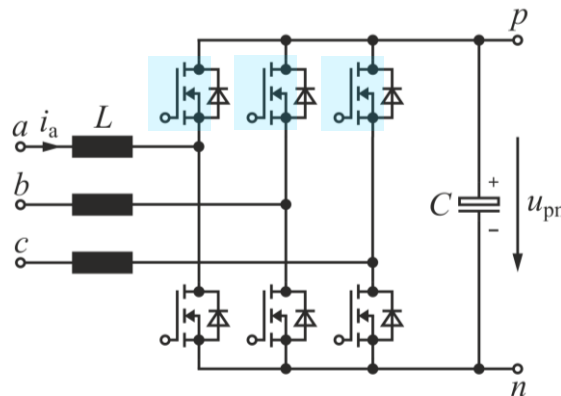
★ $10\text{kW}/\text{dm}^3$



$10\text{A}/\text{Div}$
 $200\text{V}/\text{Div}$
 $0.5\text{ms}/\text{Div}$



Fully-Controlled (Six-Switch) Bridge Rectifier



■ Output Voltage Control

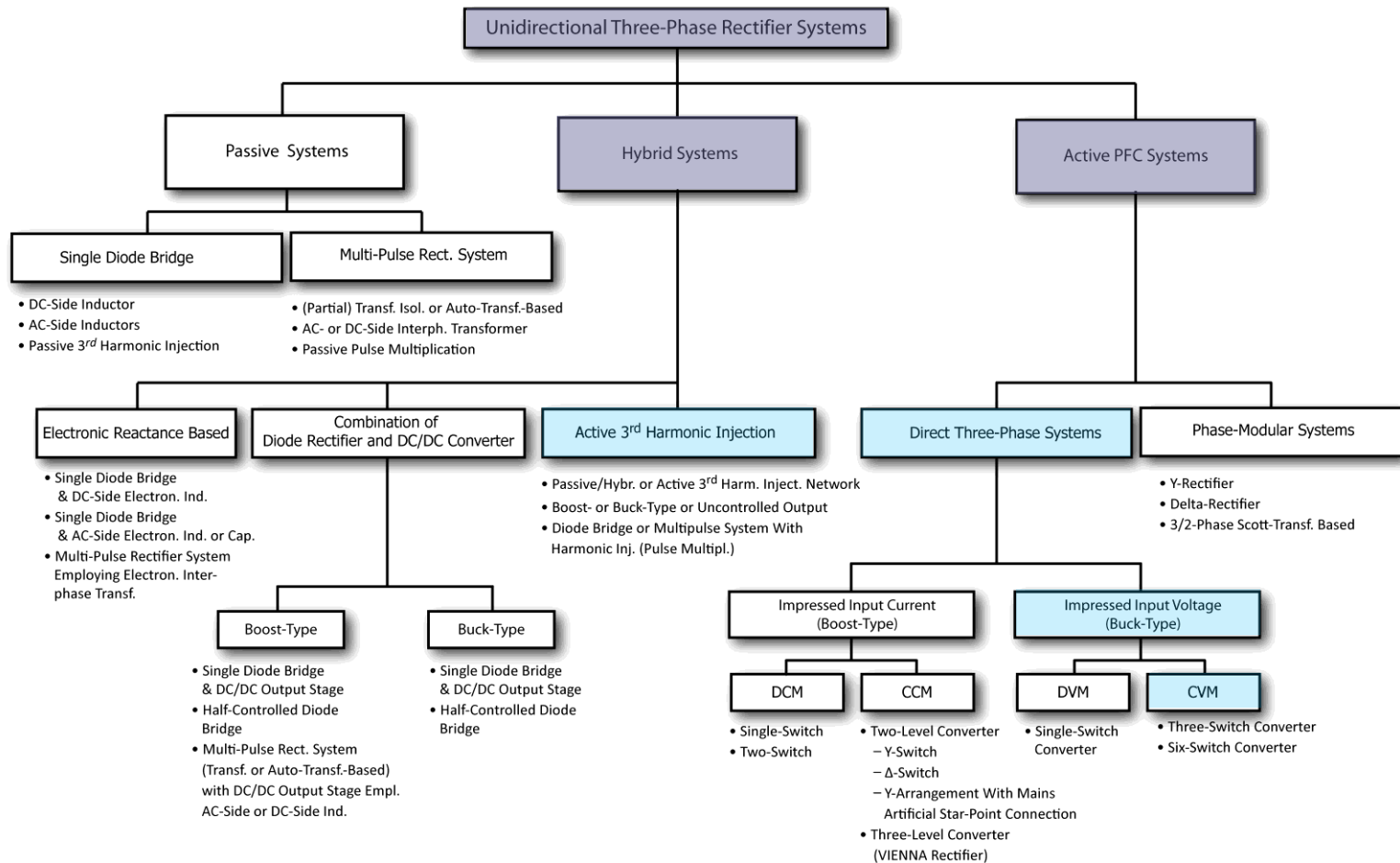
- Phase- & Bridge-Symmetry
- Sinusoidal Mains Current Control
- $\Phi = (-180^\circ, +180^\circ)$ – Bidirectional (!)



3- Φ Buck-Type PFC Rectifier Systems

- Unidirectional
- Bidirectional

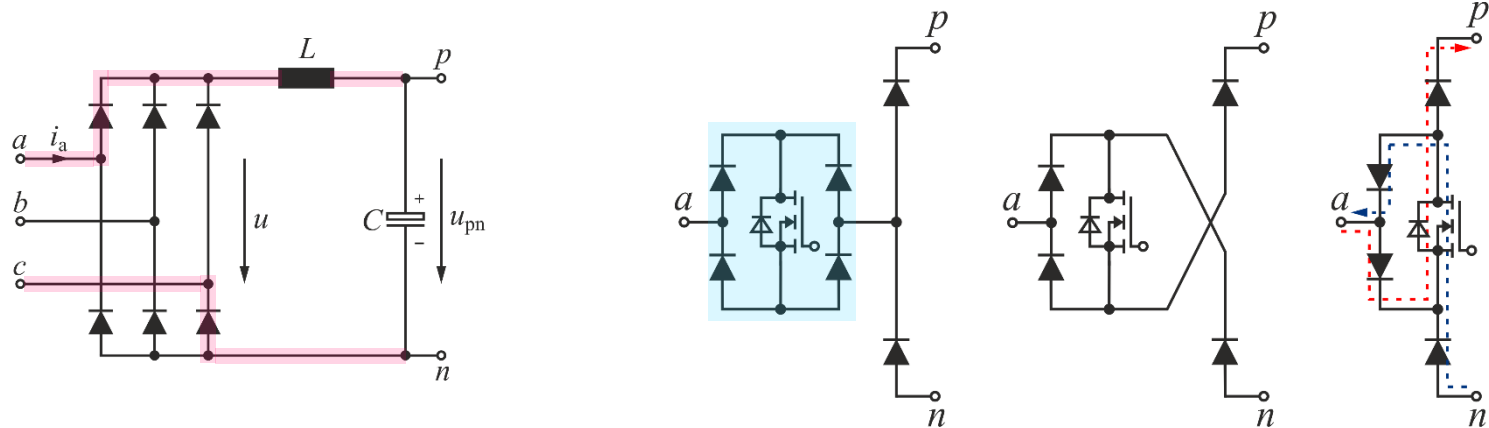
► Classification of Unidirectional Rectifier Systems



Active 3- Φ Buck-Type PFC Rectifier Systems

Three-Switch Rectifier
Six-Switch Rectifier

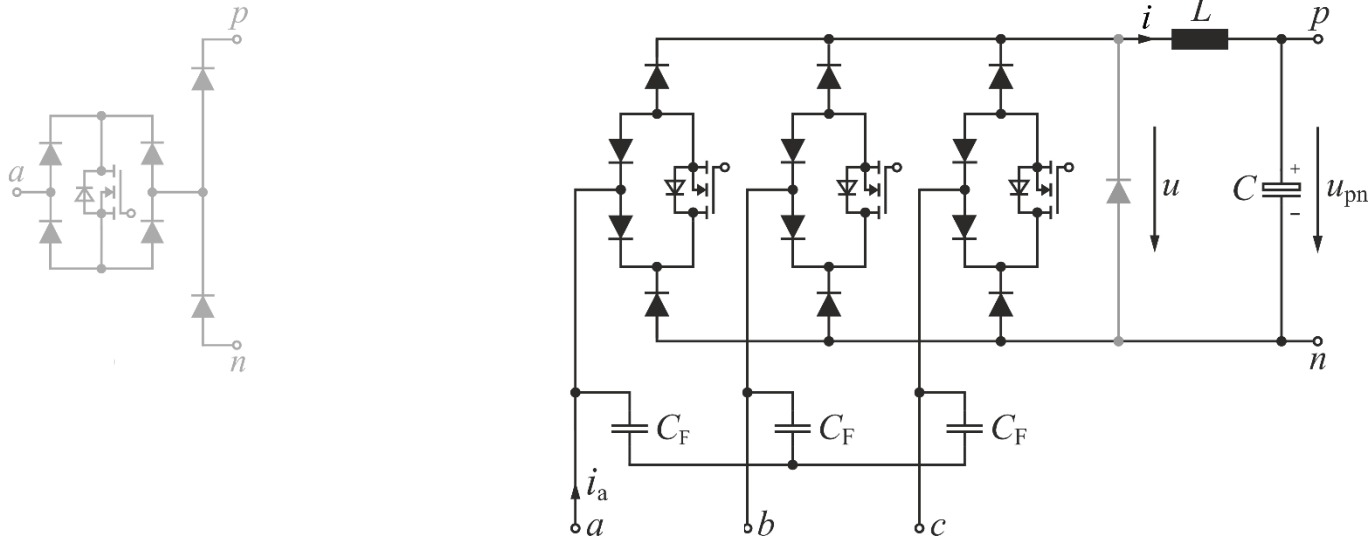
Three-Switch PFC Rectifier



■ Derivation of Rectifier Topology

- Controllability of Conduction State
- Phase-Symmetry / Bridge-Symmetry

Three-Switch PFC Rectifier

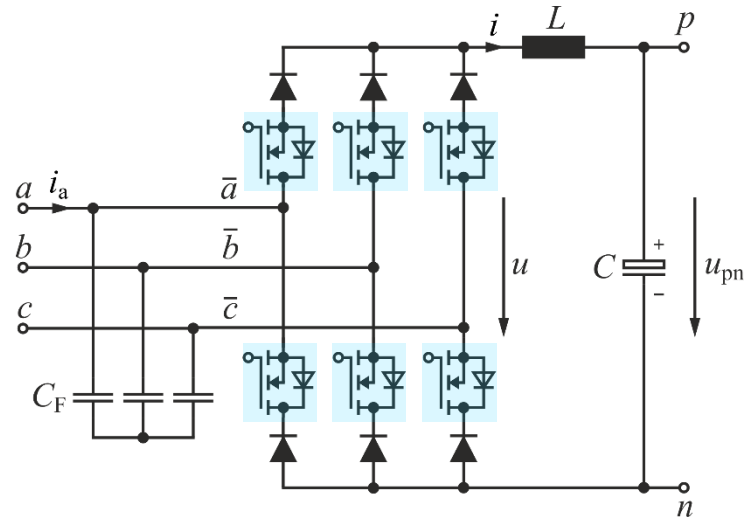
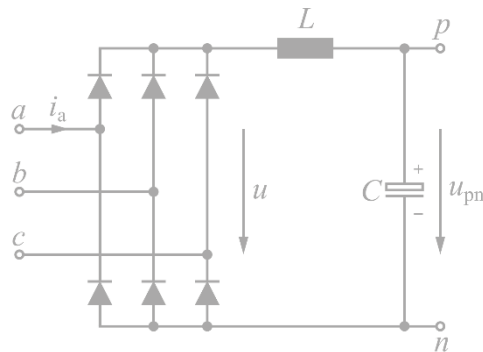


- Output Voltage Control
- Sinusoidal Mains Current Control
- $\Phi = (-30^\circ, +30^\circ)$

→ Relatively High Conduction Losses



Six-Switch PFC Rectifier



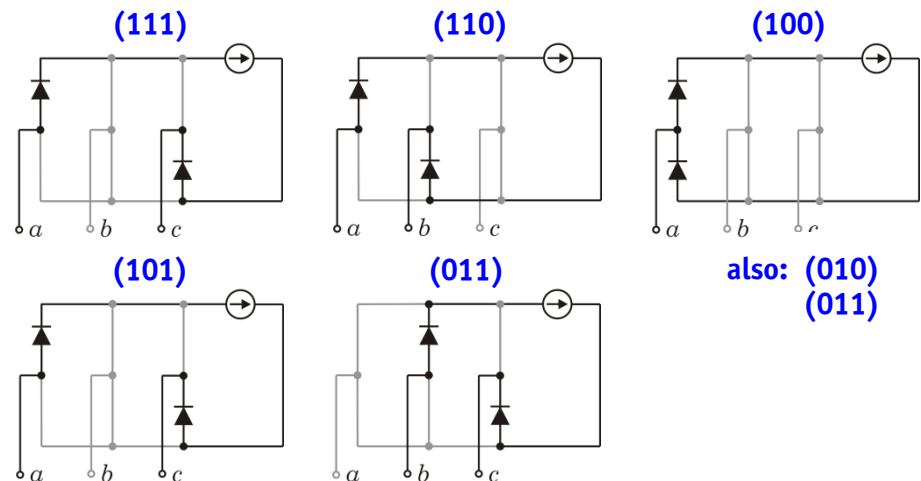
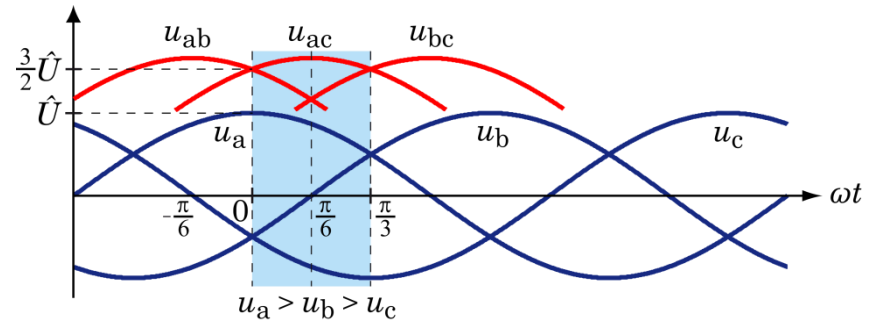
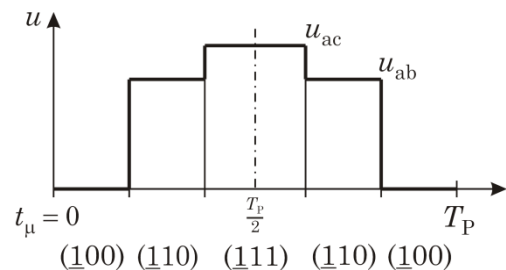
- Controllability of Conduction State
- Phase-Symmetry / Bridge-Symmetry

- Output Voltage Control
- Sinusoidal Mains Current Control
- $\Phi = (-90^\circ, +90^\circ)$



► Modulation Scheme

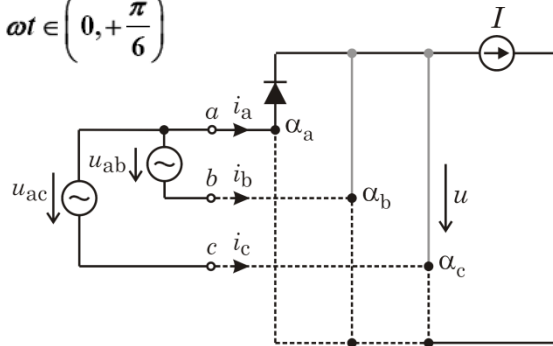
- Consider 60°-Wide Segment of the Mains Period; Suitable Switching States Denominated by (s_a, s_b, s_c)
- Clamping to Phase with Highest Absolute Voltage Value, i.e.
 - Phase a for $\omega t \in \left(-\frac{\pi}{6}, +\frac{\pi}{6}\right)$,
 - Phase c for $\omega t \in \left(+\frac{\pi}{6}, +\frac{\pi}{2}\right)$ etc.
- Assumption: $\omega t \in \left(0, +\frac{\pi}{6}\right)$



- Clamping and “Staircase-Shaped” Link Voltage in Order to Minimize the Switching Losses

► Input Current and Output Voltage Formation

- **Assumption:** $\omega t \in \left(0, +\frac{\pi}{6}\right)$



- **Output Voltage Formation:**

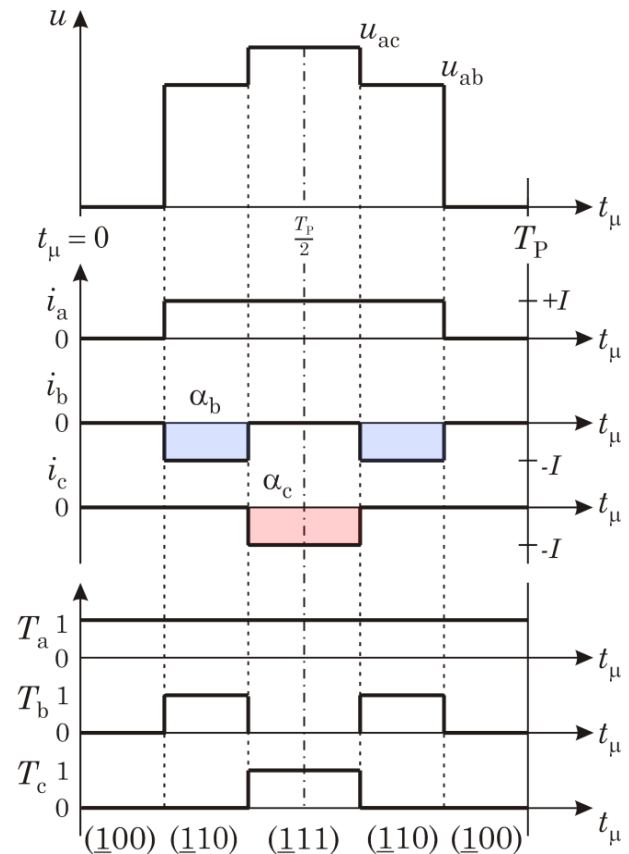
$$\bar{u} = u_{ab} \cdot \alpha_b + u_{ac} \cdot \alpha_c$$

$$P_{\text{link}} = P_{\text{input}}$$

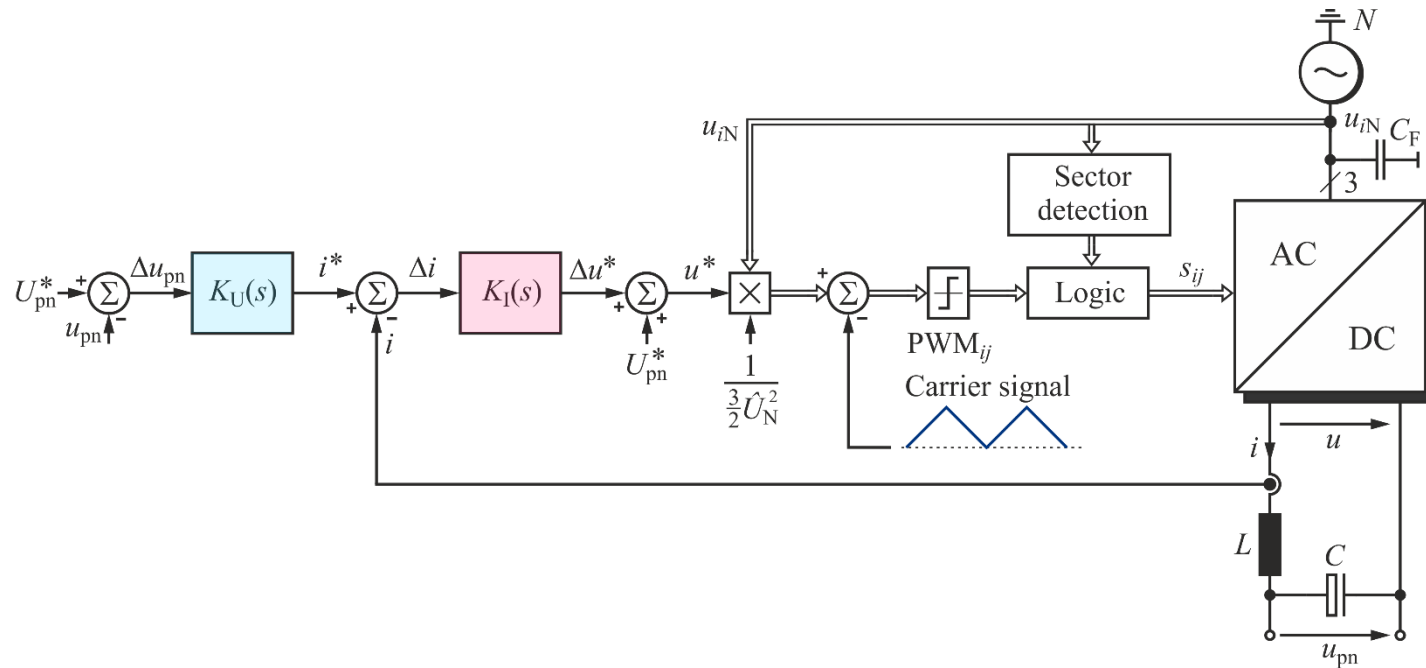
$$\bar{u} \cdot I = \frac{3}{2} \cdot \hat{U} \cdot \hat{I}^*$$

$$\bar{u} = \frac{3}{2} \cdot \hat{U} \cdot \frac{\hat{I}^*}{I} = \frac{3}{2} \cdot \hat{U} \cdot M$$

- Output Voltage is Formed by Segments of the Input Line-to-Line Voltages
- Output Voltage Shows Const. Local Average Value



Control Structure



■ Output Voltage Control & Inner Output Current Control

► Experimental Results

■ Ultra-Efficient Demonstrator System

$$U_{LL} = 3 \times 400 \text{ V (50 Hz)}$$

$$P_o = 5 \text{ kW}$$

$$U_o = 400 \text{ V}$$

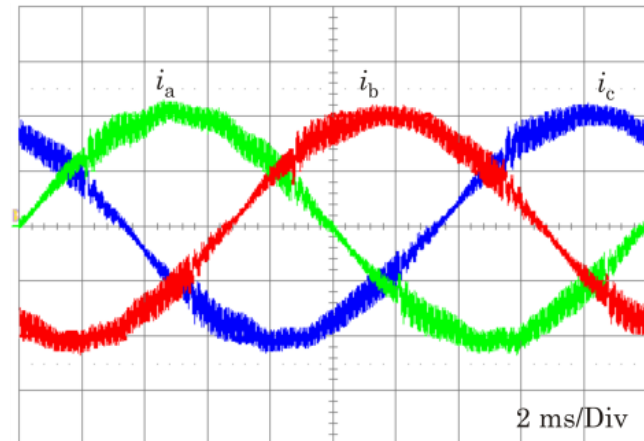
$$f_s = 18 \text{ kHz}$$

$$L = 2 \times 0.65 \text{ mH}$$

$$\eta = 98.8\% \text{ (Calorimetric Measurement)}$$



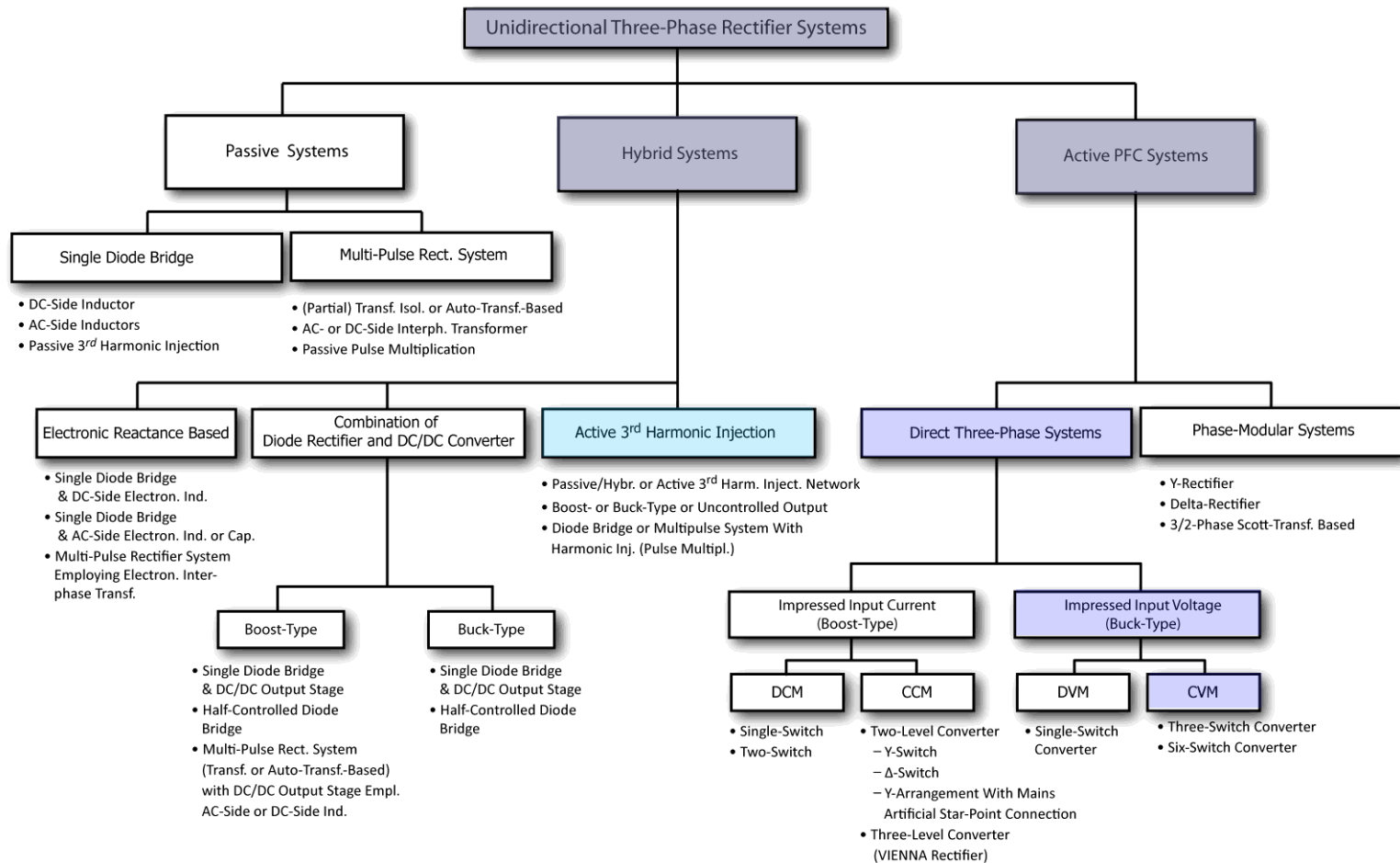
Input Phase Currents (5 A/Div)



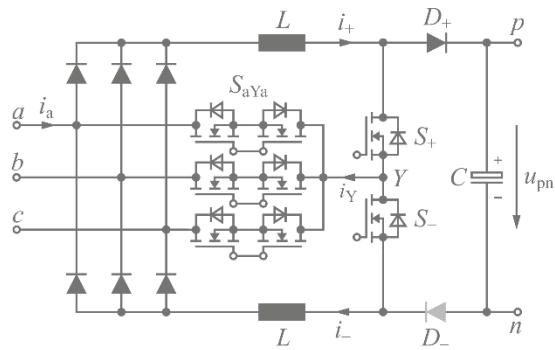
3rd Harmonic Inj. Buck-Type PFC Rectifier Systems

SWISS Rectifier

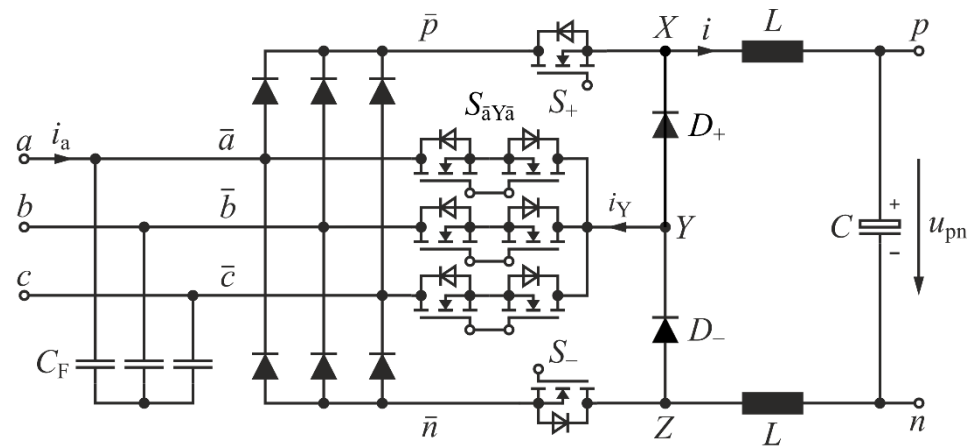
► Classification of Unidirectional Rectifier Systems



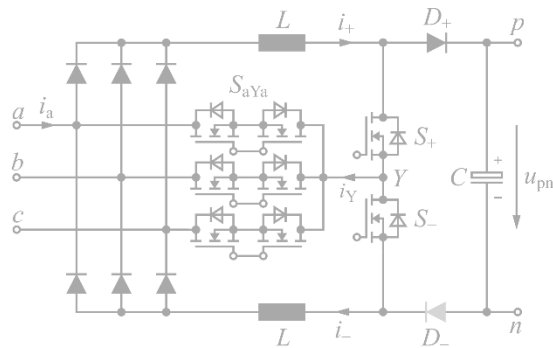
SWISS Rectifier



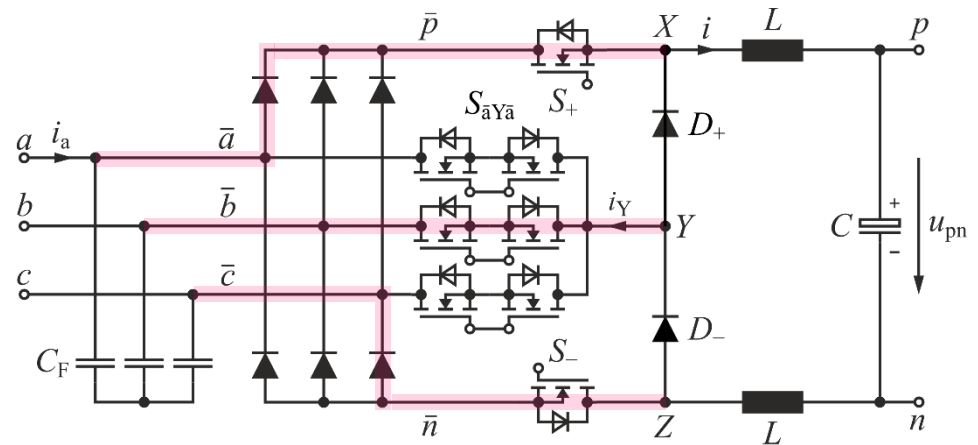
■ 3rd Harmonic Inj. Concept



SWISS Rectifier



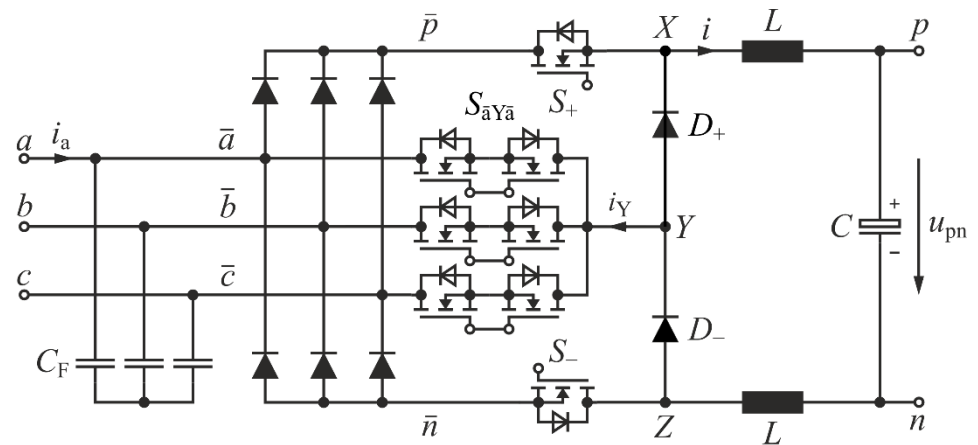
- Output Voltage Control
- Sinusoidal Current Control



SWISS Rectifier

- Output Voltage Control
- Sinusoidal Current Control

→ Low Complexity

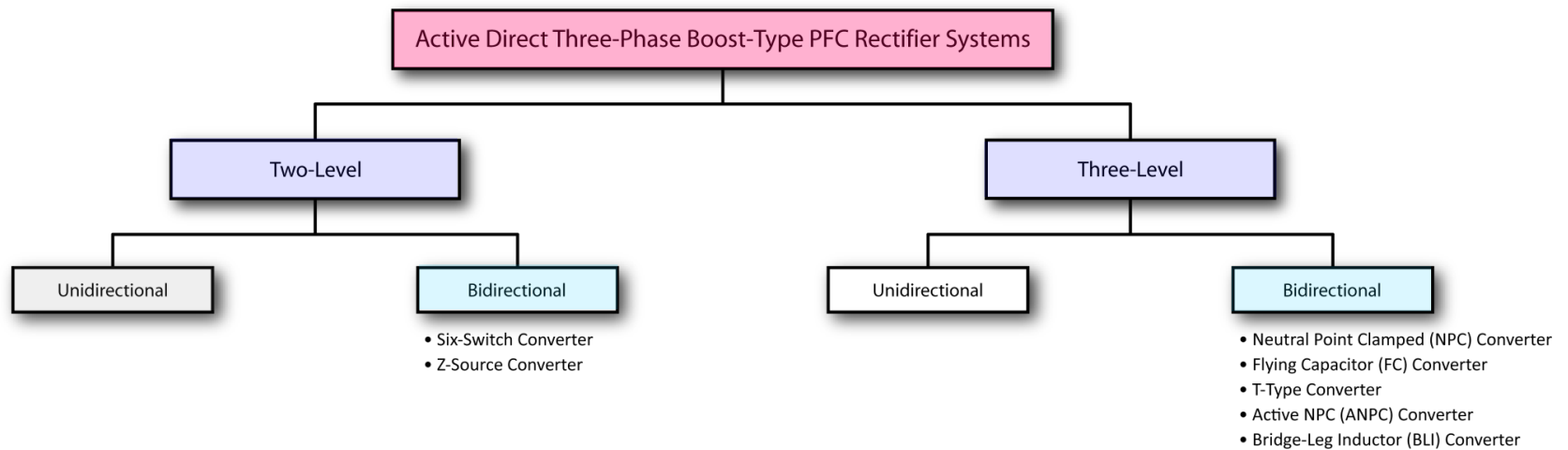


Bidirectional PFC Rectifier Systems

- *Boost-Type Topologies*
- *Buck-Type Topologies*

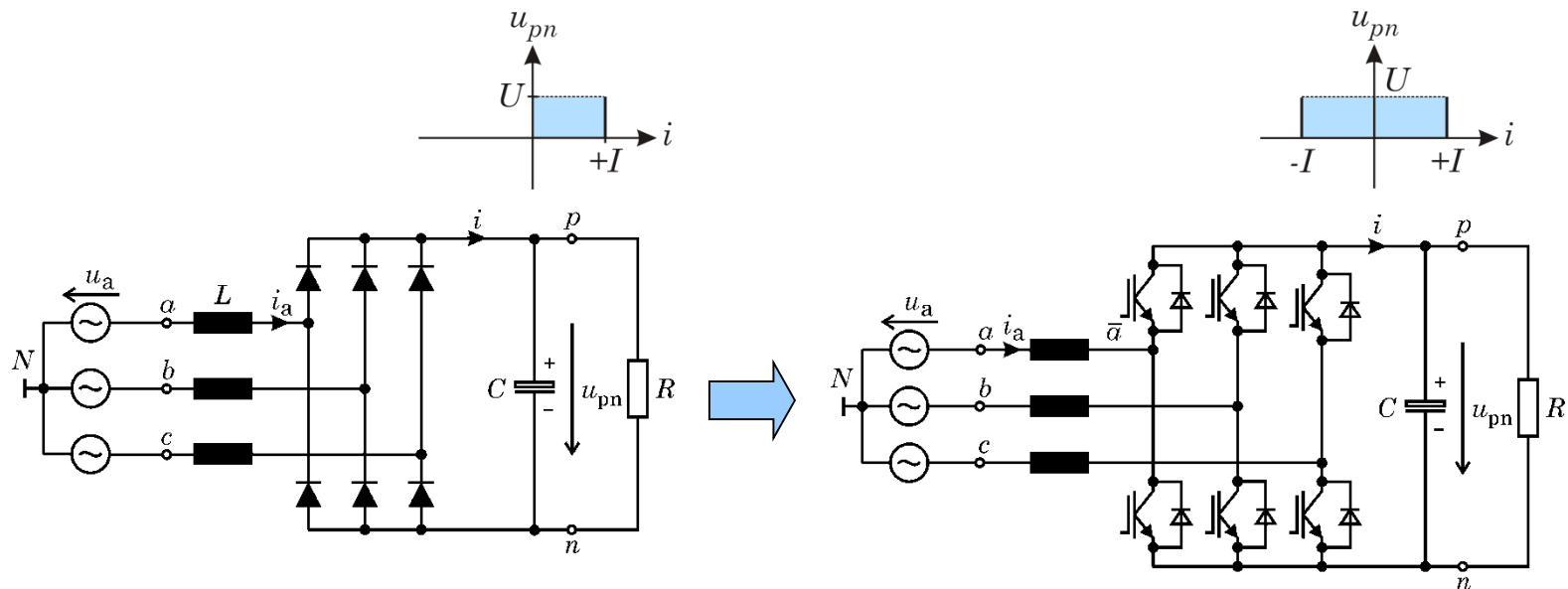
Boost-Type Topologies

► Classification of Bidirectional Boost-Type Rectifier Systems

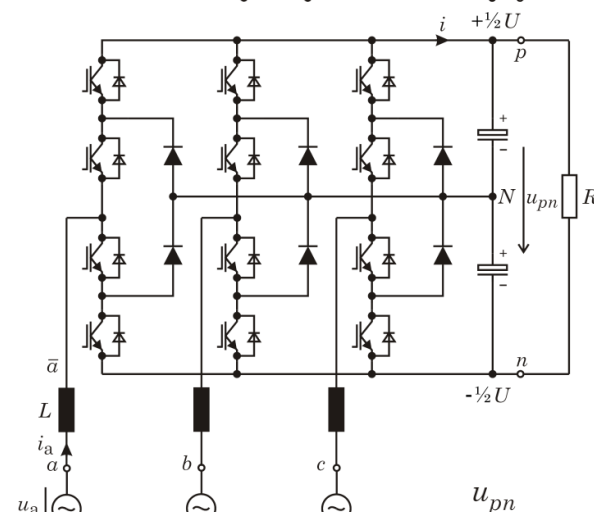
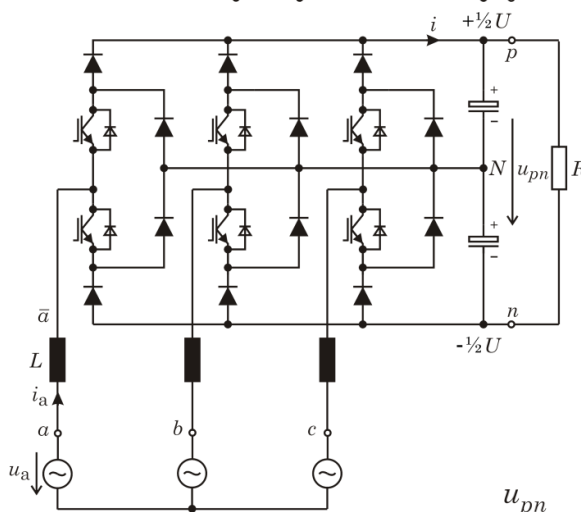
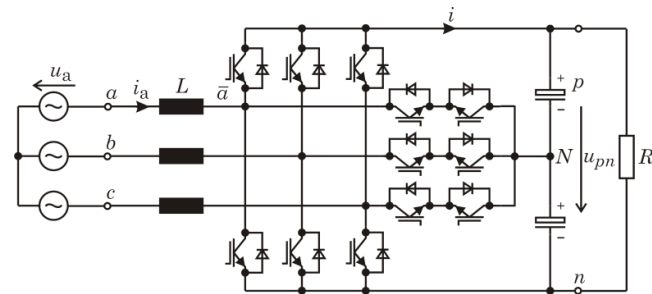
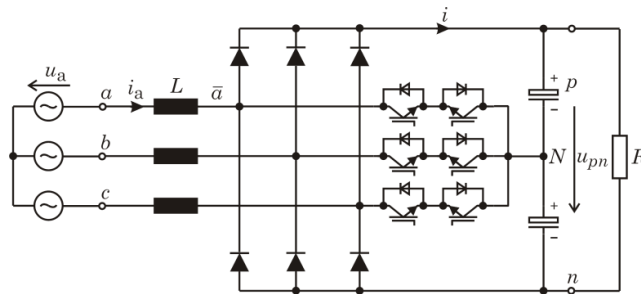


► Derivation of Two-Level Boost-Type Topologies

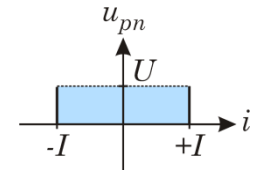
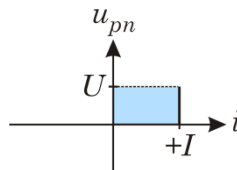
- Output Operating Range



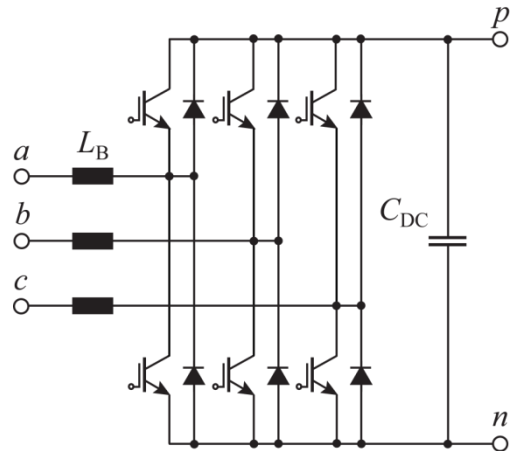
► Derivation of Three-Level Boost-Type Topologies



- Output Operating Range

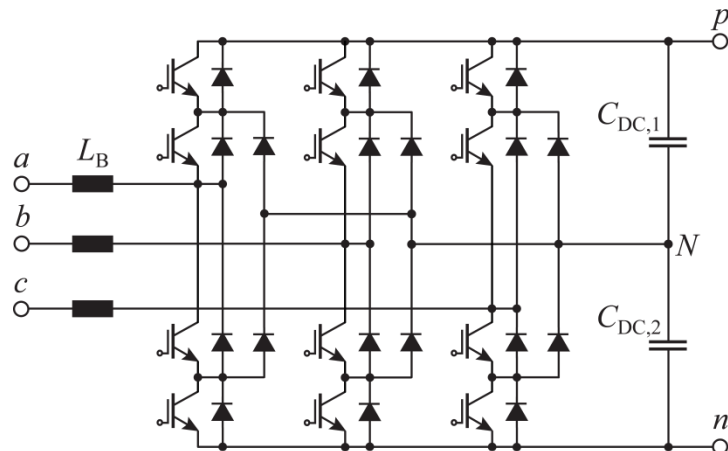


► Comparison of Two-Level/Three-Level NPC Boost-Type Rectifier Systems



• Two-Level Converter Systems

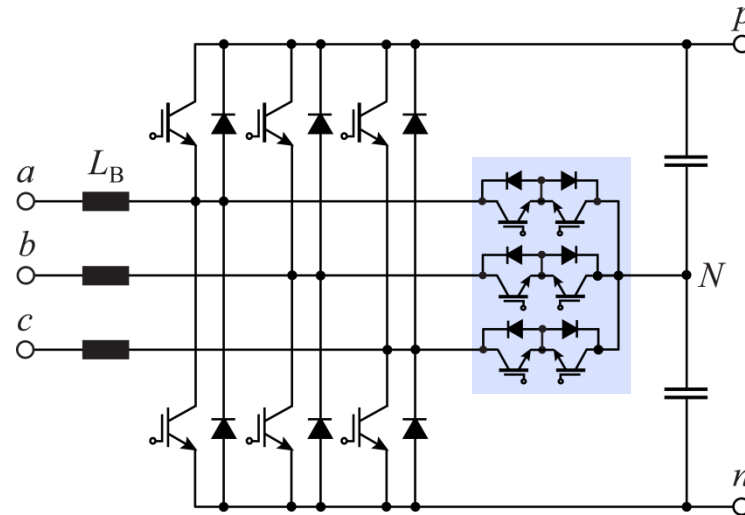
- + State-of-the-Art Topology for LV Appl.
- + Simple, Robust, and Well-Known
- + Power Modules and Auxiliary Components Available from Several Manufacturers
- Limited Maximum Switching Frequency
- Large Volume of Input Inductors



• Two-Level → Three-Level Converter Systems

- + Reduction of Device Blocking Voltage Stress
- + Lower Switching Losses
- + Reduction of Passive Component Volume
- Higher Conduction Losses
- Increased Complexity and Implementation Effort

► T-Type Three-Level Boost-Type Rectifier System

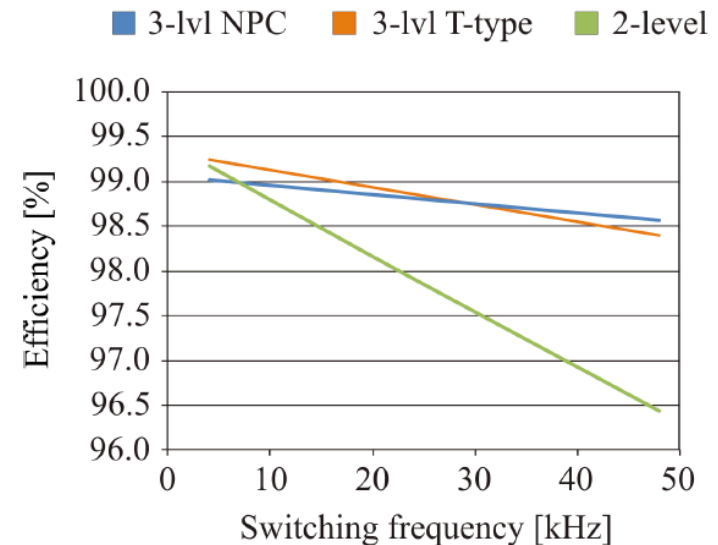


- + Semiconductor Losses for Low Switching Frequencies
Lower than for NPC Topologies
- + Can be Implemented with Standard Six-Pack Module
- Requires Switches for 2 Different Blocking Voltage Levels

► Pros and Cons of Three-Level vs. Two-Level Boost-Type Rectifier Systems

- + Losses are Distributed over Many Semicond. Devices; More Even Loading of the Chips → Potential for Chip Area Optimization for Pure Rectifier Operation
- + High Efficiency at High Switching Frequency
- + Lower Volume of Passive Components
- More Semiconductors
- More Gate Drive Units
- Increased Complexity
- Capacitor Voltage Balancing Required
- Increased Cost

- Moderate Increase of the Component Count with the T-Type Topology



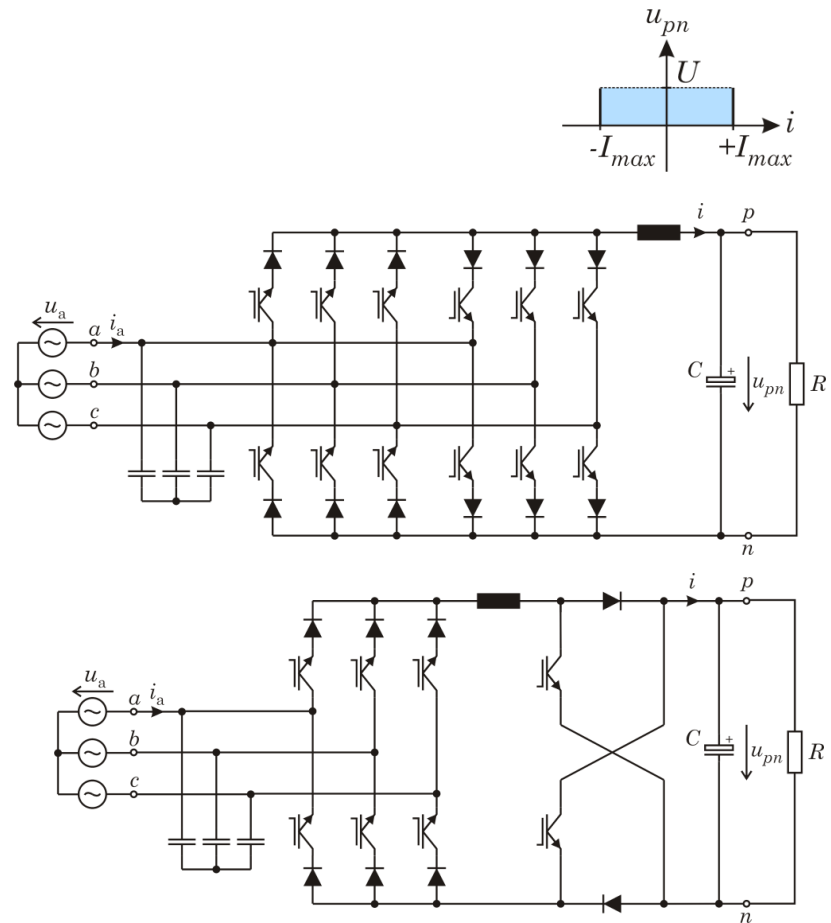
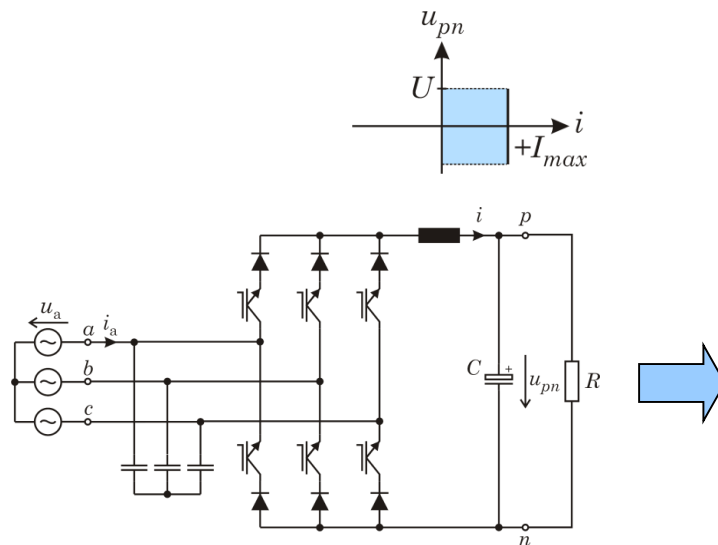
Consideration for 10kVA/400V_{AC} Rectifier Operation; Min. Chip Area, $T_{j,max} = 125^{\circ}\text{C}$

- Multi-Level Topologies are Commonly Used for Medium Voltage Applications but Gain Steadily in Importance also for Low-Voltage Renewable Energy Applications

Buck-Type Topologies

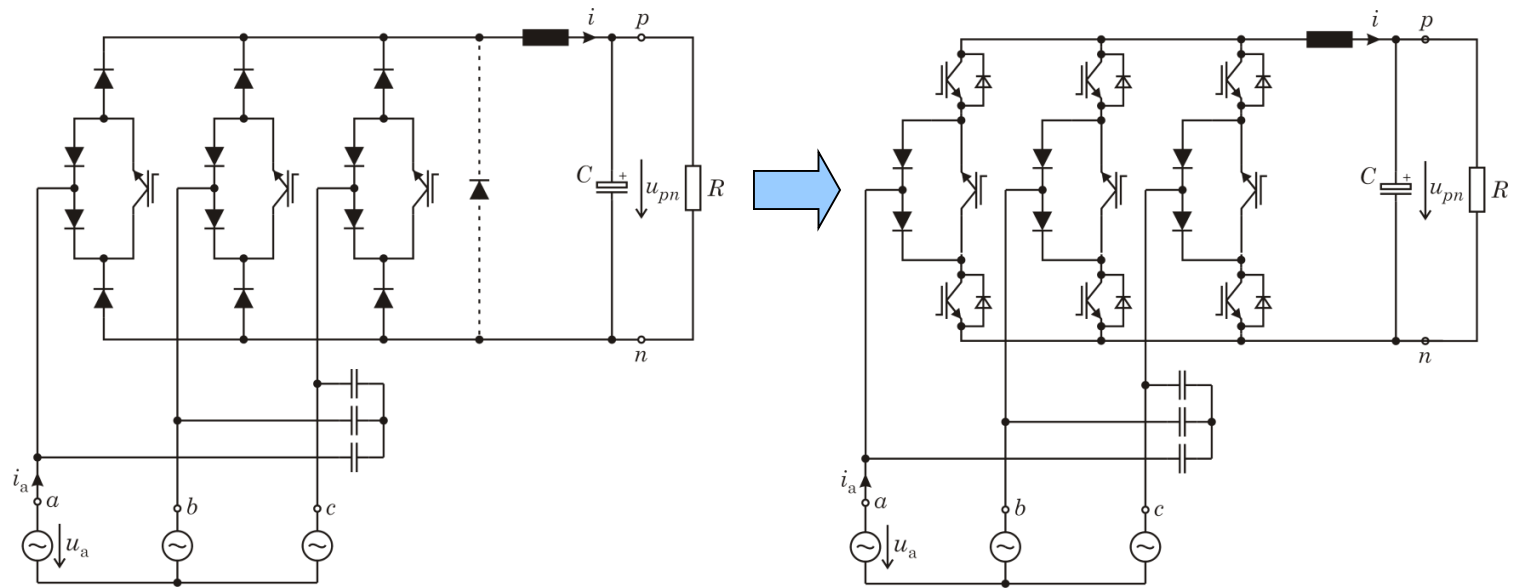
► Derivation of Unipolar Output Bidirectional Buck-Type Topologies

- Output Operating Range

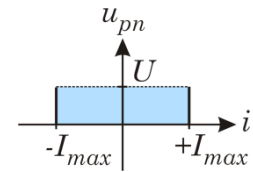
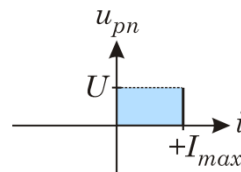


- System also Features Boost-Type Operation

► Derivation of Unipolar Output Bidirectional Buck-Type Topologies



• Output Operating Range



Thank you!

About

Johann W. Kolar (F'10)



received his M.Sc. and Ph.D. degree (summa cum laude / promotio sub auspiciis praesidentis rei publicae) from the University of Technology Vienna, Austria. Since 1984 he has been working as an independent international consultant in close collaboration with the University of Technology Vienna, in the fields of power electronics, industrial electronics and high performance drives. He has proposed numerous novel converter topologies and modulation/control concepts, e.g., the VIENNA Rectifier, the SWISS Rectifier, the Delta-Switch Rectifier, the isolated Y-Matrix AC/DC Converter and the three-phase AC-AC Sparse Matrix Converter. Dr. Kolar has published over 450 scientific papers at main international conferences, over 180 papers in international journals, and 2 book chapters. Furthermore, he has filed more than 110 patents. He was appointed Assoc. Professor and Head of the Power Electronic Systems Laboratory at the Swiss Federal Institute of Technology (ETH) Zurich on Feb. 1, 2001, and was promoted to the rank of Full Prof. in 2004. Since 2001 he has supervised over 60 Ph.D. students and PostDocs.

The focus of his current research is on AC-AC and AC-DC converter topologies with low effects on the mains, e.g. for data centers, More-Electric-Aircraft and distributed renewable energy systems, and on Solid-State Transformers for Smart Microgrid Systems. Further main research areas are the realization of ultra-compact and ultra-efficient converter modules employing latest power semiconductor technology (SiC and GaN), micro power electronics and/or Power Supplies on Chip, multi-domain/scale modeling/simulation and multi-objective optimization, physical model-based lifetime prediction, pulsed power, and ultra-high speed and bearingless motors. He has been appointed an IEEE Distinguished Lecturer by the IEEE Power Electronics Society in 2011.

He received 9 IEEE Transactions Prize Paper Awards, 8 IEEE Conference Prize Paper Awards, the PCIM Europe Conference Prize Paper Award 2013 and the SEMIKRON Innovation Award 2014. Furthermore, he received the ETH Zurich Golden Owl Award 2011 for Excellence in Teaching and an Erskine Fellowship from the University of Canterbury, New Zealand, in 2003.

He initiated and/or is the founder/co-founder of 4 spin-off companies targeting ultra-high speed drives, multi-domain/level simulation, ultra-compact/efficient converter systems and pulsed power/electronic energy processing. In 2006, the European Power Supplies Manufacturers Association (EPSMA) awarded the Power Electronics Systems Laboratory of ETH Zurich as the leading academic research institution in Power Electronics in Europe.

Dr. Kolar is a Fellow of the IEEE and a Member of the IEEEJ and of International Steering Committees and Technical Program Committees of numerous international conferences in the field (e.g. Director of the Power Quality Branch of the International Conference on Power Conversion and Intelligent Motion). He is the founding Chairman of the IEEE PELS Austria and Switzerland Chapter and Chairman of the Education Chapter of the EPE Association. From 1997 through 2000 he has been serving as an Associate Editor of the IEEE Transactions on Industrial Electronics and from 2001 through 2013 as an Associate Editor of the IEEE Transactions on Power Electronics. Since 2002 he also is an Associate Editor of the Journal of Power Electronics of the Korean Institute of Power Electronics and a member of the Editorial Advisory Board of the IEEEJ Transactions on Electrical and Electronic Engineering.

About

Roman Bosshard (S'10)



received the M.Sc. degree from the Swiss Federal Institute of Technology (ETH) Zurich, Switzerland, in 2011. During his studies, he focused on power electronics, electrical drive systems, and control of mechatronic systems. As part of his M.Sc. degree, he participated in a development project at ABB Switzerland as an intern, working on a motor controller for traction converters in urban transportation applications. In his Master Thesis, he developed a sensorless current and speed controller for a ultrahigh-speed electrical drive system with CELEROTON, an ETH Spin-off founded by former Ph.D. students of the Power Electronic Systems Laboratory at ETH Zurich.

In 2011, he joined the Power Electronic Systems Laboratory at the Swiss Federal Institute of Technology (ETH) Zurich, where he is currently pursuing the Ph.D. degree. His main research area is inductive power transfer systems for electric vehicle battery charging, where he published five papers at international IEEE conferences and one paper in the IEEE Journal of Emerging and Selected Topics in Power Electronics.